

POLITECNICO DI TORINO

Corso di Laurea Magistrale in Ingegneria Civile

Tesi di Laurea Magistrale

**Form Finding and Optimal Brick Tessellation for
Static Equilibrium of a Pierced Vault**



Relatore:

Dr. Amedeo Manuello Bertetto

Correlatori:

Dr. Fabio Bazzucchi

Prof. Paolo Maggiore

Dr. Davide Masera

Candidato:

Federico Riberi

Luglio 2018

“Fare o non fare, non c’è provare”

Acknowledgements

È veramente difficile riuscire a descrivere quello che si prova alla fine di questo percorso iniziato sei anni fa quando uscivo per la prima volta dalle porte del Politecnico felice per essere riuscito ad esservi ammesso. In questi anni veramente tante cose sono successe e tutte mi hanno portato a questo traguardo, non solo accademico e professionale, ma soprattutto umano e personale.

In queste poche righe vorrei provare a esprimere la mia gratitudine per aver avuto la grandissima fortuna di poter vivere questa lunga e difficile avventura, per chi mi ha accompagnato e per chi ha creduto in me, perché di una cosa sono certo: da solo non ce l'avrei mai fatta.

Questo lavoro di tesi in particolare, è stato reso possibile da chi in questi mesi mi ha dato fiducia e la possibilità di portare avanti un progetto, un'idea e un sogno che solo un anno fa era un'idea embrionale nella testa di uno spaurito studente di ingegneria. Il dott. Fabio Bazzucchi e il dott. Amedeo Manuello sono stati i primi a credere con me alla possibilità di creare un nuovo metodo progettuale per la costruzione di strutture in pura compressione e a credere che potessimo insieme raggiungere questo obiettivo. Ovviamente solo un primo passo è stato fatto ma senza ombra di dubbio nella giusta direzione. A loro va il merito di avermi guidato lasciandomi la libertà di cercare le mie risposte lungo il cammino, correggendo la rotta quando necessario, sempre avendo rispetto dei miei tanti tentativi alla cieca e della mia inesperienza. A loro va la mia gratitudine per aver sempre creduto in me e nel nostro progetto.

Grazie a tutti i dottorandi del DISEG, i professori e soprattutto i tecnici del MASTRLAB che mi hanno accudito in questi mesi.

Il ringraziamento più grande spetta di diritto alla mia famiglia che per me significa tutto e che da tempo si è decisamente allargata componendosi di quelle persone con le quali ormai mi sento legato in un modo che solo all'interno di una famiglia riesci a sperimentare e che le prossime righe non riusciranno a riassumere.

Grazie al mio Babbo, il mio eroe e la mia colonna portante, l'uomo che vorrei poter diventare. Grazie alla mia Mamma, la persona che mi ha insegnato a capire quali sono le

cose più importanti della vita. Grazie alla mia stupenda e magnifica sorellina, la mia Strega, perché, anche se forse non gliel'ho mai detto, è ciò che di più prezioso ho al mondo.

Grazie a Mattia, l'amico e il fratello con cui ho sempre e da sempre condiviso tutto, con cui sono cresciuto e che sempre e da sempre è stato ed è al mio fianco.

Grazie ai miei 4 compagni di viaggio: Luchino, Lu, Dalmass e Salo, rigorosamente ricordati come li chiamo sempre. Per voi non credo che possano esistere parole adatte a descrivere quello che abbiamo vissuto insieme e quello che provo. Siete la mia forza, insieme abbiamo sudato, pianto, faticato, riso; insieme siamo diventati ingegneri, insieme siamo "forse" diventati grandi, insieme siamo diventati fratelli e insieme voglio continuare a crescere.

Grazie a Bea, quella persona che nonostante tutto quello che può succedere non mi abbandona mai e crede sempre in me.

Grazie a Chia e Noe, le migliori compagne di classe e di banco del mondo, le amiche che sempre so essere al mio fianco.

Grazie a Vali, Eli, al mio buon Carluzzo, Michele, Paolino, Davide ai miei coinquilini, a tutti i compagni di avventura e a tutte quelle persone che sanno il posto speciale che hanno nel mio cuore e che mi hanno sempre sopportato e supportato.

GRAZIE!

Abstract

The design of vaulted structures is living a true renaissance thanks to the computer aided graphic statics. The fundamental work, mostly done by Block, have brought a series of computer tool for the research of the vault form by analyzing the thrust network lines. This thesis firstly explores the load-carrying efficiency of different piercing pattern of a simple vault, generated by RhinoVault. As a main result, from FEM analysis, the more stable pattern was found in the uniform distribution of 29 holes along the diagonals. As a second stage, the more suitable tessellation of the voussoirs was examined to guarantee both equilibrium and manufacturing. Planes and surfaces map were employed to create a 3D printed mould system where to pour concrete and realize the bricks. Realized elements were assembled to create a table scale model of the vault.

Contents

| | |
|--|-----|
| Acknowledgements | 5 |
| Abstract..... | 7 |
| 1. Introduction..... | 13 |
| 2. An Historical Approach to Form Finding..... | 15 |
| 3. An Overview of Structural Form Finding Methods | 35 |
| 3.1. Force Density Method..... | 37 |
| 3.2. Dynamic Relaxation Method..... | 41 |
| 3.3. Particle-Spring System | 49 |
| 3.4. Thrust Network Analysis..... | 52 |
| 4. Form Finding and Linear Buckling Load Analysis for Pierced Vaults: A Case Study | 59 |
| 4.1. Rhino VAULT | 62 |
| 4.2. Starting Attributes | 67 |
| 4.3. Opening Patterns..... | 70 |
| 4.4. Form Finding Process | 72 |
| 4.5. Pierced Vaults Structural Analysis..... | 83 |
| 4.5.1. Mesh Element..... | 85 |
| 4.5.2. Geometric Attributes | 85 |
| 4.5.3. Material Attributes | 86 |
| 4.5.4. Supports..... | 86 |
| 4.5.5. Loads Attributes | 87 |
| 4.5.6. Post Processing Phase | 89 |
| 4.6. Linear Buckling Load Analysis..... | 99 |
| 5. Scaled Prototype Realization | 113 |
| 5.1. The Geometry | 114 |
| 5.2. First Tessellation Pattern Trial..... | 115 |
| 5.3. Voussoirs Fabrication | 121 |
| 5.4. Falsework Fabrication | 129 |
| 5.4.1. Constraints Fabrication..... | 133 |
| 5.5. Construction Phases Scheme..... | 136 |
| 5.6. Second Tessellation Pattern Trial..... | 139 |
| 6. Conclusions..... | 147 |

| | |
|--|-----|
| APPENDIX A | 151 |
| A.1 Grasshopper 3D | 153 |
| A.2 Digital Simulation – Particle-Spring System | 156 |
| Bibliografia | 166 |
| Attachments | 167 |

1. Introduction

In this thesis I want to sponsor an architecture and design philosophy in which geometry, sustainability and structural requirements work together to follow what nature teaches us: to optimize ourselves to survive, to optimize ourselves to be fit, to optimize ourselves to be healthy for us and for the ones who interact with us and for our planet, optimize ourselves to be an example.

Masonry structure are natural structures. As wood, they come from the earth and elevates from it to build spaces and volumes. This exhibits a warm and classic architecture, somehow familiar in its way. However, there is no reason why a masonry structure can't be *modern* or *innovative*. The examples of the last years, and the new attention to this building typology, have evidenced their continuous potential to be an actual architectural solution. Digital Fabrication and Additive Manufacturing have opened a new area of possibilities, from eco-sustainability and easy construction, to transparency.

The main object of this work is to take a first step in a direction where a design tool for latticed masonry shells would be developed, starting from a given topology and obtaining the optimized grid and stiffness.

First of all, a look and an overview on historical aspects of Form Finding is led, with a focus on the most important architects and engineers who developed the building philosophy of the resistance by shape, the compression-only structures design and the introduction of numerical approaches with computers in the design process in the last decades.

After, a brief description of modern form finding techniques is presented showing how modern designers approach Form Finding. The objective of the chapter is to show that Form Finding has to be seen as a fundamental part of the whole design process, not only as a first conceptual and preliminary phase.

The central part of the thesis deal with a theoretical case study where compression-only pierced shell geometries are designed with the Thrust Network Analysis developed by Philippe Block.

The shape of the vaults is reached through the value variation of some chosen parameters: lowering degree and piercing pattern. After, global structural stability analysis has been made varying: the previous parameters values, slenderness and load-cases.

In the end, one of the analyzed pierced vaults is chosen and a scaled prototype is realized with the help of Additive Manufacturing techniques.

2. An Historical Approach to Form Finding

During centuries from the classical age until nowadays, the most important example of form finding was always around us: the arch. This structural element represents one of the biggest discoveries of the building history of mankind. For the first time, a structure doesn't have to carry loads because of its material characteristics; it's the shape that determine if the structural element will be able to carry loads or not.

“Ut pendet continuum flexile, sic stabit contiguum rigidum inversum. As hang the flexible line, so but inverted will stand the rigid arch” (Hooke, 1676). This sentence was written by Hooke in 1675 as an anagram inside a totally unrelated book: *A description of Helioscopes and other instruments*. The anagram solution was not published until the author death but this let us know that he understood that if he could solve the problem of the shape of the catenary, he would at the same time found which is the correct shape of the perfect arch able to carry load in a compression state. (Heyman, 1998)

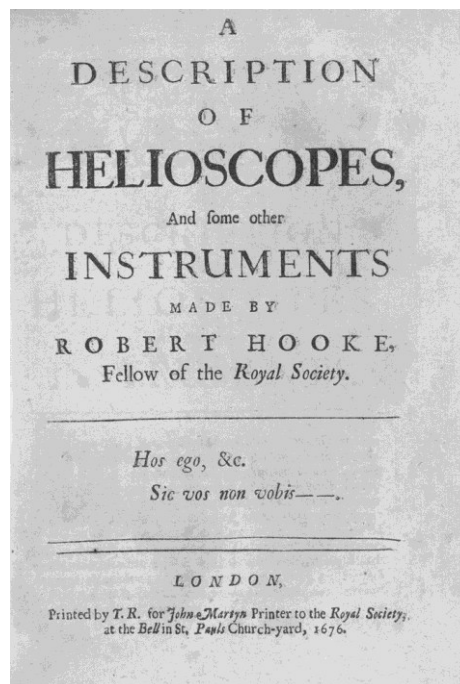


Figure 1: Hooke's 1675 book cover of "A Description of Helioscopes and Other Instruments"

Robert Hooke is defined as the England's Leonardo Da Vinci, a genius for his time. *“He was among the world's leading talents in designing and making scientific instruments and clocks, mechanical engineering, material science, and structural mechanics, as well as astronomy, microscopy, chemistry, biology, physics, surveying and architecture”*

(Addis, 2007). Hooke was a good friend of Christopher Wren and they became building designers together by accident when they were called to restore and rebuild the heart of London after the terrible fire in 1666. *“They were the first building designers who had a good mathematical and scientific understanding of forces, derived from their work at the Royal Society. They used to work with mathematical model to represent the complexity of the planetary motion so they turned this knowledge into the building design”* (Addis, 2007).

Hooke’s anagram explains why masonry construction or arches and domes developed in such an incredible way across the last two thousand years of history mostly when structural analysis theory was not born yet and when mathematical theorems were not applied to the building design. Centuries of building experience taught, surely with no consciousness about it, that since arches and domes are simple compression structures, their stability is independent from their scale, and every dimension of a structural model can be increased proportionately to erect the real structure. That is way no engineering science was necessary in the past to design, model and build pure compression structures: that’s all because the stability is only a geometry matter and it is almost independent from the stiffness or the strength of the masonry. (Larena, 2009)

At the time in which Hooke worked, there were big arguments between the most important scientists on the scene and not only for scientific reasons. It is impossible to leave out Newton from the dissertation.

Intellectually, Hooke was probably nearly as able as Newton, and he was certainly even more touchy and vain; but in other respects they were men of totally different temperaments and interests. [...] Newton’s vision of the Universe may have been wider than Hooke’s, but his interest in science was much less practical. [...] It is true that Newton became Master of the Mint and did the job well, but it seems that his acceptance of the post had a little to do with any desire to apply science and a lot to do with the fact that this was a ‘place under Government’ which, in those days, conferred a much higher social position than his fellowship of Trinity, not to mention a higher salary. I don’t think he had much time or inclination to indulge in the sins of the flesh. In short, Newton was well constituted to detest Hooke as a man and to loathe everything he stood for, down to and

including elasticity. It so happened that Newton had a good fortune to live on for twenty-five years after Hooke died, and he devoted a good deal of this time to denigrating Hooke's memory and the importance of applied science. Since Newton had, by then, an almost God-like position in the scientific world, and since all this tended to reinforce the social and intellectual tendencies of the age, subjects like structures suffered heavily in popularity, even for many years after Newton's death. (Gordon, 1978)

However, during this period often the statements, like the one secrecy did by Hooke, were not fully supported by mathematical proofs and the problem of catenary was one of them. At the end of the century seems that Leibniz, Huygens and Bernoulli gave their solution to the problem but was only David Gregory in 1697 that published the mathematics. There were some mistakes inside the analytical solution but what he wrote was essential for the work of Coulomb almost 80 years later:

*In a vertical plane, but in an inverted situation, the chain will preserve its figure without falling, and therefore will constitute a very thin arch, or fornix; that is, infinitely small rigid and polished spheres disposed in an inverted arch of a catenaria will form an arch; no part of which will be thrust outwards or inwards by other parts, but, the lowest part remaining firm, it will support itself by means of its figure... And, on the contrary, none but the catenaria is the figure of a true legitimate arch, or fornix. **And when an arch of any other figure is supported, it is because in its thickness some catenaria is included.** Neither would it be sustained if it were very thin, and composed of slippery parts. From Corol. 5 it may be collected, by what force an arch, or buttress, press a wall outwardly, to which it is applied; for this is the same with that part of the force sustaining the chain, which draws according to a horizontal direction. For the force, which in the chain draws inwards, in an arch equal to the chain drives outwards. [...]* Gregory asserts that if any thrust line can be found lying within the masonry, then the arch will stand. (Heyman, 1998)

One of the first and most important application of the anagram comes from Wren and it is displayed in Saint Paul's Cathedral. The building is one of the masterpiece where the weight of a huge building can be addressed from the top to the foundations. "The building

even incorporates flying buttresses, though unlike in medieval cathedrals, they are hidden from view, as they did not suit the Baroque architectural style. The main structural element of this cathedral is a cone made of brick, which carry the weight of the lantern. Inside this, and visible from the interior of the cathedral, is a lightweight hemispherical brick shell with an oculus” (Addis, 2007) that is supported by the brick cone. For the design of the cone, Wren used the principle written by Hooke. So “the most efficient and economical shape for the brick cone was calculated to be an elongated, gentle paraboloid”. (Addis, 2007) In the hanged model idea, the shape was given by a gravity concentrated load in midspan.

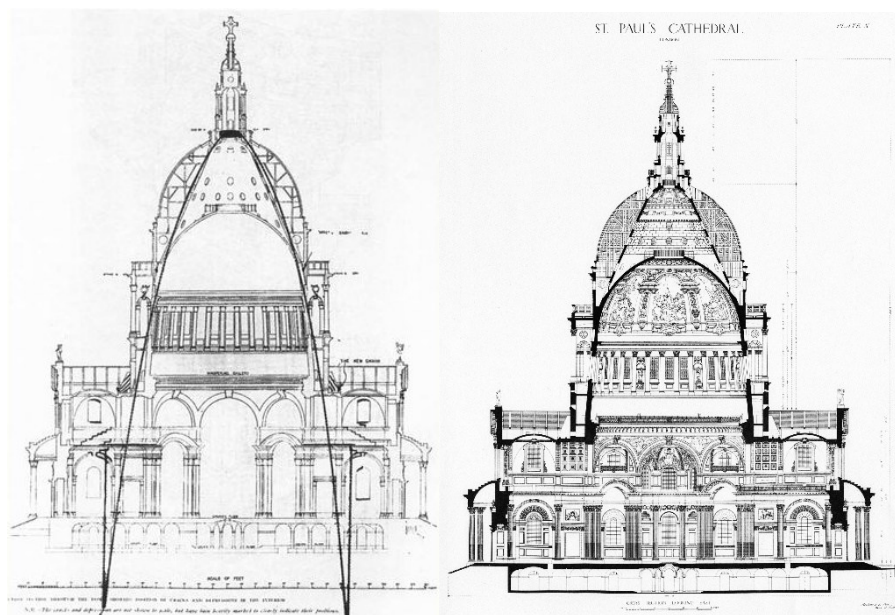


Figure 2: (a) The inverted hanging chain in front of the section of the dome of the St. Paul Cathedral in London by Christopher Wren (1720) and (b) the architectural section of the building

A second remarkable example of application of the so called Hooke’s second law, comes from Italy and from the dome of St. Peters during the XVIII century. It “had developed cracks running up from the drum along generators, and dying out near the crown; these meridional cracks divided the dome into portions approximating half spherical lunes (orange slices)” (Heyman, 1998). Giovanni Poleni, academic from University of Padova, in 1740 was called as consultant after other unsatisfactory designers. He criticized his colleagues because the models of collapse they presented, did not correspond to the behavior of the dome as indicated by the cracks. He assumed that masonry had large compression strength and zero tensile strength that is fair considering what nowadays is known about masonry behavior. He divided the dome into fifty lunes and considered the

equilibrium of this quasi two dimensional arch tapering to zero thickness at the crown. He observed that such an arch would be stable if the line of thrust lay entirely within the thickness of the masonry as expected. Defining the shape of a stable arch as the inversion of the corresponding hanging catenary, he made a model using weights proportional to the distribution of weight in a pair of lunes and the weight of the lantern, and determined the shape of the thrust line experimentally. Three years later, Le Seur, Jacquier and Boscovich, made a different study of the dome concluding that extra ties were necessary for the stability of the dome to contain the horizontal thrusts. Poleni saw their work and he agreed with them because of his estimation of the tie force coming from the horizontal pull of the hanging chain. (Addis, 2007) (Heyman, 1998)

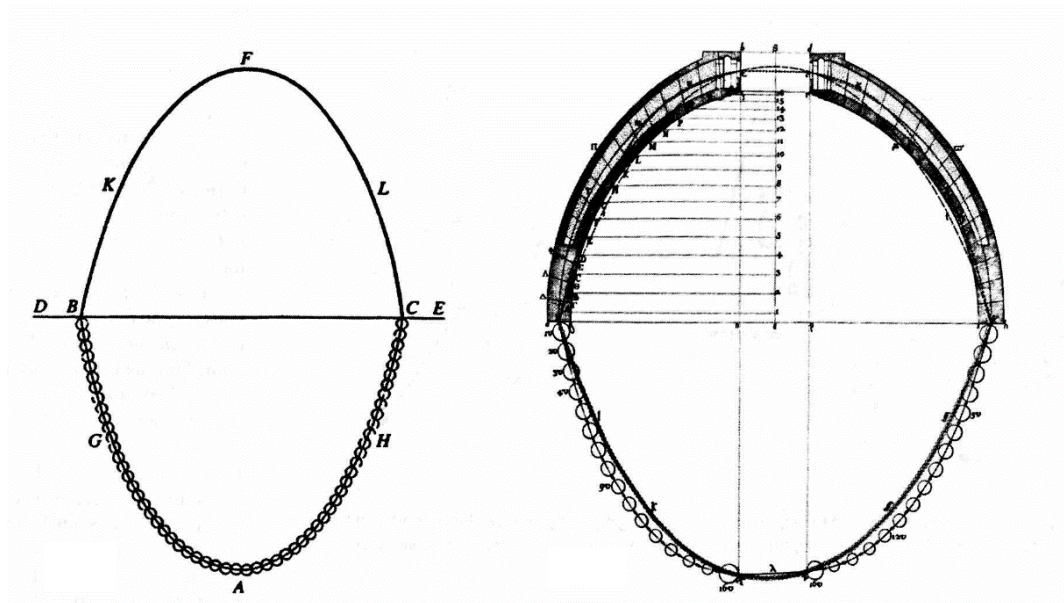


Figure 3: Poleni's drawing of Hooke's analogy between an arch and a hanging chain, and his analysis of the Dome of St-Peter's in Rome (1748)

“It may point out that the simple catenary is not a parabola, as in many texts both terms are used as synonyms; in fact, it has the shape of the hyperbolic cosine.” (Huerta, 2006) However, Hooke's second law could also be seen as a precocious statement of the Lower Bound Theorem.

This approach illustrated by Hooke was not widely divulged in continental Europe, but it was being mentioned in some French treatises of the XVIII century. In Germany Hubsch carries out some research on this idea to demonstrate the uselessness of buttresses during the design of a church in the XIX century.

“Around 1840, the line of thrust theory is postulated making more rigorous the intuitive experimental approach of the English engineers” (Huerta, 2006). Now it was possible to calculate and draw a line of thrust without models, using mathematical analysis or graphical methods.

The most important graphical method that attempt to calculate structures using primarily graphic methods, is the Graphic Statics. One of the father of this method is Maxwell who, between 1864 and 1870, established that for certain trusses, the nodes and polygons representing the geometry have reciprocal polygons and nodes in the force domain. (Beghini, 2014)

Graphic statics is easy to apply for one and two dimensional problems to be solved. This approach can be extended to the third dimension but it need a very complex geometrical procedure. However, some explanations about this method will be presented in the following chapters. (Rippmann, 2016)

A new formal language based on the use of hanging models was only introduced through the work of German architect Friedric Gosling and more prominently, through the creation of the Catalan architect Antoni Gaudi.

Gaudi’s work convers all aspects of architecture: layout, ornamentation and stability. He also incorporates other arts: sculpture, painting and photography. For Gaudi, structural design was an integral part of architectural design from its initial stages. It was not restricted to a mere stability check.

In order to understand the structural component of Gaudi’s architecture, is useful to understand the traditional Catalan building methods. The procedures concerned are all based on the use of an especially resistant, broad, flat tile an inch thick and 6 by 12 inches in area. These tiles courses are usually laminated in a sufficient number of layer in order to achieve the desired moment of inertia at any point of interest. Part of the efficiency of this masonry building kind derives from the excellence of the tiles, which are frequently harder than stone. The character of the mortar employed is crucial. It is quite thick occupying the 50 cent of the depth of the masonry. Nowadays the strength of the mortar became so high that masonry usually beaks.

Traditional building methods and Graphic Static were two of the most important aspects that influenced Gaudi's architecture. Gaudi used the concept of catenary arches in a completely original way: to integrate the structural design in the process of architectural design.

"Gaudi used the concept of catenary arches in a completely original way: to integrate the structural design in the process of architectural design. It is not a matter of verifying the stability of a certain design; it is a matter of projecting, from the start, using stable shapes". (Huerta, 2006)

Gaudi found catenary and parabolic curves aesthetically pleasant and he used them even when he could have used other kinds of shapes. He didn't want to apply the traditional method in which a vault is designed, giving it a certain shape and dimensions and, then, its stability is checked using graphic methods; he wanted to apply a design method that allowed him to obtain equilibrated forms directly. He devised his own method for creating masonry compression structures by extending into three dimensions Robert Hooke's axiom stating that the form of a stable arch is that of an inverted hanging chain. To establish the form for the vault of a chapel, Gaudi created a three-dimensional model using wires and bags of sand to represent the weight of the masonry elements and canvas to visualize the vaults. When inverted, this would give a stable arrangement of masonry columns and vaults.

The architectural projects by Gaudi that hold the greatest interest are two unfinished structures: the Colonia Guell chapel and the Church of the Sagrada Familia, on which he worked from 1884 until his death in 1926. Although unfinished, *"Gaudi's intentions with regard to both buildings are well known from his drawings, models, and photographs, so that we can actually study his structural theory and practice as though the two edifices had in fact been completed"* (Collins, 1963). In particular, the Colonia Guell chapel is the one all designed using empirical considerations. The form and the shape of the whole structure and of its constituent parts are governed by the material used for their construction: masonry. A masonry vaults need to follow as closely as possible the thrust network of forces acting on and inside the analyzed structure. Gaudi recovered most of his data about materials and their behavior from direct tests. In the standard process he needed to use these advices through the subject of graphic statics as usual at the time. The

three dimensional forms involved in the process required a very high difficult geometrical and analytical approach by means of projective geometry and diagrams very hard to be read. So he implemented three dimensional hanging models, funicular models that represented the true arches in inverted position. (Collins, 1963) (Huerta, 2006)

Specifically thinking about the Colonia Guell Chapel is known that this church is part of an ambitious industrial complex, in the town of Santa Coloma de Cervello (Barcelona).

The project starts from Eusebi Guell, owner of a large textile factory; his intention was to build a quartier beside Barcelona for the workers of the factory. As great patron of Gaudí, he involved the architect in the project in 1890. Guell's intention was not only to build a place for the workers to sleep and rest and live with their family, he wanted to create a new living center with its own personality that join social and economic life. So it was important for him to build facilities to help develop culture, sport and arts. Also the religious component was important for Guell, so he asked Gaudí to design and realize a new chapel, instead of the one (too small for the growing population) that could accommodate all the inhabitants.

However, little did Güell imagine that Gaudí would make a proposal as sober, stern and radical. The architecture was based on the task of making Güell a place of worship, that harmonized with the unconventional architecture of the workers' homes in Güell's Colony, and with the nearby forest and the slope of the hill where it would be projected.



Figure 4: The Crypt of Colonia Guell

One of the most characteristic features of this construction is undoubtedly its structure. A way that comes from a study model that retains, called “stereostatic model or polifuncular model” by which Gaudí calculated the structure of the future church. A model of the church at 1:10 that grew to more than 4.5 meters high and hung by string from the ceiling by two points and the suspending weights were bags of pellets. In this way he could draw an inverted bow in the air and Gaudí spent time photographing and he then put his drawings of the future arches onto paper, forming the profile of the church. Again the modernist genius, whose rule was “with two rulers and a ball of string all the architecture is generated”, demonstrated in Güell’s colony’s own physical knowledge of gravity and pressure, along with his intuition and experience, helped to create a unique structure which was formed as an “experiment” of architectural solutions that were then also incorporated into the Sagrada Familia.

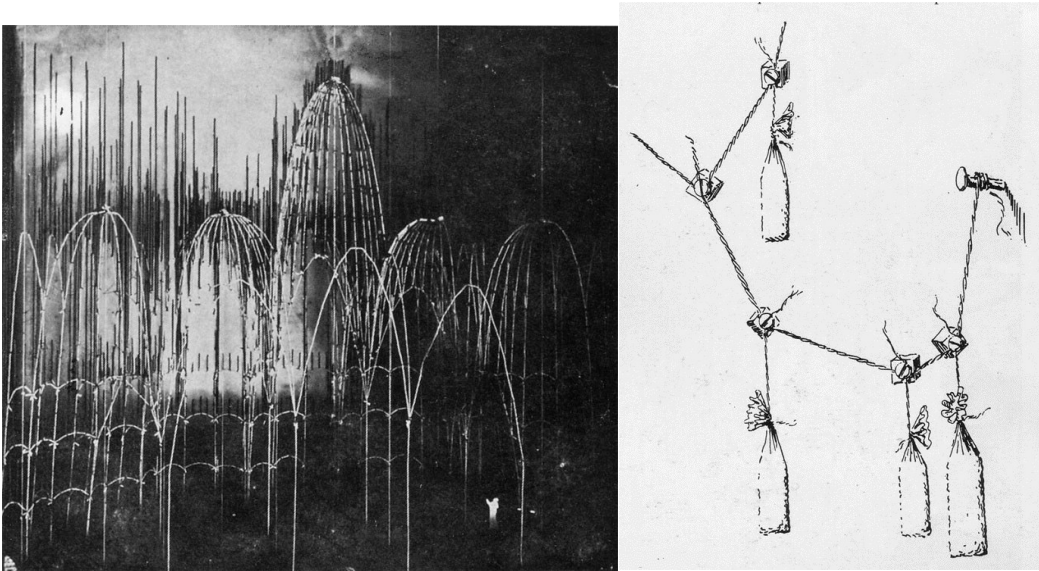


Figure 5: (a) First stereostatic model for a previous study and (b) Small sacks filled with pellets



Figure 6: Hanging model for the Sagrada Familia



Figure 7: View of the Sagrada Familia

By the beginning of the second half of the 20th century the use of hanging models was refined. One of the most important designer of those years working and thinking about form finding was the Swiss Heinz Isler. He was one of the father of concrete shell design and he was interested in thin shell topic since he was a student. Indeed, he was the only one between hundred students to choose a master degree thesis in which he studied thin shell.

Isler is also remarkable for his simple experiment where he showed that straight and flat elements were not as efficient as curved ones, indeed a curved plastic element, the one used by him, can resist more than 30 times greater load then the same element when it is flat.

It is well known that *“the general mathematical theory of shells did little to stimulate design; rather, the construction of shells stimulated academics to study the theory.”* (Billington, 1985). He also used the geometric similarity between hanging structures and dome or shell structures. For many years after the heyday of concrete shells in 1950s, he has continued to produce concrete shell roofs using an elegant design procedure. He first establishes a suitable plan for the roof, then uses a hanging fabric model to generate the statically-correct geometry, which he then measures and scales up to generate the

dimensions of the finished shell of reinforced concrete. In his remarkable paper *New Shapes for Shells*, presented at the first conference of the International Association for Shell and Spatial Structures, in Madrid in 1959, Isler proposed three methods of form finding. Of these three, he considered the hanging cloth reversed to be the most satisfactory and this was the method he used to find the shape of his most iconic works such as the roofs of the N1 autobahn service station at Deitingen and the Sicli factory in Geneva. The paper concluded with a sketch, by Isler, shown in figure, indicating 39 potential shell forms and an *etc.*, suggesting that there might be an infinite number yet to be discovered.



Figure 8: Isler's examples of the endless forms possible for shells, from his IASS conference paper in 1959

“For form finding of his shells Isler loaded the fabric surface with a plaster of his own formula developed to maximize mouldability when wet whilst maintaining a constant on the curved fabric and minimizing cracking of the drying surface. However, Isler also realized the shortcomings of this technique, due to the influence of fabric weave and its orientation relative to the boundaries. To minimize these effects, for more accurate modelling of the hanging surface, Isler employed a selected high-quality latex rubber membrane which has consistent isotropic properties”. (Chilton, 2012)

From the almost potentially infinite shapes that can be found using these form finding methods the choice of the shape that will be effectively designed and built by the engineer is governed, according to Isler and what he wrote on the blackboard of IASS conference in 1959, to some key factors:

- Functional;
- Shaping;
- Artistic expression;
- Statics;
- Construction;
- Cost.

In the photography that record these words, Isler emphasized shaping and cost. (Chilton, 2012)



Figure 9: Service Station at Deitingen Sud (1968)



Figure 10: Sicli SA Factory in Geneva (1969)

Hanging models also played a fundamental role in the work of Frei Otto. Otto specialized in lightweight tensile and membrane structures, and pioneered advances in structural mathematics and civil engineering. He founded the Institute for Lightweight Structures at

the University of Stuttgart in 1964 and headed the institute until his retirement as university professor. He used physical models as integral part of the process of designing cable-net or membrane structures. He developed completely new kind of structures where is present a double curvature with a high level of pre-stress to prevent the membrane or steel cables form deflecting excessively under snow or wind load, and from vibrating or flapping in a wind. To design his structures, he developed a completely new design and manufacturing process: the soap film models. Those models presented the greatest technical challenge because no one ever made bubbles up to a meter across that would last long enough to be studied and measured. It was very difficult to be accurate enough in the measurement because that model has to scaled up to almost hundred times to become the real structures and in the up scaled situation, the solution has to satisfy the requirements of the fabric and cable manufacturers. This design method let Otto to build the cable net roof of the German Pavillon at Expo 67 in Montreal and the 135 metres cable-net roof over the stadium at the 1972 Munich Olympics.

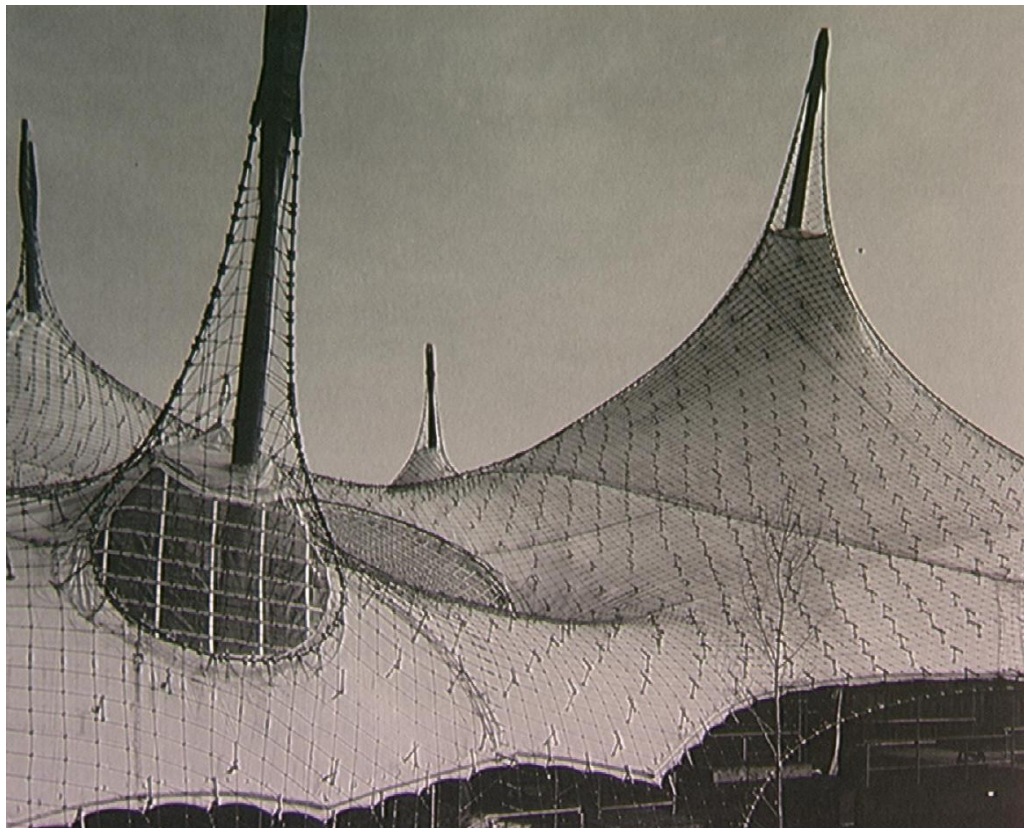


Figure 11: German Pavillon at Expo 67 in Montreal

Jörg Schlaich, project leader at Leonhardt & Andrä, the structural firm of the project, doubted the precision of the physical models, and pushed for the development of computational methods for the analysis and cutting pattern generation. During this phase Linkwitz proposed to measure the models precisely applying close range photogrammetric methods which would allow for a simultaneous determination of the 3-D geometry of the model without touching it. Also from this analysis it was realized that the models were by no means precise enough to derive the cutting pattern for an equal mesh cable net made from steel. In 1971 Linkwitz and Schek discovered a new formulation of the figure of equilibrium of forces, the force-density formulation. They realized that this was more appropriate for solving the problem, especially that of finding good initial geometry. The general formulation of the static equilibrium problem as mathematical relation between geometry and inner forces is non-linear and has to be solved iteratively. To solve the problem was studied a mathematical *trick*: the forces in action were substituted by the ratio between force and length of the element; this ratio is called *force density* and let the designer to write linear equilibrium equations to solve the system that now is all linear and lightweight and fast from a computational point of view. The system became again non-linear when constraints are imposed to the structure. In this case the system is solved through gradient-based methods such as the Gauss-Newton method. This method, called from that time Force Density Method (FDM), was the one used to calculate in a numerical way the geometry of the Olympic roof and some years later of the Multihalle in Mannheim.

Each set of force density values creates a unique equilibrium form and the potential of this approach for form finding on the computer enabled the optimization of equilibrium geometry, but did not yet offer an alternative for the model-based design and for finding process. (Grundig, Moncrieff, Singer, & Strobel, 2000) (Lachauer, 2015)

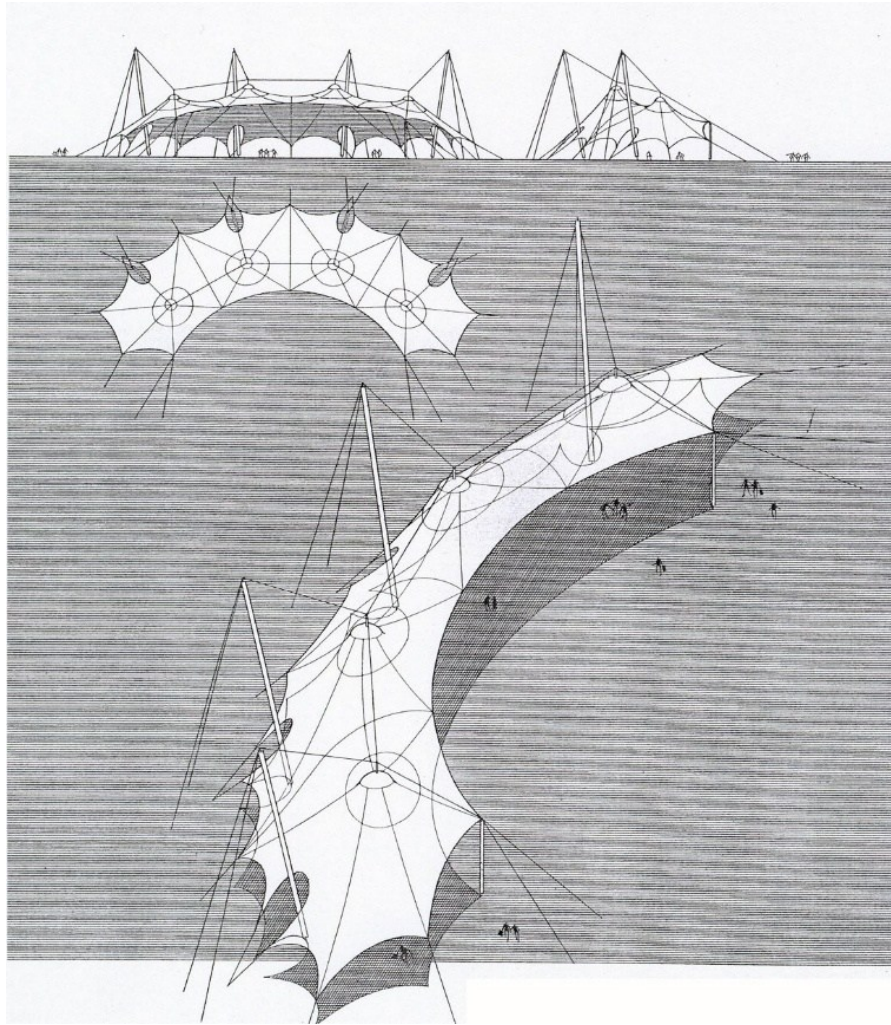


Figure 12: cable-net roof over the stadium at the 1972 Munich Olympics

Frei Otto's model studies were not restricted to tensile structures. He and his research teams looked at every possible form of structure. His particular fascination, however, was with forms generated in nature and the natural world was always an inspiration for Otto during his career. Thinking about that, it is easy to understand that he was fascinated by what Hooke wrote in his anagram and by the design approach Gaudi had for his main structures. Otto was so interested in Gaudi's works that he also made a reconstruction of the hanging model of the crypt of Colonia Guell by the Catalan architect. (Addis, 2007)

According to this, one of the most important structure designed and built by Frei Otto was the Multihalle in Mannheim in Germany, realized in 1975 as exhibition building for the Garden Festival. Even if in 1970s the computers were already born, computational analysis was still in its childhood. That's way a physical model, a hanging one, was create to design the Multihalle.

Two companies were involved in the realization of the physical model: Mutschler & Partners and Atelier Warmbronn. The first company was the architectural firm of the project while the second one was the Frei Otto's own company. They realized a small suspended chain model of the structure under design process: the chosen scale for the model was 1:500 and it was created during a workshop led by Otto by himself in Warmbronn in Germany. They used wire thread spread all over the surface area of the model in order to find the approximate length and width of the gridshell.

In designer's mind those threads would represent the wooden "branches" forming the gridshell in the final structure. The suspended model was found as a good representation for the Mannheim Multihalle behavior because, always thinking about Hooke's second law, it was put under entirely tensile forces only coming from self-weight. It is important to consider that in a lightweight structure like this one, the self-weight is only a little and negligible percentage of the whole forces field involving the gridshell; snow and wind are two of the most important conditioning forces acting on the structure but in order to find the form, considering self-weight or, in general, gravitational loads, is instead a good solution both in the early and the advanced phases of the project. In this situation, all the forces acting on the surface are transmitted only by means of axial forces. Applying Hooke's teaching and inverting the suspended model, bending moments will always be null and all the internal forces that were fully in tension become fully in compression.

During design phases of the Multihalle, this was very important because wooden lathes can resist axial forces well because the forces act along the axis of the beam but are poor at resisting shear forces that act in orthogonal direction with regard to the axis of the beam.



Figure 13: Multihalle Mannheim

During the realization of the hanging chain model, the designers knew that the representation of the real structure in scale couldn't be able to consider every single element of the real structure both grid and node. They needed to find a way to scale up well to real size the model and all the considerations coming from the analysis. They decided to represent only one grid element instead of three of them.

“The wire mesh was created using surprisingly simple materials: it consisted only of a wire rod with hooks at both ends approximately 15 millimeters in length, and a wire ring approximately 2.5 millimeters in diameter. While the wire represented the timber beams of the gridshell the rings represented the nodal joints. This arrangement of chain elements allowed the production of a mesh of any size, and also ensured that the angles could be freely displaced. This angular freedom provides the possibility to produce either a curved or planar form using this quadrangular equal-meshed net. Once the net was completed to the approximate proportions, it was suspended on a final framework which consisted of brass support columns, plexiglass, and brass wire boundaries. The edge lengths were then adjusted to fix any minor inconsistencies in the form of the smooth domes. The next step was using the model to realize the fully formed structure”. (Mihalik, Tan, & Zengeza, 2013)

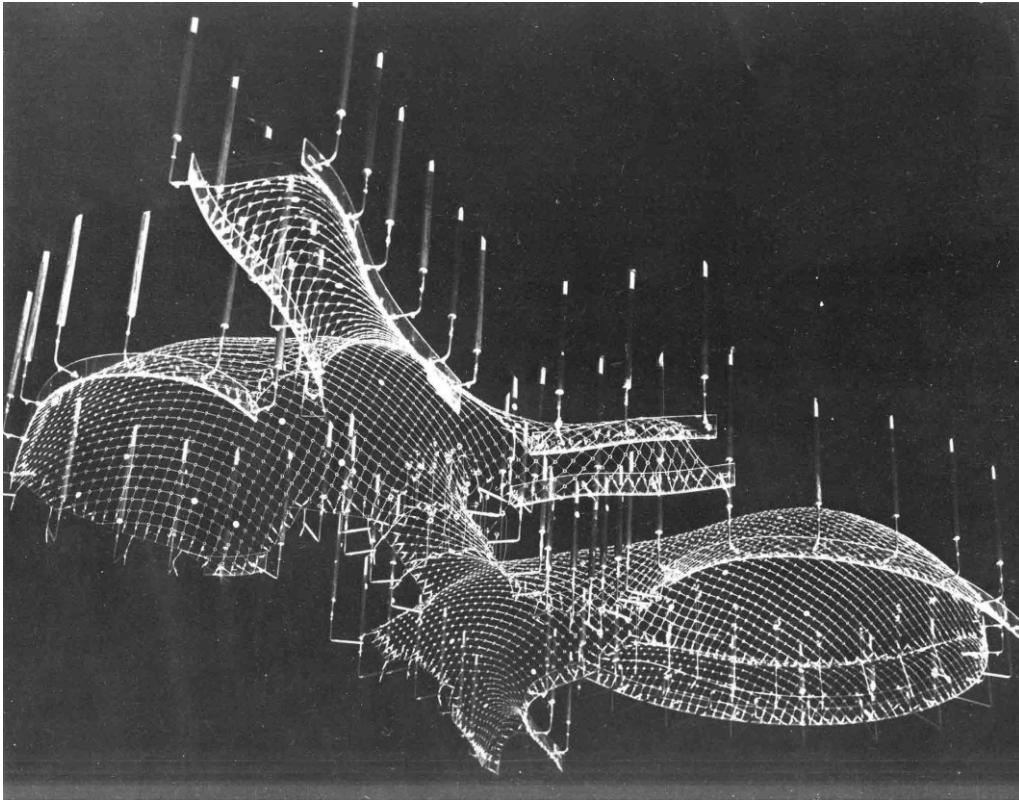


Figure 14: Hanging Model for Multihalle Mannheim

To ensure that neither would occur, a computer analysis of the structure was undertaken by the engineers at Arup's firm. The computer model of the roof was simplified like the physical one. The analysis revealed the likelihood that the shell would indeed buckle in some places, and it was decided to increase its resistance to buckling by using two orthogonal grids of laths. Despite the thicker gridshell, the building is surely one of the boldest structures ever constructed and, though originally intended as a temporary building, is still in use.

3. An Overview of Structural Form Finding Methods

Form finding can be defined as the “*forward process in which parameters are explicitly directly controlled to find an optimal geometry of a structure which is in static equilibrium with a design loading*” (Adriaenssens, Block, Veenendaal, & Williams, 2014)

To find the right or even just one feasible form for a structure or a membrane or a double curved surface the designer could use both physical and numerical methods. Physical models were used a lot during the past decades before the rise of personal computers. They deal with the construction, in scale, of the structure object of the design process. As written in the previous chapter, they could be realized with different methodologies develop during the centuries starting from the Hooke’s second law, passing through Gaudi’s hanging models, Isler’s physical models and theories about concrete shells, until Frey Otto and his soap film models for the search of the minimal surface for in-tension structures and his hanging models. Remarkable is the procedure used by Isler of the membranes hanged and covered by his own made elastic rubber that let the designer to fix the form after the initial wet membranes got dry. This method is used also nowadays in wind tunnels to study particular kind of membranes’ deformations.

Numerical methods for form finding are the most applied design approaches for membrane structures even if they are governed by compressive or tensile state of stress. Sometimes physical and numerical methods are used both. First the numerical one is applied to find the geometry of the structure and after the physical model is realized but only to represent the chosen shape; this choice reduce a lot costs of experimental tests during the design process. Through numerical representation is possible to create the desired shape of the structure function of constraints, both structural and geometrical ones, and of stresses supposed. Different numerical methods are implemented nowadays, both linear and non-linear. (Casagrande, 2011)

“By the early 1980s, the speed of computer had increased sufficiently for complex iterative calculations to become feasible [This let the designer to use numerical

models and numerical form finding methods in the design not only as a test or a scientific experiment but as integrative part of the design process]

The designer first inputs the approximate surface geometry of a membrane, its support conditions and the elastic properties of the membrane material. The computer then analyzes the structure and finds the equilibrium form, if there is one, for the given input conditions. If this form is not what the designer wanted, the input conditions can be altered and the new equilibrium shape calculated. This highly interactive approach to form-finding effectively gives the designer the feeling of experimenting with a physical model in the real world. Not only do such programs find the equilibrium form, they can compute the stresses in the membrane. this allows the identification of areas that are overstressed, understressed, or unstressed in one direction, leading the membrature to wrinkle". (Addis, 2007)

"In the last five decades several methods of form finding have been developed. Earlier methods were typically applied to discrete cable-net structures and extended by later methods to surface elements for membrane structures. It is possible to categorize these in three main families:

- ***Stiffness matrix methods*** are based on using the standard elastic and geometric stiffness matrices. These methods are among the oldest form finding methods and are adapted from structural analysis;
- ***Geometric stiffness methods*** are material independent, with only a geometric stiffness. In several cases, starting with the force density method, the ratio of force to length is a central unit in the mathematics. Several later methods are presented as generalizations or extensions of the force density method, introduced in the previous chapter, independent of element type, often discussing prescription of forces rather than force densities.
- ***Dynamic equilibrium methods*** solve the problem of dynamic equilibrium to arrive at a steady-state solution, equivalent to the static solution of static equilibrium." (Block & Veenendaal, 2012)

"An overview and comparison of structural form finding methods has been presented by Veenendal and Block. Their research discusses and compares the methods of form finding

through three design examples. [...] Their work focuses on the process of which the methods find the form with respect to factors such as time and number of iterations. In addition, they present the potential development of new and hybrid methods based on the results.” (Bertin, 2013)

In the following sections will be presented the most important numerical methods used by designers during the form finding process.

3.1. Force Density Method

The Force Density Method (FDM) is one of the most used form finding methods for the design of shells, membranes and cable net structures. The procedure of the method has been developed by Schek and Linkwitz between 1971 and 1974 (years of their scientific publications about the topic) with regard to the stadium roof in Munich for Olympic Games of 1972. The first and most important idea that is important to remind is that this method is one of the first studied to be used with a computer.

The authors of the method had to deal with a very high non-linear problem as the stadium roof was.

The following analytical explanation of the method is the translation from italian of *Introduzione all'analisi automatica di sistemi strutturali composti da funi*, book written by E. Casagrande in 2011.

The method relies on the assumption that the ratio of tension force to length of each cable can be constant, transforming a system of non-linear equations to a set of linear equations which can be solved directly. To better explain how the FDM works, is solved an easy example of cable-net structure.

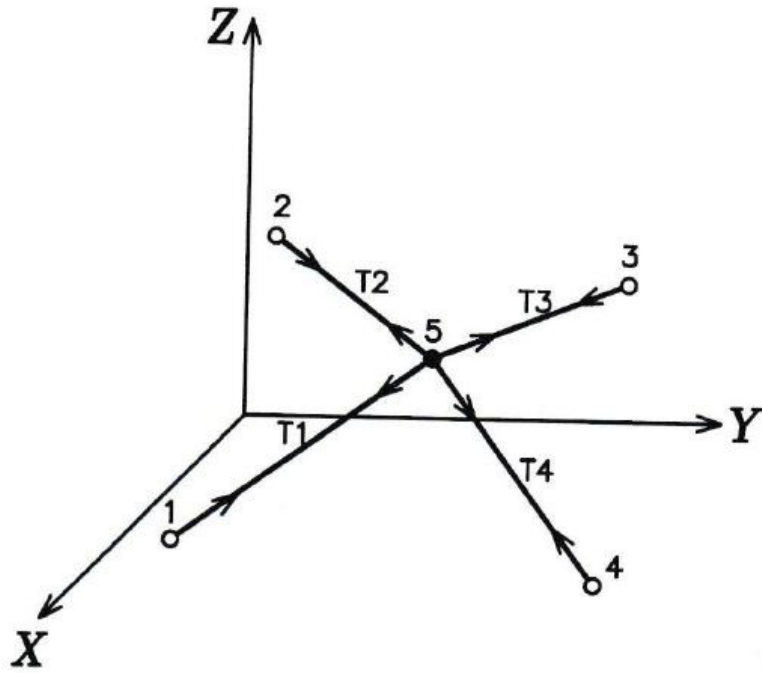


Figure 15: Cable-net structure scheme

The simple structure has 5 structural nodes and one of them is free subjected to a random force set (P_x, P_y, P_z) and 4 pre-stressed elements subjected to a pre-stress force T_i . The equilibrium equations are written with regards to the node 5; they are written for each bar and for each principal direction with the help of director cosins:

$$\frac{(x_p - x_n)}{L_m} = \frac{L_{mx}}{L_m} = c_x$$

$$\frac{(y_p - y_n)}{L_m} = \frac{L_{my}}{L_m} = c_y$$

$$\frac{(z_p - z_n)}{L_m} = \frac{L_{mz}}{L_m} = c_z$$

The bars are all connected to free node so the equilibrium equations for each direction can be written as follows:

$$T_1 \cdot c_{x1} + T_2 \cdot c_{x2} + T_3 \cdot c_{x3} + T_4 \cdot c_{x4} = P_x$$

$$T_1 \cdot c_{y1} + T_2 \cdot c_{y2} + T_3 \cdot c_{y3} + T_4 \cdot c_{y4} = P_y$$

$$T_1 \cdot c_{z1} + T_2 \cdot c_{z2} + T_3 \cdot c_{z3} + T_4 \cdot c_{z4} = P_z$$

The step after deal with the substitution of the first three equations in the latter three obtaining:

$$T_1 \cdot \frac{(x_5 - x_1)}{L_1} + T_2 \cdot \frac{(x_5 - x_2)}{L_2} + T_3 \cdot \frac{(x_5 - x_3)}{L_3} + T_4 \cdot \frac{(x_5 - x_4)}{L_4} = P_x$$

$$T_1 \cdot \frac{(y_5 - y_1)}{L_1} + T_2 \cdot \frac{(y_5 - y_2)}{L_2} + T_3 \cdot \frac{(y_5 - y_3)}{L_3} + T_4 \cdot \frac{(y_5 - y_4)}{L_4} = P_y$$

$$T_1 \cdot \frac{(z_5 - z_1)}{L_1} + T_2 \cdot \frac{(z_5 - z_2)}{L_2} + T_3 \cdot \frac{(z_5 - z_3)}{L_3} + T_4 \cdot \frac{(z_5 - z_4)}{L_4} = P_z$$

The system is non-linear because the element lengths are directly dependent to the extreme nodes coordinates of the row which they are connected. Now is introduced the constant term, called force density coming from the ratio between the tension of the element and its own length:

$$q_m = \frac{T_m}{L_m}$$

In this way, the previous system can be written as follows:

$$q_1 \cdot (x_5 - x_1) + q_2 \cdot (x_5 - x_2) + q_3 \cdot (x_5 - x_3) + q_4 \cdot (x_5 - x_4) = P_x$$

$$q_1 \cdot (y_5 - y_1) + q_2 \cdot (y_5 - y_2) + q_3 \cdot (y_5 - y_3) + q_4 \cdot (y_5 - y_4) = P_y$$

$$q_1 \cdot (z_5 - z_1) + q_2 \cdot (z_5 - z_2) + q_3 \cdot (z_5 - z_3) + q_4 \cdot (z_5 - z_4) = P_z$$

The system written as above is linear in the unknown q_m .

The same problem is now exposed from a matrix point of view in order to extend the solution also to more complicated problems.

For the generic element length:

$$L_{mx} = x_p - x_n = [1 \ -1] \cdot \begin{bmatrix} x_p \\ x_n \end{bmatrix} = [C_s] \cdot [X]$$

Using this notation the projected length of each element in the three principal directions can be summed up as follow:

$$[L_{mx}] = [C_s] \cdot [X]$$

$$[L_{my}] = [C_s] \cdot [Y]$$

$$[L_{mz}] = [C_s] \cdot [Z]$$

\mathbf{Q} is the diagonal matrix containing the density force values. So the equilibrium equations of each single bar can be written in the following system:

$$[Q_{mx}] = [Q] \cdot [L_{mx}]$$

$$[Q_{my}] = [Q] \cdot [L_{my}]$$

$$[Q_{mz}] = [Q] \cdot [L_{mz}]$$

And the global system of equilibrium equations for each free node is:

$$\sum Q_{mx} = P_x$$

$$\sum Q_{my} = P_y$$

$$\sum Q_{mz} = P_z$$

The following step is to substitute the value of $[Q_{mi}]$ inside the sum that can be written as $[C]^T$; the equilibrium is found as:

$$[C]^T \cdot [Q] \cdot [C] \cdot [X] = P_i$$

It is also possible to separate the matrix $[C]$ in two parts: the first one will contain the constraints nodes while the latter the free ones.

The Force Density Method is one of the easiest methods for form finding processes for membrane structures and in particular cable-net structures. The computer has to work only with linear systems so the method is lightweight from a computational point of view. However, with this method the value of the forces T_i of the single element is not known *a priori* because all the algorithm work with the ratio, with the force density (that are coefficients). This procedure gives back a system, a shape, a structure which tensional state is unknown. So this method can be applied in a functional way only if the designer has a good experience because he determines the shape of the structure acting on

coefficient without physical relations. Initial values for these force densities need to be chosen for the first-order form-finding. There is nothing that informs the user on how to distribute the forces to obtain a desired three-dimensional shape. There is also no option to constrain a solution to a predefined solution space. Often the shape of the structure is imposed by architectural or functional constraints. When this happens, the designer needs to understand that the equilibrium values of the force densities are found in an iterative optimization process. (Southern, 2011) (Casagrande, 2011) (Rippmann, 2016) (Block, Thrust Network Analysis: Exploring Three-dimensional Equilibrium, 2009)

3.2. Dynamic Relaxation Method

Differential equations can describe nearly all systems undergoing change. They are ubiquitous in science and engineering as well as economics, social science, biology, business, health care, etc. Many mathematicians have studied the nature of these equations for hundreds of years and there are many well developed solution techniques. Often, systems described by differential equations are so complex, or the systems that they describe are so large, that a purely analytical solution to the equations is not tractable. It is in these complex systems where computer simulations and numerical methods are useful.

Dynamic Relaxation Method systems modify the form-finding problem into a dynamic problem. They simulate the behavior of physical form-finding experiments, such as network of hanging chains or a soap bubble experiment. The method uses a network of linear elements with simulated elastic behavior, initial rest length and lumped, nodal masses. Dynamic Relaxation is mostly used to improve given input shapes, but does not allow the designer to easily interact with the optimization process. The basis methodology of dynamic relaxation is a numerical discretization of the structural form into a particle spring system. The dynamic relaxation method was created without the dynamic interpretation to solve mathematical equations with the finite difference method. Only later the method was introduced to dynamic characteristics to help the solution of engineering problems and not only mathematical problems anymore. the first applications of the method were on linear problems but the growth of computer processor and the specific characteristics of the analytical solution, let the method to be implemented and

applied also for non-linear applications. In this way it was possible to use it for form finding processes.

Dynamic relaxation method was initially used for structural analysis in in different engineering fields because the solution is found without complex operations on stiffness matrix.

The following analytical explanation of the method is the translation from italian of *Introduzione all'analisi automatica di sistemi strutturali composti da funi*, book written by E. Casagrande in 2011.

The method finds the equilibrium of a structural system with masses, concentrated on nodes. They move like a harmonic system with damping around the equilibrium position. The equation which rule the motion of the node I in a generic direction d is:

$$\mathbf{P}_{id} = \left[\sum \mathbf{K}\delta \right]_{id} + \mathbf{M}_{id}\delta''_{id} + \mathbf{C}\delta'_{id}$$

\mathbf{P} is the external loads array, the first term of the second part of the equation is the internal forces array, \mathbf{M} is the masses array and \mathbf{C} is the viscous damping coefficient. δ variables are respectively the nodal vectors of accelerations ($''$), velocities ($'$) and displacements.

After the introduction of the main equation, the residual array is introduced from the difference between the external loads array and the internal forces array. This difference creates a motion of the system based on the following relation:

$$\mathbf{R}_{id} = \mathbf{P}_{id} - \left[\sum \mathbf{K}\delta \right]_{id} = \mathbf{M}_{id}\delta''_{id} + \mathbf{C}\delta'_{id}$$

the structural system reaches the equilibrium condition when the residual array tends to zero. The equation can be approximated with finite differences method if the acceleration term is considered as the ratio between velocity and time lapse. n is the time lapse in which the calculus is done:

$$\mathbf{R}_{id}^n = \mathbf{M}_{id} \frac{\delta_{id}^{n+\frac{1}{2}} - \delta_{id}^{n-\frac{1}{2}}}{\Delta t} + \mathbf{C} \frac{\delta_{id}^{n+\frac{1}{2}} - \delta_{id}^{n-\frac{1}{2}}}{2}$$

Pointing out velocity terms:

$$\delta_{id}^{n+\frac{1}{2}} = \delta_{id}^{n-\frac{1}{2}} \cdot \frac{\frac{\mathbf{M}_{id}}{\Delta t} - \frac{\mathbf{C}}{2}}{\frac{\mathbf{M}_{id}}{\Delta t} + \frac{\mathbf{C}}{2}} + \frac{\mathbf{R}_{id}^n}{\frac{\mathbf{M}_{id}}{\Delta t} + \frac{\mathbf{C}}{2}}$$

With the velocity definition written as above, the displacements at time $n+1$ can be found as:

$$\delta_{id}^{n+1} = \delta_{id}^n + \delta_{id}^{n+\frac{1}{2}} \Delta t$$

The method repeats the last but one equation in an iterative way in order to determine the displacements array until the difference between internal and external loads, becomes lower than a fixed value, a tolerance.

The dynamic relaxation method stability is conditioned, according to the previous equations, by time lapse, arrays containing mass terms (\mathbf{M}) and damping coefficients (\mathbf{C}). These variables are necessary because the method goal is to find the system's equilibrium position and not to follow the dynamic behavior of the structure. It is important to determine clever time lapses and \mathbf{M} and \mathbf{C} values in order to have a stable behavior and a sure convergence of the method. The initial values to assign to variables were analyzed in different studies. Some of those results are written in the following section.

- **Time Lapse**

Time Lapse parameter is very important because it could influence both stability behavior and computational speed. Indeed, if this parameter is changed, nodes relative speeds and nodes relative displacements will be subjected to big variations and also the evaluation of kinetic energy will be strongly influenced. Two schemes for time lapse choice are analyzed: *constant time lapse* and *Qiang procedure*.

- *Constant time lapse*

The constant time lapse assumption is the most used method. According to Underwood in his *Dynamic relaxation in computational method for transient analysis*, the time lapse has to be:

$$\Delta t \leq \frac{2}{p_{max}}$$

Assuming p as the maximum value of structure time period. The period is function of the stiffness matrix and mass matrix according to the following expression:

$$p = \sqrt{\frac{\mathbf{K}}{\mathbf{M}}}$$

Where \mathbf{K} is the structure stiffness matrix and \mathbf{M} represents the masses concentrated in the nodes. According to Underwood, the value should have to be included between 1 and 1.1, but for sake of simplicity often the value 1.0 is used. However, values a bit higher than one return a better convergence of the solution.

- *Qiang procedure*

This method is presented by Shizhong in his *An Adaptive dynamic relaxation method for non-linear problems* and it is founded on Rayleigh wave's theory and the minimum time period of the structure. For each iteration, time lapse is given by the following relation:

$$\Delta t = \frac{2}{\sqrt{1 + p_0}}$$

This scheme is usually applied for non-linear solving problems; indeed, the time lapse value changes every iteration.

- **Mass**

Another important parameter which is able to influence the dynamic relaxation method is the mass acting in order to understand nodes speed and the kinetic energy of the whole system.

Four solutions to write the mass matrix are presented:

- Unary mass;
- Mass proportional to the stiffness;
- Mass proportional to the sum of absolute values;
- Gerschgorin method.
 - *Unary mass*

The matrix \mathbf{M} is built multiplying by identity matrix \mathbf{I} a numerical coefficient g :

$$\mathbf{M} = g\mathbf{I}$$

This method is easy to be implemented but it is not the best one for form finding processes because matrix mass is kept constant for every iteration: that means a bigger number of iterations and more time necessary to solve the problem.

- *Mass proportional to the stiffness*

In this method the mass matrix is built as a multiple of the stiffness matrix:

$$\mathbf{M} = g\mathbf{K}$$

The method is very close to the first one but with better performances from a computational point of view; indeed, for each iteration, the mass is subjected to a variation proportional to the stiffness variation. This process ensures a faster convergence of the solution.

- *Mass proportional to the sum of absolute values*

In this scheme the mass matrix \mathbf{M} is determined as the sum of the absolute values of every row of the stiffness matrix \mathbf{K} :

$$m_{ii} = \sum_{j=1}^{ndof} |k_{ij}|$$

It is clear that bigger is the number of degrees of freedom of the structure, more is the computational time for the form finding process. The increase in the operations number is compensated by a bigger numerical stability of the whole process because of the continue updating of the matrix each iteration. The big disadvantage is that for this scheme, is necessary to upload the whole stiffness matrix of the structure.

- *Gerschgorin method*

This method, unlike the previous three, is created from mathematical basis. It is very efficient, mostly for non-linear analysis:

$$m_{ii} \geq \frac{1}{4} \Delta t^2 \sum_{j=1}^n |k_{ij}|$$

- **Damping coefficient**

The damping coefficient \mathbf{C} is one of the other most important parameters of the analysis which influence a lot the numerical stability and the convergence of the dynamic

relaxation method. Many researches has been done to find the best way to decide a value for this coefficient and most of all are based on Rayleigh theories.

- *Dynamic method*

This method is presented by W.J. Lewis in his *Tension Structures – Form and Behavior*; according to his job, the method comes from a structural system composed by one mass and a spring. N is the number of iterations composing a complete oscillation cycle, m is the system mass and f is the fundamental frequency of the system. With those assumptions, the viscous damping coefficient is given by the following relation:

$$C = 4\pi m f$$

The method has big advantages from a computational point of view because the C value changes at every iteration.

- *Underwood Method*

The Underwood method tries to evaluate the variable c . the coefficient is then found as the product of the coefficient end the matrix mass:

$$c_n = 2 \left\{ \frac{\mathbf{x}_n^T \mathbf{K}_n \mathbf{x}_n}{\mathbf{x}_n^T \mathbf{M}_n \mathbf{x}_n} \right\}^{\frac{1}{2}}$$

The \mathbf{M} of the expression is evaluated with the Gerschgorin method, while \mathbf{K}_n is the diagonal matrix defined as follow:

$$K_n^i = \frac{F_i(x^n) - F_i(x^{n-1})}{\Delta t \cdot x_i^{m-\frac{1}{2}}}$$

Where F_i is the node i internal force. This method is used a lot in the non-linear analysis because guarantees a fast convergence of the solution.

- **Dynamic relaxation method with kinetic energy**

The dynamic relaxation method can be implemented with some differences using kinetic energy. In this case at every iterative step the kinetic energy is calculated and when the maximum value is reached, the velocity array is initialized to zero and a new iterative step begins.

The equation can be written as:

$$\mathbf{R}_{id} = \mathbf{M}_{id} \delta''_{id}$$

The acceleration terms are written with finite difference method:

$$\mathbf{R}_{id}^n = \mathbf{M}_{id} \frac{\delta_{id}^{n+\frac{1}{2}} - \delta_{id}^{n-\frac{1}{2}}}{\Delta t}$$

The relations that give back the velocity and displacements can be written as:

$$\delta_{id}^{n+\frac{1}{2}} = \delta_{id}^{n-\frac{1}{2}} + \frac{\mathbf{R}_{id}^n}{\mathbf{M}_{id}} \Delta t$$

$$\delta_{id}^{n+1} = \delta_{id}^n + \delta_{id}^{n+\frac{1}{2}} \Delta t$$

When the kinetic energy comes to the maximum value, the velocity array is set to zero and the operative procedure restart from the last found layout. The kinetic energy peak is found from the comparison between the KE at i iteration with KE at $i-1$ iteration. Indeed, if the last value is lower it means that the peak has been overpassed.

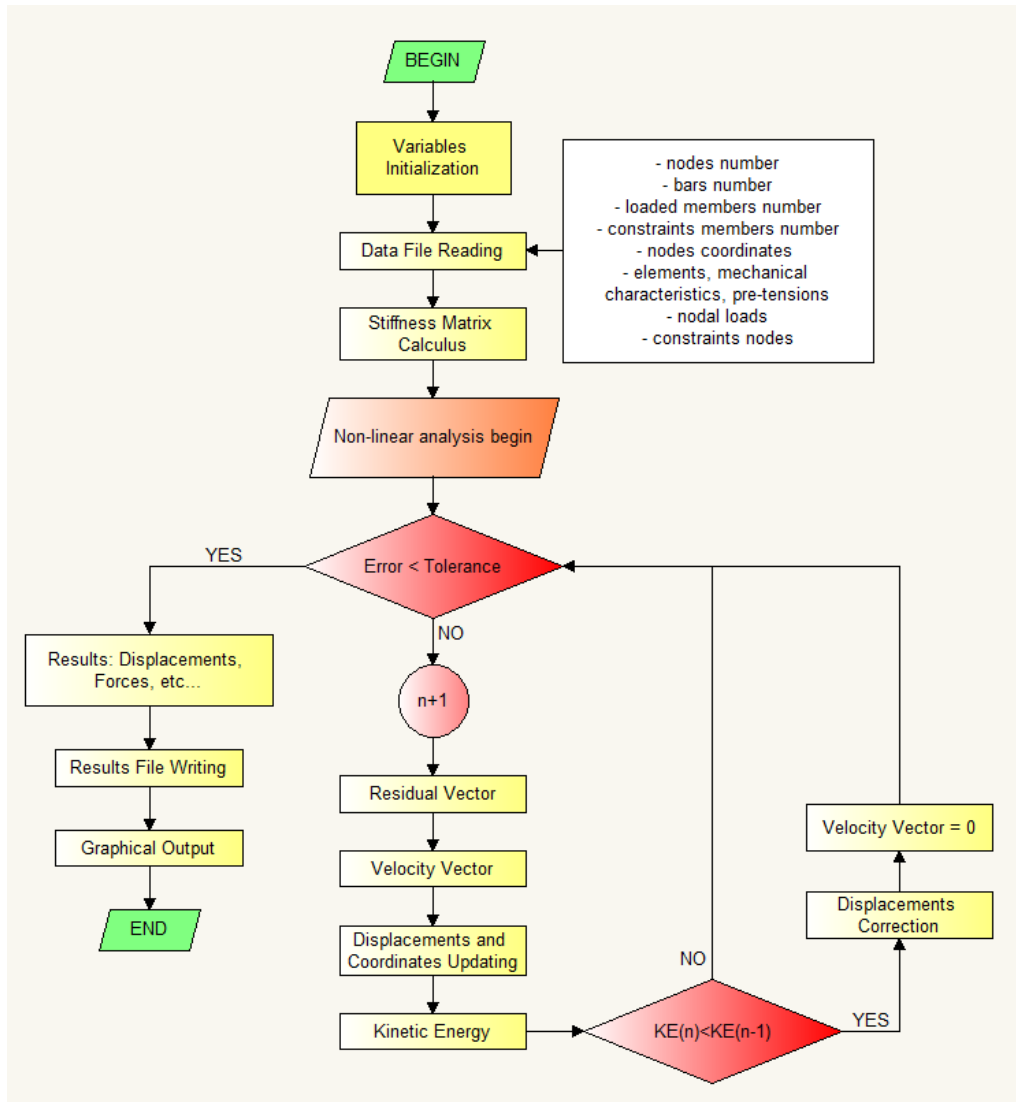


Figure 16: Dynamic Relaxation Method Flow Chart

3.3. Particle-Spring System

Force Density Method and Dynamic Relaxation Method are very useful to solve structural problems where is necessary to find the equilibrium position of a structural network subjected to a well-known system of internal and external forces and/or when pre-stressed load states are present. When the typical form finding problem is assigned for structure that has to be in a fully compression or tension state of stresses under self-weight or gravitational loads, those two approaches seems to be not very suitable. The best representative example is the one of the suspended hanging chain model.

During the years, researchers tried also to apply Finite Element Analysis to the world of form finding but without success. This happened because of the presence of big displacements while the system is moving trying to find his equilibrium position. Big displacements in this environment are the cause for numerical instabilities and the results can't be correct also because all the theory of Finite Element Analysis is based on small displacements. The Finite Element Analysis is not able to represent in the correct way those situations so also that way was abandoned for form finding process.

Witnesses of this situation are both Axel Killian and John Ochsendorf at MIT. They developed a new methodology for form finding based on the previous Dynamic Relaxation method but able to represent the stress state of a structure fully in compression or in tension.

Their goal was to represent by numerical and computational perspectives, the behavior of a physical model like the ones created in the past for the design of some of the most important shell structures of the last two centuries. As illustrated in the previous chapter, architects and engineers as Gaudì, Isler, Otto were used to design their structure with hanging models.

Killian and Oschendorf knew that a method developed in the computers world and most of all in the Computer Aided Design environment would be able to represent and model hanging structure under various loading conditions and evaluate their behavior in real time. So Particle Spring System was created.

“Particle-spring systems are based on lumped masses, called particles, which are connected by linear elastic springs. Each spring is assigned a constant axial stiffness, an

initial length, and a damping coefficient. Springs generate a force when displaced from their rest length. External forces can be applied to the particles, as in the case of gravitational acceleration.” (Kilian & Ochsendorf, 2005)

If the initial geometry of the particle spring system is known, two principal approaches can be applied to find the equilibrium: implicit and explicit solvers.

Kilian and Ochsendorf observed that implicit solvers are more useful to solve structural problems. They are more stable, from a numerical point of view, considering the high spring stiffness used in the model to minimize the initial strain of the spring length at the beginning of the solving procedure. Using high spring stiffness small changes in length value will be observed while the solver is working and in the final condition. Small changes are not easy to be recognized and evaluated by an explicit solver that could return a wrong solution for the problem. That's why implicit solvers have to be preferred for the structural form finding process. The two researchers of MIT developed their method using the Runge-Kutta solver aiming to reach the equilibrium of each particle.

“Each particle in the system has a position, a velocity, and a variable mass, as well as a summarized vector for all the forces acting on it. A force in the particle-spring system can be applied to a particle based on the force vectors direction and magnitude. Alternatively, the magnitude of the force can be calculated using a function as in the case of springs. Springs are mass-less connectors between two particles that exercise a force on the particles based on the spring's offset from its rest length. Particles can be restrained in any dimension, so it is straightforward to add supports by restraining the displacement vectors of an individual particle.” (Kilian & Ochsendorf, 2005)

When the solving procedure starts, the system is not in equilibrium and all the process is governed by the motion of the springs and the mass nodes trying to find their equilibrium position. The particle-springs movement goes on until the internal equilibrium of the forces is found or the analysis is interrupted.

A good way to help the system to reach the equilibrium is the application of a damping coefficient to each spring or with other methods if more useful. Often can be applied by

the developer of the system termination criteria for the solver: a tolerance value for nodes velocity, for instance.

Killian and Ochsendorf presented in their paper some examples about their new method that was implemented on a Java code developed by Greenwald in 2003 to apply the method on a CAD environment.

They also affirmed that the method is useful for three-dimensional structure: that's because also for those kind of structure is possible to use the term *funicular* in order to consider a structure in compression or tension only state of stress under a given loading. This situation is a little bit harder to be solved because the problem is more complex because of the multiple load paths which are possible. Multiple load paths indeed, means multiple possible forms for the structure. This is possible because only by changing the rest length or the stiffness of a single spring, the whole shape of the structure under loads will be different.

Trying to understand the conclusions made by Killian and Ochsendorf it is possible to say that this new method is useful because is possible to have real time results of the analysis and also is possible to see step by step every change in the structure and in the supposed solution both during the solving procedure and after a change in the system stiffness or in the variation of the rest length of a spring.

The Particle Spring System can be also seen as an application of the Lower Bound Theorem because it is always able to find the equilibrium of the structure under a given loading combination. As known from the structural analysis, this means that the given loading conditions is lower than the collapse condition so we are sure that the found shape will be stable even if it is not the most optimized solution. The method is also useful for the designer because it let him to better understand in an intuitive way how the structure works, which is the flow forces and which could be the optimal shape for his structure.

One of the biggest disadvantage of the method is its computational weight. It could be expensive, from a computational point of view, for a desktop computer if the nodes number is bigger than one thousand. The method still works but it could be hard to see results in real time, losing one of the most important qualities of the method because the designer isn't able to understand step by step what is happening to the structure while it

is finding its equilibrium condition and it will be hard for him to interact with the structure under motion.

3.4. Thrust Network Analysis

In order to understand the Thrust Network Analysis is fundamental to introduce some concept about graphical methods and in particular about Graphic Static.

Since the Ancient times, the classical age, the gothic period and so on, a lot of heuristic and geometrical design methods were applied by architects and builder to realize structures and also to experiment with spectacular works like the gothic cathedrals during the Middle Age. All those buildings weren't realized with the support of analytical theories or knowledge. Everything was known from experience, from word of mouth between generations of builders or textbook full of drawings.

The most important graphical method, developed in the second half of the XIX century is the Graphic Statics. This method was initially developed by Karl Culmann, professor of Civil Engineering at the Swiss Federal Institute of Technology (ETH) in Zurich, between the 1864 and 1866 with the publication of his work *Die Graphische Statik* where he summed up all the work made by his predecessors in the previous centuries. His method is based on third Newton's law and he used a graphical representation of internal and external forces acting in and on the structure, considering both magnitude and direction.

The method presented is composed by two principal diagram called *form diagram* and *force diagram*. The first diagram represents, in a two-dimensional world, the geometry of the structure including its external loads while the second one represents the equilibrium of the forces.

Matthias Rippman, in his doctoral thesis in 2016, summed up three general but fundamental characteristics of the two diagrams:

“The relation between form and force diagrams is called reciprocal (Maxwell, 1864), having the following topological, geometrical and structural properties:

- *The form and force diagrams are dual figures, i.e. both diagrams have the same number of edges, and each node with a valency higher than one in one*

diagram corresponds to a space, formed by a polygon of edges, in the other, and vice versa;

- *Each edge e in the form diagram has a corresponding edge e^* , parallel to edge e , in the force diagram;*
- *The length of edge e^* in the force diagram is, at a chosen scale, equal to the magnitude of axial force in edge e in the form diagram.” (Rippmann, 2016)*

If the two diagrams are built following the previous indications, the reciprocal relationship guarantee the in-plane static equilibrium of all internal loads. It is important to remind that if the structure is statically indeterminate, more than one reciprocal diagrams are present for the same form diagram.

The graphic statics, for its own representation, can be used in a bidirectional way: it is possible to

“construct the force diagram from the form diagram or apply the inverse process and construct parts of the form diagram from an intended force diagram. [this fact can also be interpreted as:]

“structural analysis of determinate structures is conducted by drawing the form diagram, and subsequently constructing the force diagram; structural design or form finding is conducted by constructing the geometry of the structure form chosen constraints of the force diagram”. (Lachauer, 2015)

This consciousness about graphic static was the main input for the birth of the Thrust Network Analysis by Philippe Block and John Ochendorf only a few years later the invention of the Particle Spring System. They studied this method not only to design new structures in a compression-only or tension-only state of stress but also for the analysis of historic structures in unreinforced masonry.

Within this method, Block uses reciprocal diagrams in order to relate the geometry of the three dimensional equilibrium networks to the internal forces present inside the structure. They used an algorithm similar than the one used for the Force Density Method because they understood that was important to linearize the constraints in order to take into account the high indeterminacy of the problem included in funicular structures.

In the following rows, the most important assumption necessary for the Thrust Network Analysis are written directly from the Doctoral Thesis work by Philippe Block where the method is presented:

“assumption b) and c) are specific for masonry:

- a) *The structural action of the vault is represented by a discrete network of forces with discrete loads applied at the vertices [...];*
- b) *A compression only solution in equilibrium with the applied loads and contained within the vault’s geometry represents a valid, i.e. stable, equilibrium state of vault [...];*
- c) *Masonry has no tensile capacity; sliding does not occur; and the stresses are low enough so that crushing does not occur (infinite compression is assumed) [...];*
- d) *All loads need to be vertical.*

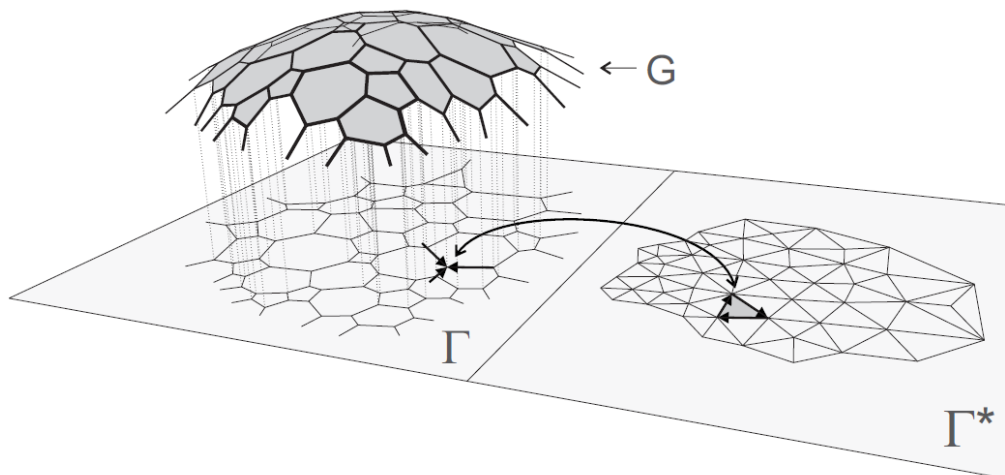


Figure 17: Relationship between the compression equilibrium shape, the thrust network (G), its planar projection (primal grid Γ) and the reciprocal diagram (dual grid Γ^*)

“ . (Block, Thrust Network Analysis: Exploring Three-dimensional Equilibrium, 2009)

Every time Block refers to equilibrium structures or solutions he is referring to compression funicular structure in equilibrium with the external applied loads only by means of compressive or axial forces, without any internal bending.

One of the rule imposed by Block to apply his method is the constraint of only vertical loads to be applied to the analyzed structure. Matthias Rippmann in his doctoral thesis

affirm that the equilibrium problem can be solved if we divide the solving procedure in two main steps:

- STEP 1: Solution of the so called “horizontal equilibrium”;
- STEP 2: Solution of the “vertical equilibrium”.

These two steps are also the ones used in the tool developed by Block Research Group at ETH in Zurich, called Rhino VAULT, implemented to use the Thrust Network Analysis. The tool, a plug-in for Rhinoceros, will be explained in detail in the following chapters of this Thesis.

The first step of the analysis is introduced because one observation is done: the vertical loads will be not present in the form diagram if it is considered as the horizontal projection of the thrust network G , as can be seen in the previous figure. Therefore, the in-plane equilibrium of the form diagram can be also considered as the horizontal equilibrium of G and this is not dependent by the applied vertical loads. The magnitude of the external loads is given by a scale factor of the force diagram: in this way for a given force diagram in equilibrium with the respective form diagram, and considering a given scale factor, a unique thrust network G , in equilibrium with the external loads, can be found for the given supports vertices.

The presented approach let the designer to manipulate different and multiple degrees of freedom as the ones described in the figure taken by Rippmann’s thesis:

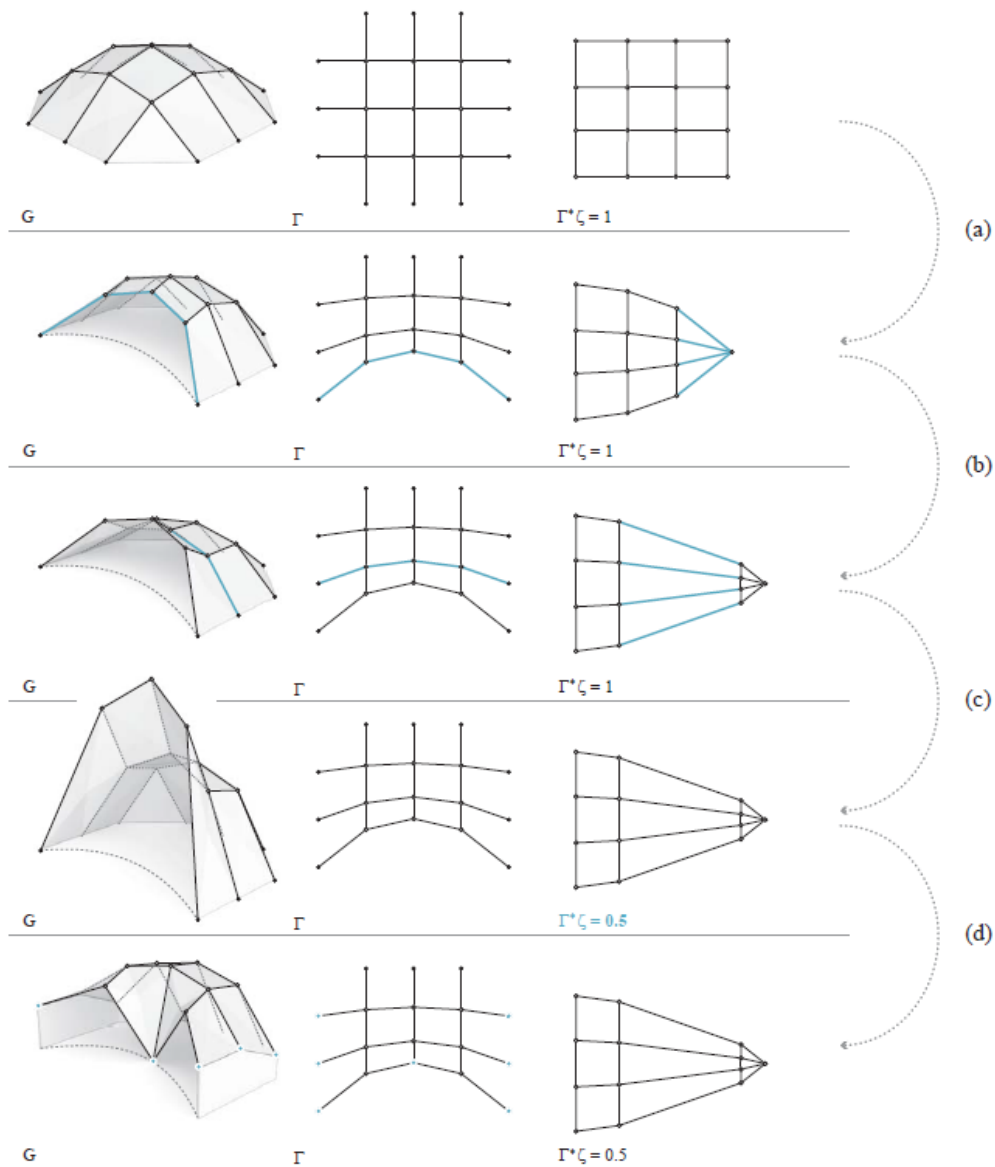


Figure 18: Modification of the design parameters in TNA: (a) Modification of the layout of forces represented by Γ ; (b) (re-)distribution of the (horizontal) forces represented by Γ^* ; (c) the vertical rise of the equilibrium network G , inversely proportional to scale of Γ^* ; (d) the definition of supports and the heights in G . (Rippmann, 2016)

Block, in his thesis, gave an overview of the main steps to do to complete the solving procedure of form finding:

- **Construction of the primal grid Γ** : the designer has to think at his structure as if it is composed by a network of forces representing a possible load paths acting throughout the structure;

- **Formulation of nodal height constraints:** the solution can be found if a solution space is defined; this means a definition of a sort of masonry vault's transversal section with regard to values of extrados and intrados;
- **Attribution of nodal loads:** always remember the rule of the method that constrain the designer to apply only vertical loads, nodal loads have to be applied to the structure: both representing self-weight and live loads;
- **Formulation of the nodal constraints about vertical equilibrium:** there are a defined number of branches converging in every node of the network and they must be in equilibrium. The forces acting through them are written in function of the own length of every one of them in the form diagram, the unknown components of the force diagram and the previously defined nodal heights;
- **Generation of the force diagram:** the force diagram is created following the rules of reciprocal diagrams and applying the desired scale factor;
- **Linearization of the constraints:** Block uses a linear optimization of the constraints in order to be able to solve only by means of linear equations, the form finding problem;
- **Solution for the G grid using linear optimization:** the solution is found using the analytical procedure illustrated in Block's doctoral thesis;
- **Update of the dual grid:** the solution found with the linear optimization has to be checked by the designer and often it is not satisfactory. The constraints will be updated and the dual grids could be manipulated. The process is done in an iterative way until a satisfactory solution is found.

In particular, when the designer manipulates the diagrams, he is explicitly manipulating the distribution of forces acting throughout the network. That's why the network created on the vault is only a hypothesis of load path between the infinite paths possible. This manipulation, indirectly, is also changing the stiffness of single parts of the structure and this is independent from the choice of material.

“all internal vertices need to be in horizontal equilibrium, which is guaranteed if, for edges coming together at internal vertices in Γ , their corresponding edges in Γ^ form closed polygons, representing closed polygons of force vectors [...]. In other words, to*

guarantee equilibrium solutions, it is necessary that all corresponding edges in Γ and Γ^ are parallel.*” (Rippmann, 2016)

A lot more could be written about Thrust Network Analysis but for specific and more complete explanation about the method, it suggested to refer to the original texts written by Block and his collaborators during the last decade.

4. Form Finding and Linear Buckling Load Analysis for Pierced Vaults: A Case Study

During the last decades several form finding methods were presented and shown. Each one has got its own strength and its own weakness different tool by tool. In the previous chapters of this work their histories and their own characteristics were illustrated.

It is important to understand that the form finding process is not an aesthetic, artistic, philosophic approach used for the early design phases to create some new and upsetting shape. It is not a support for the fantasy or the intuition of the architect or the engineer to discover shapes never supposed.

The form finding process has to be seen as an important step for the structural analysis and design of the final structure. It helps to explore the universe of shape solutions that a shell could assume to accomplish its structural objective. If a funicular structure is searched, a form finding method will be able to guarantee a pure membrane stress state in compression under self-weight or, generally speaking, a good structural shape already in an early design phase.

With this approach all the constraints coming from the architectural design (height, surface to be covered, openings and supports numbers) and from geometrical or building constraints like obstacles or support positions and so on, are converted into design drivers, enabling flexible and innovative design solutions. The other important skill necessary for a form finding method is the speed and intuitiveness in order to help designer in the solutions universe exploration.

Scope of this chapter is to analyze different pierced funicular structures and to compare them in order to understand the best holes' pattern which return a structure with the desired thickness and pierced area percentage. This goal has to be reach considering a masonry structure.

The structures analyzed, in masonry, have to be funicular shells with membrane stress state in compression because they are assumed to have no bending or traction strength. The initial design shape is discovered by mean of the Thrust Network Analysis. The method, illustrated in the previous chapter, is the most intuitive and flexible tool to

develop the following analysis. Graphical methods and Graphic Statics give to the form finding process high flexibility and intuitiveness.

The method is very comfortable for this study because it is easy to interact with the form of the future structure and its flow of forces. The tool that implement the TNA lets the user to freely change openings number, shape and dimension. Smoothing techniques presents inside the tool guarantee that holes don't generate big stress concentration next their boundary.

The study begins with the choice of the perimeter the shell structure will cover. It is known that the funicular shell will present a double curvature so surely her projection on the horizontal plane will have a shape like the one supposed. It is important to notice that the shape drawn is only a first trial and it will be changed during the form finding process in order to achieve the horizontal and vertical equilibrium. The second step of the analysis is made using the tool released by the Block Research Group which implement the Thrust Network Analysis for practical applications. With the tool the shape of the shells is found; for each shell, the same height is imposed considering three different lowering conditions.

In the form finding phase 4 pattern are considered. What does it mean?

The same shell structure, first found with the TNA, will be modified creating holes in different number and positions on the surface; the openings number is an increasing variable different step by step and scheme by scheme.

The following step of the study will take place exporting each found shell structure in a Finite Element environment in order to discover how stresses behave in the different conditions present. Indeed, each of the structure will be structural analyzed considering 5 different constant thickness values. It will be also checked if the found shape respect the most important dogma of the study: the structure is characterized by a compression-only stress state. This is checked looking at the eccentricities of the axial forces respect to the transverse section.

This Finite Element Analysis step of the study is developed in LUSAS analyst environment.

The comparison between different structures belonging to the same pattern is governed by the equivalent Von Mises stress. This value will be illustrated in function of the

thickness of the structures and in function of the percentage of holed area related to the total area of the shell surface. Only a little number of vaults are analyzed in this step because the goal is only to validate the form finding theory applied.

The main part of the analysis, however is not lead thinking about the tension state of compression. A linear buckling load analysis is done.

To understand why this kind of analysis is necessary, in the following lines is quoted David Bushnell, one of the leader in Buckling of Shells, from the introduction in the article published in 1981:

“In order to produce efficient, reliable designs and to avoid unexpected catastrophic failure of structures of which thin shells are important components, the engineer must understand the physics of shell buckling. [...] To the laymen buckling is a mysterious, perhaps even awe-inspiring, phenomenon that transforms objects originally imbued with symmetrical beauty into junk.” (Bushnell, 1981)

The shells belonging to the different patterns will be loaded by uniformly distributed loads representing dead load and variable or accidental loads and a linear buckling analysis is done in the Finite Element modeling environment. The buckling load is found, for each structure considering different work cases: three lowering degree values, five slenderness values, 4 hole patterns and symmetrical and anti-symmetrical load conditions.

The results are commented in the following sections but the complete dossier of graphs and values tables is presented as attachment at the end of the work.

4.1. Rhino VAULT

The TNA is applied by mean of the tool developed by Block Research Group: Rhino VAULT. The algorithm is developed as a free plug-in for Rhinoceros V4 and V5. The Graphical User Interface let the designer to interact with the reciprocal diagrams and to control all the form finding procedure. The tool was implemented by Lorenz Lachauer and Philippe Block in 2011 with the first release for Rhinoceros in 2012. The latest releases use *RhinoScript* for the graphical interface features but a lot of component of the algorithm are written in C# and Python programming languages and some processes could be manually controlled working on the software's Application Programming Interface (API). The structure of Rhino VAULT is based on the typical Thrust Network Analysis approach; the following flowchart try to resume this process. It is better illustrated in Matthias Rippmann's Doctoral Thesis *Funicular Shell Design: Geometric Approaches to Form Finding and Fabrication of Discrete Funicular Structures*.

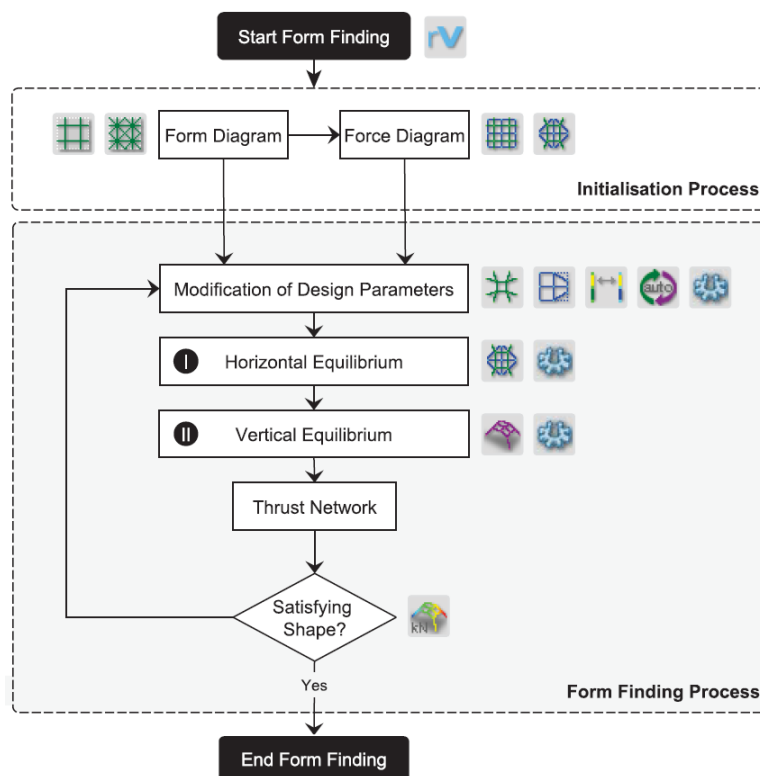


Figure 19: TNA-based form finding framework showing the key operations and corresponding Rhino VAULT buttons: initialization process, modification of the design parameters, computing the horizontal and vertical equilibrium (Rippmann, 2016)

The method implemented with Rhino VAULT uses the two most important element of Graphic Static: the form and force diagram. The TNA was explained in the previous chapter but it is important to remember the principle that lead the whole method: the form and force diagram are in horizontal equilibrium when the corresponding edges in both diagrams are parallel and properly oriented. Furthermore, for a given horizontal projection (the form diagram) and the equilibrium of the horizontal force components and their scale factor, a unique thrust network, in equilibrium with the given loading, is then found for the given support vertices, which represents the shape of the compression-only structure.

In other words, the form diagram gives a representation of the boundary conditions of the structure analyzed and its plan's dimensions while the force diagram defines the horizontal force components in the structure, and how they are proportionally distributed/related. Rhino VAULT was specifically developed to help designer letting him to interact with the equilibrium process manipulating the two diagrams in a bidirectional and interactive manner.

Rhino VAULT is not a stand-alone software but it is implemented in the Rhinoceros environment so it uses the same CAD and the same general user interface. Using the tool is possible by mean of the typical toolbar layout like all the commons commands present in Rhinoceros.

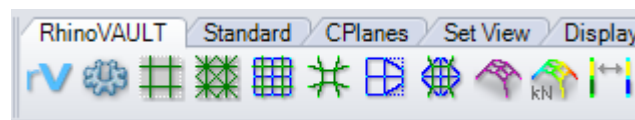




Figure 20: The Rhino VAULT toolbar

The different options given by the tool are now described trying to help to better understand how the tool works:

-  **_rvInitiate**: when Rhinoceros is opened, the library that included all the Rhino VAULT is not already loaded so if the user needs to start a form finding process is necessary to initiate the tool: in this way libraries are loaded and the software can be used;

- 
_rvSettings: this command button opens a window where is possible to change particular issues of the plugin. In this way it is allowed, for instance, to choose if visualize the thrust network mesh scheme or the color diagrams about the force magnitude present inside the different parts of the found structure. Furthermore, is possible to change some calculations parameters like the number of the process iterations during form finding;

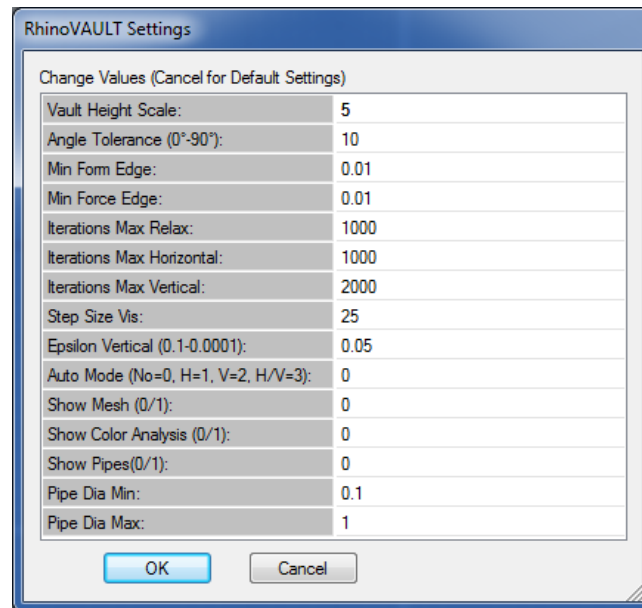



Figure 21: The default settings to control the different commands of Rhino VAULT

- 
_rvForm: this command is used after the definition of an untrimmed surface by the user. That surface must represent the projection of the perimeter of the final structure. The command interacts with the CAD environment and generate an initial projection of the layout of forces in plan. The user can choose freely the topology of the layout including open-edges. The final nodes of these chosen-to-be open edges will remain their position and thus represent support of the structure. This form diagram can also be drawn completely manually, with the help of Rhinoceros commands or external drawing software. It is important to remember that the tool works only if there are not present overlappings or duplicate edges and that all edges are assigned to the *01_FormEdges* layer. Indeed, it is important to notice that every single object used to visualize and store the most recent Rhino VAULT result is assigned to a specific layer. This process

is completely automatic and controlled by the plugin but it is important not to play with these layers and to keep them clean and free from each element that is not linked with a specific Rhino VAULT definition;

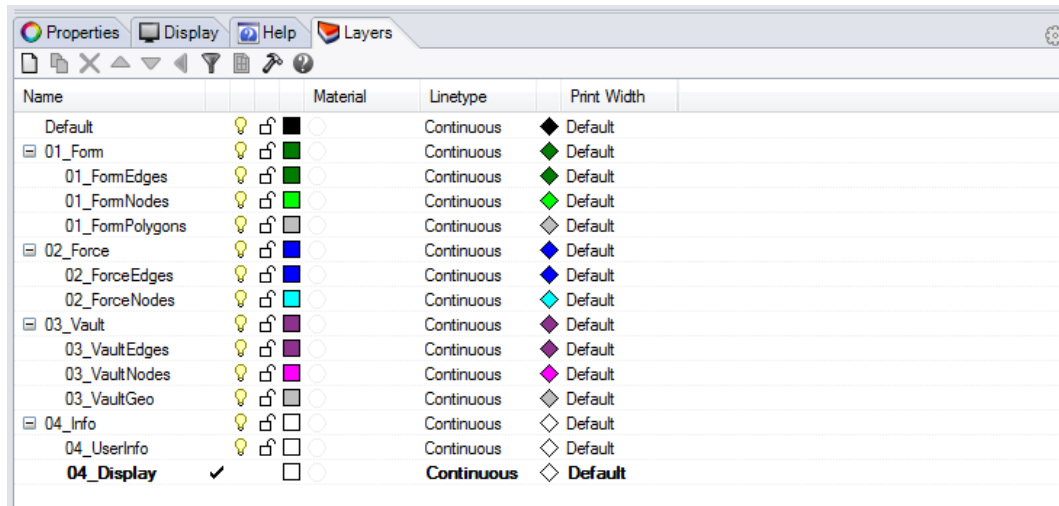








Figure 22: Default layer structure of Rhino VAULT inside the Rhinoceros CAD's environment

- 
_rvFormTri: this command is similar than the previous one; in this case it is possible to automatically generate a form diagram whose pattern is made of triangular elements and not quadrangular like the default procedure. This command is not used a lot also because it slows down a lot the computational speed of the whole process because it introduces more nodes than the default options so for the same surface a bigger number of equations need to be solved and the result is not better than using the default command. A triangular based form diagram could be useful to describe flow of forces difficult to be represented with the quadrangular scheme;
- 
_rvDual: this command button generates a dual diagram for the defined form diagram. It could be seen as the first force diagram representation trial. To generate it, the software generates an initial rotate dual network that is obviously not the equilibrated force diagram. This means that between the two diagrams vectors are not parallel and oriented in the right direction. The tool shows the edges that are not in equilibrium and shows the specific angle deviation. Bigger are the values of the angle deviation, more difficult will be the research for the horizontal equilibrium state. In particular conditions, it is impossible to find the

equilibrated condition with a specific number of the iteration of the TNA algorithm. It is suggested to manually control those big values operating on the two diagrams before the algorithm starts to work; Rhino VAULT tool helps the user in this procedure because critical angle deviation values for the equilibrium are represented in red;

-  **_rvRelax**: often could be important to improve the distribution of vertices in the form or force diagram such that connected edges form smoother, more continuous paths. The way in which every node or edge is involved in this process could be controlled through the command button **_rvModify** illustrated below. This happens because is possible to change the virtual inertia of the elements, deciding which are the elements that have to move and how much;
-  **_rvModify**: inside this command button is possible to find several tools useful to modify and manipulate both form and force diagrams and also the thrust network after the form finding process is completed. Some of those tools involve geometrical features: the two diagrams can be scaled and/or moved, both the whole diagrams or part of them. It is also possible to manipulate the supports changing their height or projecting them onto an existing surface or mesh. It also possible to design supports that guarantee only vertical thrust. A very important function, used a lot for the analysis object of this section, is the one that let the user to define openings in the structures. This is possible because the tool basically changes the applied loads of the nodes surrounding the opening. One of the last important tools implemented by this command is the one that changes the inertia of individual nodes affecting both the relax function and the horizontal equilibrium research;
-  **_rvHorizontal**: with this command button the research for horizontal equilibrium is done. The procedure can be weighted to give priority to the geometry of either form or force diagram. Practically, this means that one can choose which diagram will be adapted less during the solving process that enforces parallelity;

-  **_rvVertical**: is used to find a thrust network by solving the vertical equilibrium based on the computed horizontal equilibrium. The vertical equilibrium of the forces ensures a compression-only solution under dominant self-weight. The solution can be visualized by a network of lines, pipes and a continuous mesh. If the vertical equilibrium fails to fully compute the thrust network will be shown in red.

4.2. Starting Attributes

Before the illustration of the whole procedure followed for this study, the 4 patterns used to generate increasing number of openings onto the surface for different lowering conditions of the founded funicular shell structure are presented. The flow of forces discretization level is known from the application of Thrust Network Analysis by mean of Rhino VAULT: the holes' pattern has to be create with respect to this discretization. Each hole in the first trial form diagram is create deleting an area corresponding to 2x2 quadrangular elements as it can be seen in the following figure:

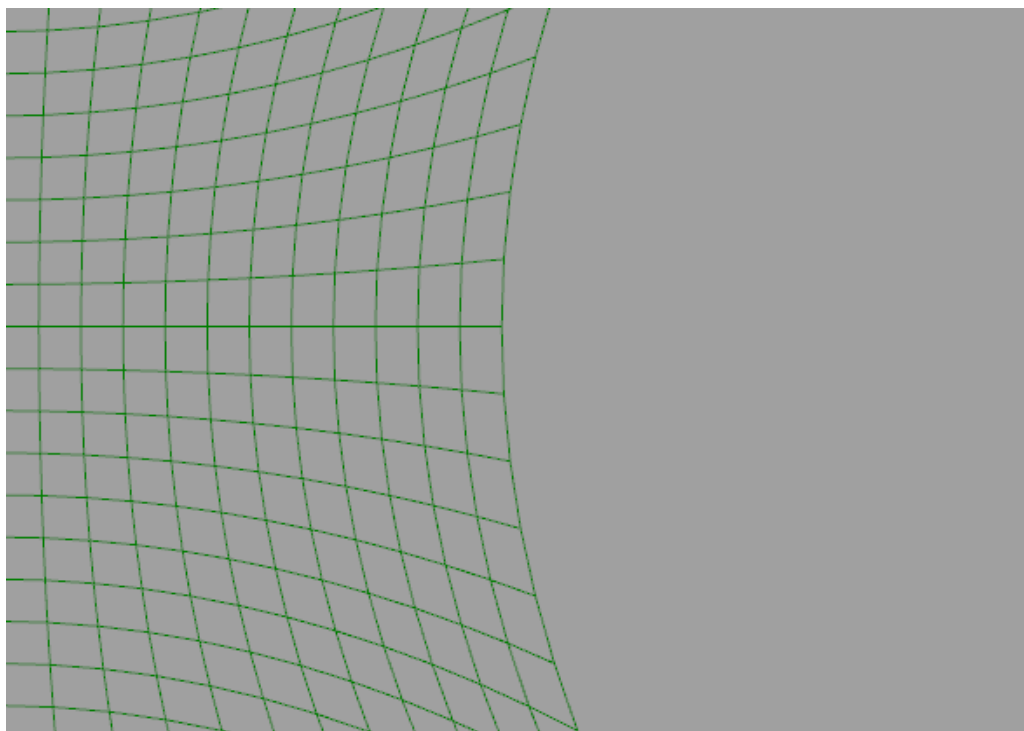


Figure 23: portion of a trial form diagram before form finding and before the hole creation

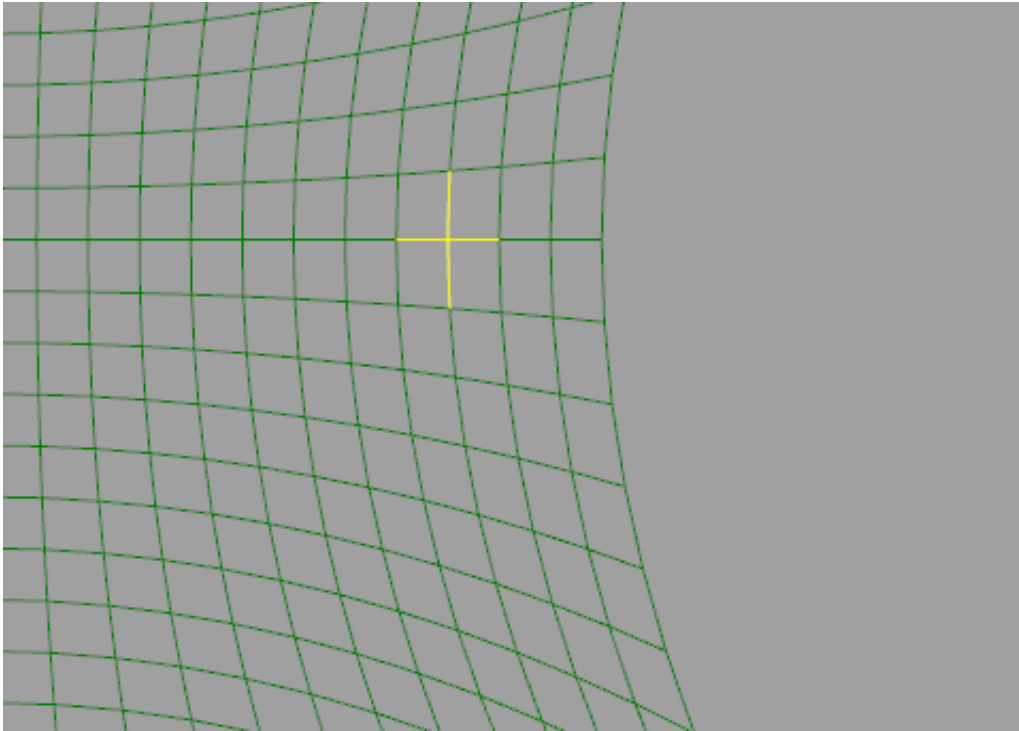


Figure 24: portion of a trial form diagram before form finding - in yellow the edges that have to be deleted to create a new hole

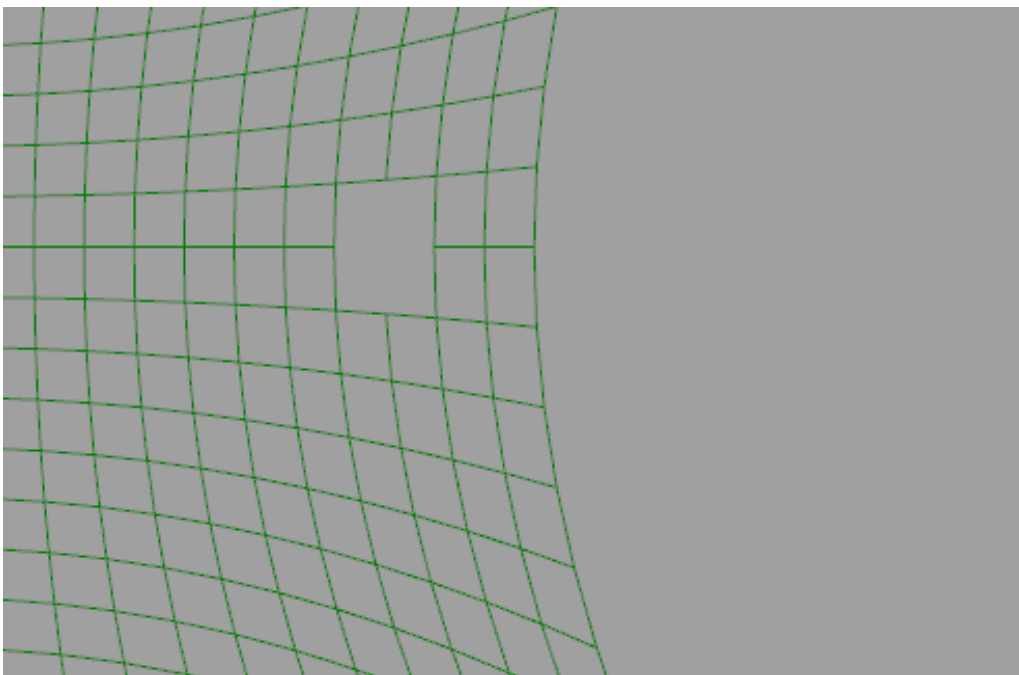


Figure 25: portion of a trial form diagram before form finding and after the creation of the hole from a 2x2 quadrangular element area

To define the pattern some rule has to be imposed:

- The distance between two holes has to be at least of 1 quadrangular element;
- The position of the holes respects the symmetry of the starting geometry shape;
- The distance between a hole and one of the boundaries has to be at least of 2 quadrangular elements.

Because of the discretization used for the definition of the form diagram, the chosen dimension (using as measure unit the quadrangular element) of the holes and the defined rules, the larger grid of holes that could be generated is made by 7x7 holes, that means a total maximum number of 49 holes.

4 patterns are created.

The choice of the patterns is not randomly realized. In a first phase of the study, only the first of them was generated. The first hole in the center was placed thinking about the Pantheon's Dome in Rome where is known that the central circular hole helps to drop down the stress concentration in the central and higher fraction of the dome. The other holes were placed trying to keep the geometrical and structural symmetry of the original shape, the one without holes, from the center towards the boundary edges of the structures, filling with holes, step by step, the surface.

The second and third patterns are generated to observe the behavior of the structures if the central hole is created only in a second time. Numerical results revealed that this curiosity was justified. The two patterns are different from each other because in the holes grow in number from boundaries towards the center following two different paths. After the central hole is placed the holes fill the shell surface.

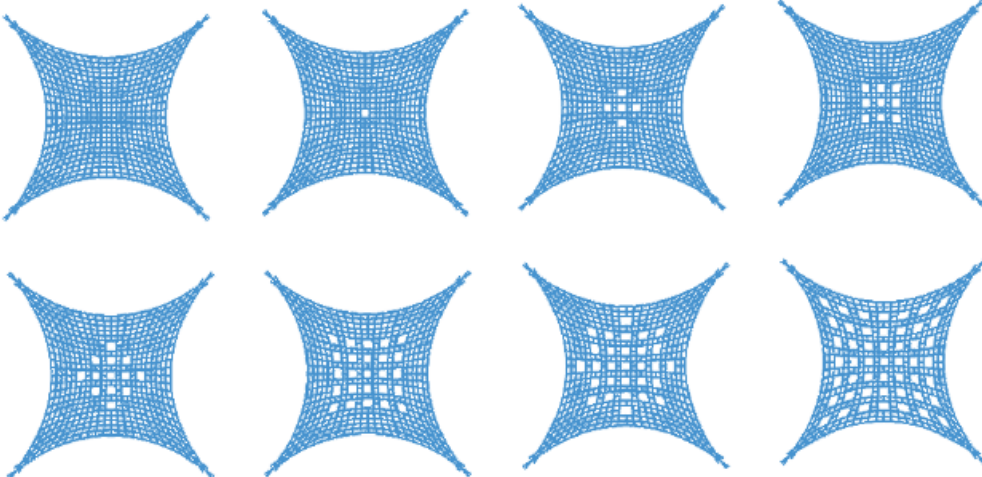
For a serviceable state load condition numerical results shew that the third pattern seemed to be the best one, but it was also clear that the central hole was truly helpful from a structural and strength point of view. Indeed, the *Pattern 4* is generated very close to the third one but with two main differences: the openings filling path is inverted and is changed the path after the 13th hole.

In the next pages are illustrated with schematic representations, the 4 chosen patterns. In the attachments are also reported figures representing the patterns and consequently all

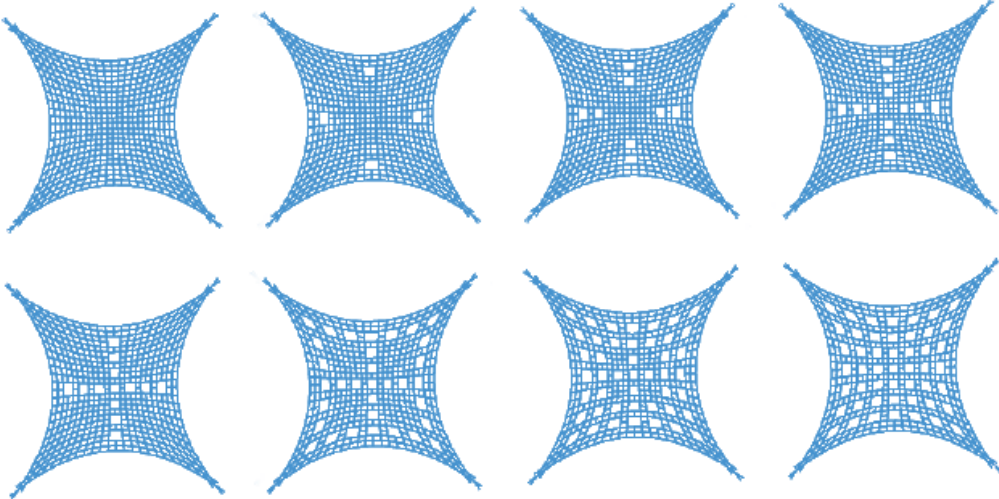
the found structures after the form finding process trying to help to figure the reader out the real shape of the analyzed shells.

4.3. Opening Patterns

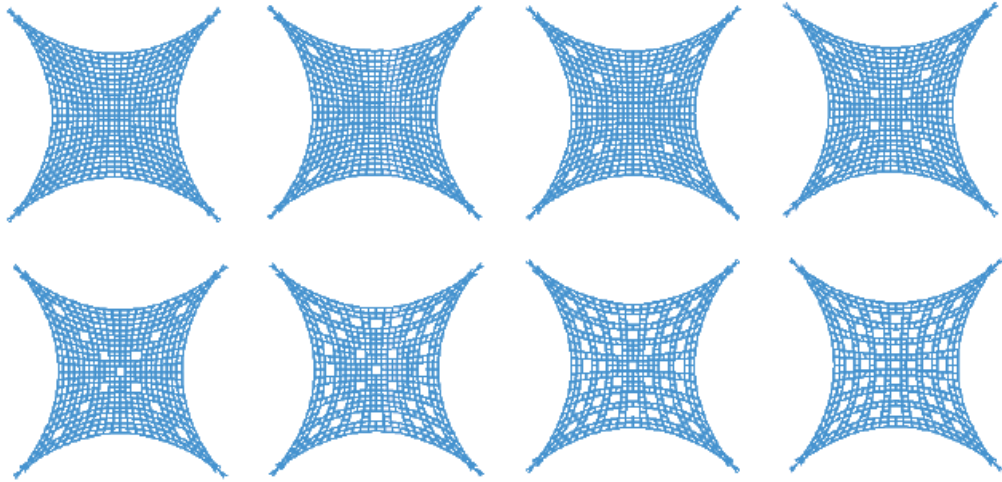
- **Pattern 1**



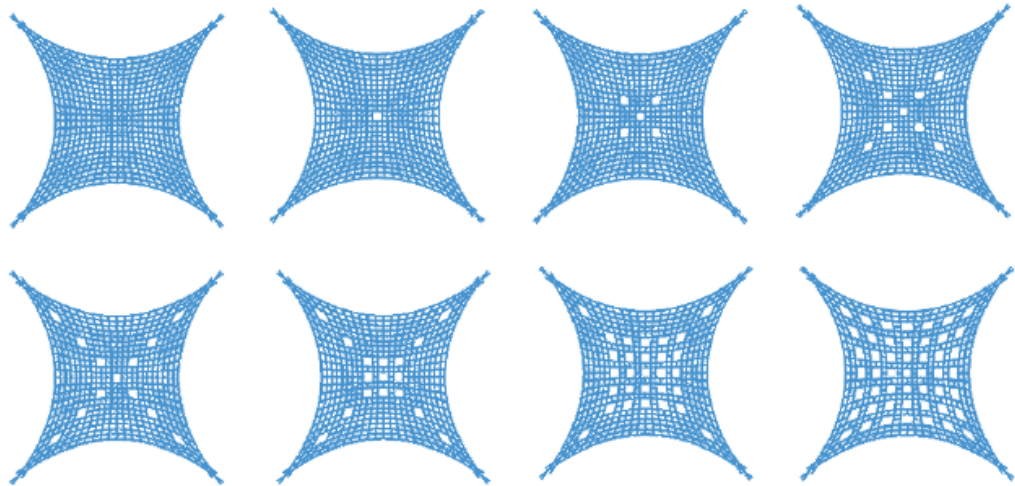
- **Pattern 2**



- **Pattern 3**



- **Pattern 4**



4.4. Form Finding Process

The case study does not have any kind of constraint by geometrical or structural point of view because the study is not made for a real structure subjected to all design phases. For this reason, all the geometrical data and input and furthermore, number and nature of constraints, number of openings, material characteristics, structure thickness and so on are all arbitrary in order to give the as most general interpretation as possible of the obtained values and results.

However, the study is done to give a practical contribute to real design of structures. The geometry of the structure is think to let it suitable as a temporary structure like an exhibition pavilion, auditorium, concert hall and so on or also as a stable structure.

The selected area to be covered is a square with sides of 16 meters. The maximum height of the new shell structure will be 2.5, 5 or 7.5 meters in function of the lowering degree considered and this values has to be reached in the center of the covered area. The structure will be supported only in 4 points at the 4 square corners. The structure will present a compression-only state of stress for gravitational loads so it will follow the ancient principle of the *catenaria* in three dimensions that means that the shell will present a double curvature shape after the form finding process.

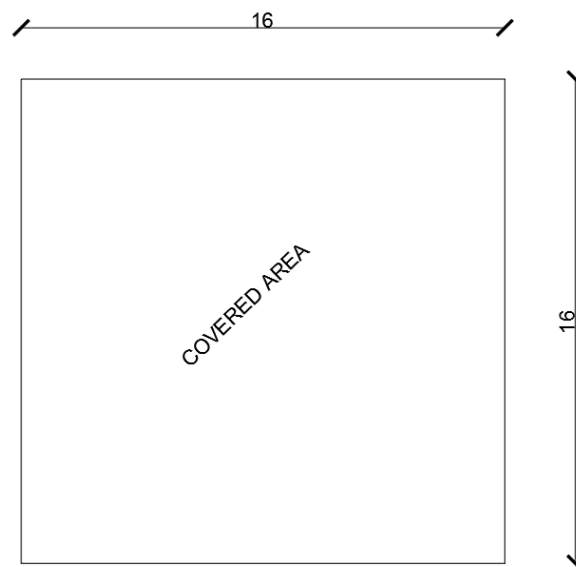


Figure 26: Perimeter of the covered area

It is obvious that this perimeter could not be considered as the projection of the perimeter of the final shell structure also thinking about it as a first trial. Keeping the 4 corner points steady, a new trial perimeter is generated. The chosen shape would be more similar to the 3-D catenary solution. It is illustrated in the next figure:

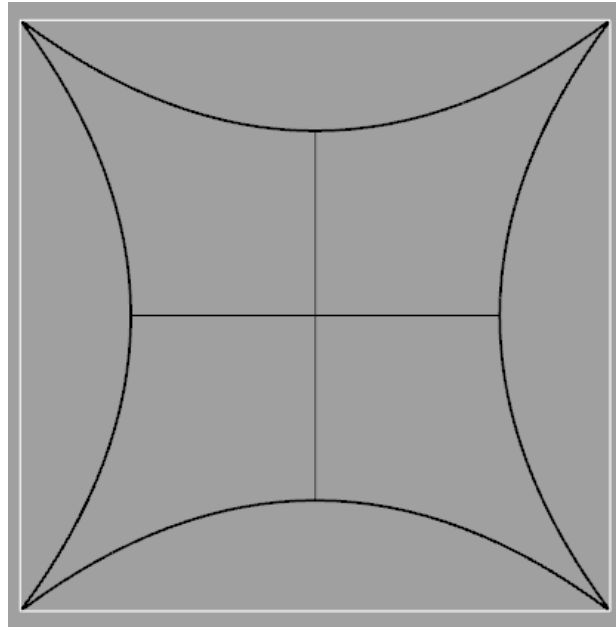


Figure 27: the trial projection on horizontal plane of the funicular shell structure

The illustrated shape is not an arbitrary choice but comes from the projection of the shell structure found with the Particle Spring System during the study of the behavior of that form finding method and illustrated in Appendix A. It was observed that the horizontal projection of the hanging model has a shape very similar to the one used now.

The perimeter is drawn directly in Rhinoceros 3-D CAD environment; in this way the drawing is already ready to be subjected to form finding process with Rhino VAULT. Every side of the original square is considered as a curve governed by a second order equation, a parabola, described by the position of three points: the initial, the final and the middle curve one. The shape in the figure is obtained moving each middle curve point towards the center of the square of 6 meters.

All the steps are presented with regard to the structure with thirteen holes of the third pattern with maximum height of 5 meters; this is true also for numerical results and values. However, as written previously, the whole results will be illustrated at the end of

this dissertation as attachment. This choice wants to help understanding the following steps.

After Rhino VAULT's library is loaded by Rhinoceros, the obtained shape is selected to generate the form diagram used in the TNA. The selected surface has been divided in a 25x25 quadrangular grid: this means that each side is subdivided in 24 segments.

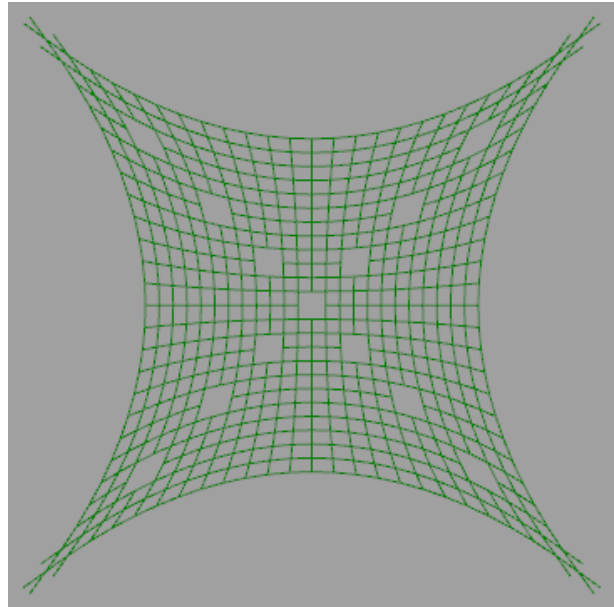


Figure 28: first trial form diagram for the 13 Holes' shell of the pattern 3

In the figure is shown how this first trial form diagram is made. It is important to focus on the corners of this diagram. Few branches-like segments are present. This is explained because the forces may go to a number of discrete supports, such as columns or buttresses. If we have considered a punctual support for the shell structure at each corner, the algorithm would not have been able to find the horizontal equilibrium regardless of all the other parameters and/or variables. Adding these supports let the algorithm to find the convergence.

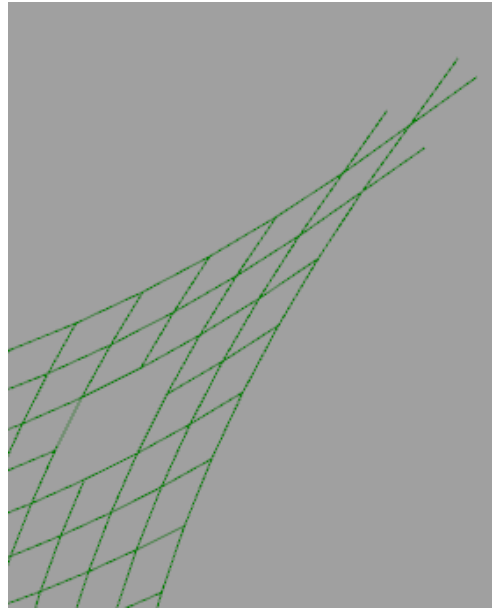


Figure 29: Support conditions – Detail

The tool creates a force diagram that doesn't respect the horizontal equilibrium. It could be seen as a first trial, a break point to start the equilibrium condition research. The default setting creates it from a rotation of 90 degrees of the lines composing the edges of the initial form diagram. Unsupported boundaries of a funicular structure form a three-dimensional edge arch. The horizontal forces in the unsupported edge arches are represented in the force diagram by fan-shaped set of edges converging in one vertex. As written above, the framework allows for the creation of irregular openings in complexly shaped funicular networks. Openings are generally represented by faces in the form diagram with more than four vertices. These openings comprise a funicular polygon in the form diagram for the horizontal thrust applied to it. These funicular polygons can be seen in the force diagram because of the Graphic statics' rules. In the form diagram an opening must be represented by a convex face; this result in a star-like configuration of corresponding edges in the force diagram. It is obvious that more circular-like is the openings in the form diagram, less accentuated will be the stress concentration around the hole's boundaries.

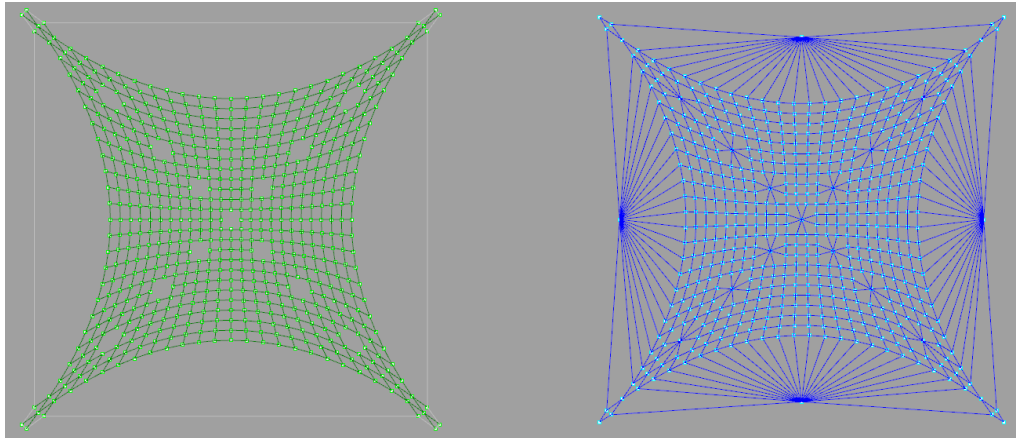


Figure 30: Initial Form and Force diagram

The initial Force Diagram does not represent the equilibrated state but the plugin lets the user know which are the edges that present a direction angle deviation bigger than a tolerance angle (imposed by user) that means which are the edges that, for a given tolerance, are not parallel in the form and force diagram. In the form diagram this info is also available; in this way it is easier for the designer to understand which would be the critical edges that could determine a non-convergence of the solution. The developers of the software suggest always to check if there are edges with too much big deviation angles and to manually modify them. For instance, a deviation angle bigger than 100° may not allow the system to reach the convergence of the horizontal equilibrium.

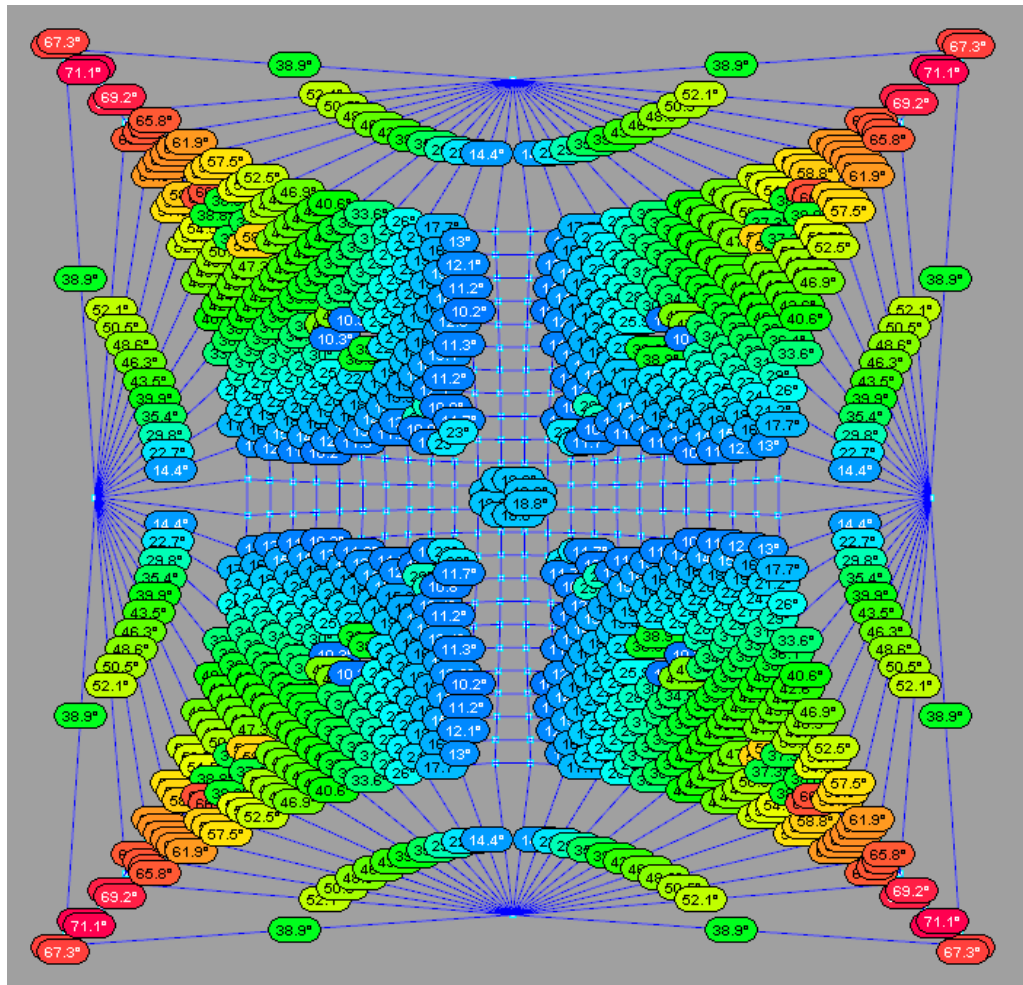


Figure 31: Initial Force diagram - In evidence the direction angle deviations between same edges in form and force diagram

The following step of the study is the relax of the form diagram. This function was presented during the description of the tool commands. The framework lets the users to operate on the form of the two diagrams in order to smooth the shape of the edges. This could be useful if seems difficult to find a convergence to horizontal equilibrium.

Laplacian mesh smoothing techniques, applied to existing form diagrams, are used to improve the distribution of vertices in the form diagram such that connected edges form smoother, more continuous load paths [...]. The smoothing method is extended such that individual vertices and/or constrain vertices to lie on user-defined guide curves to form unsupported edge arch or opening geometries. (Rippmann, 2016)

During this process is possible to assign different value of *inertia* to every single point or edge. This allows for a smart control of the relaxing movements of the diagrams. This

function is included inside the command button `_rvModify`. Every edge or points weight is assigned with a parametric value included between 0 and 1. Weight 0 for a point means that point will not move during relax phase; weight 1 for a point means that point has no *inertia* and it is completely free to move. This is the default condition for the points.

In the case study value 0 is assigned to the support points while a value 0.15 is assigned to the boundary edges points. This value has been chosen to let the form of the diagram to be smoothed without change too much the initial shape.

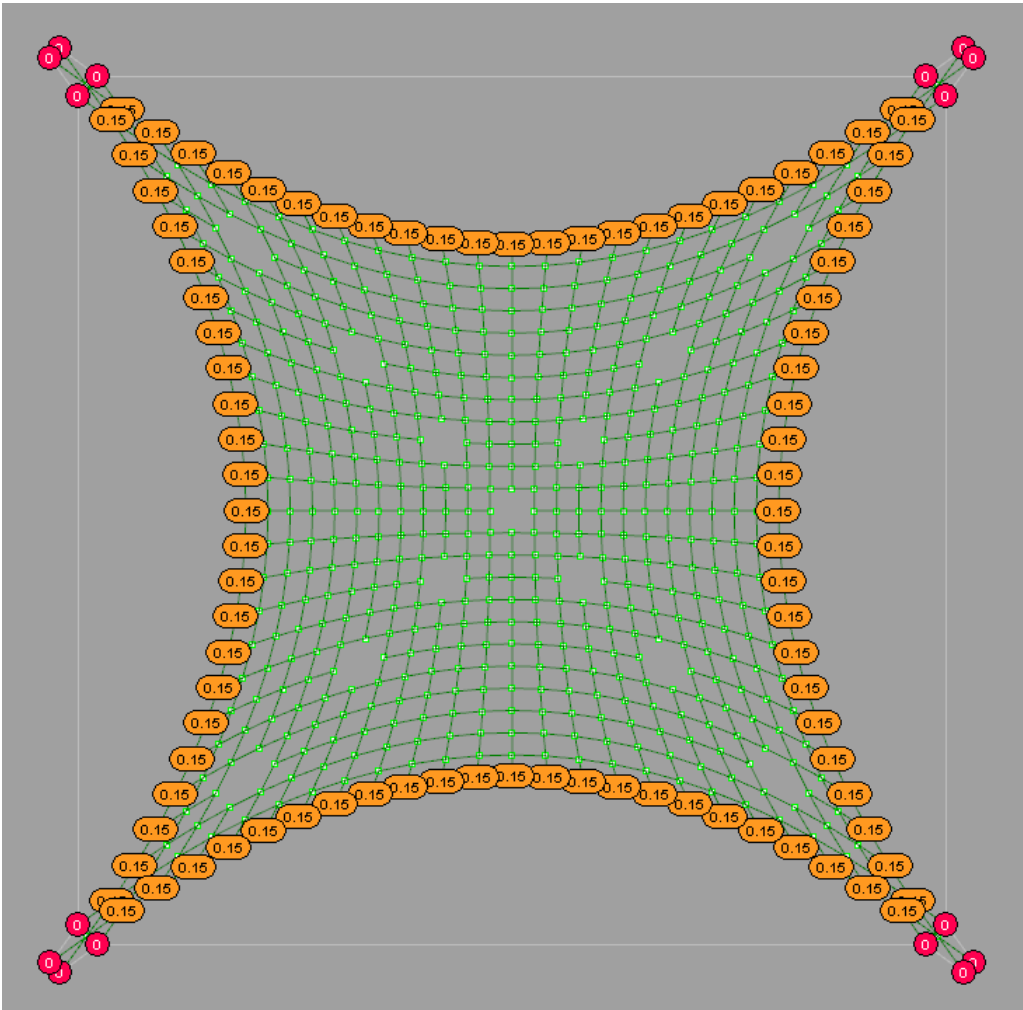


Figure 32: using `_rvModify/ConstraintNodes`

The openings boundaries were not constrained during relax phase. This has been done because in this way the holes would smooth their shape in order to guarantee a lower stress concentration when the funicular shell structure would be found.

Next figure shows the relaxed form diagram and his relative force diagram:

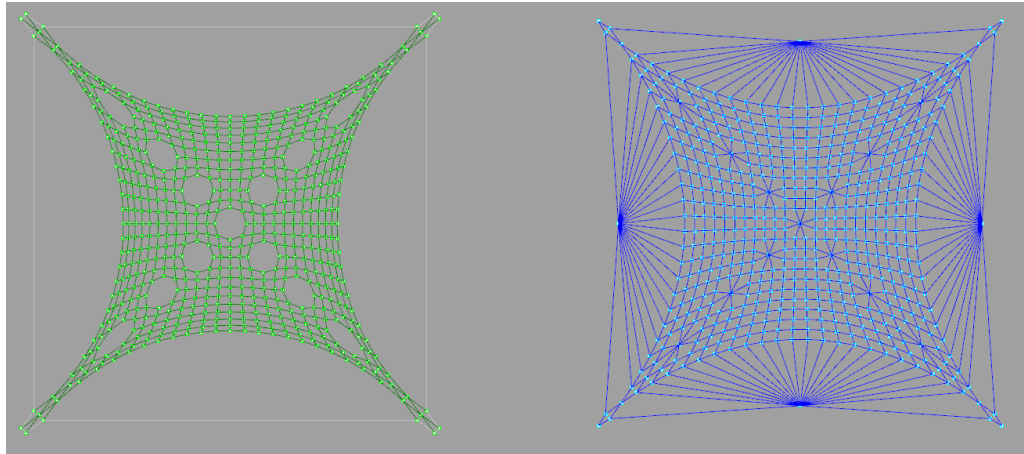


Figure 33: Relaxed form diagram and its relative force diagram

The resulting diagram is not only smoothed but the edges of the form and the force diagram present deviation angle values smaller than before the process.

After this operation, the form and the force diagrams are ready to be subjected to the real form finding process. The horizontal equilibrium is found varying the shape only of the force diagram. The equilibrium is found for every structure analyzed with a different number of iterations. For the structure used to illustrate the study reached convergence after 399 iterations. In the next figure is represented the force diagram in equilibrium:

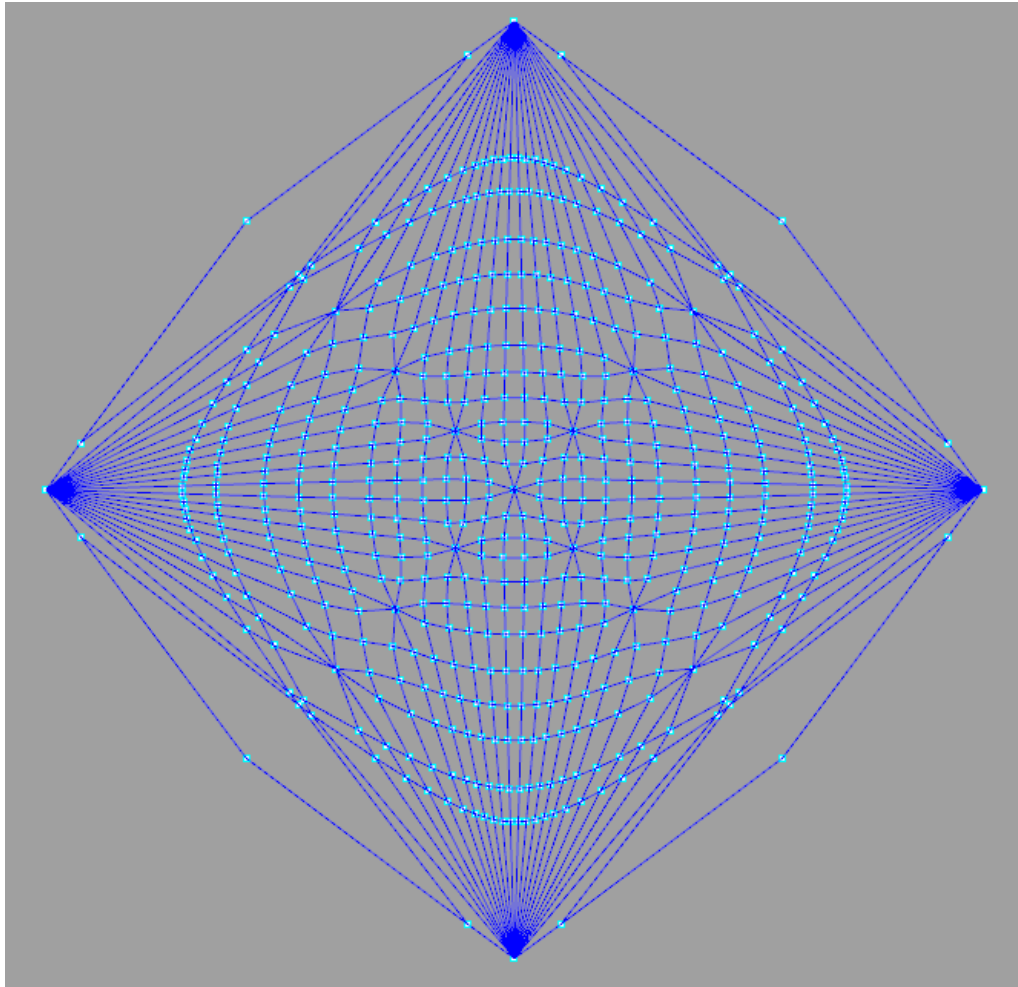


Figure 34: Force Diagram after the Horizontal Equilibrium is reached

The following step is the search for vertical equilibrium, second most important step of the Thrust Network Analysis. Remembering that for a given horizontal projection and equilibrium of the horizontal force components and a given scale of the force diagram (1 for the case study) a unique thrust network, in equilibrium with the given loading is found for the given support vertices, the form finding process is now completed.

Also in this case, such as for the horizontal equilibrium research, the equilibrium is found after a different number of iterations, different case by case. The height of the found structure is always function of the scale of the force diagram. Indeed, the found funicular structure is the only one in equilibrium if the scale of the diagram is equal to 1.

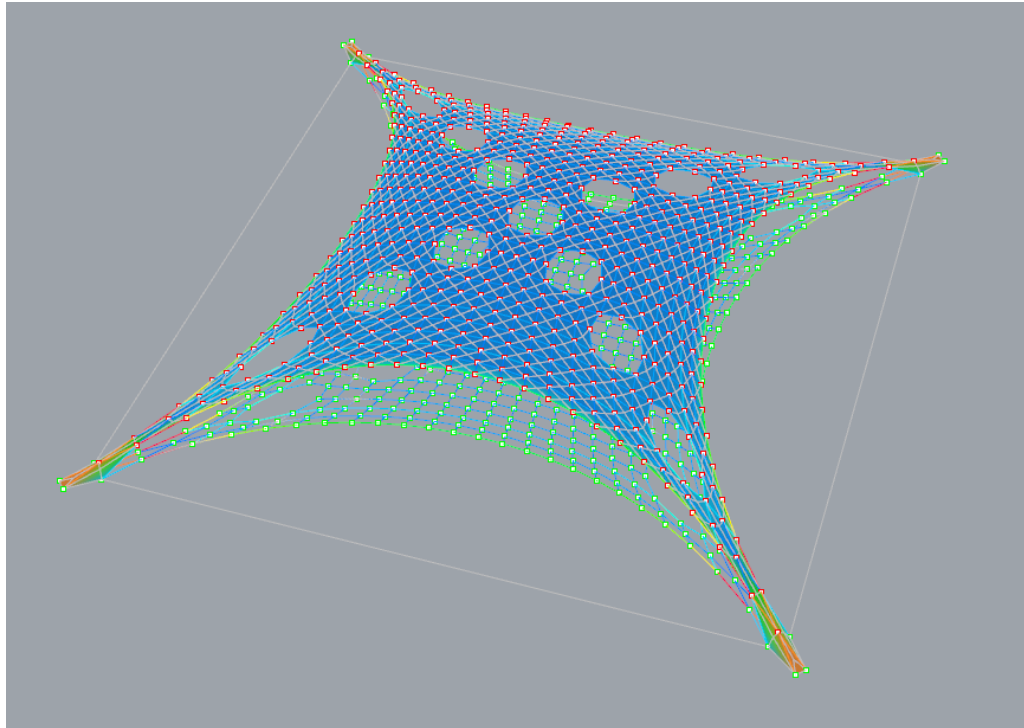


Figure 35: Shell Structure from TNA

The structure found with the TNA and represented above has not the height desired: it is only 3.03 meters high. To reach the 5 meters desired and imposed for the case study it is necessary to change the scale factor of the force diagram.

The sets of external loads are not defined for this form finding process. According to Block (Block, Thrust Network Analysis: Exploring Three-dimensional Equilibrium, 2009) the problem in analysis is not linear but the TNA works solving systems of linear equations. However, is not possible to find an exact proportion between scale factor and height of the funicular shell.

In an iterative way, the different values for all the shells were found. For instance, the scale factors for the vaults 5 meters tall are represented in the following tables:

| PATTERN 1 | | PATTERN 2 | | PATTERN 3 | | PATTERN 4 | |
|-----------|--------|-----------|--------|-----------|--------|-----------|---------|
| No Hole | 0.7515 | No Hole | 0.7515 | No Hole | 0.7515 | No Hole | 0.7515 |
| 1 Hole | 0.746 | 4 Holes | 0.712 | 4 Holes | 0.719 | 1 Hole | 0.746 |
| 5 Holes | 0.6658 | 8 Holes | 0.669 | 8 Holes | 0.6877 | 5 Holes | 0.673 |
| 9 Holes | 0.618 | 12 Holes | 0.615 | 12 Holes | 0.636 | 9 Holes | 0.63254 |
| 13 Holes | 0.586 | 13 Holes | 0.588 | 13 Holes | 0.614 | 13 Holes | 0.614 |
| 25 Holes | 0.488 | 33 Holes | 0.488 | 33 Holes | 0.504 | 17 Holes | 0.565 |
| 29 Holes | 0.461 | 45 Holes | 0.399 | 45 Holes | 0.4035 | 29 Holes | 0.474 |
| 49 Holes | 0.36 | 49 Holes | 0.36 | 49 Holes | 0.36 | 49 Holes | 0.36 |

Table 1: Scale Factor Table

The application of those factors ends the form finding process. All the structures present now the right height value and they could be analyzed with a Finite Element Solver to understand how the pierces condition the global stability of the structures.

4.5. Pierced Vaults Structural Analysis

The second main step of the study is about the structural analysis of the found funicular shells.

In this paragraph two different approaches are present. The first one is about the analysis of some of the structures looking at their Von Mises stresses under serviceability load conditions while the second one, the most important one, is about the linear buckling load analysis. In that case, more load conditions are included considering both symmetrical and anti-symmetrical load-cases. Three lowering degree conditions are introduced in order to better understand the behavior of the structures.

In the following sections all the conditions are described to be applied for the first approach analysis. The specific conditions applied for the second one are introduced in the specific paragraph about buckling analysis.

The analysis is done by mean of a Finite Element Solver: LUSAS 15.1 in its academic version. As written in the User Manual: LUSAS is an associative feature-based Modeller. The model geometry is entered in terms of features which are discretized into finite elements in order to perform the analysis. The finite elements are the computational answer to designer question: *What would happen if I did this to my new design and I need to answer only by means of nature schematization?*

Carpinteri wrote in his *Scienza delle Costruzioni 2*: the finite element method is a discretization method; instead of the displacements continuous function, the problem unknowns are the displacements of a finite points number. It is also an interpolation method because after the displacements of the nodes are determined, the method tie them with as most regular as possible functions. (Carpinteri, 1992)

Increasing the discretization of the features will usually result in an increase in accuracy of the solution, but with a corresponding increase in solution time and disk space required. The features in LUSAS form a hierarchy, that is Volumes are comprised of Surfaces, which in turn are made up of Lines of Combined Lines, which are defined by Points.

The model is a graphical representation of geometric features as points, lines, surfaces, volumes and assigned attributes as materials, loading, supports and mesh.

Describing how the study has been done, the same shell structure used for the form finding process will be considered.

Only the structures 5 meters tall are considered in this first structural analysis phase.

The geometry of the structure has been exported as a .dxf file from Rhinoceros to the CAD environment in order to trim the structure: only a quarter of the structure is considered for the structural analysis. The geometry exported from Rhinoceros are not points and lines but the triangular mesh generated by Rhino VAULT at the end of the form finding process. That mesh illustrated in the figure below, is composed by triangular elements; the discretization is made up on the original discretization of the form diagram; in this way higher is the level of the discretization of the form diagram in the early stages of the process, higher will be the number of mesh.

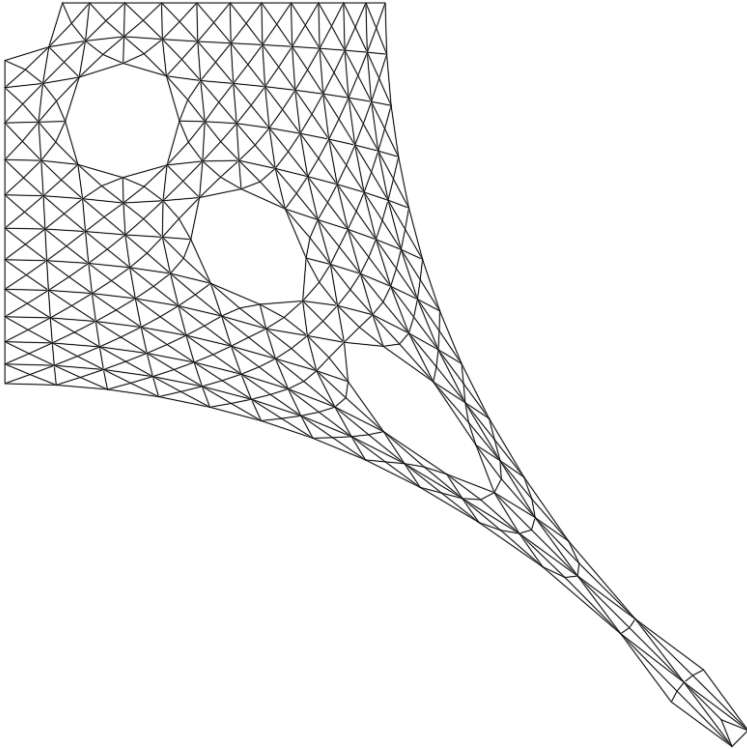


Figure 36: 1/4 of the shell structure - in evidence the mesh discretization made up by Rhino VAULT

The presented geometry has been imported in the LUSAS 3-D CAD environment. LUSAS recognize the geometry imported but all the lines composing the mesh in the .dxf file were not interpreted by the software as surface and/or mesh element. User has to create all the surface elements in order to assign the desired surface finite element to every single mesh element which the imported geometry is made up.

4.5.1. Mesh Element

The TSL6 finite element has been chosen for the structural analysis. It is a semiloof triangular element and its characteristics are described according to LUSAS' User Manual:

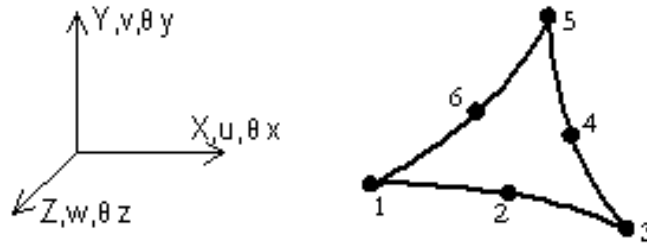


Figure 37: Semiloof element - TSL6

- **Element Group:** Shells;
- **Element Subgroup:** Semiloof shells;
- **Element description:** a family of shell elements for the analysis of arbitrarily curved shell geometries, including multiple branched junctions. The elements can accommodate generally curved geometry with varying thickness and anisotropic and composite material properties. The element formulation takes account of both membrane and flexural deformations. As required by thin shell theory, transverse shearing deformations are excluded;
- **Number of Nodes:** 6 anticlockwise;
- **Freedom:** U, V, W: at corner nodes. U, V, W, θ_1 , θ_2 : (loof rotations) at mid-side nodes;
- **Node coordinates:** X, Y, Z at each node.

All the other properties about this element are well described in the cited LUSAS' User Manual.

4.5.2. Geometric Attributes

The other geometrical feature necessary to the Modeller to understand how the structure is characterized in the three dimensions is the thickness of the shell elements. 5 thickness values were initialized:

- $t_1 = 30 \text{ cm}$;
- $t_2 = 25 \text{ cm}$;
- $t_3 = 20 \text{ cm}$;
- $t_4 = 15 \text{ cm}$;
- $t_5 = 10 \text{ cm}$.

4.5.3. Material Attributes

Referring to Italian D.M. 17/01/2018 *Aggiornamento delle Nuove Norme Tecniche Per Le Costruzioni*, the material for the structure has been chosen, a masonry kind obviously. As the other parameters, also the mechanical characteristics of masonry are arbitrarily chosen. The chosen kind is referred to a common building situation with isotropic characteristics.

The following mechanical characteristics refer to Table C8 A.2.1 of the *Circolare 2 febbraio 2009, n. 617 – Istruzioni per l'applicazione delle “Nuove norme tecniche per le costruzioni” di cui al D.M.14 gennaio 2008*:

| MASONRY KIND: SEMI-SOLID BRICKS AND CEMENT MORTAR | | | | | |
|---|------|----------------------|---|--------|-------|
| f_m | 6,5 | [Mpa] | E | 4550 | [Mpa] |
| τ_0 | 0,28 | [Mpa] | G | 1137,5 | [Mpa] |
| γ | 15 | [kN/m ³] | | | |

Table 2: mechanical characteristics of the selected masonry kind

4.5.4. Supports

As exploited in a previous section, the structure is supported in its four corners. For equilibrium reasons these supports are not considered as punctual ones but they are composed by four different points simulating a sort of buttress. Also for this situation, as for instance for the material attributes, the choice of the support condition is arbitrary with respect to the correct number of degrees of freedom. For the case study a simply supported condition has been selected. Indeed, the 4 four points present in the reduced scheme for the structural analysis have displacements in the three principal direction kept locked.

The analyzed structure is only $\frac{1}{4}$ of the real one. That happens because it is exploited its geometrical and loading-system symmetry. Additional constraints are necessary to have

the same structural behavior between the figure's model and the "complete" one. There are present two kind of constraints:

- Translation in X direction fixed and rotation about Y-axis fixed;
- Translation in Y direction fixed and rotation about X-axis fixed.

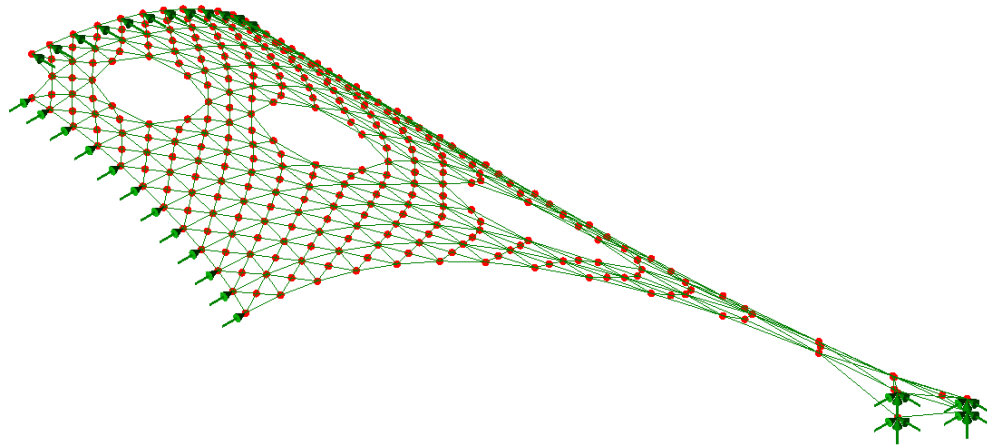


Figure 38: Support attributes description

4.5.5. Loads Attributes

In order to analyze the structure, some loads need to be applied. The density of the chosen materials is about 15 kN/m^3 and the self-weight of the structure was not applied as a load divided the square area but as a concentrated load at the top of the structure with a value equal to half of the effective resultant thinking about a thickness of 15 cm. this value has been chosen in order to consider always the same load for every structure allowing a comparison based on the same initial load data. Indeed, the different shapes due to the different holes would have totally different and incomparable results due to the different loads and mass quantity distribution. Only half of the resultant is considered because a concentrated load with a modulus equal to the resultant has bigger effects on shell's behavior, totally unrealistic; with the value that has been chosen, the author tried to represent a more representative case. However, loads value are not the central core of the analysis; they are only useful to let the comparison to be done. Furthermore, the same reasoning has been done for live loads considering a load divided by square meters of 1.5 kN/m^2 .

The total area of the shell surface without openings is: **114.92 m²**. The resultant applied for self-weight and live loads, considering half of their real value, are:

- $P = \frac{\gamma \cdot t \cdot A}{2} = \frac{15 \cdot 0.15 \cdot 114.92}{2} = 129.3 \text{ kN};$
- $Q = \frac{qA}{2} = \frac{1.5 \cdot 114.92}{2} = 86.19 \text{ kN}.$

These two are the concentrated loads applied at the structures. Obviously their application takes into account the symmetry of the problem. For the structures, like the one represented above, the loads are applied at the nodes distributed on the boundary of the opening. No load cases or loads combination has been done.

4.5.6. *Post Processing Phase*

The stress state analysis was one of the first step made during the develop of the work so only a few of the whole number of analyzed structures is considered. In particular, the structures with maximum height of 5 meters and with symmetric load conditions were analyzed. First of all is done an evaluation on the eccentricity of the loads in order to understand if the Thrust Network Analysis return the right behavior. This control confirmed the validity of the method but is not included in this work.

The main parameter of the post processing phase is the Von Mises stress:

$$[(\sigma_1^2 + \sigma_2^2 + \sigma_3^2) - (\sigma_1\sigma_2 + \sigma_1\sigma_3 + \sigma_2\sigma_3)] = \sigma_{VM}^2$$

There are present 4 different patterns including 8 funicular structures each one. Each structure has been analyzed changing its thickness through 5 different values and the results are shown by the help of graphics

In the next pages are presented two kind of graphics:

- the Von Mises stress is illustrated in function of the thickness of the funicular shell structure; one function checks with an opening's percentage of the structure;
- the Von Mises stress is illustrated in function of the opening's percentage of the structure; one function checks with a thickness value of the funicular shell structure.

The stress used and visualized in the graphics is the highest value through all the nodes of the structure

- **Pattern 1**

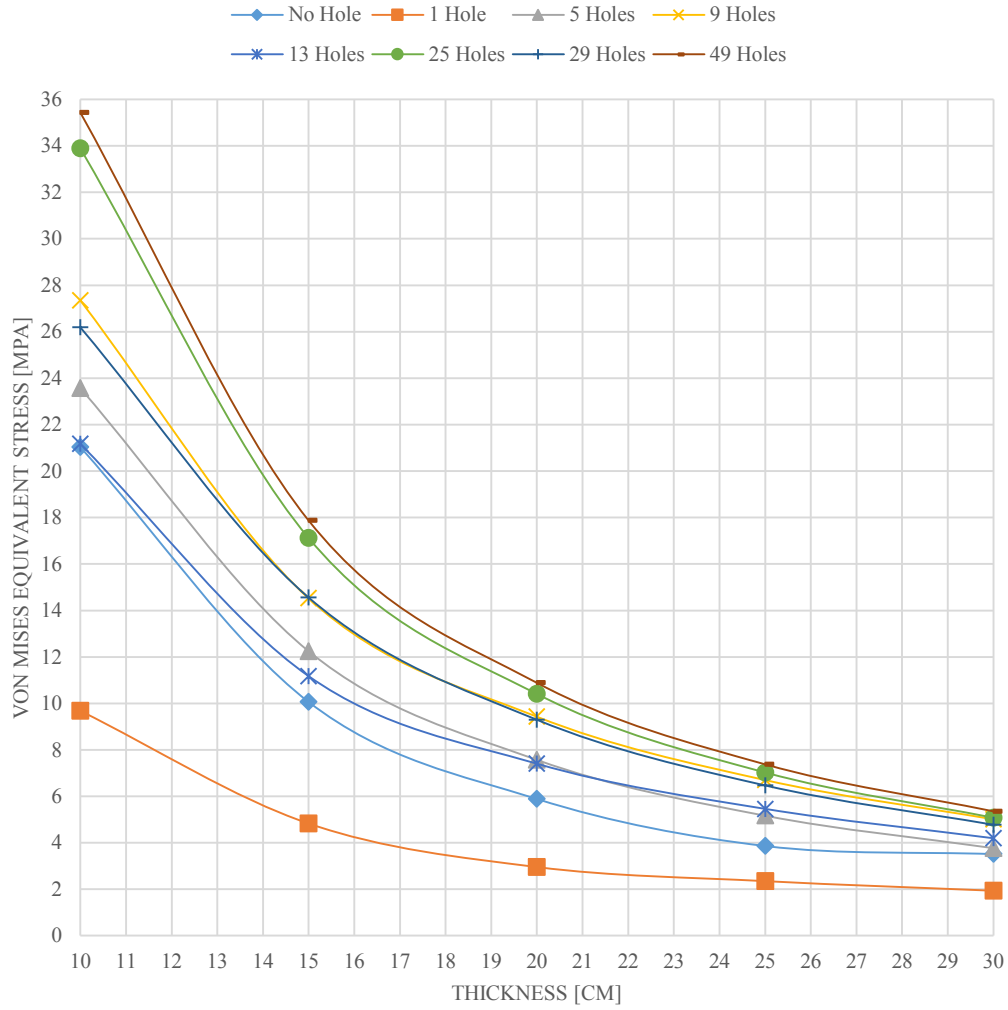


Figure 39: Pattern 1 - Graphic 1

| t | [cm] | 30 | 25 | 20 | 15 | 10 |
|---------------------|------|------|------|-------|-------|-------|
| σ_{id} [Mpa] | | | | | | |
| No Hole | | 3.52 | 3.87 | 5.89 | 10.07 | 21.03 |
| 1 Hole | | 1.94 | 2.36 | 2.96 | 4.83 | 9.68 |
| 5 Holes | | 3.78 | 5.17 | 7.57 | 12.25 | 23.57 |
| 9 Holes | | 5.01 | 6.70 | 9.43 | 14.53 | 27.35 |
| 13 Holes | | 4.19 | 5.45 | 7.40 | 11.17 | 21.17 |
| 25 Holes | | 5.08 | 7.02 | 10.41 | 17.12 | 33.89 |
| 29 Holes | | 4.77 | 6.46 | 9.29 | 14.56 | 26.20 |
| 49 Holes | | 5.36 | 7.38 | 10.89 | 17.88 | 35.44 |

Table 3: Von Mises Stresses

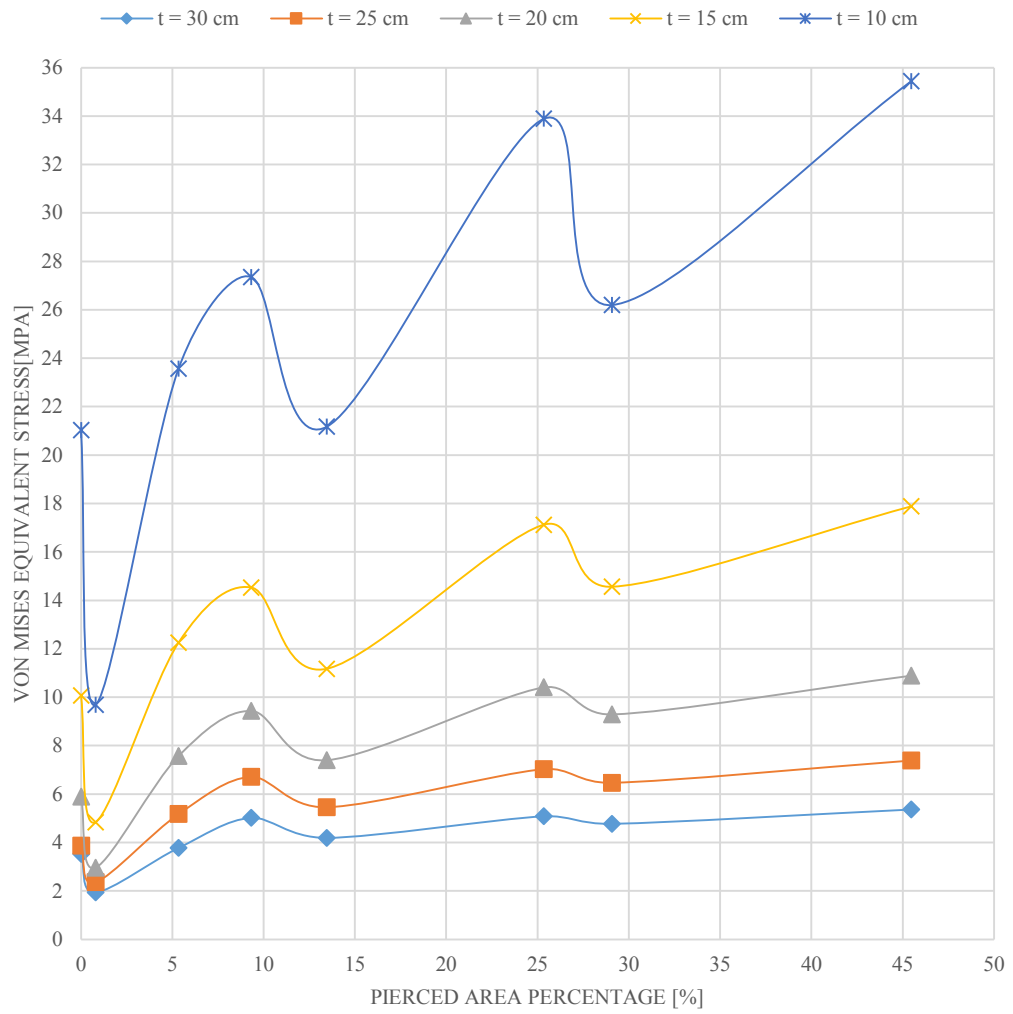


Figure 40: Pattern 1 - Graphic 2

| Pierced Area Percentage | | |
|-------------------------|-------|-----|
| No Hole | 0 | [%] |
| 1 Hole | 0.79 | [%] |
| 5 Holes | 5.34 | [%] |
| 9 Holes | 9.32 | [%] |
| 13 Holes | 13.46 | [%] |
| 25 Holes | 25.34 | [%] |
| 29 Holes | 29.08 | [%] |
| 49 Holes | 45.46 | [%] |

Table 4: Pierced Area Percentage

- **Pattern 2**

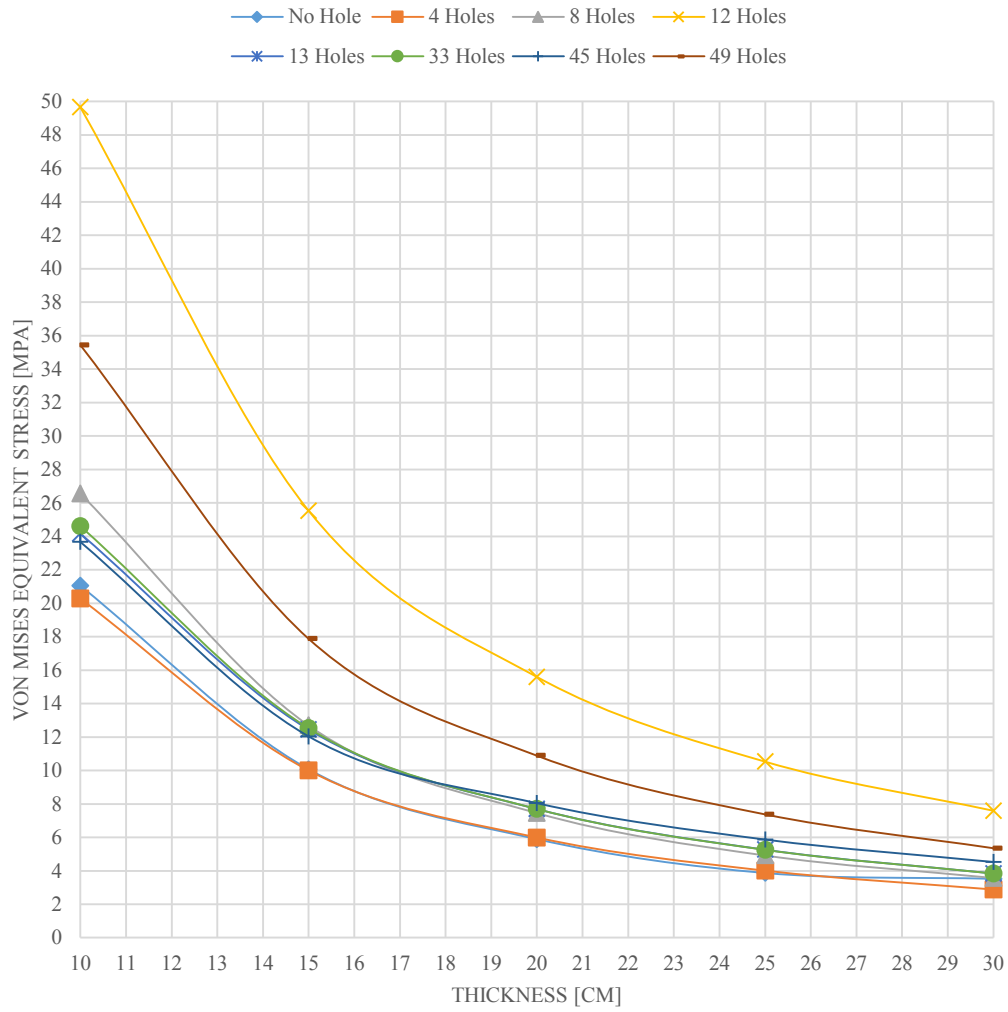


Figure 41: Pattern 2 - Graphic 1

| t | [cm] | 30 | 25 | 20 | 15 | 10 |
|---------------|------|------|-------|-------|-------|-------|
| σ_{id} | | | | | | |
| No Hole | | 3.52 | 3.87 | 5.89 | 10.07 | 21.03 |
| 4 Holes | | 2.87 | 4.00 | 5.98 | 9.99 | 20.27 |
| 8 Holes | | 3.58 | 4.92 | 7.46 | 12.69 | 26.56 |
| 12 Holes | | 7.60 | 10.53 | 15.60 | 25.53 | 49.65 |
| 13 Holes | | 3.85 | 5.27 | 7.70 | 12.45 | 24.15 |
| 33 Holes | | 3.84 | 5.25 | 7.69 | 12.52 | 24.60 |
| 45 Holes | | 4.52 | 5.86 | 8.04 | 12.03 | 23.66 |
| 49 Holes | | 5.36 | 7.38 | 10.89 | 17.88 | 35.44 |

Table 5: Von Mises Stresses

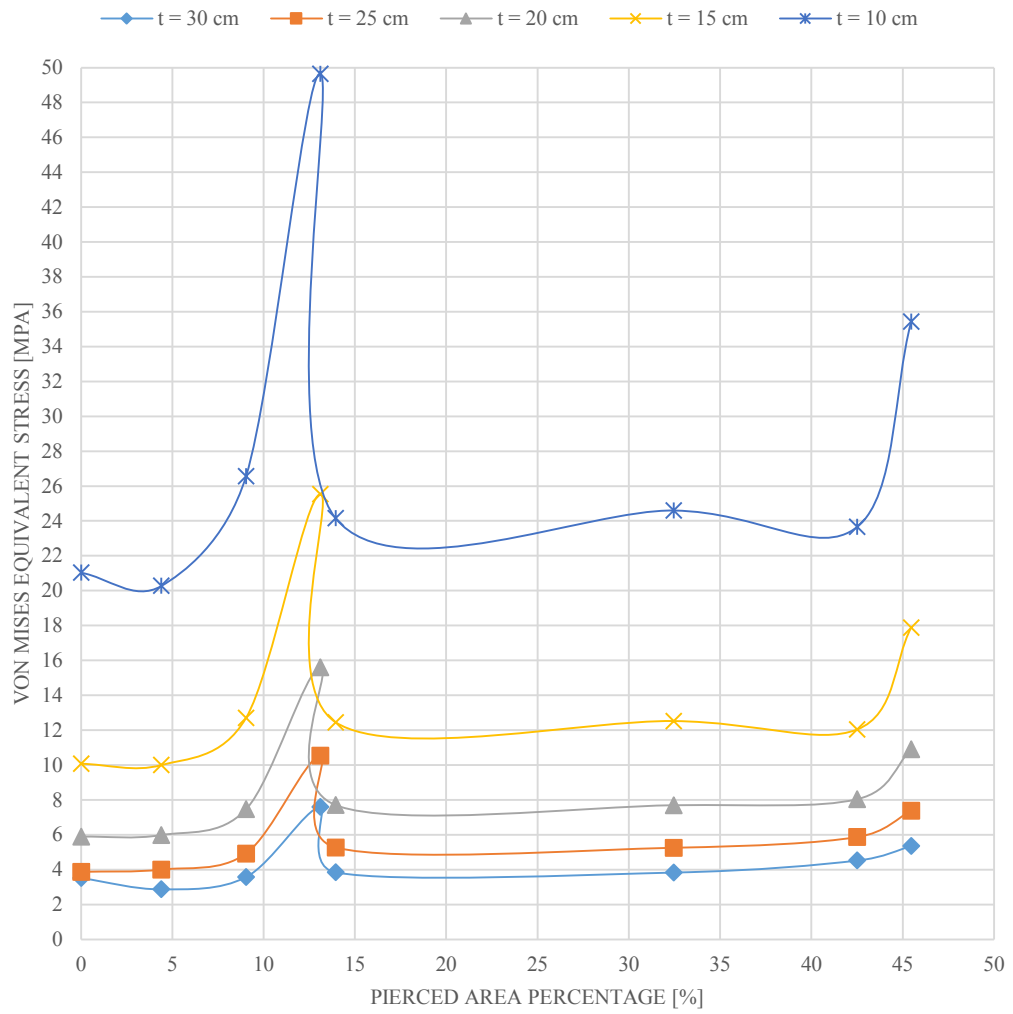


Figure 42: Graphic 2 - Pattern 2

| Pierced Area Percentage | | |
|-------------------------|-------|-----|
| No Hole | 0 | [%] |
| 4 Holes | 4.39 | [%] |
| 8 Holes | 9.03 | [%] |
| 12 Holes | 13.1 | [%] |
| 13 Holes | 13.94 | [%] |
| 33 Holes | 32.46 | [%] |
| 45 Holes | 42.5 | [%] |
| 49 Holes | 45.46 | [%] |

Table 6: Pierced Area Percentage

- **Pattern 3**

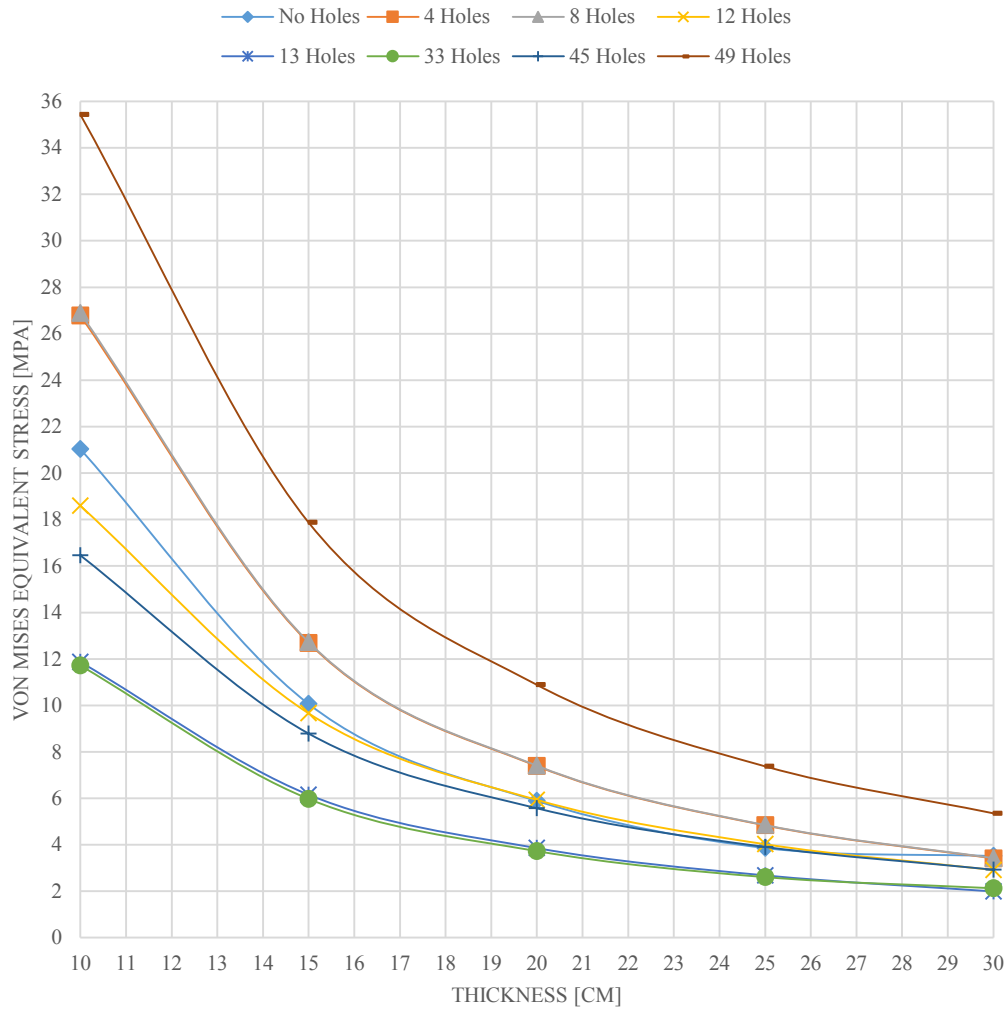


Figure 43: Graphic 1 - Pattern 3

| t | [cm] | 30 | 25 | 20 | 15 | 10 |
|---------------|------|------|------|-------|-------|-------|
| σ_{id} | | | | | | |
| No Hole | | 3.52 | 3.87 | 5.89 | 10.07 | 21.03 |
| 4 Holes | | 3.42 | 4.84 | 7.39 | 12.69 | 26.77 |
| 8 Holes | | 3.43 | 4.85 | 7.41 | 12.73 | 26.89 |
| 12 Holes | | 2.92 | 4.03 | 5.94 | 9.66 | 18.59 |
| 13 Holes | | 2.00 | 2.69 | 3.86 | 6.16 | 11.87 |
| 33 Holes | | 2.13 | 2.61 | 3.73 | 5.98 | 11.72 |
| 45 Holes | | 2.93 | 3.91 | 5.57 | 8.79 | 16.46 |
| 49 Holes | | 5.36 | 7.38 | 10.89 | 17.88 | 35.44 |

Table 7: Von Mises stresses

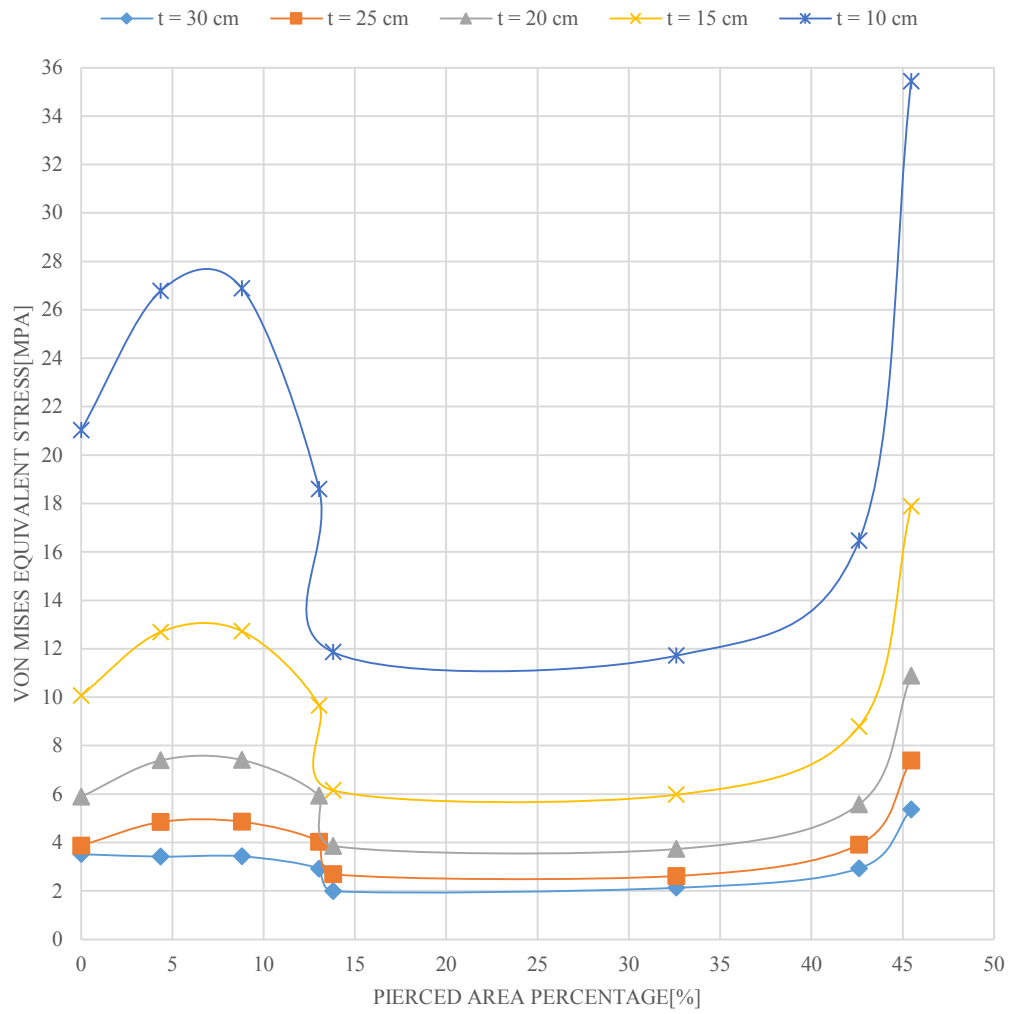


Figure 44: Graphic 2 - Pattern 3

| Pierced Area Percentage | | |
|-------------------------|-------|-----|
| No Hole | 0 | [%] |
| 4 Holes | 4.35 | [%] |
| 8 Holes | 8.81 | [%] |
| 12 Holes | 13.03 | [%] |
| 13 Holes | 13.8 | [%] |
| 33 Holes | 32.6 | [%] |
| 45 Holes | 42.6 | [%] |
| 49 Holes | 45.46 | [%] |

Table 8: Pierced Area Percentage

- **Pattern 4**

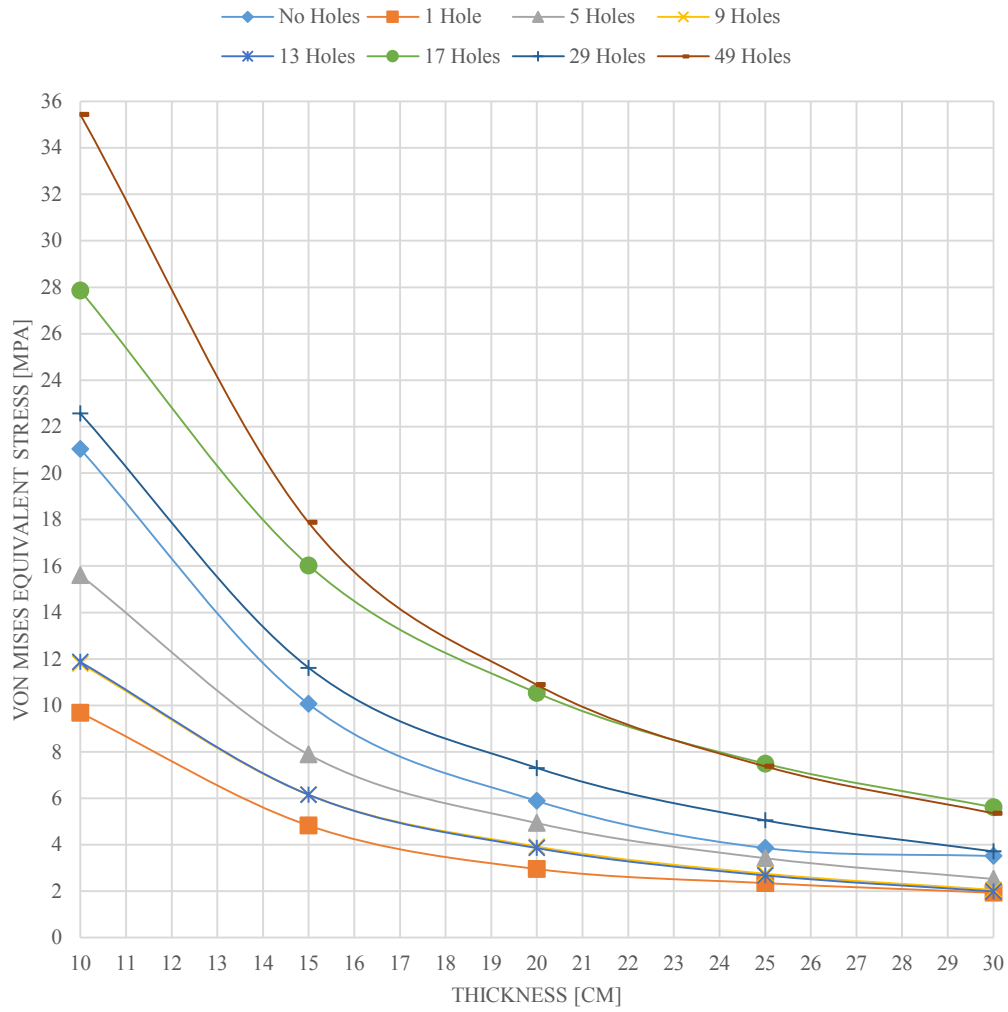


Figure 45: Graphic 1 - Pattern 4

| t | [cm] | 30 | 25 | 20 | 15 | 10 |
|---------------|------|------|------|-------|-------|-------|
| σ_{id} | | | | | | |
| No Hole | | 3.52 | 3.87 | 5.89 | 10.07 | 21.03 |
| 1 Hole | | 1.94 | 2.36 | 2.96 | 4.83 | 9.68 |
| 5 Holes | | 2.53 | 3.43 | 4.94 | 7.89 | 15.61 |
| 9 Holes | | 2.06 | 2.75 | 3.92 | 6.15 | 11.80 |
| 13 Holes | | 2.00 | 2.69 | 3.86 | 6.16 | 11.87 |
| 17 Holes | | 5.61 | 7.49 | 10.53 | 16.02 | 27.85 |
| 29 Holes | | 3.71 | 5.05 | 7.30 | 11.61 | 22.56 |
| 49 Holes | | 5.36 | 7.38 | 10.89 | 17.88 | 35.44 |

Table 9: Von Mises stresses

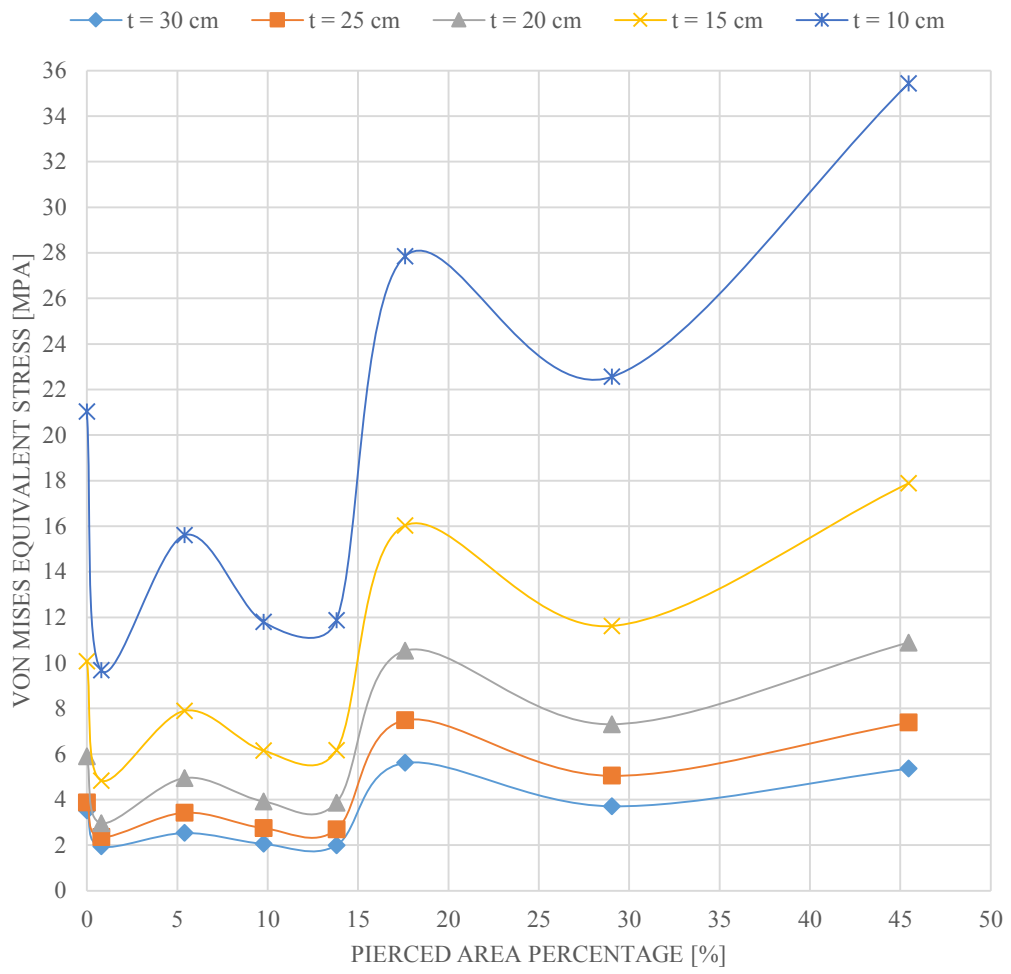


Figure 46: Graphic 2 - Pattern 4

| Pierced Area Percentage | | |
|-------------------------|-------|-----|
| No Hole | 0 | [%] |
| 1 Hole | 0.79 | [%] |
| 5 Holes | 5.4 | [%] |
| 9 Holes | 9.76 | [%] |
| 13 Holes | 13.8 | [%] |
| 17 Holes | 17.6 | [%] |
| 33 Holes | 29.04 | [%] |
| 49 Holes | 45.46 | [%] |

Table 10: Pierced Area Percentage

the results of the analysis let some considerations to be done:

- The stress trend with the decrease of the thickness is almost the same for every pattern;
- The funicular shell structure without openings is not the one with the lowest stress values; that means that if openings are placed with the right number and position can ensure a lower stress level inside the shell structure than the solution without them;
- For pattern 1 and 4 the shell structure with 1 hole, placed in the center of the structure, is the one with the lowest level of stress;
- Pattern 4 is the scheme in which the biggest number of points curve lie under a value of 6.5 MPa, the strength of the masonry kind selected;
- For Pattern 2 the solution with 12 holes, placed with a cross like scheme but without a central opening, has stress values bigger than the solution with 49 holes;
- For pattern 2, the step that involves the presence of the central opening, drop down the stresses inside the structure until the no-openings structure stress level;
- For pattern 3, the step that involves the presence of the central opening, drop down the stresses inside the structure until values lower than the ones in the solution without openings; for this pattern, with the central opening, the solution with a openings percentage lower than the one of the structure with 49 holes, are characterized by stress values lower than the one without openings.

The contour plots of the Von Mises stresses of every funicular shell structures are kept in the Attachments together with

4.6. Linear Buckling Load Analysis

“To most laymen the word ‘buckling’ evokes an image of failure of a structure which has been compressed in some way. Pictures and perhaps sounds come to mind of sudden, catastrophic collapse involving very large deformations. From a scientific and engineering point of view, however, the interesting phases of buckling phenomena generally occur before the deformations are very large when, to the unaided eye, the structure appears to be undeformed or only slightly deformed.” (Bushnell, 1981)

The goal of this analysis is to find the value of the first load multiplier that cause the elastic equilibrium instability of the structures and them deformed shape in order to understand which are the possible collapse mechanisms.

The reason why this analysis is done can be summarized again in the words of David Bushnell:

“The property of thinness of a shell wall has a consequence [...]: The membrane stiffness is in in general several orders of magnitude greater than the bending stiffness. A thin shell can adsorb a great deal of membrane strain energy without deforming too much. It must deform much more in order to adsorb an equivalent amount of bending strain energy. If the shell is loaded in such a way that most of its strain energy is in the form of membrane compression, and if there is a way that this stored-up membrane energy can be converted into bending energy, the shell may fail rather dramatically in a process called ‘buckling’ as it exchanges its membrane energy for bending energy. Very large deflections are generally required to convert a given amount of membrane energy into bending energy. The way in which buckling occurs depends on how the shell is loaded and on its geometrical and material properties. The prebuckling process is often nonlinear if there is a reasonably large percentage of bending energy being stored in the shell throughout the loading history.” (Bushnell, 1981)

From an analytical point of view, the analysis is lead as taught by the Structural Analysis. As written by Alberto Carpinteri in his *Scienza delle Costruzioni*: considering a discrete

system characterized by n degrees of freedom, and the Finite Element Model is the perfect example, the elastic equilibrium stability problem can always be written as:

$$([K] - \lambda[K_g])\{\delta\} = \{0\}$$

Where:

- $[K]$ is the **elastic stiffness matrix**;
- $[K_g]$ is the **geometric stiffness matrix**;
- $\{\delta\}$ is the **nodal displacements vector**;
- λ is a **load multiplier** that grows in a proportional way.

The eigenvalues of the problem can be found from the following condition:

$$Det([K] - \lambda[K_g]) = 0$$

The minimal eigenvalue found is called **critical loads multiplier** and it is related with the collapse solicitation for the structure. (Carpinteri, 1992)

With the LUSAS modeler and solver is possible to do a Buckling Analysis. It is important to notice that the analysis is a linear one. The problem has got big non-linearity features, both geometrical and mechanical, but for a general interpretation of the global stability behavior, the analysis offered by LUSAS is considered enough.

Indeed, a linear buckling analysis can be considered as a useful technique applied to relatively stiff structure to estimate the maximum load that can be supported prior to structural instability or collapse.

LUSAS Modeller manual gives the conditions applied by the software. It assumes that the stiffness matrix does not change prior to buckling, and that the stress stiffness matrix is simply a multiple of its initial values as explained by the previous equations. With these assumption, the linear buckling analysis can only be used to predict the load level at which a structure becomes unstable and pre-buckling displacements and their effects are negligible. The linear problem is solved only after the assemblage process of the stiffness matrix and the software prescribe that only elements with geometric non-linear capability can be used in a linear buckling analysis: this is respected by the case study because the TSL6 element used for the mesh definition has got geometric nonlinear capability.

The buckling load for a mode is obtained by multiplying the actual magnitude of the applied loading by the eigenvalue found.

Absolute displacement output is not available from the analysis but it is shown in a normalized state so the eigenvectors are normalized to unity with the maximum translational displacement degree of freedom is set to one.

As written in the introduction of this paragraph, the structures analyzed are the same used for the stress analysis under concentrated loads. However, the linear buckling analysis is feasible by the LUSAS Solver only if distributed loads are applied on the model.

In order to understand better the behavior of these kind of structures, different situations are analyzed. It is explored the behavior through the load condition (symmetrical or anti-symmetrical) and lowering condition (three different cases) variation.

The lowering degree is defined as:

$$R = \frac{D}{H}$$

Where:

- H is the maximum height of the structure counted from the support quote;
- D is the structure principal diagonal of the projection on the horizontal plane.

As written three different lowering conditions are analyzed:

$$R_1 = \frac{24}{5} = 4.8 \quad R_2 = \frac{24}{2.5} = 9.6 \quad R_3 = \frac{24}{7.5} = 3.2$$

R_1 is about the already shown structures, while in order to be able to analyzed the structures characterized by R_2 and R_3 it is necessary to repeat all the form finding process as explained in the previous sections: the input data are the same with the only difference of the height modifiable changing the scale of the force diagram when the Thrust Network Analysis is applied.

It is useful, for the interpretation of the analysis result, to get how slenderness is defined during the study:

$$\eta = \frac{D}{t}$$

Where:

- t is the thickness of the cross section of the shell structure.

5 thickness values are defined for the case study so 5 slenderness values are present:

| t | η |
|------|--------|
| [m] | [-] |
| 0.3 | 80 |
| 0.25 | 96 |
| 0.2 | 120 |
| 0.15 | 160 |
| 0.1 | 240 |

Table 11: slenderness values

Two different conditions are also analyzed about load-cases. It is important to remind that the case study is about a structure with geometrical symmetry and consequently all the considerations and results are about this construction typology. However, the first load-case is the symmetrical one in which all the vertical loads are applied as gravity uniformly distributed loads all over the upper surface of the shell structure with z-axis direction. The second load-case is the anti-symmetrical one where only the dead load is applied as gravity uniformly distributed load all over the upper surface; the anti-symmetrical case is generated because of the application of variable or accidental loads as uniformly distributes loads only on a half of the upper surface of the shell structures. Both the loads of the second load-case have to be considered as applied with z-axis direction.

In the following figure is shown the model of the structure for symmetrical loads:

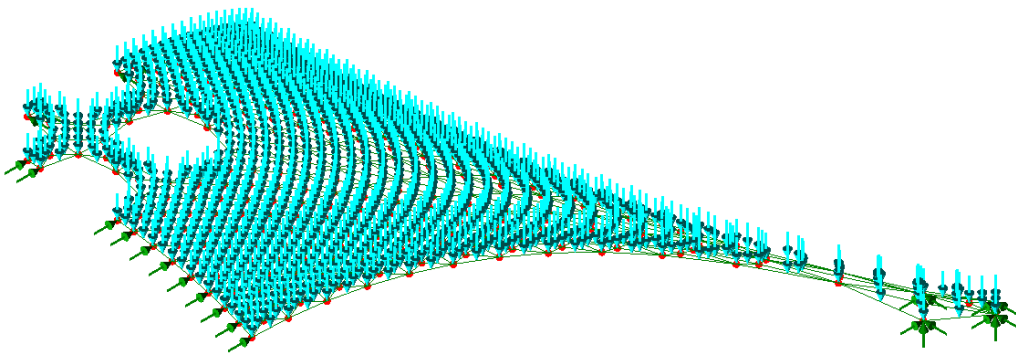


Figure 47: structural model for symmetrical load condition

The second load case and condition has to be modeled in a different way than the first in order to be analyzed in the right way from the LUSAS Modeller and Solver, for R_1 , R_2 and R_2 geometries. It is not enough to model only a quarter loaded part of the structure to represent the anti-symmetrical load-case anymore.

As shown in the following figure, a half of the structure has to be modeled in the Finite Element Modeler environment. The whole modeled structure is loaded by self-weight of the structure but only a half part of it, so a quarter part of the whole one, is subjected to live loads.

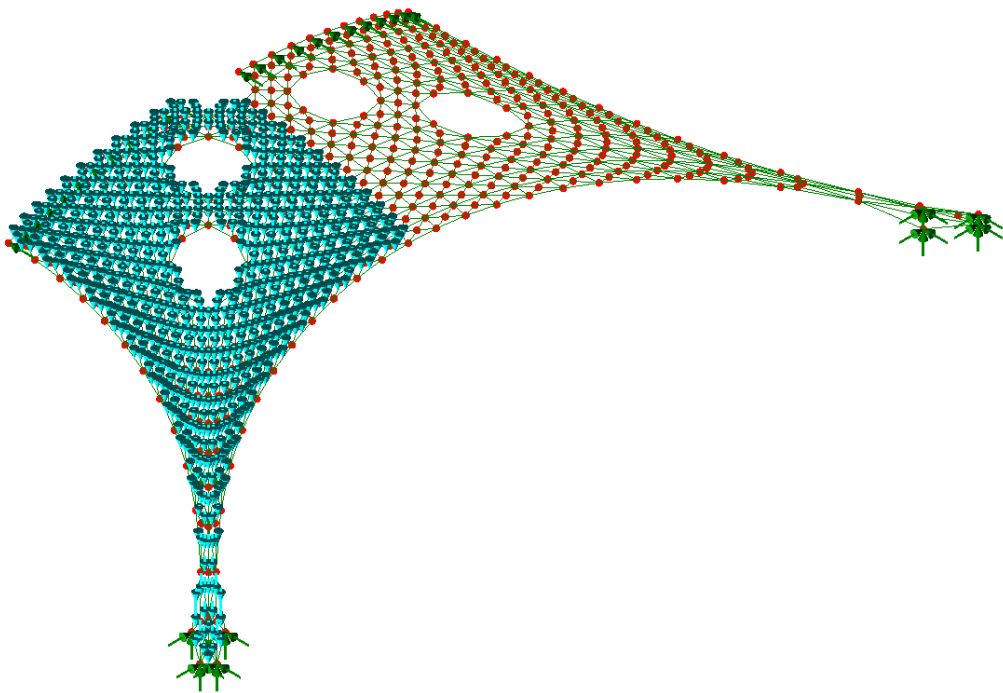


Figure 48: Structural model for anti-symmetrical load condition

The load considered and applied on the structure are:

- **Self-weight or Dead load:** the value of the uniformly distributed load is function of the slenderness of the shell structure and of the material density. In this case study a masonry kind with 15 kN/m^3 density is used. Both for symmetrical case and anti-symmetrical one this load is applied on the whole upper surface of the structure.
- **Live Loads:** the upper surface of the shell analyzed is not designed thinking about people on it so the only one gravitational live load applicable is the snow one. A value of 1.5 kN/m^2 is considered. The value is think for a structure built in Italy

in *Zone I* as defined from the *D.M. 17/01/2018*. Live loads are the ones that govern the symmetrical or anti-symmetrical condition for the structure.

The support conditions are the same illustrated in the previous paragraph and they considered the structure as hinged at the four corners.

In the next part of the section results coming from the structural analysis done with LUSAS Modeller and Solver are reported.

They are illustrated from two different point of view. The first one is composed by tables:

- **Critical load multiplier** (λ) for the current load-case, function of the slenderness of the structure;
- **Critical live load resultant**: is the resultant of the loads that is possible to apply to the structure, without considering self-weight, in incipient buckling conditions;
- **Critical uniformly distributed live load**: is the maximum uniformly distributed load that is possible to apply to the structure, without considering self-weight, in incipient buckling conditions.

The second one is composed by graphics where the previous critical values are visualized in function of the holed area percentage.

The values in the tables and in the graphics are all normalized respect to the referring maximum values of each lowering degree condition that are:

- **Maximum critical load multiplier:**

$$\lambda_{max,R_1} = 27.85$$

$$\lambda_{max,R_2} = 12.59$$

$$\lambda_{max,R_3} = 33.83$$

- **Maximum critical live load resultant:**

$$F_{max,R_1} = 13665 \text{ kN}$$

$$F_{max,R_2} = 6241 \text{ kN}$$

$$F_{max,R_3} = 17853 \text{ kN}$$

- **Maximum uniformly distributed live load:**

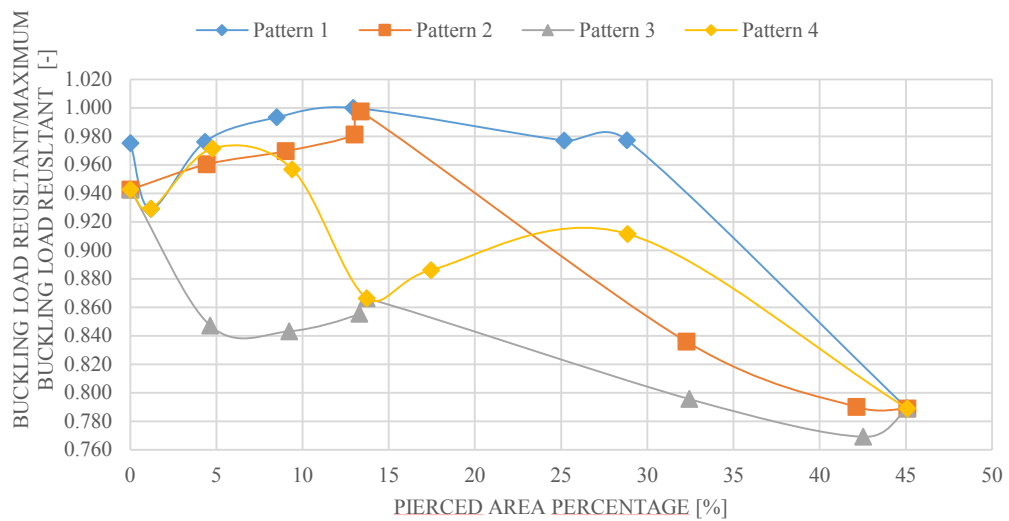
$$q_{max,R_1} = 163 \text{ kN/m}^2$$

$$q_{max,R_2} = 71 \text{ kN/m}^2$$

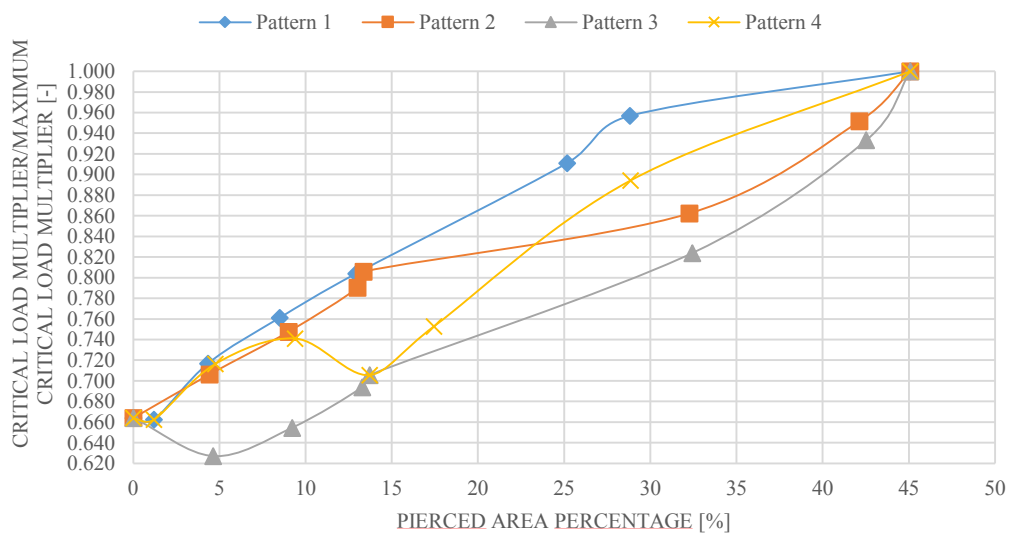
$$q_{max,R_3} = 198.5 \text{ kN/m}^2$$

All the graphics and the values obtained from the buckling load analysis are included in this paper as attachment. In this section one example of them is presented:

CRITICAL LIVE LOAD RESULTANT



CRITICAL LOAD MULTIPLIER



The two graphs are representative of the structure with lowering value of 3.2 (the 7.5 meters high one case), slenderness equal to 80 (the 30 cm thick one case) and considering a symmetrical load condition.

Each line represents one of the 4 patterns and each point represents one structure subjected to linear buckling load analysis.

From the analysis of the results of the R_1 lowering condition case it is possible to do some considerations:

- For every shell structure, when the central hole is generated, the relative structure is always more stable than the previous one both from the critical load and critical load multiplier point of view;
- Shell structures belonging to the Pattern 1 seem to be always more stable, both from the critical load and critical load multiplier point of view, than all the others. This situation seems to be independent from the holed area percentage;
- For pattern 1, that seems to be the best performer one, in the equilibrium elastic stability world, presents growing or sub-constant critical values for a holed area percentage lower than more or less 30%. It means that the structure has a better behavior if the holed areas are placed in the central part, the highest one, as far as possible from the edges and/or the constrained areas.
- An intuitive behavior can be confirmed by the analysis. Indeed, the most unfavorable conditions, always from the stability point of view, are generated when the slenderness and the holed area percentage grow and, as written above, when the distance from the edges and from the constrained area decrease;
- It is important to notice that even for the worst condition, the critical load multiplier is always bigger than 1: it means that, for the analyzed structures, each one is stable for the serviceable loads conditions. The lowest values belong to the shell structure with 8 holes of Pattern 3 with a slenderness of $\eta = 240$ and anti-symmetrical load conditions and is

$$\lambda = 2.71;$$

- The behavior trend of the critical uniformly distributed live load is always very similar to the critical load multiplier one and not to the critical live load resultant one.

The results coming from the two other lowering conditions are very close to the ones done above with some differences:

- Higher is the shell structure and so lower is the lowering value R_i , higher are the critical values both in term of load multiplier and uniformly distributed live load;
- Also for the worst condition, that means lowering value equal to 9.6 and slenderness equal to 240, the load multiplier is always bigger than one and the structures can be considered stable for serviceable load conditions;
- For lowering condition with value 9.6 for symmetric load conditions it's possible to see, through the graph analysis, a different behavior respect to all the other cases. Indeed, for slenderness smaller than 240, the curves have not the trend expected. The reason come from the modest height of the shell respect to its planar dimension that is cause of very high horizontal forces and reaction that are dangerous for structures like the one analyzed. The curves trend returns to be the known one for a slenderness value of 240 that means that in that case the weight of the structures and the applicable live loads are not higher enough to create a situation like the one described just above.

The analyzed case is only a study case and it has not the claim to represent the general behavior of compression only structure realized from a Form finding process. Indeed, no automatic algorithms were employed to create and analyze each structure in each load condition but all the process was hand controlled and realized. However, 720 different shell structures were analyzed, and the amount of data started to be too big to be an integrated part of the work and this is the reason because them are kept as attachments.

Furthermore, it is essential to give as a sort of solution, a smart representation of the results. Two graphs, illustrated in the next pages, were created to sum up all the analyses and they let the reader to explore the best found solution in function of the different parameters considered by the authors or directly chosen by the reader itself.

In order to better understand the following output some considerations are necessary:

- D is the diagonal of the horizontal squared projection of the shell structure;
- h is the maximum shell height;
- D/h is the lowering value and it is the value represented on the y-axis so three values are considered;
- *Slenderness* is the η considered and it is the value represented on the x-axis so five values are considered;
- The first graphic is referred to the critical load multiplier while the second one is referred to the critical live load resultant always considering that values without the self-weight of the structure so it represents the effective applicable load resultant to the structure;
- Circles with different radius values are present in the graphics. A number is present beside each circle and it is included between 0 and 1. This number, and consequently the circle dimensions, represents the value of the referring variable (critical load multiplier or critical live load resultant) normalized to the maximum one considering each lowering condition. This means that for each lowering condition it is present a structure with value equal to 1;
- The circles may have different colors representing the pattern which the values illustrated are referred to;
- Beside every circle is present a text line in which is written the shell structure that is represented by the circle and the number;
- Since different collapse mechanisms are present, also this feature is indicated in the output.

In the next two diagrams are also put in evidence the different mechanisms of collapse that characterize the structure when the load assumes its critical value. For the case studied two different mechanisms are present. The first one is the most general one and it is the one expected from everyone who want to load a structure like those with vertical loads and it is the one presented in the next figure. The quarter of shell represented in the image is only a general example for whole the structures which present this mechanism that are included in the light blue polygon in the graphics. This collapse mechanism can be identified with the name Mec A.

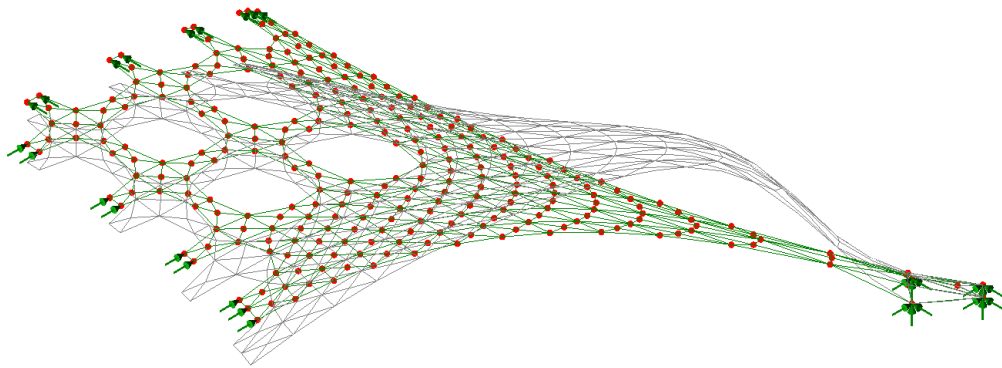


Figure 49: Mec A. Example for the first Mechanism of Collapse

The second mechanism occurs only for two of the whole number of examples presented in the two graphics and it is the one presented in the next figure as Mec B. in the graphics the structures characterized by Mec B are included in the red polygon.

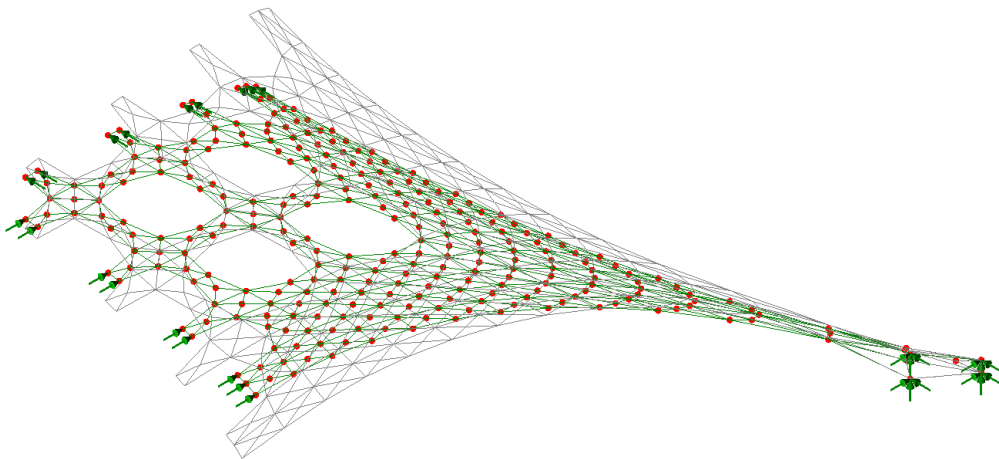


Figure 50: Mec B: Example for the second Mechanism of collapse

Even if not represented as one of the most stable case, it is important to notice that for anti-symmetrical loads it is possible to identify another mechanism of collapse. The one presented in the next figure and called Mec C. this mechanism of collapse is the one expected under the load conditions described above. In function of the slenderness and of the lowering condition the absolute magnitude of the deformed shape in collapse incipient conditions is not the same. In the figure is represented only a general example to better understand the shape of the so called Mec C.

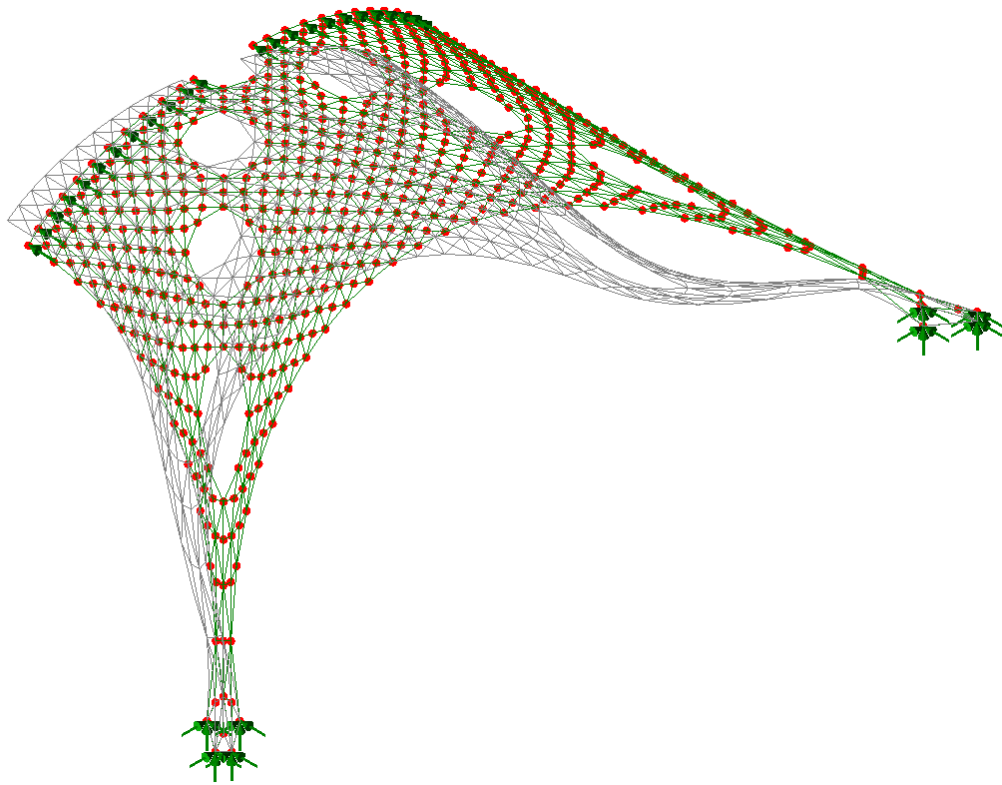
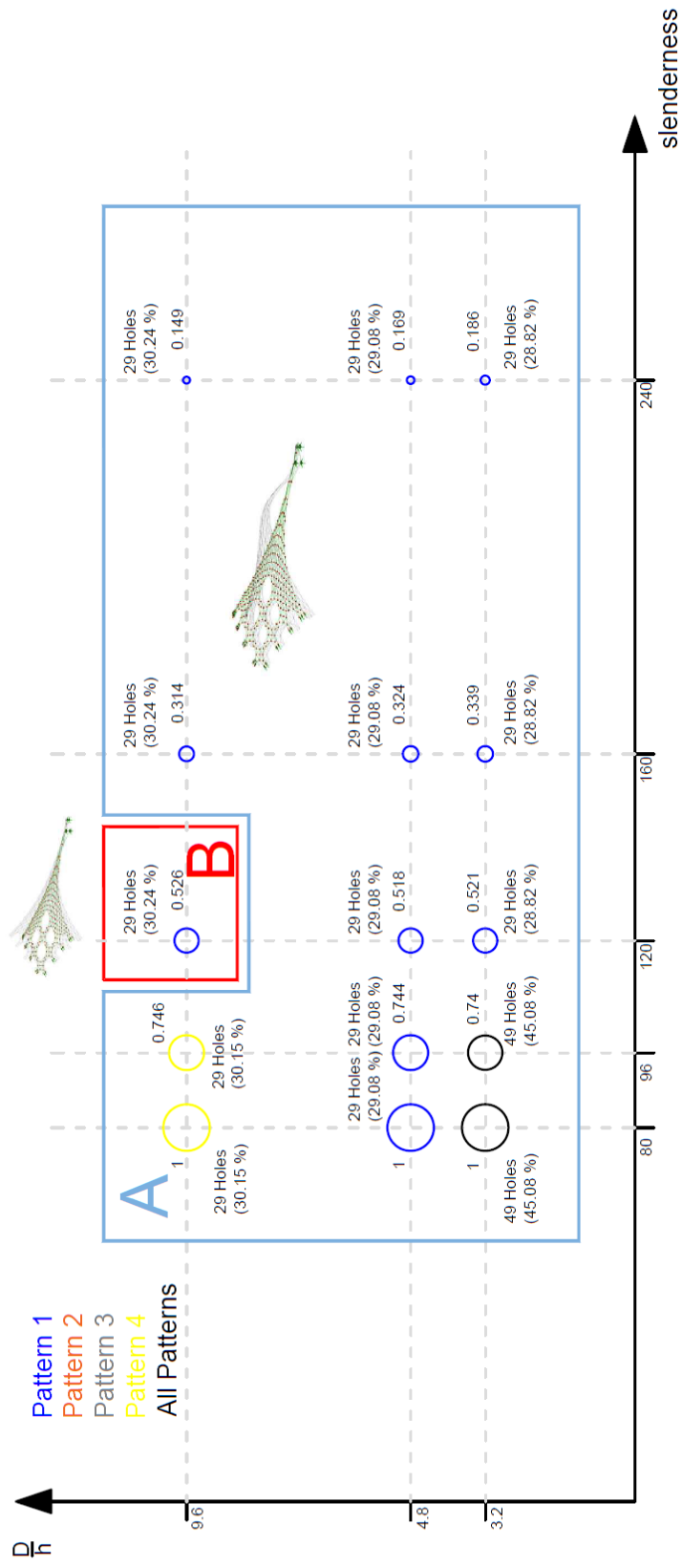
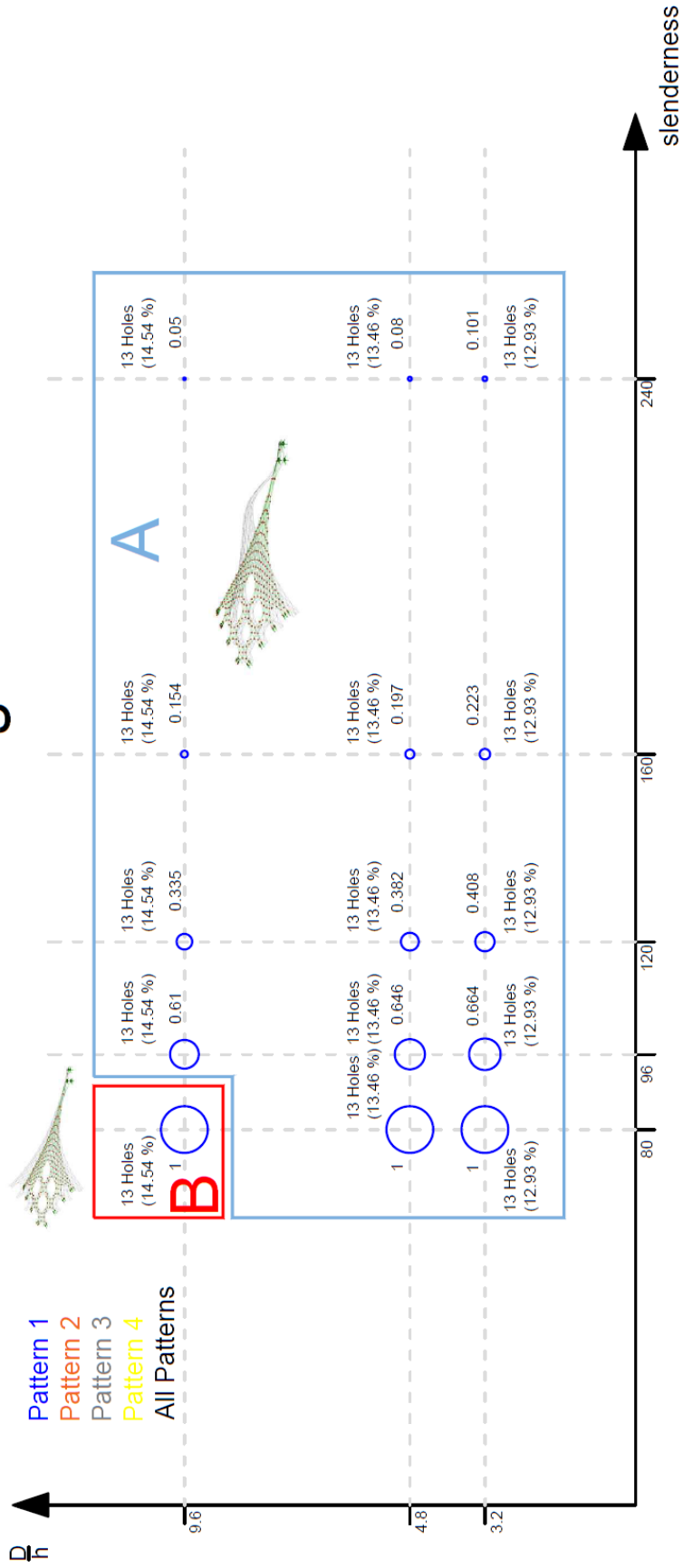


Figure 51: Mec C: Example for the second Mechanism of collapse

Critical Load Multiplier



Critical Buckling Live Load



5. Scaled Prototype Realization

In the previous chapters of this work the focus was on form finding methods applied to think, draw and design funicular shapes. Numerical methods let the designer to interact with complex geometries impossible to deal with in the physical model environment. Indeed, before the so called digital revolution the only way to study and manage the complexity of building projects was to divide them into individual parts trying to assemble them together only after in a following phase of the design process. Only a few number of architects and designers, such as Heinz Isler or Antoni Gaudì, were able to manage those complex shapes like the ones illustrated in this work and in literature without the help of contemporary CNC (Computer Numerical Control) processes.

A second great challenge is represented by the fabrication through discrete elements of the studied and designed geometries. In particular, this challenge is characterized by the condition that oblige to create a structure where discrete elements remain unconnected after the building construction. This constrain involve higher requirements than the ones used for structures where the elements are mechanically connected in order to create stiff surfaces. The first fundamental and most important requirement is the only-compression stress state when self-weight and external loads act on the structure. It affects a lot the design of the tessellation geometry. Furthermore, it is important to remind that the voussoirs will have low/negligible tensile and high compressive strength. To ensure structural stability is impossible to realize the vaults if it will not act purely in compression.

However, the relevant constraint for the fabrication process can be summed up in:

- **Architectural and tectonic requirements:** they include all the considerations that influence the overall shape also in function of the tessellation geometry and the surface texture and finish;
- **Structural requirements:** they need a design process the guarantee the static equilibrium of the final funicular shape. They determine the slenderness of the shell in order to avoid global buckling. To avoid in-plane sliding failure between discrete elements is fundamental that all the contact faces are orthogonal to the local force flow; in this way the friction resistance could be present because it is

proportional to normal forces. The voussoirs geometry has to be designed to ensure that contact faces are aligned normal to the force flow.

“A good tessellation geometry provides the necessary interlocking between blocks such that they form a stable, three-dimensional structural surface. This strategy creates, for example, a staggered stretcher bond. [...] Finally, interlocking features at the interface between neighbouring voussoirs are necessary to prevent local out-of-plane sliding”;
(Rippmann, 2016)

- **Fabrication requirements:** they are function of the construction material and its production processes.

Based on the previous consideration, in this chapter the design and the fabrication of a scaled prototype of a pierced vault is realized. The goal is to validate the global stability analysis illustrated in the previous chapter and to illustrate the link between design and fabrication processes. The prototype is realized with cement blocks casted into 3d printed formworks representing the voussoirs geometry coming from the tessellation pattern design. Furthermore, considering the construction phases, a falsework made by cardboard sheets is realized.

5.1. The Geometry

Based on the two final diagrams reported at the end of the previous chapter, one of the vaults is chosen to be realized as a scaled prototype. The main parameter which leads the choice is the critical load multiplier and the referring diagram is the first one. The vault chosen is the one with the higher value of the critical load multiplier between the structures with a slenderness value of 80 and a lowering degree value of 3.2. This mean that the pierced vault is the one with 49 holes and a pierced area percentage of 45.08 %, 7.5 meters tall and with uniform transverse section thickness of 30 cm.

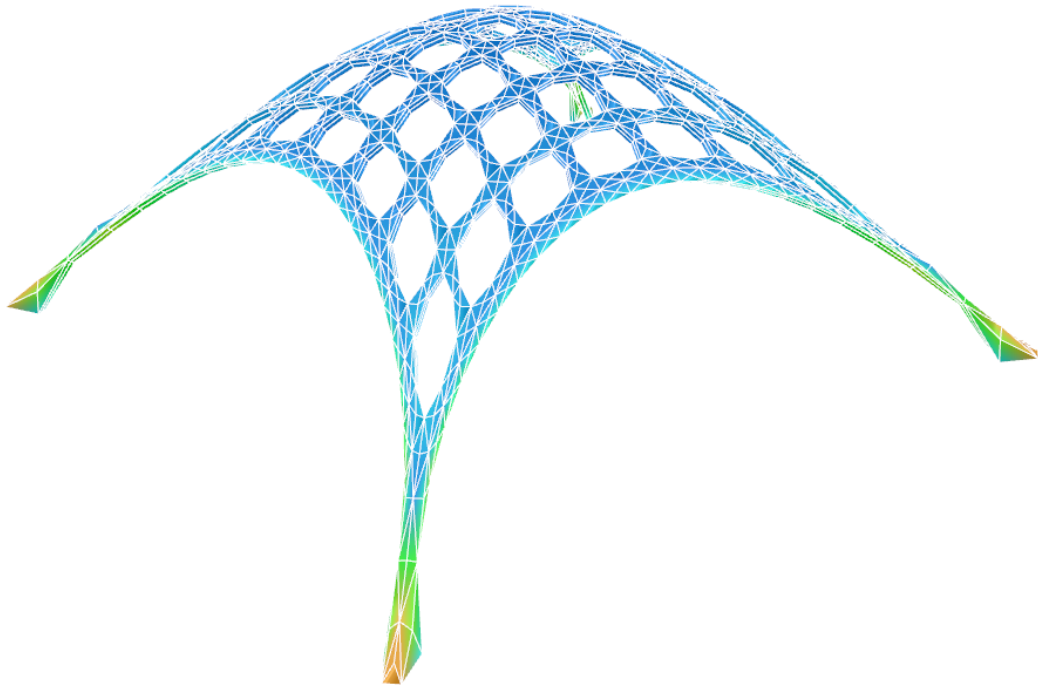


Figure 52: Geometry representation of the chosen vault from the Rhino VAULT output

The representation scale chosen, arbitrarily, is 1/16 in order to have the plan side dimension almost equal to 1 m. Consequently, the prototype will be 46,9 cm tall and it will have a uniform transverse section thickness of 18.75 mm.

5.2. First Tessellation Pattern Trial

Masonry structures have been realized for thousand years and skilled masons were capable to find the right tessellation pattern even for even the most complex shapes and structures. Based on this long history and on the requirements described in the previous section, three relevant features can be defined according to Rippmann doctoral thesis:

- *“Voussoirs should be aligned such that the load-transferring contact faces as perpendicular as possible to the local ‘force flow’ to prevent sliding failure;*
- *The tessellation pattern should be staggered or similarly laid out to ensure an interlocking voussoir arrangement;*
- *The size of voussoirs should be as uniform as possible over the entirety of the surface.”* (Rippmann, 2016)

In order to design a first tessellation pattern trial, the form diagram of the resulting geometry coming from the form finding process is considered.

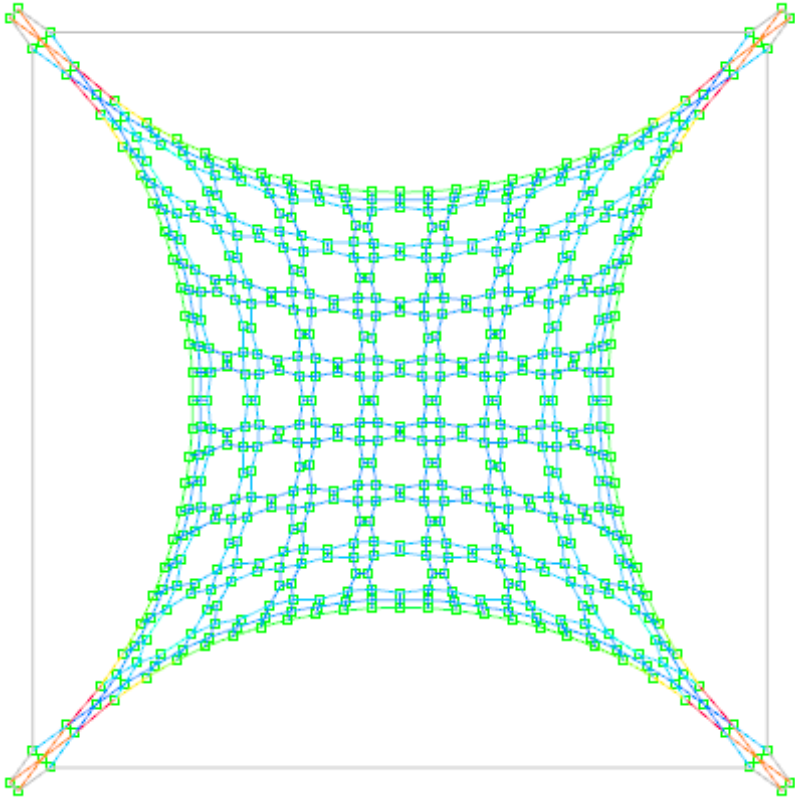


Figure 53: final form diagram of the chosen vault

The quadrangular grid could also be seen as the discretization of the flow force due to external vertical loads, so it has been used to design the tessellation pattern. Taking advantage of the double symmetry of the geometry, only a quarter of the vault is considered for the voussoirs geometry design.

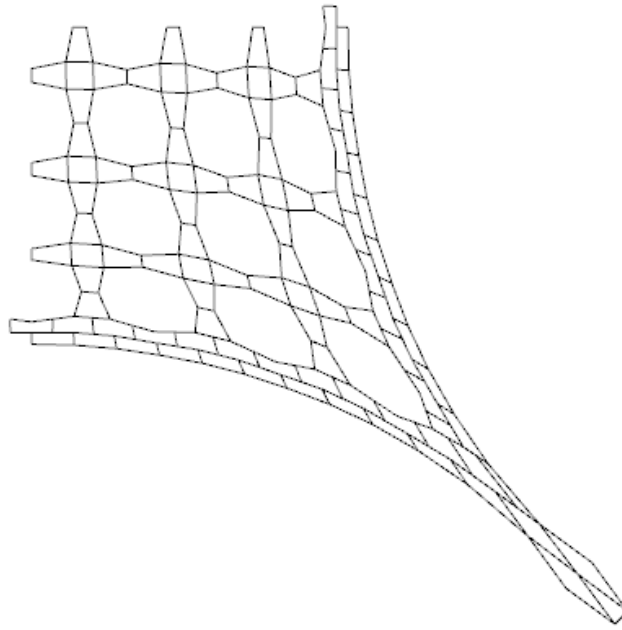


Figure 54: first tessellation pattern trial

The designed pattern is drawn on the middle surface of the vaults; this happens because the Thrust Network Analysis return the middle surface geometry of the structure after the form finding process. Therefore, is necessary to represent the real 3D volume of the vault to design the blocks geometry.

Grasshopper 3d represent the best tool to deal with the problem. The software, native inside Rhinoceros code and environment, let the designer to approach problems from an algorithmic and parametric point of view. More explanations about this tool are illustrated in the Appendix A of the work.

In figure 39 are represented the Grasshopper 3D components used to create the volume of the vault from its middle surface:

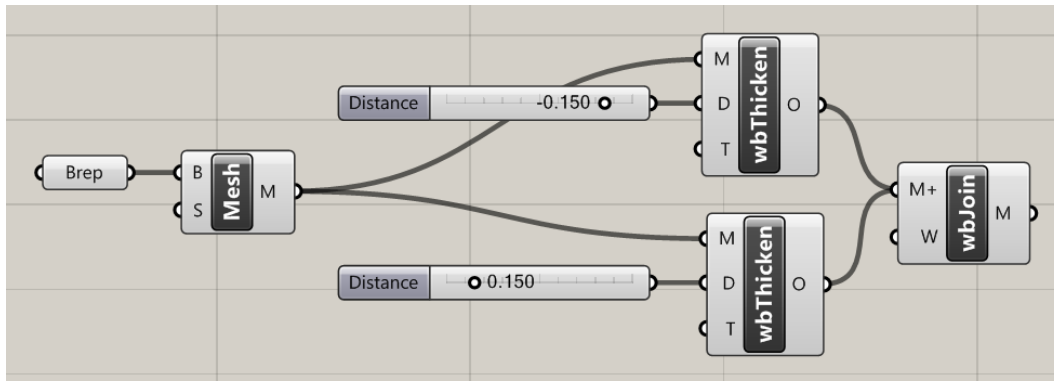


Figure 55: Grasshopper 3D code for the vault's volume representation

The first component *Brep* contain the geometry of the vault. The term *Brep* represent a geometrical parameter defined as a non-abstract class that allows the programmer to create a shape consisting of multiple and/or trimmed surfaces. A *Brep* maintains many lists of geometric entities, including faces, edges, trims, loops and vertices. All of these are associated with each other via topological relationships. Indeed, the vault's geometry is represented as a polysurface in the Rhinoceros CAD environment and it is seen as a *Brep* from Grasshopper.

The second component convert the *Brep* element in a *Mesh* element. This step is necessary because the components that create the volume of the selected geometry manage only *Mesh* elements. These components are included in a suite called *Weaverbird*.

Weaverbird is a topological modeler that contains many of the known subdivision and transformation operators, readily usable by designers. Instead of doing the work repeatedly, or sometimes using complicated scripts, this plug-in reconstructs the shape, subdivides any mesh, even made by polylines, and helps preparing for fabrication.

In particular, the *Weaverbird's* *Mesh Thicken* component, computes a new mesh as a closed solid from a starting offsettable and oriented mesh. Indeed, setting the *Distance* parameter on 0.15 m and -0.15m, it was possible to find the volume of the vault above and below its middle surface. The results are presented in figure 40a and 40b.

The last component represented in figure 39 join the two meshes created into 1 closed *Mesh*.

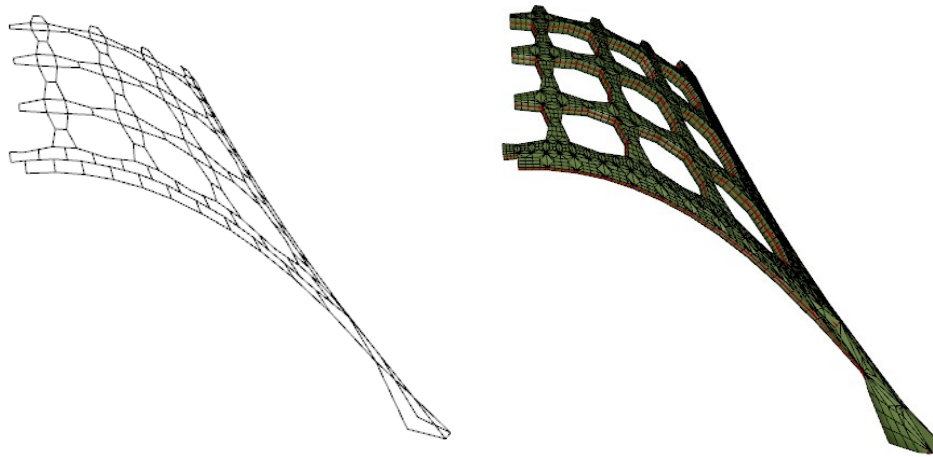


Figure 56: geometry of the vault before Grasshopper 3d, including the first tessellation pattern trial (a) and geometry of the vault after Weaverbird's Mesh Thicken (b)

In the following step, the voussoirs are created from the obtained 3D geometry of the vault. The closed mesh representing the structure is divided into its line components through Weaverbird's Mesh Edges component inside Grasshopper 3D environment. Starting from the tessellation pattern illustrated above, the volume of each block is pulled out from the complete geometry of the structure, ordered with a numerical code and classified.

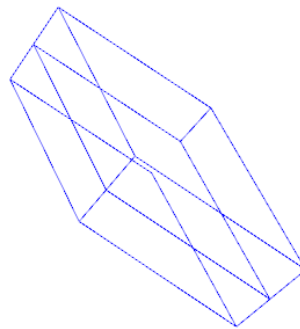


Figure 57: Example of Pulled out Voussoir - Block n.45

The complete voussoirs' classification is illustrated in figure 42. The numerical code starts from the number 08 because the first seven blocks were joint together in order to create the base of the structure.

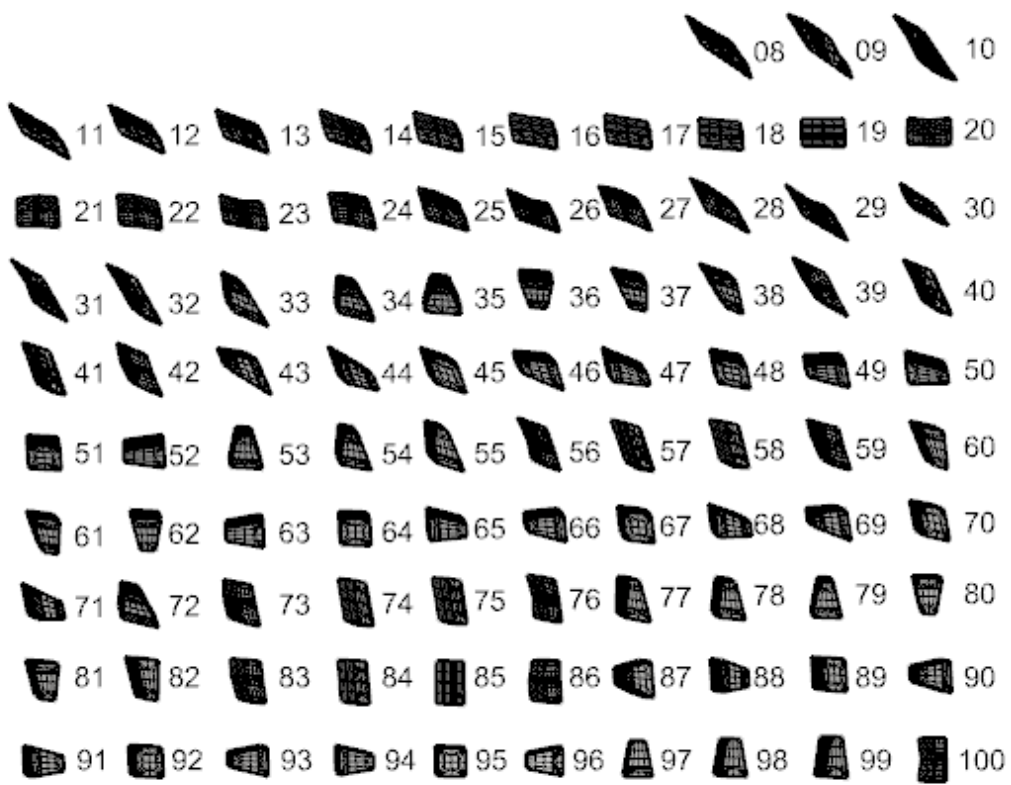


Figure 58: Voussoirs' classification and codification

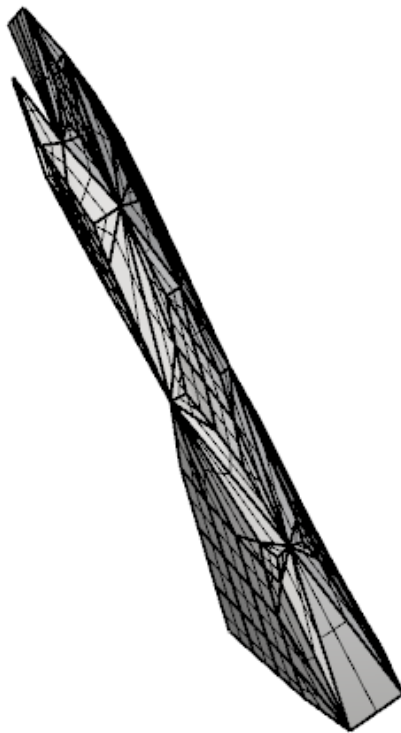


Figure 59: Base element

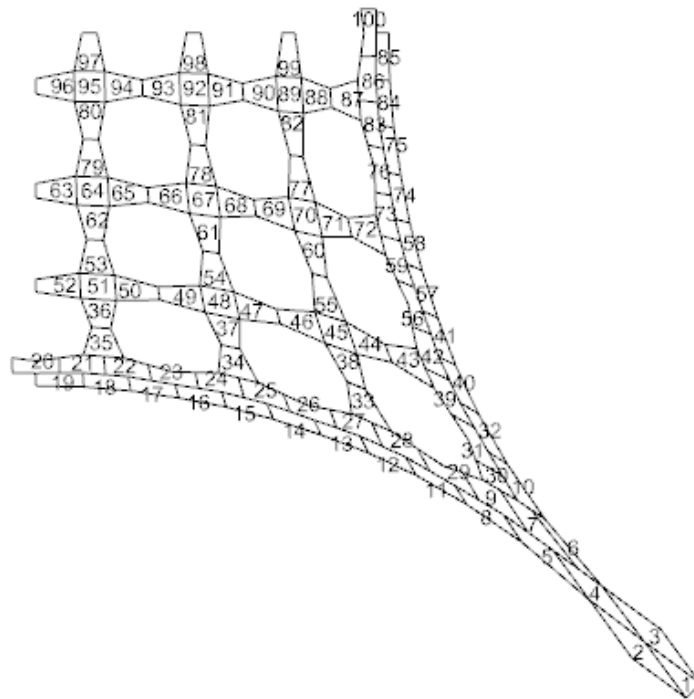


Figure 60: *Voussoirs' classification and codification*

5.3. Voussoirs Fabrication

The designed voussoirs, scaled to the prototype dimension have to be fabricated and assembled together to build the vault's prototype. In the last section their geometry has been designed paying attention to their contact faces that have to be normal to the local force flow.

The voussoirs have to be realized in cement so a mould system has to be designed for the casting. The material choice, that has got a high density value, comes from the necessity to have the as big self-weight as possible to materialize the compression between contact faces in order to have enough friction contribute to keep the blocks aligned.

The real challenge in the formworks realization is that they need a high geometrical accuracy and they are quite small: they are only 18.75 mm tall and their plan's dimension are variable between less than 2 cm and almost 5-6 cm.

The Additive Manufacturing technology has been chosen to realize them.

The term Additive Manufacturing references technologies that grow three-dimensional objects one superfine layer at a time. Each successive layer bonds to the preceding layer

of melted or partially melted material. It is possible to use different substances for layering material, including metal powder, thermoplastics, ceramics, composites, glass and even edibles like chocolate.

Objects are digitally defined by computer-aided-design (CAD) software that is used to create .stl files that essentially slice the object into ultra-thin layers. This information guides the path of a nozzle or print head as it precisely deposits material upon the preceding layer. Or, a laser or electron beam selectively melts or partially melts in a bed of powdered material. As materials cool or are cured, they fuse together to form a three-dimensional object.

This technology is composed essentially by three steps:

- Creation of a digital 3D model. Some criteria are present to divide digital models in printable or unprintable ones. The main one is that they have to be represented by a closed mesh;
- Conversion of the digital model into a coded based machine-readable format. The most common file extension is the .stl (Standard Tessellation Language).

“This file format is supported by many other software packages; it is widely used for rapid prototyping and computer-aided manufacturing. STL files describe only the surface geometry of a three dimensional object without any representation of color, texture or other common CAD model attributes. The STL format specifies both ASCII and binary representations. Binary files are more common, since they are more compact. An STL file describes a raw unstructured triangulated surface by the unit normal and vertices (ordered by the right-hand rule) of the triangles using a three-dimensional Cartesian coordinate system.”
(Ciobota, 2012)

- 3D printing the object.

Stereolithography (SLA), Selective Laser Sintering (SLS) and Fuse Deposition Modeling (FDM) are three of the most popular 3D printing techniques. FDM is the technology chosen to realize the formworks.

“FDM printing was developed in 1988 by Scott Crump. FDM printers form geometry by melting plastic filament and depositing thin layers additively on a platform. The FDM printers [...] require support structures for overhanging parts. Some FDM printers can print multiple materials, in this way supports can be printed in a material that is easy to remove; such as water soluble filament. FDM printers use two types of plastic; ABS [the Lego plastic], or an organic version: PLA” (Tedeschi, 2014)

The formwork has to be designed from the block geometry using the same GH-code (Grasshopper Code) used to create the volume of the vault. However, some difference is present. First of all, for each block only the lateral surface has to be considered and modelled as a polysurface and converted by Grasshopper in a mesh element.

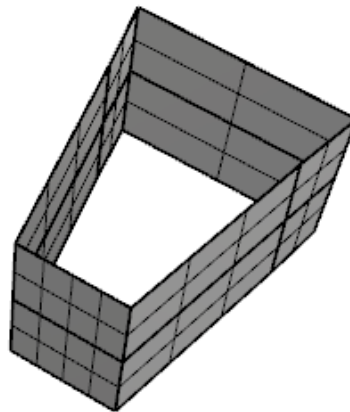


Figure 61: Example of a CAD formwork model for GH-code - Block n.97

Referring to Figure 39 where the GH-code is shown, the Distance parameter is now set with the value of 0.002. It means that the designed formwork will be 2 mm thick.

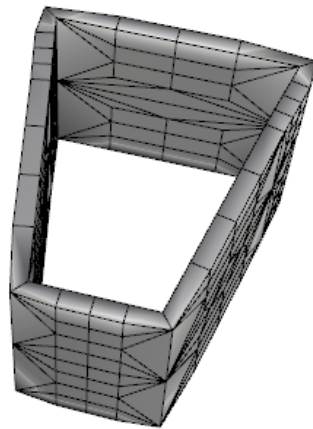


Figure 62: Example of a 3D formwork model ready to be exported and printed - Block n. 97

The designed formwork is represented in Rhinoceros CAD Environment as a closed mesh element so it is suitable to be exported as a STL file.

In order to be printed with the FDM technology the STL file needs to be elaborated by one of the freeware commercial softwares available on internet that process the digital model changing different parameters useful for the desired object realization: Ultimaker Cura Software and Makerbot Print are the two software chosen in function of the different 3d printers used for the Additive Manufacturing process.

The most relevant parameters set up for the 3D printing process are:

- Filament material: PLA;
- Filament diameter: 1.75 mm;
- Layer Height: 0.2 mm;
- Fill density: 30 %;
- Print Speed: 80 – 150 mm/s;
- Printing temperature: 215 °C.

Regarding the four base elements, they have not been realized in cement and their geometry has been directly fabricated with the FDM technique with the same settings of the formwork elements.

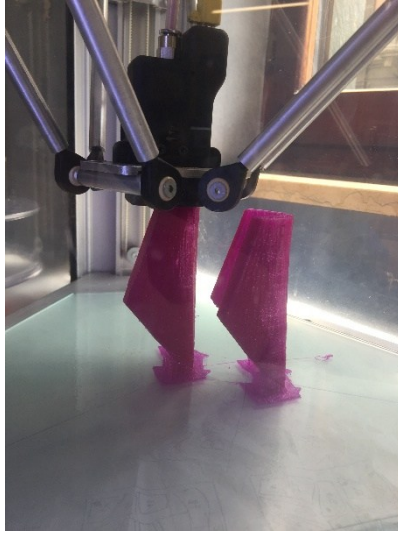


Figure 63: 3D printing of the bases

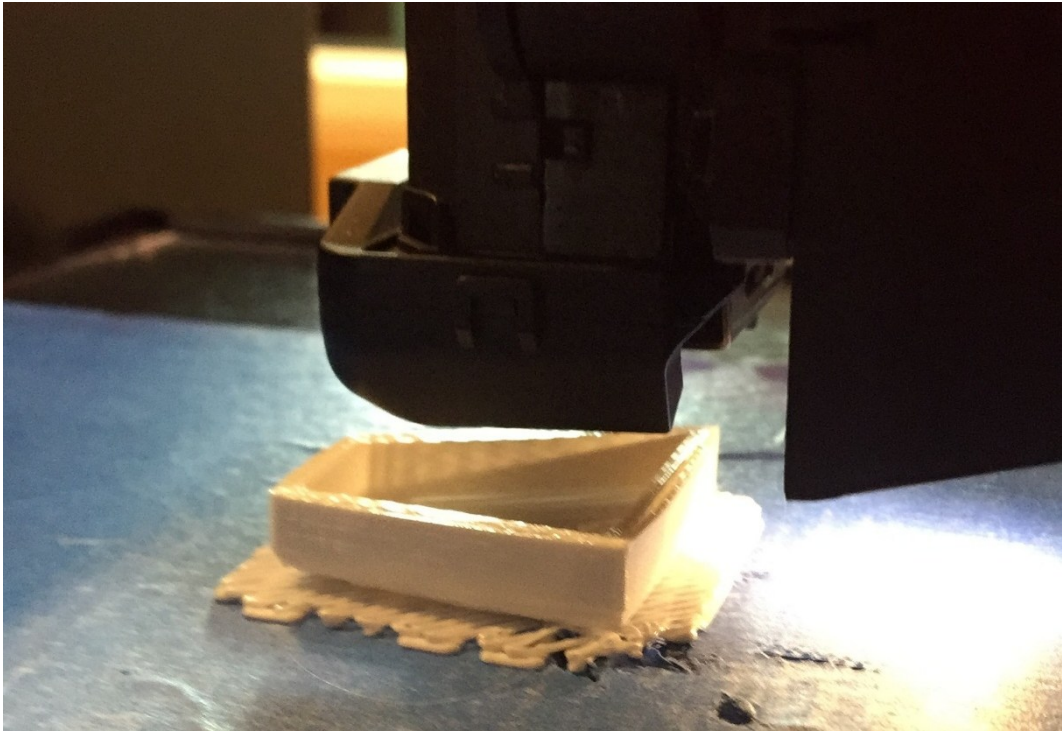


Figure 64: 3D printing of a formwork – Block n.97

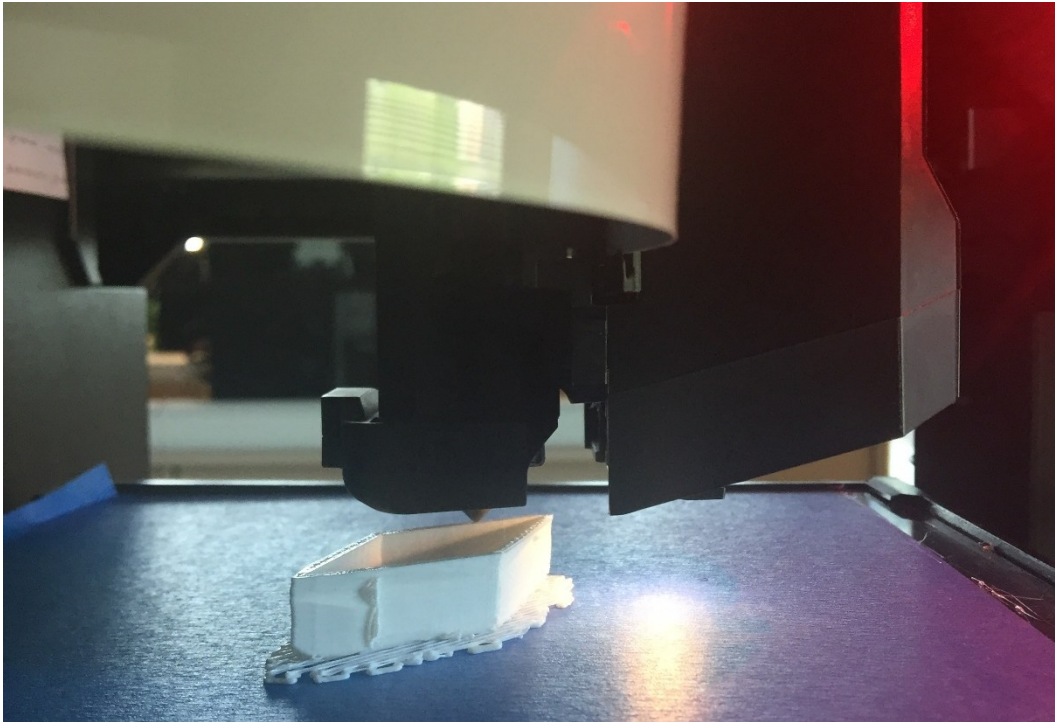


Figure 65: 3D printing of a formwork – Block n.45

The following step of the fabrication process, at the end of the formworks 3D printing dealt with the casting of the cement and the final realization of the voussoirs. This operation took place in the Mastrlab inside the Department of Structural and Geotechnical Engineering of the Politecnico di Torino. There the cement was mixed with water with a ratio almost equal to

$$\frac{a}{c} \cong 0.4$$

This value guarantees a good workability of the mixture and the block after demoulding operations return a block with good mechanical characteristics. During casting operations, a higher ratio value has been tested but the demoulded voussoir were too much brittle and not suitable for the vault realization.

It is important to notice that the moulds made with PLA material own good elastic characteristics but they are also very stiff and it was impossible to demould the brick without break them or the brick itself. Furthermore, the formworks needed to be recycled for at least three times in order to realize all the blocks of the four parts of the vaults. The problem has been solved dividing them into two different parts; these two parts were

mechanically jointed for casting operations, deassembled in the demoulding phase and jointed again for a new cast.

The following pictures try to help better understanding what has been explained in the last paragraph:



Figure 66: Formworks assembled and positioned for cast operations

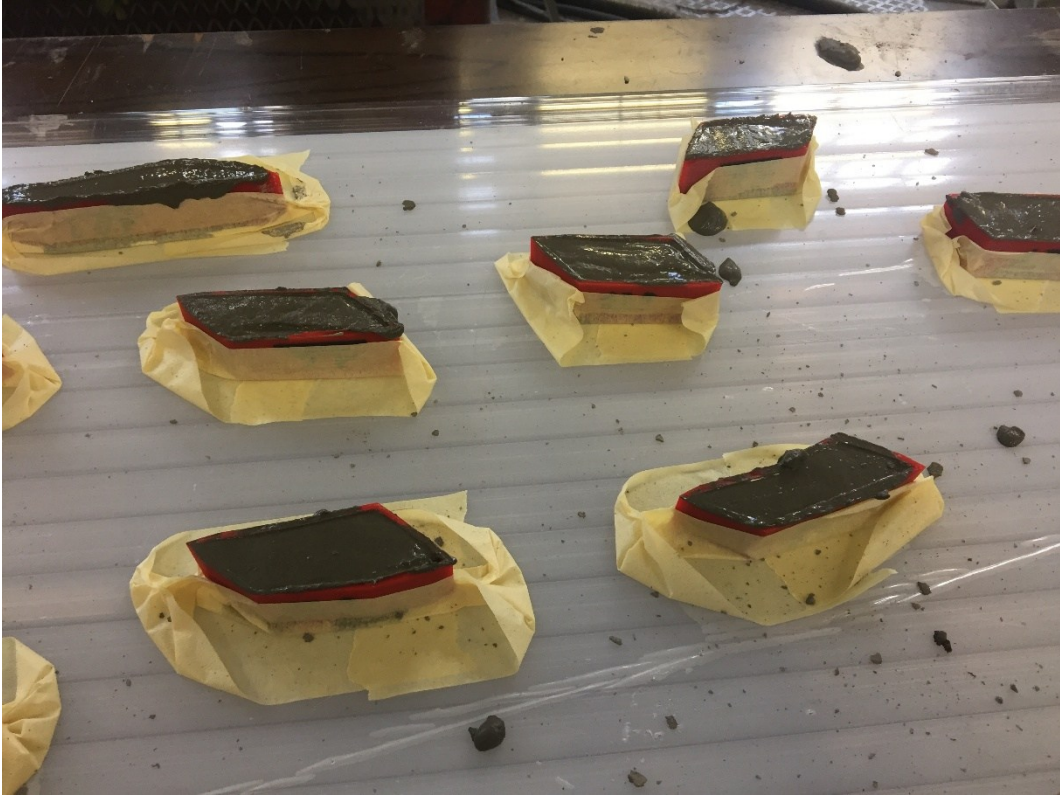


Figure 67: voussoirs after the cast



Figure 68: Demoulding operation

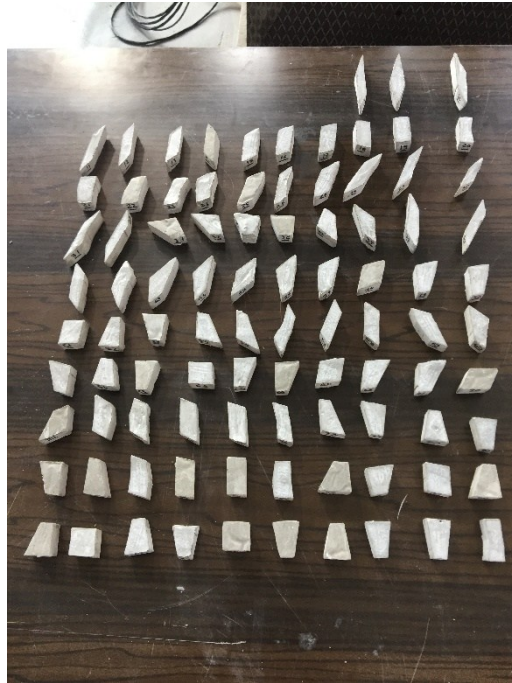


Figure 69: The voussoirs at the end of the fabrication process

5.4.Falsework Fabrication

From the first roman arch to the most important domes built during the centuries, falseworks have always been an integrated part of the project. They are essential for structures realization in a building step where they are not able to support themselves and external loads. Furthermore, sometimes the falsework design become as important as the structure design itself.

Also for the vault's prototype realization, a falsework has to be designed and fabricated. The solution found for the prototype can't be considered suitable for the 1:1 scaled vault. Indeed, different issues, materials required and fabrication systems lead to solutions incompatible for the two cases.

In this paragraph, only the prototype's falsework is discussed and the 1:1 solution will be matter of future studies.

The most important issues considered during design phases were that the falsework:

- has to follow the intrados shape of the vault with the as most precise geometry as possible;

- has to be realized with poor material: it can't be as expensive as the vault because it is only a temporary structure;
- has to be stable enough to carry all the prototype's self-weight and all the other external loads acting on it during construction phases;
- needs to be removed at the end of the construction and during the removal operation it is fundamental to avoid damages to the already built vault.

A solution considering fixed support cardboards has been realized and its design has been developed into the Rhinoceros 3D CAD environment. The result is represented in the following picture:



Figura 1: 3D falsework concept design

The falsework is composed by 37 cardboard sheets in each direction with a variable inter-axis of almost 2 cm. That distance has been designed in order to avoid the drop of one or more blocks from the top of the falsework during the construction. Every sheet represents the intersection between a vertical plane and the intrados of the vault and they have been found using Rhinoceros features. The falsework has got a base of 77.2x77.2 cm and it is 26 cm tall. Every cardboard sheet is characterized by 37 cuts used to join each sheet to the other. This connection solution is illustrated in the following pictures.

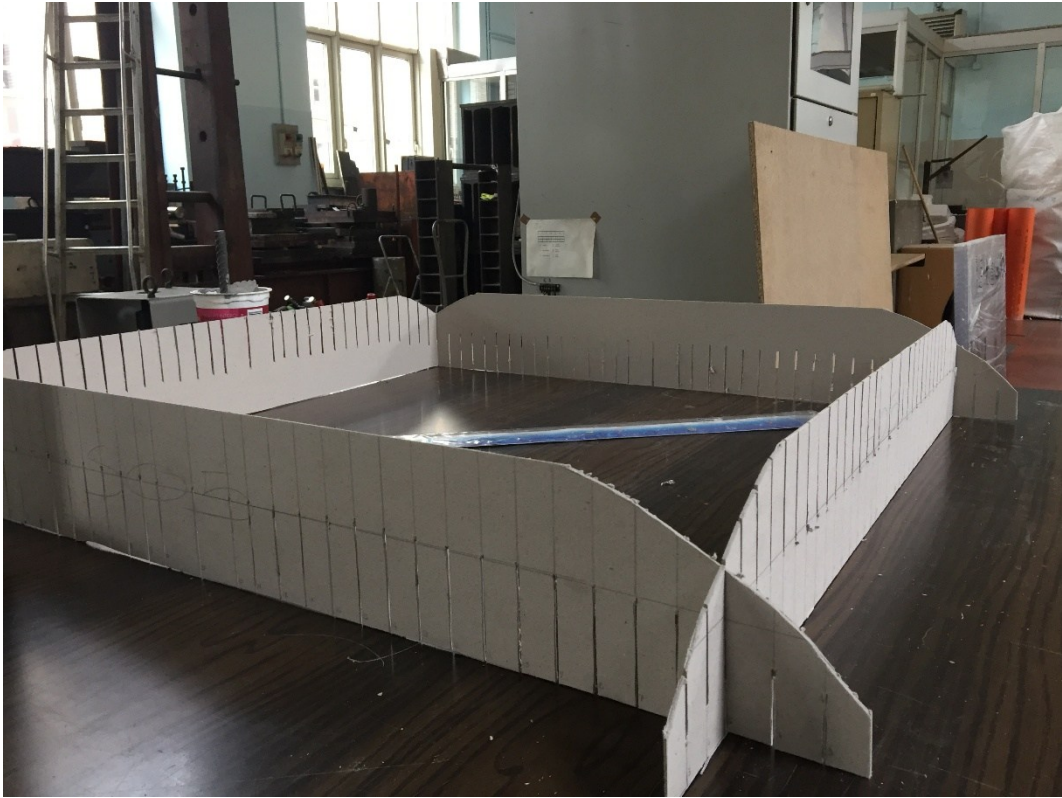


Figure 70: Falsework connection system example

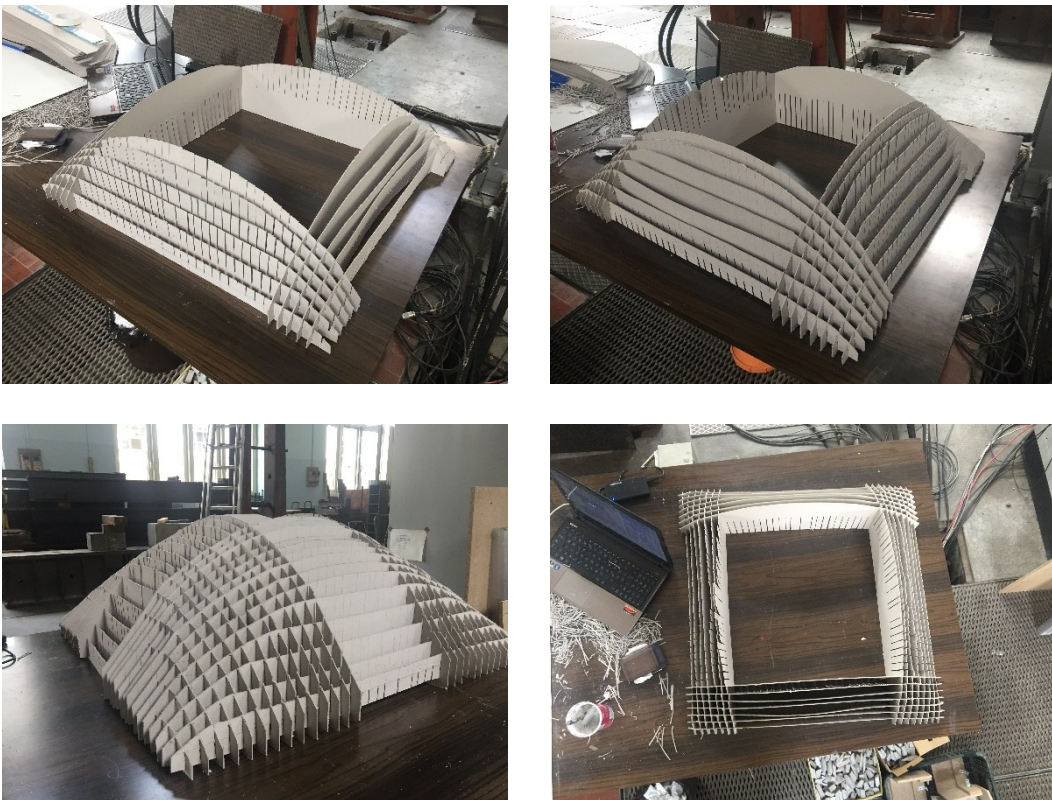


Figure 71: falsework construction phases

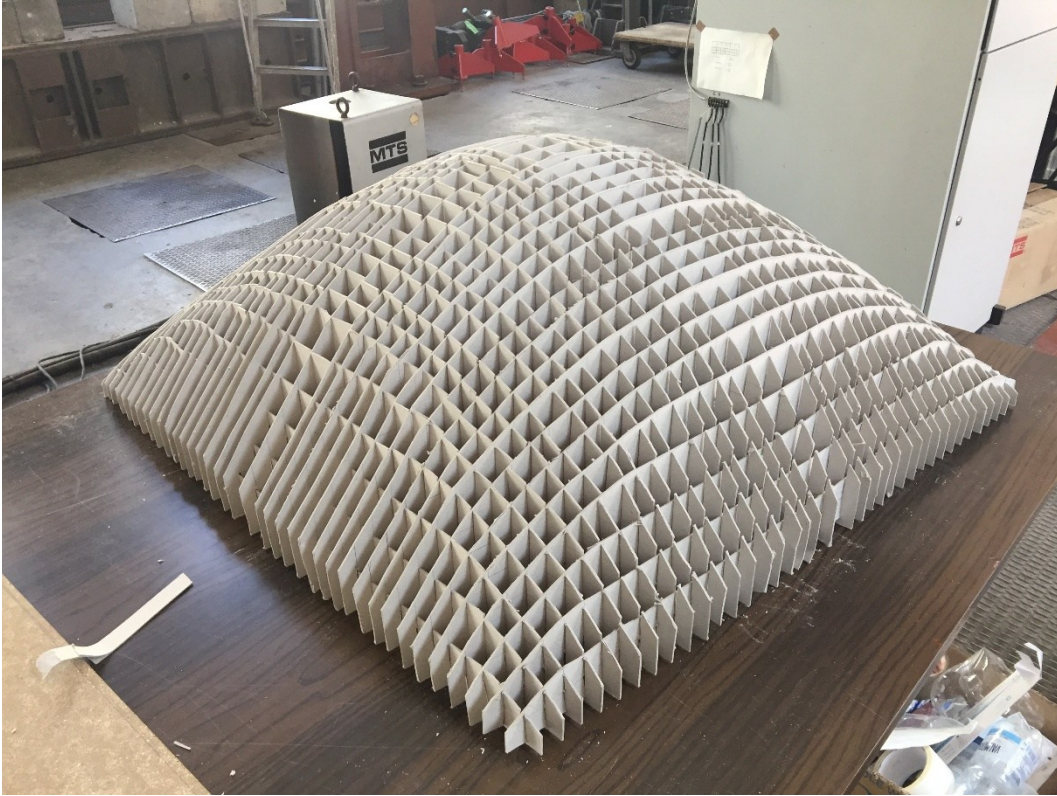


Figure 72: the ended cardboard falsework

The realized falsework lays on a plywood panel 10 mm thick and with a base equal to the falsework one. All the structure is supported in 4 points by mean of 4 threaded bars. The right height of the falsework is ensured rotating the threaded bars.

The falsework supporting system has been designed in order to solve the fourth issue presented previously: the falsework has to be removed at the end of the vault construction. Indeed, the threaded bars, the threaded holes in the plywood panel where the bars are inserted and the whole falsework are designed and dimensioned for this reason.

At the end of the construction, the plywood panel goes down through the contemporary rotation of the threaded bars until the top of the falsework is lower than the boundary arches of the vaults. Finally, the falsework is extracted.



Figure 73: the falsework positioned on the plywood panel supported by 4 threaded bars

5.4.1. Constraints Fabrication

The structural self-weight and the external loads acting on the vault come to the ground through the 4 base supports. The structure is compressed-only by definition, so at the base the reaction will have the same direction of the local flow forces. Furthermore, the support reaction has to be stronger enough to guarantee the stability of the structure, so a constraint has to be designed and realized.

A squared plywood panel 1 cm thick and 112,7 cm wide is used as base for the whole prototype. At its corners, the base elements need to be placed and right there the base constraints have to be fabricated. 4 plywood boxes 14x14x6.3 cm are assembled as elevation for the structure. This solution creates the additive height needed by the falsework to be extracted.

Two little plywood panels 15 cm high have been placed at the external corner of each box. With the help of the vinyl glue, all these elements were joint together.

The thrust coming from the base element is counteracted by the two panels at the corner of the box. The overturning of the base support and the static equilibrium is guarantee

from eight steel brackets, two at each corner, which connect the structural system composed by box and panels to the base panel.

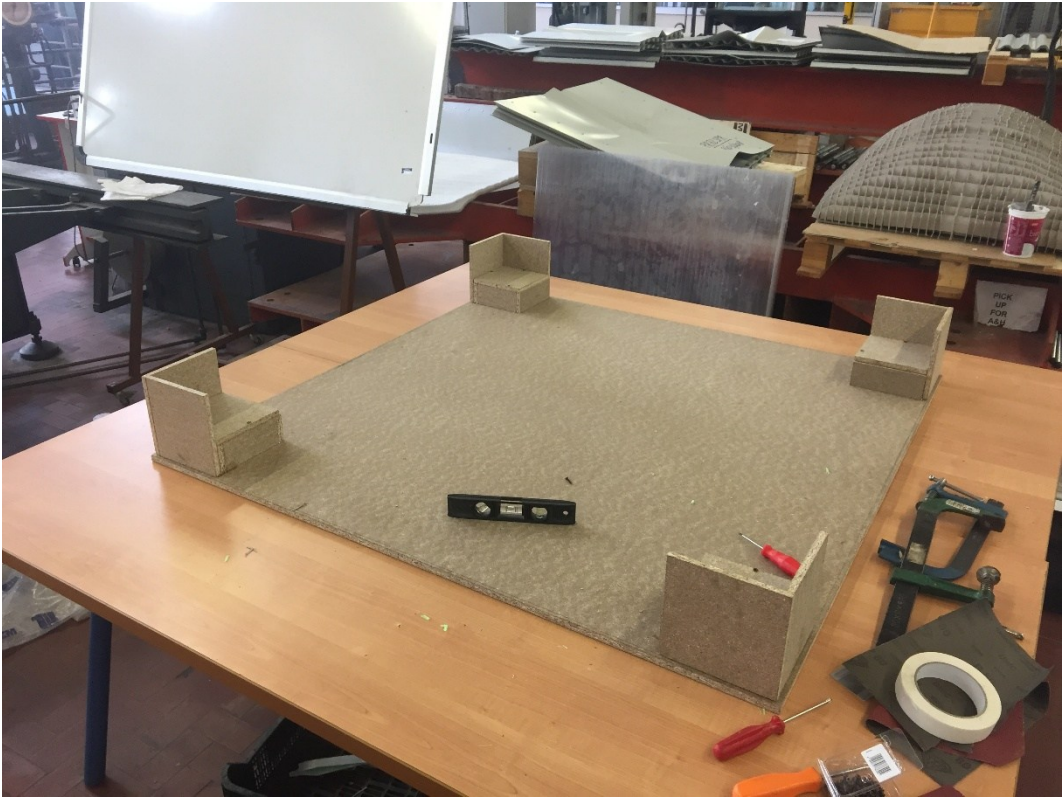


Figure 74: Base of the Prototype fabrication - At each corner is present the base element constraint



Figure 75: Base constraint detail

Unfortunately, it was not possible to place and lock the bottom face of the base element perfectly adherent to the upper face of the constraint plywood box. That means that there the structural hinge is not present and the base element is free to rotate around its supporting point. For this reason, a tie system made by string has been placed avoiding the rotation of the base element.

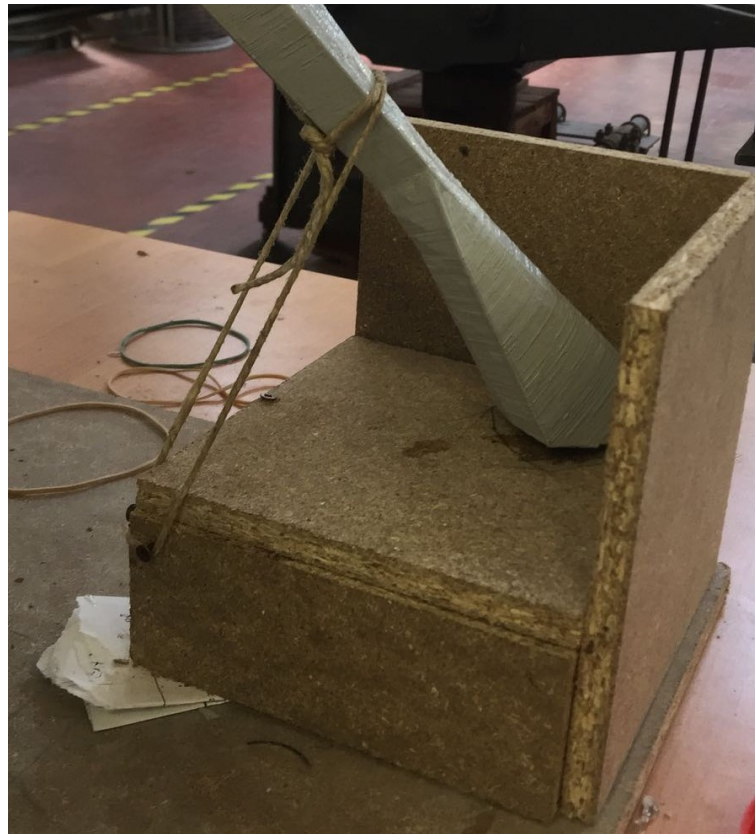


Figure 76: The tie system

5.5. Construction Phases Scheme

In this chapter, the prototype construction phases are shown through some illustration from the 3D model realized with Rhinoceros.

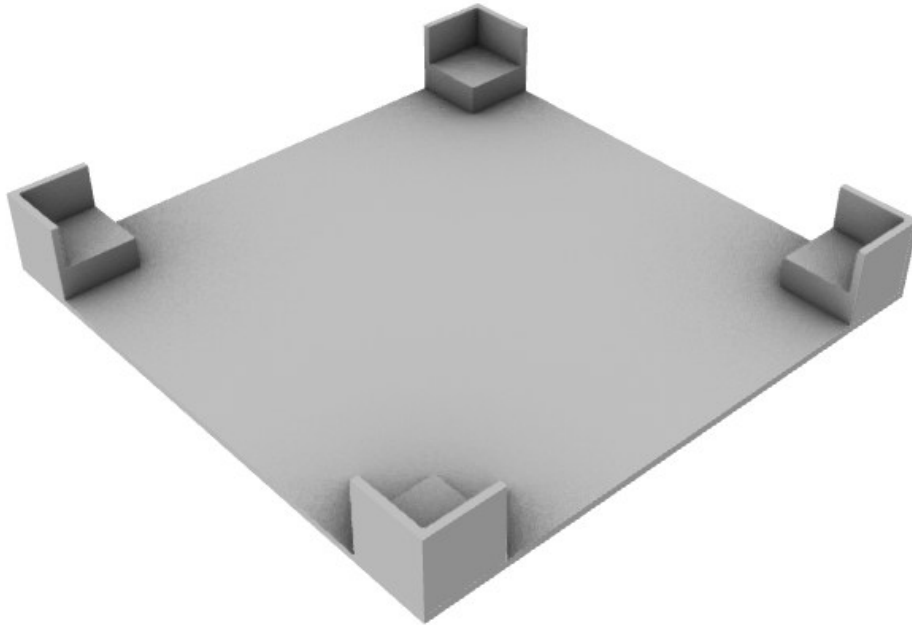


Figure 77: 1st Step - Base plywood panel and Constraints fabrication

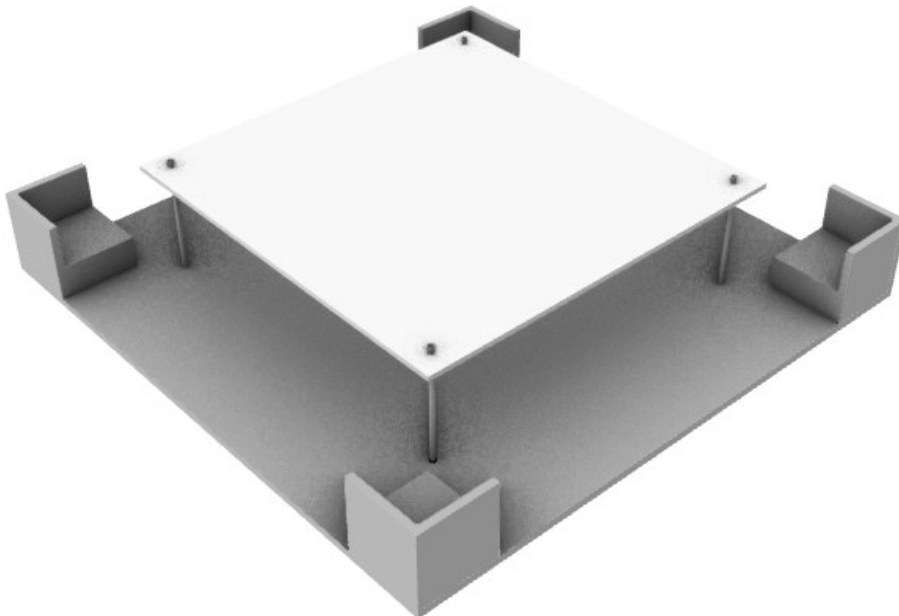


Figure 78: 2nd Step - threaded bars and falsework panel positioning

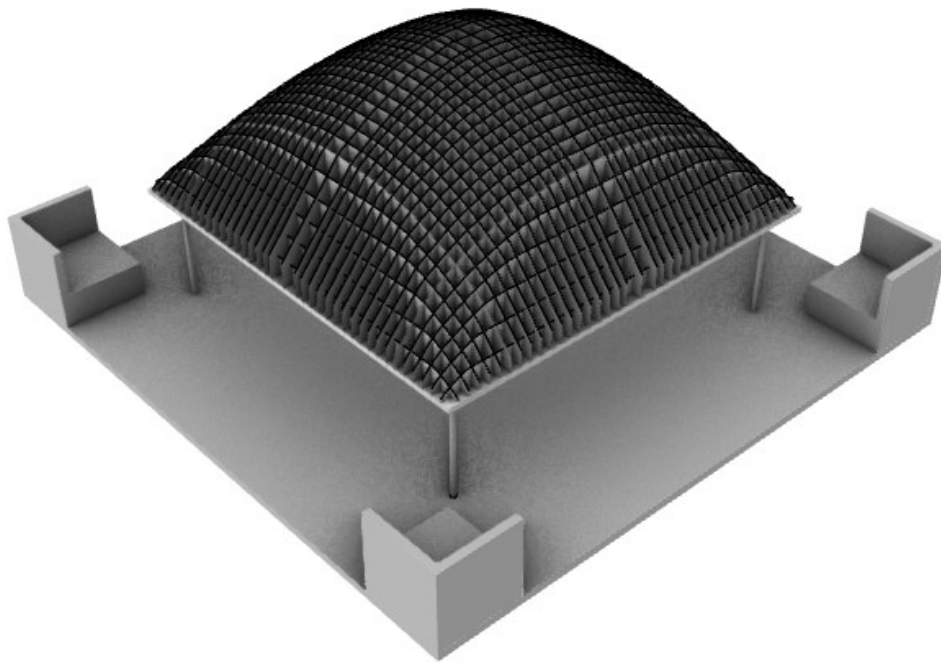


Figure 79: 3rd Step - Cardboard falsework positioning and height adjustment

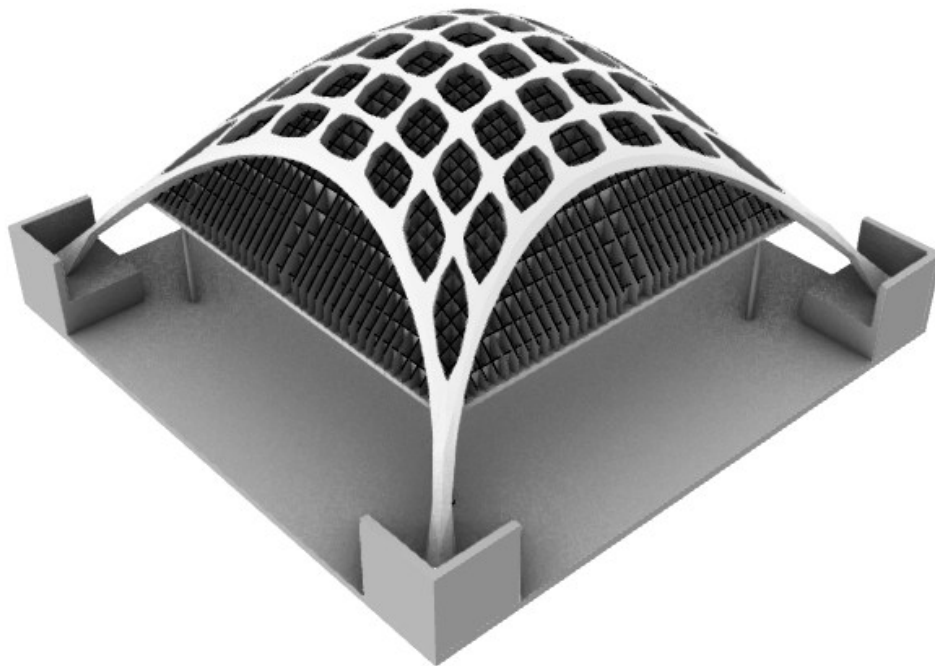


Figure 80: 4th Step - Vault fabrication through the voussoirs assembly

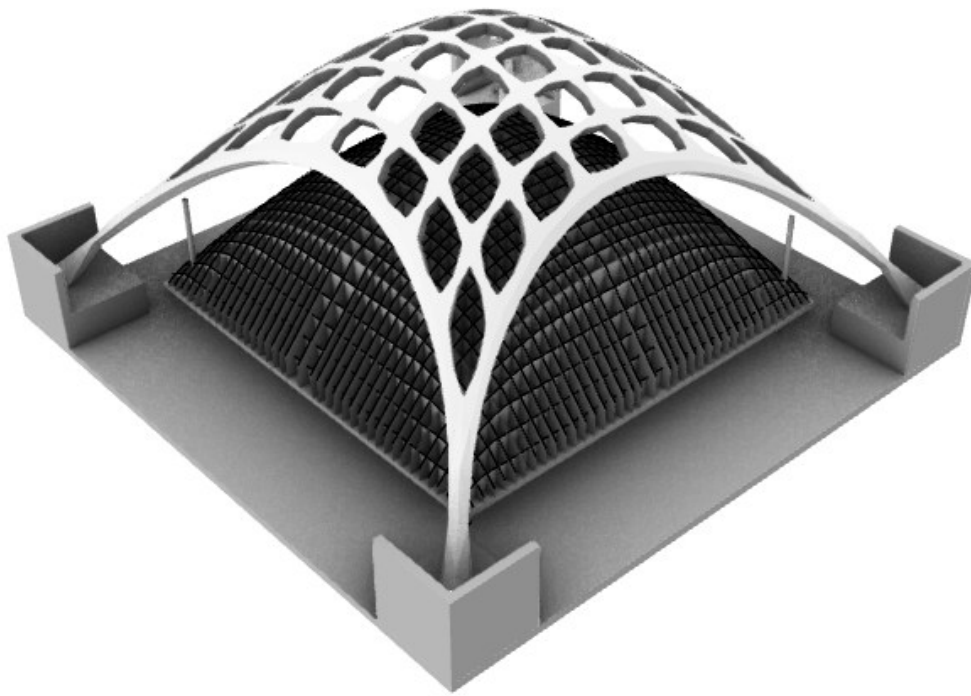


Figure 81: 5th Step - the falsework is casted off through the contemporary rotation of the four threaded bars

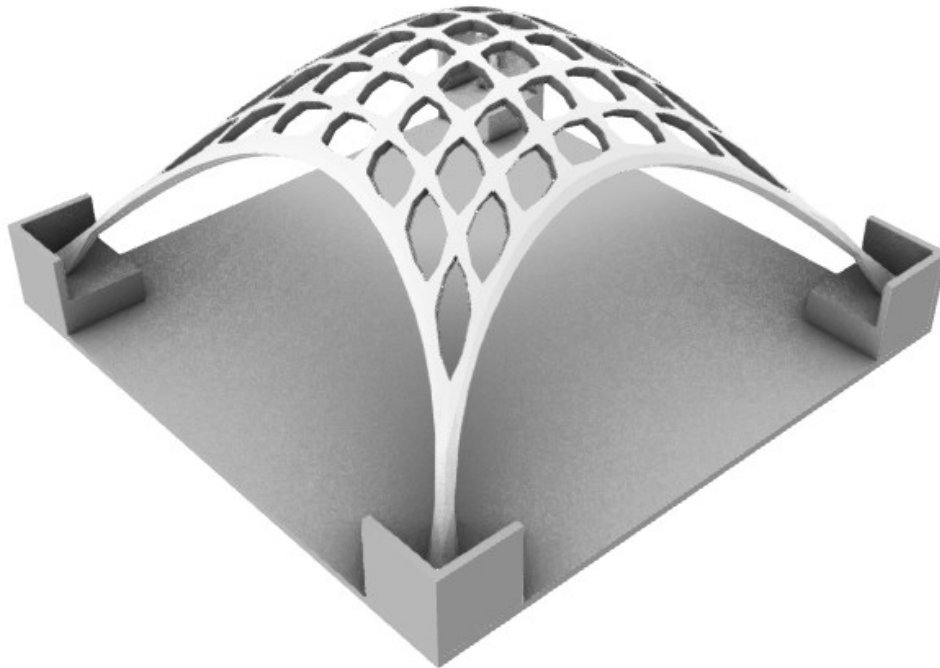


Figure 82: 6th Step - the falsework is removed and the prototype is ready

5.6. Second Tessellation Pattern Trial

When the construction phase started and the first voussoirs have been positioned, a serious problem about the tessellation pattern design came out. Indeed, the blocks placed on the boundary edges of the vault started to slide along their contact faces. That happens for two main reasons: the first one is the very low compressive stress that acts during construction phases that is not able to create a friction force between the blocks strong enough to keep the voussoirs aligned. The second main reason is the load-transferring contact faces design of the blocks of the boundary edges. Despite they are designed and realized perpendicular to the local force flow, their geometrical orientation is favorable to sliding phenomena for low compressive stresses. The issue is visible in the following pictures:

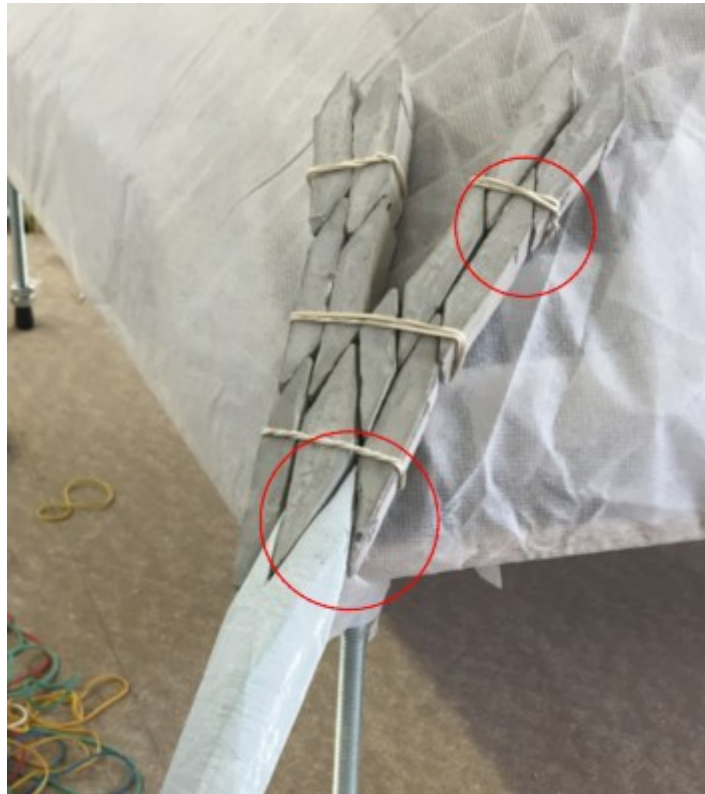


Figure 83: Sliding surfaces detail 1

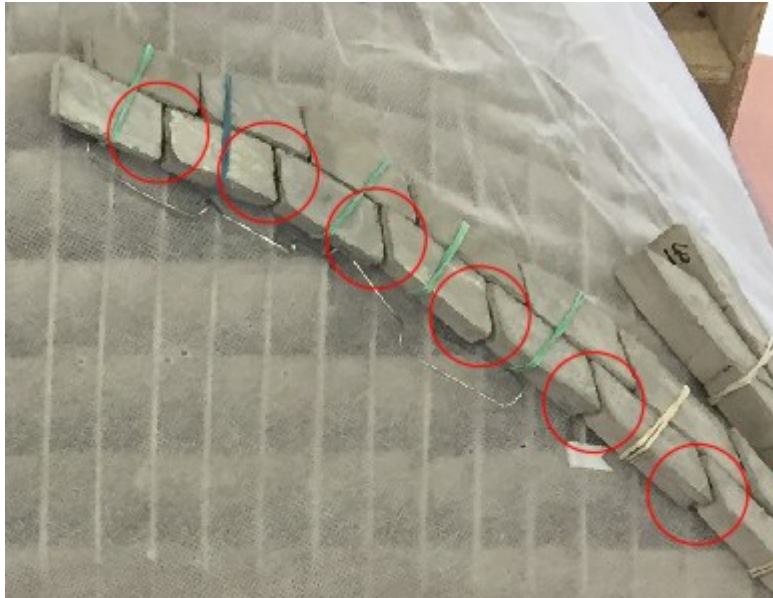


Figure 84: Sliding surfaces detail 2

The problem has been solved through the partial tessellation pattern design variation. Indeed, a complementary part of the base has been designed in Rhinoceros and 3D printed while the blocks which present a favorable sliding contact surface were redesigned changing the geometrical orientation of the *dangerous* surfaces in order to prevent new sliding phenomena.

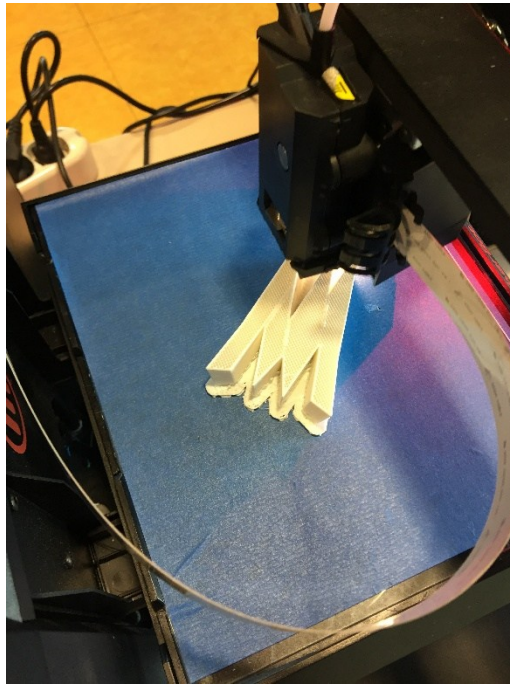


Figure 85: Base element complementary part fabrication

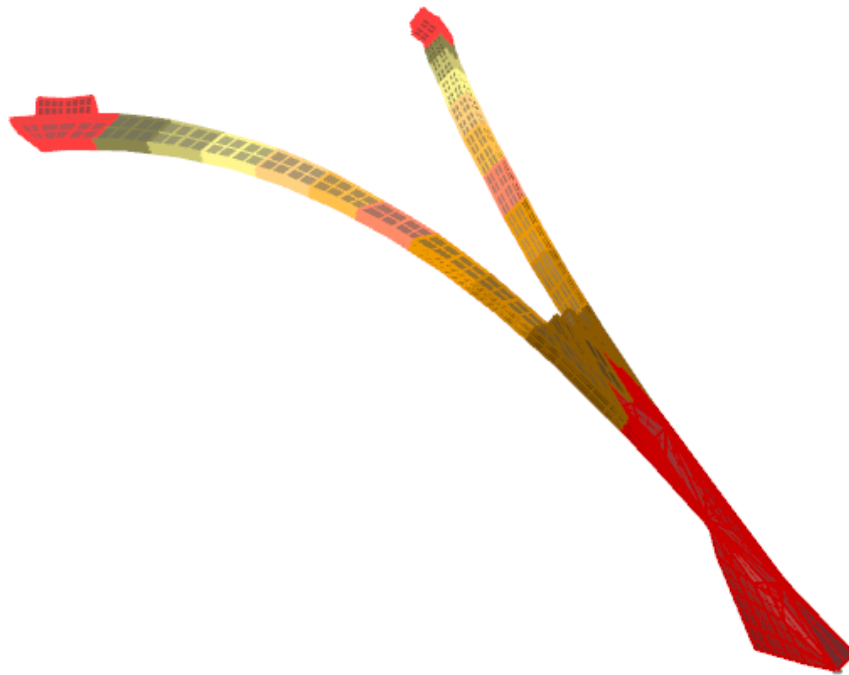


Figure 86: Redesigned voussoirs represented in the 3D CAD environment

However, the most important problem has not been solved because the friction force between the contact surfaces is not strong enough to keep the blocks perfectly aligned and in their own position even if they are staggered and properly laid out. A shear key introduction between the voussoirs seems to be the fittest solution for the sliding surfaces problem. Even if it was not possible to be applied for every block, rubber bands has been placed between the blocks of the boundary edges. They let the voussoirs able to move and slide but the ones connected to each other simulate the presence of a bigger voussoir which presents a shear key able to avoid sliding phenomena. In the end, in order to handle the inaccuracies due to the model fabrication, rubber pieces were placed and the compression state of stress of the vault has been reached.



Figure 87: Prototype realization – picture 1

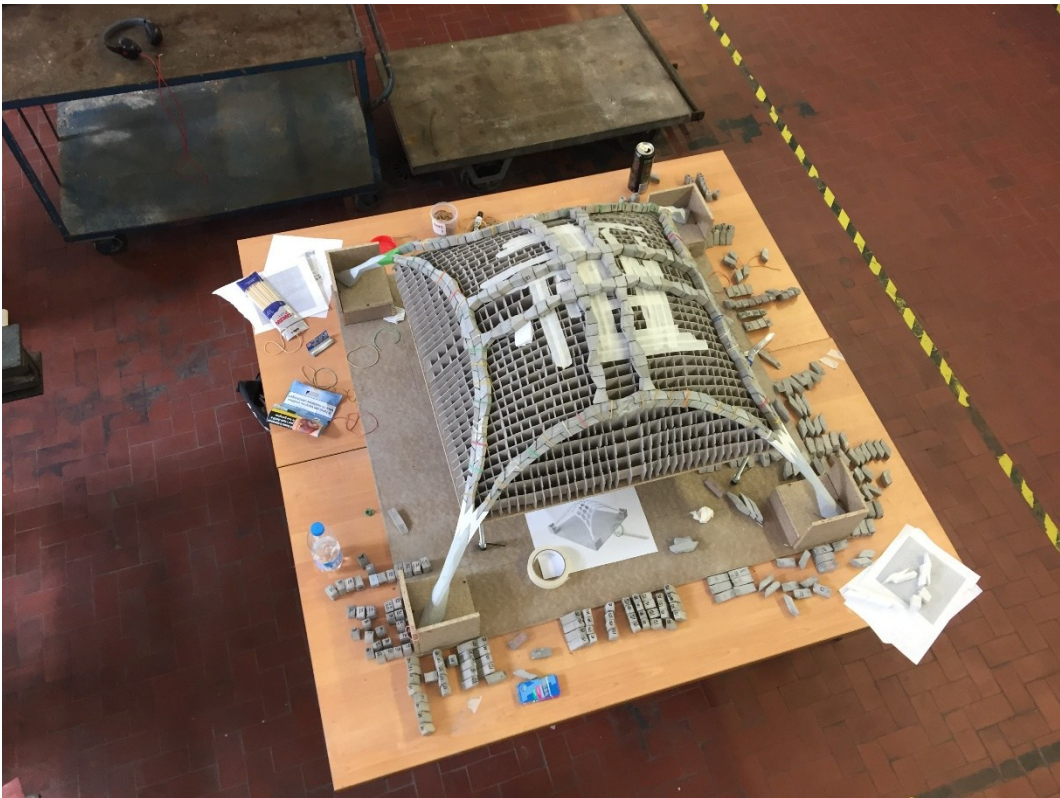


Figure 88: Prototype realization - picture 2

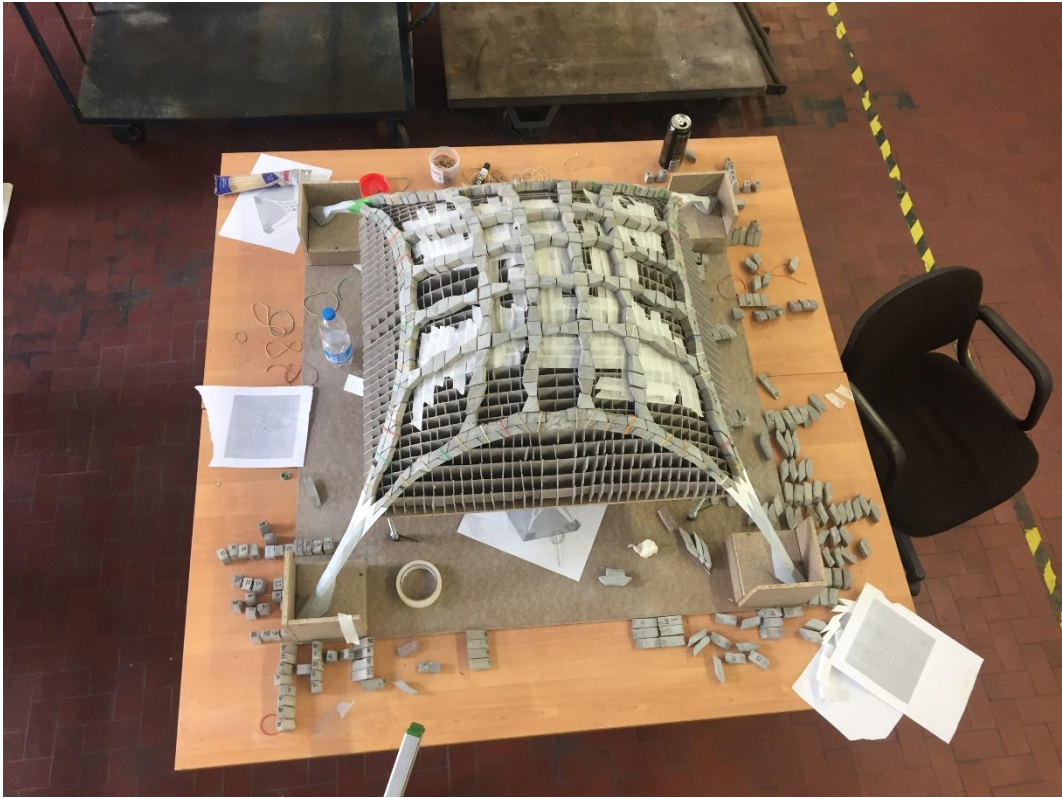


Figure 89: Prototype realization - picture 3

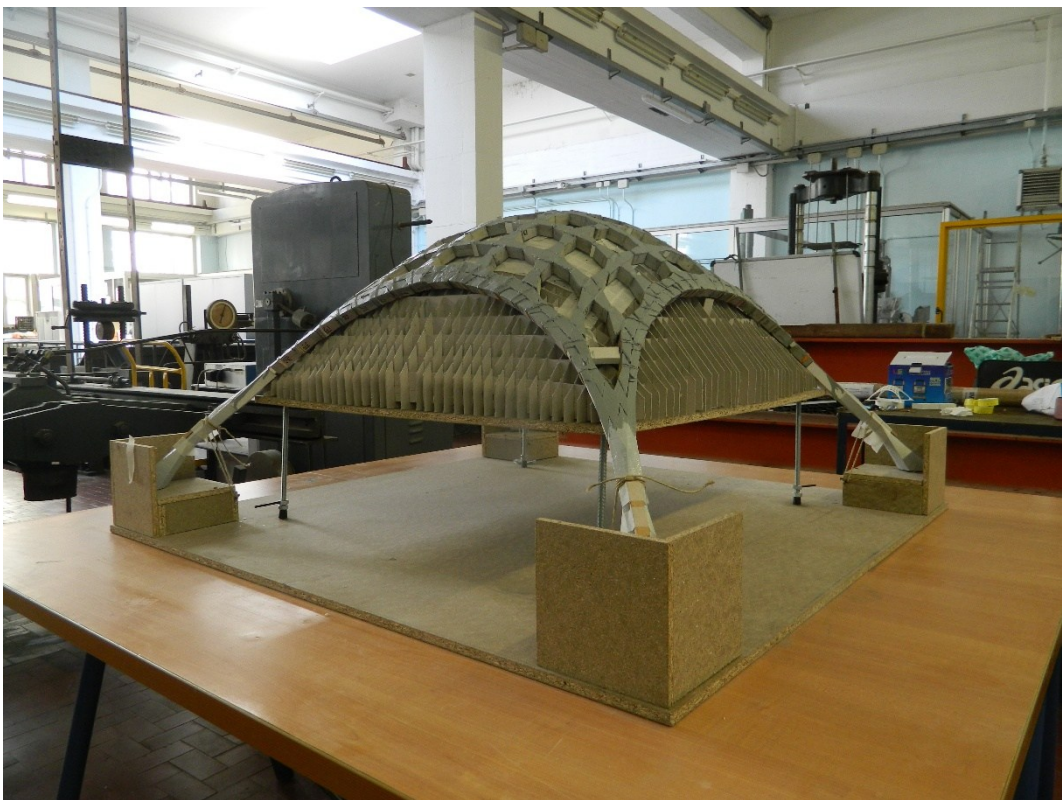


Figure 90: Ended prototype construction

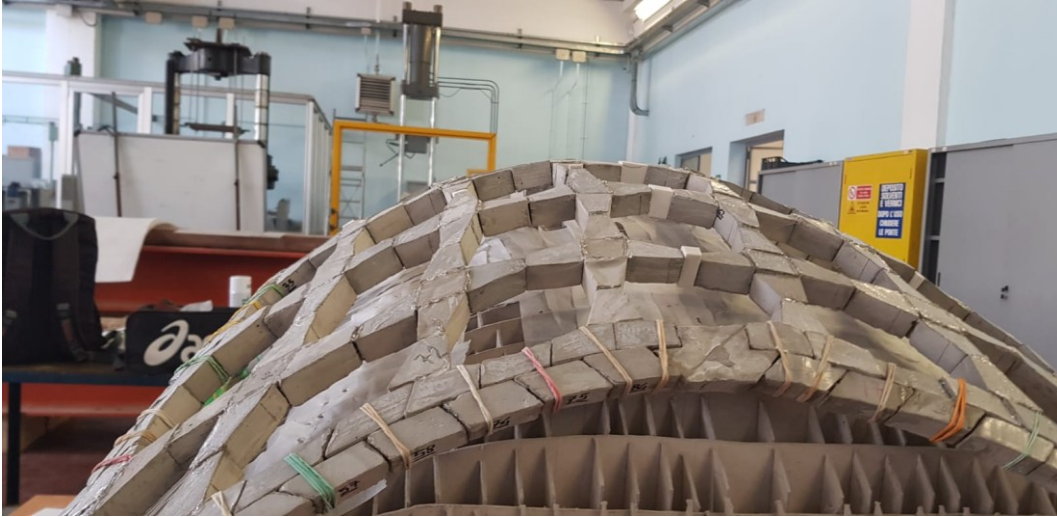


Figure 91: The ended prototype during falsework removal phase – picture 1



Figure 92: The ended prototype during falsework removal phase – picture 2



Figure 93: The ended prototype during falsework removal phase – picture 3



Figure 94: The ended prototype during falsework removal phase – picture 4



Figure 95: The scaled prototype

6. Conclusions

Thinking about a new design process and approach where Form Finding and Additive Manufacturing could be the leading tools in the design of Free Form structures and most of all in compression-only latticed masonry shell structures, the results coming from this work show how these methods could really be the most useful instruments. However, only a first step in the overall developing process has been done.

The leading numerical form finding techniques has been analyzed and the Thrust Network Analysis seems to be the optimal solution. Indeed, it return a compression-only three-dimensional structure shape only by mean of a geometrical method, the Graphic Statics, based on easier bi-dimensional rules. This approach, more intuitive than analytical ones, has been implemented directly as a plug-in into Rhinoceros environment delivering to engineers and architects a tool able to answer to any requirement from a topological and geometrical point of view.

A case study has been created in order to validate form finding results and to analyze the static equilibrium of the designed pierced vaults. The influence of different parameters on structural stability has been shown through a global linear buckling load analysis and through the comparison between the outputs of those analysis. Two final diagrams have been realized showing the most stable solutions from a Critical Load Multiplier and Critical Buckling Load Resultant point of view. 720 different linear buckling load analysis has been realized with the Lusas FEM Solver varying slenderness, lowering degree, piercing pattern and load-case conditions. Outputs evidence how the vaults with 13 holes considering the Pattern 1, is the most stable solution from the Critical Buckling Load Resultant point of view, while 29 holes solution, always considering the Pattern 1, is the most stable one from the Critical Load Multiplier point of view. However, for slenderness equal to 80, lowering degree equal to 3.2 and symmetrical load conditions, the 49 holes solution becomes the most stable solution.

Another fundamental challenge for the development of the proposed design approach is the tessellation pattern design and the voussoirs design and fabrication. The most important rules that have to be considered are the ones written by Rippmann (Rippmann, 2016) in his work and , thinking about future researches about the topic, it is clear that in

this phase of the design process the architect or the engineer will always need to contribute with his experience and his knowledge in order to find a fit solution in the tessellation pattern design unattainable by a software .

The FDM printing technique can be considered as a useful instrument in the bricks fabrication. Indeed, this technology is very useful to realize formworks where a millimeter accuracy is necessary for cast bricks realized with stone material. Furthermore, it is also perfect to realize the whole block. This 3D printing technique let the designer to produce them with different densities and different materials, that means different mechanical characteristics, always considering a sub-millimeter accuracy of the printed voussoir. Moreover, this second solution is great when shear keys needed to be realized in order to avoid sliding surfaces phenomena.

A specific introduction of a parametric approach with tool as Grasshopper 3D is fundamental thinking about future development of the proposed design method; together with Structural Optimization, algorithms like Genetic Algorithms will radically change the designer overtures to the vault project because from a given topology he will be able to obtain a latticed masonry shell with the optimized grid and stiffness; this will be possible only setting some initial fundamental geometrical and structural parameters.

However, after the scaled prototype realization, the first future step will be the analysis of the dynamic equilibrium of the vault under seismic action through a shake table machine. Two main factors will be considered during these analysis: number and inclination of contact faces. All the tests will be done considering previous FEM analysis on the modal modes of the vault. The vault, designed only for vertical loads, will be also probably tested considering an isolation system. During the analysis a monitoring system composed by optical fibers will be directly applied on the vault to study structure strains under seismic actions comparing the obtained values with FEM results.

The scaled prototype realization, evidenced that shear keys are a very important help in the vault construction. Indeed, one of the future development of this research will be the study of the optimal shear keys design in order to provide the as best as possible interlocking between the voussoirs. Furthermore, the shear keys will be used as fundamental element in the design of self-supported vaulted structures.

This work and all its future developments present a lot of possible application in the research field and in the building landscape. Vaults realized with this approach could be used, for instance, in Shelter Design. They are sustainable structures both from an economical and environmental point of view because of the fabrication techniques considered and because they could be realized with stone material.

Moreover, this design and building approach could be the solution in lunar and mars constructions where is impossible to use classical building techniques and to carry over there the building machines used on Earth and where it is necessary to use only stone materials present on those ground.

APPENDIX A

The Particle Spring System created by Killian and Ochsendorf can be easily implemented in a parametric or algorithmic modeling environment.

This approach is born when architects and engineers had to face problems like form finding. Indeed, the conventional drawing can be considered as an additive process where the complexity of the concept and the goal of the designer is reached by means of addition and overlaps of completely different signs and symbols on paper. The additive process is driven by the additive logic that is submitted to two main limits: the act of drawing does not allow the creation of interrelations between the different entities involved. The second limit is given by the exclusion of physically relevant aspects that rule the form generation in nature and in the real world, not on a paper. The Computer Aided Design is, from this point of view, only the translation of the additive logic from paper and analogical world to the digital one.

The first and most important designers involved with form finding such as Gaudi, Isler, Otto and others looked to self-formation processes in nature as a way to organize buildings and the traditional drawing techniques were not able to help them in the process. This can be one of the reasons that explain why they relied on physical models: soap films looking for minimal surfaces and hanging models looking for compression-only vaults. The passage to the parametric and algorithmic modeling techniques happened from the 1980's when computers started to have enough computational power to face those kind of problems. In order to understand this modeling technique it is important to remind that it is necessary to exceed the additive logic using editing and programming techniques inside the designing software. This type of modeling relies on **algorithms**.

It is known that algorithms can also lead to geometries and not only to mathematical results. If an editor is implemented inside a CAD environment, for instance, it is possible to create 3D geometries simply by manipulating the standard set of primitives provided by the software or defined by a sequence of instructions. The easiest example is represented by the line that can be seen in two ways: as a sign on a paper or in the CAD; as defined by two points, the start and the end of the line ones. Each point is defined by

three coordinates in the reference system $\{x,y,z\}$. the procedures that make this possible have to be expressed in a specific program language that produces two outputs:

- The algorithm;
- The output of the algorithm constituted by the desired geometries.

“The final output is not just a ‘digital sign’ but it can be considered as an interactive digital model responding to variations in the input by manipulating the entire system”
(Tedeschi, 2014)

In the last years the software developers understood that it was necessary to create a scripting that could be accessible to users with little or no programming skills. So they invented editing environments in which the programming process is led by the same visual objects usually used to create algorithms: **node diagrams**.

The technique, so called visual scripting, is based on two main working environments that generates the two outputs written above; a visual editor and a 3D modeling environment are present. As output for this process the designer is able to interact with a parametric diagram, visual expression of the algorithm, and the parametric 2D or 3D geometry coming from the solution of the algorithm. The parameters are the most important element of the “equation” because they allow the designer to interact with the geometry by mean of an intuitive logic approach based on their variation and manipulation.

Associative models that explore different configurations through control of the input parameters can be found using parametric diagrams.

A.1 Grasshopper 3D

The world of algorithmic modeling is dominated by Grasshopper, the most popular and advanced tool available nowadays. The software is not a standalone application but is designed as a plug-in for Rhinoceros. It is an editor based on all the principles described before born in 2007 with the *Explicit History* name from the work of David Rutten at Robert McNeel & Associates (the company which release Rhinoceros). The actual name of the tool was established only the year after, in 2008. During these years the community of users and developers grew a lot and involves students, professionals and academics. If the user has got a Rhinoceros license, the Grasshopper plug-in is free and it runs on the version 5.0 or higher of the software.

Grasshopper is become the leading tool in the algorithmic modeling landscape not only for its own editing capacities but also thanks to different environmental situations that can be sum up as follow:

- Wide, dynamic and growing community: one of the most important skills of this tool is the presence of a network of users that share challenging problems, knowledge, discoveries, helping each other in the growth of the common knowledge of the formal exploration and this is possible directly from the tool's official download internet site: www.grasshopper3d.com;
- Constant Updating: updating and improvements are often available on the web and bug fixing and new features are usually based on users feedbacks.
- Ecosystem: Grasshopper is not a close environment but a wide set of plug in is always available on the official internet site and is common that those application are developed from independent programmers, users of the tool themselves;
- Software and hardware interaction: one of the biggest potentiality of the plug in is the capability to interact with other software and also with hardware components: for instance, Microsoft Excel, Adobe Photoshop, Autodesk Revit, Arduino, Kinect and so on. Moreover, the interaction is not only about file compatibility and interchange, but also about real time interaction between the algorithmic modeling environment and the external world.

As described in the general description of the algorithmic modeling environment, Grasshopper editor is composed by a window that works in parallel with the 3D-modeling

environment of Rhinoceros using it to interact with geometries and to see how the algorithm is working.

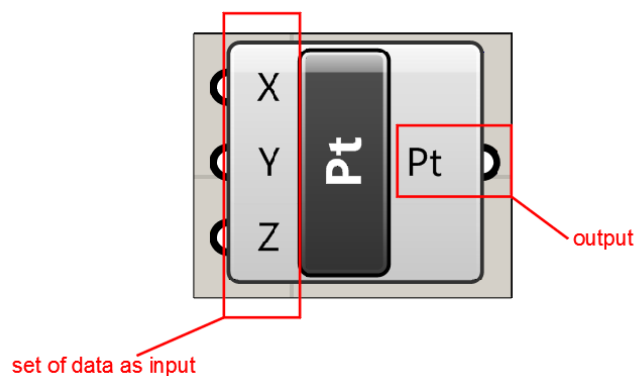
The algorithms created with Grasshopper are node diagrams made of connected components. It is obvious that the connections have to be properly designed in order to follow the logic sequence of step in the modeling process. The components are created to represent: primitives such as points, curve and surfaces; geometric operations and other categories. They are grouped in several tabs each organized in panels.

The algorithms are created in the editor window in the so-called “canvas”: there the components are placed by the designer and properly connected.

In order to better understand how the Particle Spring System can be implemented with Grasshopper a little explanation about how components work is given.

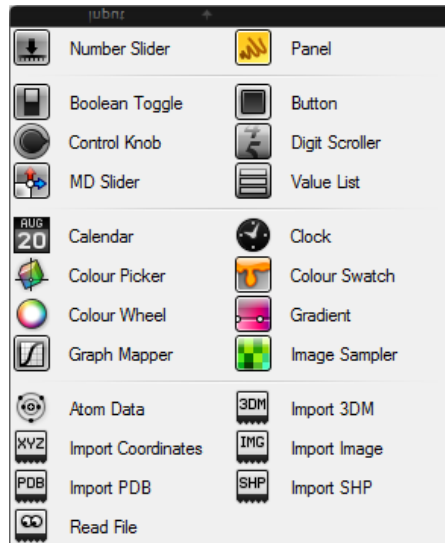
The components can be divided in three principal categories:

- **Standard Components:** they perform operations on data. It means they receives a set of data as input which is processed to generate an output. In the next figure is shown, as example, the component that generate a point in the 3D-modeling environment of Rhinoceros:



A 1: Standard Component example

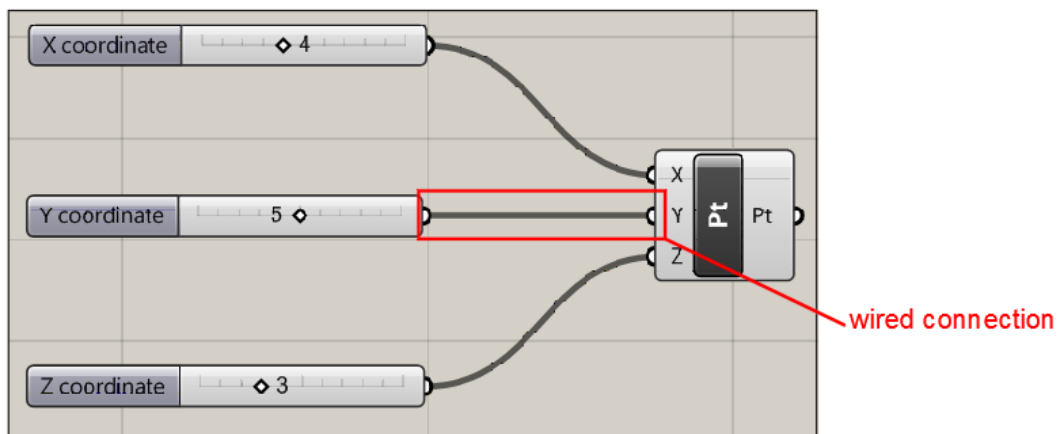
- **Input Components:** they provide data such as numbers, colours etc, which can be modified by the user. They do not expect input data. The following figure represents the standard panel of Grasshopper where are present the input components available for the user:



A 2: Input components

- **Container Components:** they can collect data in several ways and often are used as input for other components; they are characterized by a black-hexagonal icon.

In order to build algorithms, Grasshopper uses wired connections to set data between components; in this way wires conduct data from the output of a component to the input of another component.



A 3: Wired connection example

It is important to remember that the wires connect only the output of a component with the input of a one that does not precede it in the logical stream.

“the data stream can be imagined as a fluid that flows through the components from left to right.” (Tedeschi, 2014)

A.2 Digital Simulation – Particle-Spring System

In this paragraph will be discussed how to implement the Particle Spring System in Grasshopper environment. How the method work has been shown in chapter 2 of this work, so here is only exposed the procedure to apply it for the form finding of a compression only structure.

The strength of Grasshopper in the improvement of the Particle Spring System is that usually the typical software packages which solve the procedure are not integrated with a CAD or a 3D-modeling environment. David Rutten's tool, instead, exploit its "ecosystem" to develop an instrument able to interact with the "external CAD world".

Daniel Piker and his team developed and released **Kangaroo**, a physics based particle spring system engine, easy to use, designer oriented and fully integrated in Grasshopper environment.

Quoting Daniel Piker's words:

"Like the reversal of gravity to find ideal forms for masonry arches, I think an environment which allows the designer to play, to flip and twist the Laws of Nature, to cross the wires and combine forces in a way that might be impossible in the real world – all within an easy but powerful visual programming environment and with rapid feedback – could make a fertile ground for the growth of powerful and exciting new techniques.

Kangaroo is designed to be extensible to include several other types of forces, such as electrostatics – as I worked with before in Jellyfish. These different forces could then be applied simultaneously in various combinations. Other things I might also add at some point include collisions and friction.

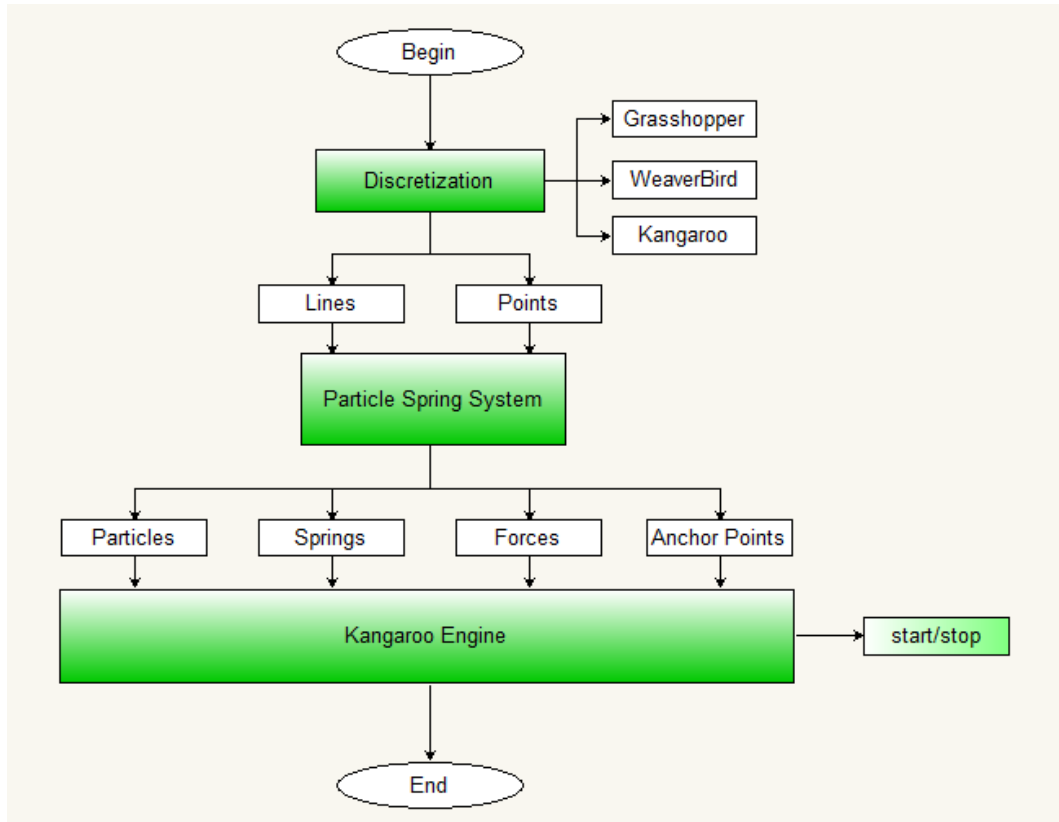
This becomes something like a sandbox game – Virtual worlds which behave according to the laws of physics we intuitively recognise."

One of the most interesting features of Kangaroo is that allows the designer to interact with form also during simulations, in real time through two interaction methods:

- **Direct Interaction:** the designer directly manages anchor points, spring properties and forces;

- **Parametric Interaction:** the most important one. The properties are parametrically linked to other parts of the 3D model.

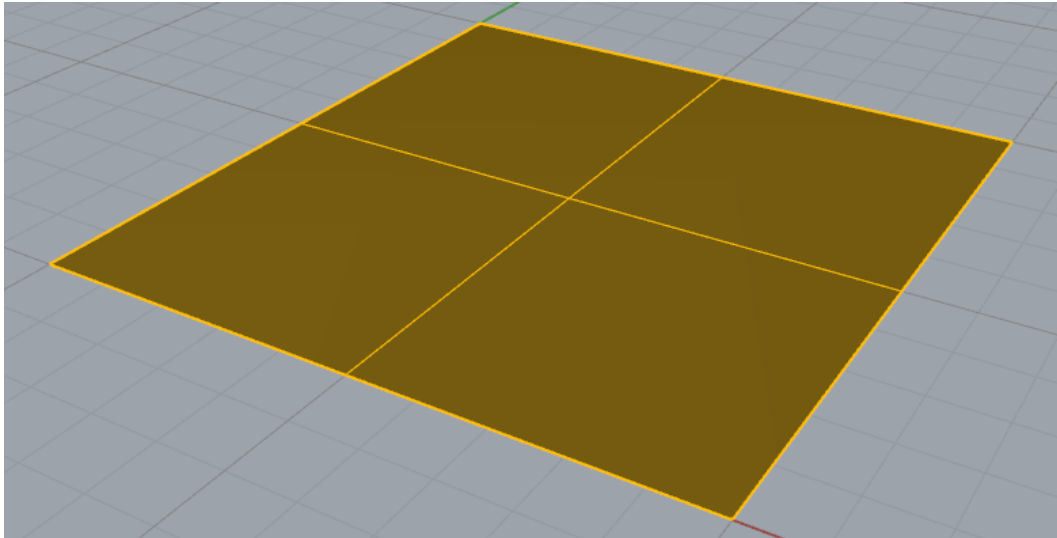
The workflow followed by the algorithm can be summarized in the following flow chart:



A 4: Particle-Spring System algorithm

The specific explanation of each part of the diagram is explained with the example of a compression only structure which form has been found from this algorithm.

The first step is the choice of the area that will be covered by the structure after the form finding process. A squared area of 10x10 m is chosen for this application and a surface object is created in the 3D modeling environment (Rhinceros).

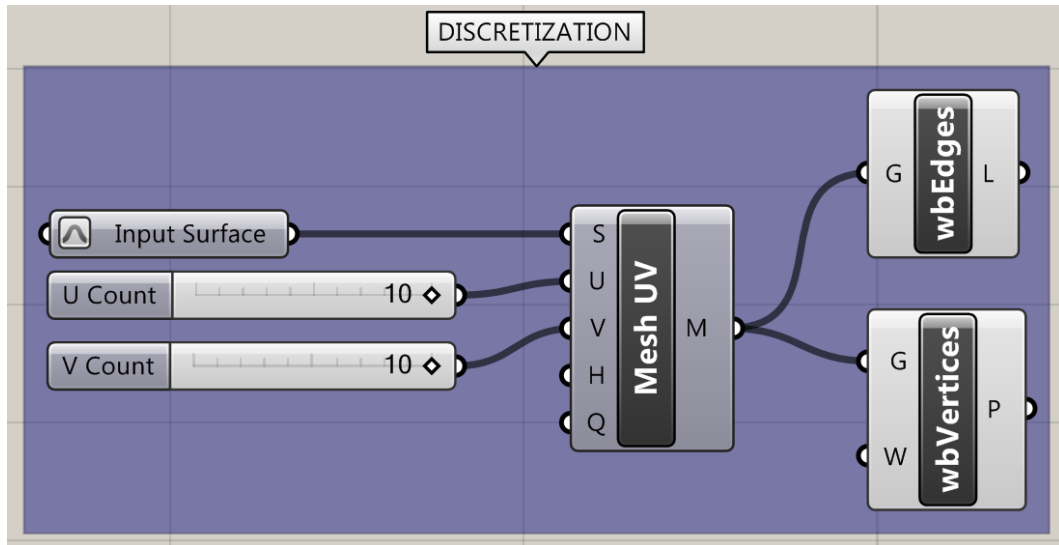


A 5: Base Surface

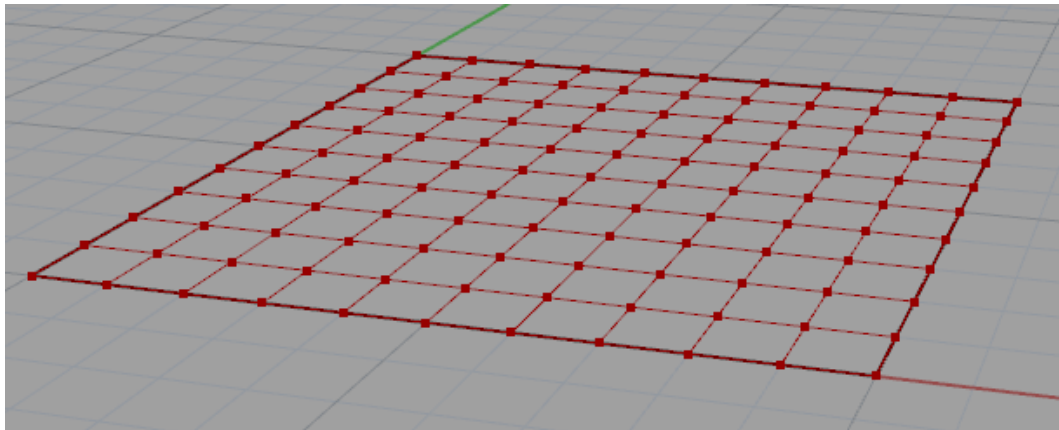
The selected surface will become a NURBS surface that will represent the structure after the form finding. Non Uniform Rational Basis Spline (NURBS) is a mathematical model commonly used in computer graphics for generating and representing curves and surfaces.

In order to represent the membrane behavior of the future structure is necessary to define a grid of springs. The most common technique is to convert the NURBS surface in a mesh. Then the edges and the vertices are extracted to turn into springs and particles.

The following figure describe the visual diagram used in Grasshopper to discretize the input surface and after the discretized object in output is reported.



A 6: Discretization GH-code



A 7: Discretized surface

before the description of the following step of the simulation is important to evidence and explain how the component that convert line into springs works.

The component name is “Springs From Lines” and is present in the Kangaroo plug-in. It was created following the Hooke’s law:

“displacements or size of the deformation of a body (treated as a spring) is directly proportional to the deforming force or load.” (Tedeschi, 2014)

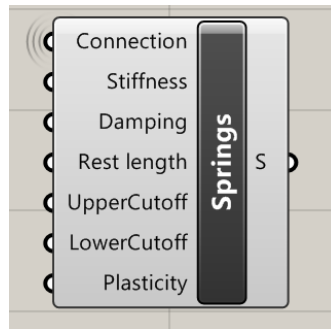
$$F = kx$$

With:

- F applied force;

- k positive constant called *stiffness* which value depends on material and cross sectional geometric properties of the elastic body.
- x is the deformation, the change in length of the body.

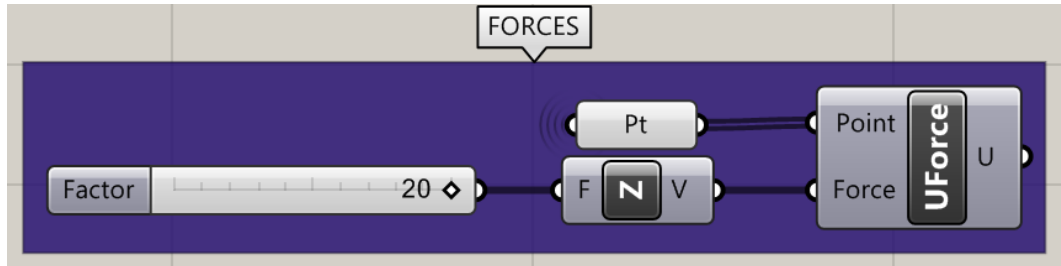
The algorithm in Grasshopper sees the line as a single spring with specific features that have to be precisely described from the designer to the component in order to have a correct interpretation of the right mechanical behavior of the future spring.



A 8: Kangaroo's spring component

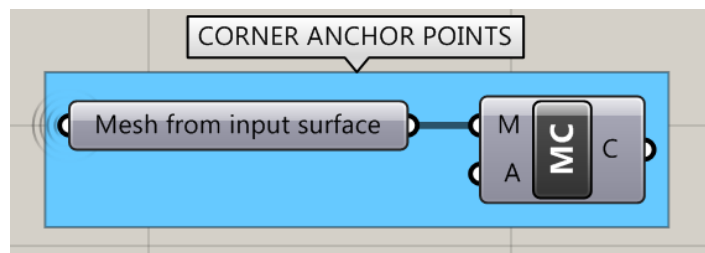
- **Connection:** with this term the component asks as input the lines that have to be considered as springs from Kangaroo during the simulation;
- **Stiffness:** is the k term of the Hooke's law equation. The higher is the value of this number, the lower will be the deformation of the structure under a force applied with the same value;
- **Damping:** this term has not the same meaning of the one in dynamic analysis of the structures but it only represents the deformation velocity without influence on the final shape structure;
- **Rest Length:** is the length that each line, or spring, reaches when the load is removed. If the rest length is the same of the start length, perfectly elastic behavior of the element is achieved. In the other cases, the length difference is an index of the presence of pre-tension inside the element if the rest length is smaller than the start length or the presence of a relaxation of the element if the rest length is bigger than the start length;
- **Upper/lower cutoff:** sets limits for the springs to operate, below or above respectively;
- **Plasticity:** the maximum elastic deformation.

Forces are applied as vectors applied at the nodes of the model in z direction where is supposed that the mass are concentrated. In the algorithm they are applied with positive sign so they are directed upward. This choice has been done in order to find the shape of a structure already overturned as the Hooke's second law teaches us.



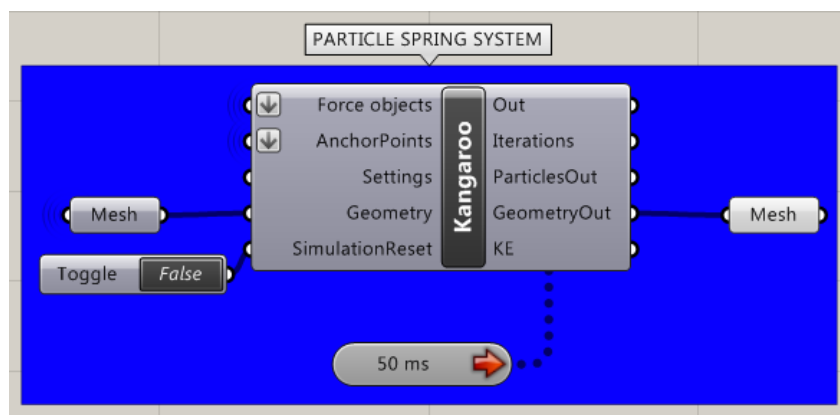
A 9: Force definition GH-code

The chosen anchor points are the corners of the input surface and are identified by Grasshopper using the following components:



A 10: Anchor points definition GH-code

At the end the model ready for the form finding process is formed by a membrane, anchored at its corners deformed by nodal forces directed along z axis and resisted by spring with a stiffness value.



A 11: Kangaroo's Particle-spring system component

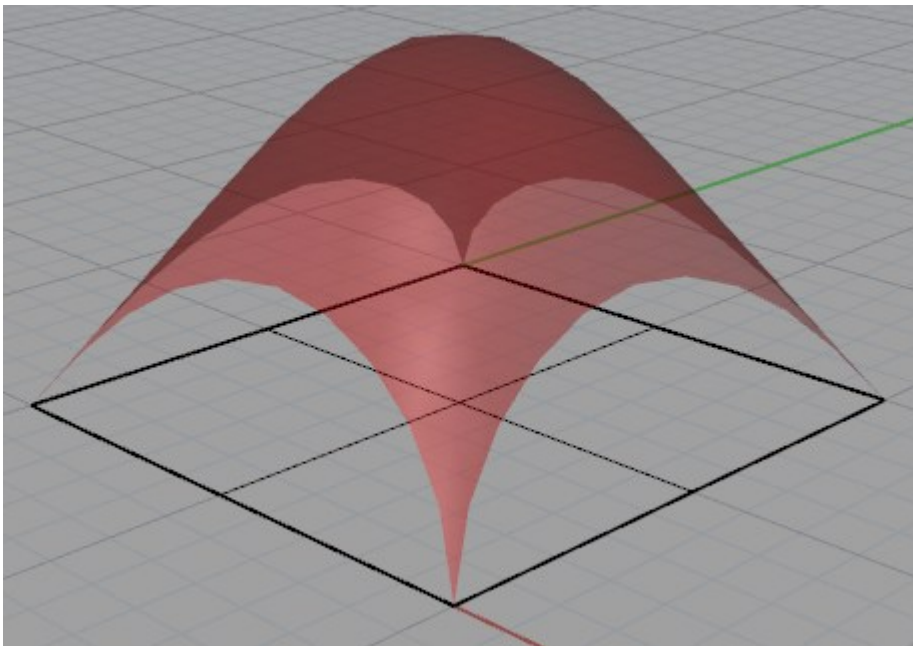
Double-clicking the Boolean toggle switching from True to False initiates the membrane simulation. If the minimal surface is the goal of the form finding process is possible to obtain it pointing to 0 the rest length of the springs.

As explained in the previous chapters the simulation ends, from a theoretical point of view, when the kinetic energy of the system reaches the zero values. With this simulation the energy converges to zero and the designer can stop the engine when the kinetic energy is contained under a desired tolerance value.

During the simulation is possible to interact with the model and the algorithm changing stiffness of the springs, damping, rest length, forces values, anchor points and so on paying attention that some errors can occur if *“the points are not returned to their original position before stopping and starting a new simulation”*. (Tedeschi, 2014)

It is not possible to change the mesh discretization while the simulation is running.

At the end, a shape for the structure is found and, for the example presented, the result is the one reported in the following figure:



A 12: Vault shape after form finding process

The presented shape guarantees a compression-only structure under gravitational loads. This affirmation is verified by the structural analysis. If the geometry is imported in a Finite Element modeling environment and meshed with shell elements, under vertical

loads the eccentricity of the loads is always contained in few millimeters (considering a thickness of the shell structure of about 30 cm).

In general, is very important to remind what prof. Adriaenssens wrote in her article: *“during the form finding process the values of all numerical quantities (EA and load) are arbitrary since it is only their ratios that effect the shape.”* (Richardson, Adriaenssens, Coelho, & Bouillard, 2013)

This example and this treatment evidence that if a designer need to solve form finding problems knowing only some initial geometrical parameters, with Grasshopper and Kangaroo, it will be able to create and handle his own tool which results are reliable and very useful for the following and more detailed design phases.

Bibliografia

- Addis, B. (2007). *Building: 3000 Years of Design Engineering and Construction*. London - New York: Phaidon Press.
- Adriaenssens, S., Block, P., Veenendaal, D., & Williams, C. (2014). *Shell Structures for Architecture: Form Finding and Optimization*. New York: Routledge.
- Beghini, L. L. (2014, March). Structural Optimization Using Graphic Statics. *Structural and Multidisciplinary Optimization*, p. 351-366.
- Bertin, T. B. (2013). *Evaluating the Use of Particle-Spring System in the Coceptual Design of Grid Shell Structures*. Cambridge.
- Billington, D. P. (1985). *The Tower and the Bridge*. Princeton: Princeton University Press.
- Block, P. (2009). *Thrust Network Analysis: Exploring Three-dimensional Equilibrium*. Cambridge: MIT press.
- Block, P., & Veenendaal, D. (2012). An Overview and Comparison of Structural Form Finding Methods for Genreal Networks. *International Journal of Solid and Structures* 49, 3741-3753.
- Bushnell, D. (1981, September). Buckling of Shells - Pitfall for Designers. *The American Institute of Aeronautic and Astronautics Journal Vol. 19*, p. 1183-1226.
- Carpinteri, A. (1992). *Scienza delle Costruzioni Vol.2*. Bologna: Pitagora Editrice Bologna.
- Casagrande, E. (2011). *Introduzione all'analisi automatica di sistemi strutturali composti da funi*. Padova: Coop. Libreria Editrice Università di Padova.
- Chilton, J. (2012). Form-finding and Fabric Forming in the Work of Heinz Isler. *Second International Conference on Flexible Formwork*. Bath.
- Collins, G. R. (1963). Antono Gaudi: Structures and Form. *Perspecta, Vol. 8*, 63-90.
- Gordon, J. (1978). *Structures or Why Things Don't Fall Down*. London: Pengin Books.
- Grundig, L., Moncrieff, E., Singer, P., & Strobel, D. (2000). A History of the Principal Developments and Applications of the Force Density Method in Germany 1970-1990. *Fourth International Colloquium in Computation of Shell & Spatial Structures*. Chania-Crete.
- Heyman, J. (1998). *Structural Analysis: A Historical Approach*. Cambridge: Cambridge University Press.
- Hooke, R. (1676). *A Description Of Helioscopes and Some Other Instruments*. London: T.R. for John and Martin Printer to Royal Society at The Bell in St. Pauls Church-yard.

- Huerta, S. (2006, May 20). Structural Design in the Work of Gaudi. *Architectural Science Review*, p. 324-339.
- Kilian, A., & Ochsendorf, J. (2005). Particle-Spring System for Structural Form Finding. *Journal of the International Association for Shell and Spatial Structures Vol.46*.
- Lachauer, L. S. (2015). *Interactive Equilibrium Modelling: A New Approach to the Computer-aided Exploration of Structures in Architecture*. Zurich: ETH Library.
- Larena, A. B. (2009). Shape design methods based on the optimization of the structure. Historical Background and application to contemporary Architecture. *Proceedings of the Third International Congress on Construction History*. Cottbus.
- Mihalik, J., Tan, M., & Zengeza, S. (2013). *Mannheim Multihalle: Hanging Chain*. Tratto da Evolution of German Shells: <http://shells.princeton.edu/Mann2.html>
- Richardson, J. N., Adriaenssens, S., Coelho, R. F., & Bouillard, P. (2013). Coupled Form Finding and Grid Optimization Approach for Single Layer Grid Shells. *Engineering Structures Vol. 52*, 230-239.
- Rippmann, M. (2016). *Funicular Shell Design: Geometric Approaches to Form Finding and Fabrication of Discrete Funicular Structures*. Zurich: ETH Library.
- Southern, R. (2011). The Force Density Method: A Brief Introduction. *Technical Report TR-NCCA-2011-02*.
- Tedeschi, A. (2014). *Algorithms-Aided Design: Parametric Strategies Using Grasshopper*. Brienza: Le Penseur.

Attachments

LOAD MULTIPLIER: TABLES

| PATTERN 1 – SYMMETRICAL LOAD – R ₁ | | | | | | |
|---|-----|-------|-------|-------|-------|-------|
| η | [-] | 80 | 96 | 120 | 160 | 240 |
| λ/λ_{\max} [-] | | | | | | |
| No Hole | | 0.674 | 0.498 | 0.346 | 0.218 | 0.115 |
| 1 Hole | | 0.695 | 0.514 | 0.357 | 0.223 | 0.117 |
| 5 Holes | | 0.745 | 0.551 | 0.383 | 0.240 | 0.126 |
| 9 Holes | | 0.803 | 0.597 | 0.417 | 0.264 | 0.141 |
| 13 Holes | | 0.849 | 0.633 | 0.442 | 0.280 | 0.149 |
| 25 Holes | | 0.955 | 0.715 | 0.501 | 0.317 | 0.168 |
| 29 Holes | | 1.000 | 0.744 | 0.518 | 0.324 | 0.169 |
| 49 Holes | | 0.972 | 0.715 | 0.483 | 0.287 | 0.136 |

| PATTERN 2 – SYMMETRICAL LOAD – R ₁ | | | | | | |
|---|-----|-------|-------|-------|-------|-------|
| η | [-] | 80 | 96 | 120 | 160 | 240 |
| λ/λ_{\max} [-] | | | | | | |
| No Hole | | 0.674 | 0.498 | 0.346 | 0.218 | 0.115 |
| 4 Holes | | 0.712 | 0.526 | 0.366 | 0.229 | 0.120 |
| 8 Holes | | 0.750 | 0.553 | 0.383 | 0.239 | 0.124 |
| 12 Holes | | 0.811 | 0.600 | 0.416 | 0.260 | 0.136 |
| 13 Holes | | 0.837 | 0.620 | 0.431 | 0.270 | 0.141 |
| 33 Holes | | 0.871 | 0.639 | 0.435 | 0.262 | 0.126 |
| 45 Holes | | 0.922 | 0.676 | 0.456 | 0.270 | 0.127 |
| 49 Holes | | 0.972 | 0.715 | 0.483 | 0.287 | 0.136 |

| PATTERN 3 – SYMMETRICAL LOAD – R ₁ | | | | | | |
|---|-----|-------|-------|-------|-------|-------|
| η | [-] | 80 | 96 | 120 | 160 | 240 |
| λ/λ_{\max} [-] | | | | | | |
| No Hole | | 0.674 | 0.498 | 0.346 | 0.218 | 0.115 |
| 4 Holes | | 0.657 | 0.478 | 0.325 | 0.198 | 0.100 |
| 8 Holes | | 0.682 | 0.496 | 0.336 | 0.204 | 0.102 |
| 12 Holes | | 0.731 | 0.532 | 0.361 | 0.219 | 0.110 |
| 13 Holes | | 0.752 | 0.548 | 0.372 | 0.227 | 0.114 |
| 33 Holes | | 0.815 | 0.599 | 0.408 | 0.245 | 0.116 |
| 45 Holes | | 0.909 | 0.665 | 0.449 | 0.266 | 0.125 |
| 49 Holes | | 0.972 | 0.715 | 0.483 | 0.287 | 0.136 |

| PATTERN 4 – SYMMETRICAL LOAD – R ₁ | | | | | | |
|---|-----|-------|-------|-------|-------|-------|
| η | [-] | 80 | 96 | 120 | 160 | 240 |
| λ / λ_{\max} [-] | | | | | | |
| No Hole | | 0.674 | 0.498 | 0.346 | 0.218 | 0.115 |
| 1 Hole | | 0.657 | 0.478 | 0.325 | 0.198 | 0.100 |
| 5 Holes | | 0.740 | 0.548 | 0.380 | 0.238 | 0.125 |
| 9 Holes | | 0.763 | 0.566 | 0.393 | 0.247 | 0.130 |
| 13 Holes | | 0.752 | 0.548 | 0.372 | 0.227 | 0.114 |
| 17 Holes | | 0.814 | 0.595 | 0.406 | 0.248 | 0.127 |
| 29 Holes | | 0.949 | 0.696 | 0.475 | 0.290 | 0.146 |
| 49 Holes | | 0.972 | 0.715 | 0.483 | 0.287 | 0.136 |

| PATTERN 1 – ANTI-SYMMETRICAL LOAD – R ₁ | | | | | | |
|--|-----|-------|-------|-------|-------|-------|
| η | [-] | 80 | 96 | 120 | 160 | 240 |
| λ / λ_{\max} [-] | | | | | | |
| No Hole | | 0.506 | 0.402 | 0.301 | 0.203 | 0.111 |
| 1 Hole | | 0.521 | 0.414 | 0.310 | 0.207 | 0.113 |
| 5 Holes | | 0.569 | 0.451 | 0.335 | 0.223 | 0.121 |
| 9 Holes | | 0.618 | 0.490 | 0.364 | 0.243 | 0.133 |
| 13 Holes | | 0.658 | 0.520 | 0.385 | 0.256 | 0.140 |
| 25 Holes | | 0.796 | 0.619 | 0.450 | 0.292 | 0.157 |
| 29 Holes | | 0.831 | 0.641 | 0.461 | 0.296 | 0.158 |
| 49 Holes | | 0.855 | 0.636 | 0.436 | 0.264 | 0.128 |

| PATTERN 2 – ANTI-SYMMETRICAL LOAD – R ₁ | | | | | | |
|--|-----|-------|-------|-------|-------|-------|
| η | [-] | 80 | 96 | 120 | 160 | 240 |
| λ / λ_{\max} [-] | | | | | | |
| No Hole | | 0.506 | 0.402 | 0.301 | 0.203 | 0.111 |
| 4 Holes | | 0.531 | 0.422 | 0.315 | 0.210 | 0.114 |
| 8 Holes | | 0.564 | 0.445 | 0.329 | 0.217 | 0.115 |
| 12 Holes | | 0.616 | 0.485 | 0.358 | 0.235 | 0.125 |
| 13 Holes | | 0.640 | 0.504 | 0.372 | 0.244 | 0.130 |
| 33 Holes | | 0.702 | 0.541 | 0.384 | 0.237 | 0.114 |
| 45 Holes | | 0.797 | 0.596 | 0.409 | 0.246 | 0.118 |
| 49 Holes | | 0.855 | 0.636 | 0.436 | 0.264 | 0.128 |

| PATTERN 3 – ANTI-SYMMETRICAL LOAD – R ₁ | | | | | | |
|--|-----|-------|-------|-------|-------|-------|
| η | [-] | 80 | 96 | 120 | 160 | 240 |
| λ / λ_{\max} [-] | | | | | | |
| No Hole | | 0.506 | 0.402 | 0.301 | 0.203 | 0.111 |
| 4 Holes | | 0.489 | 0.389 | 0.288 | 0.189 | 0.098 |
| 8 Holes | | 0.514 | 0.405 | 0.296 | 0.191 | 0.097 |
| 12 Holes | | 0.552 | 0.433 | 0.315 | 0.202 | 0.103 |
| 13 Holes | | 0.570 | 0.447 | 0.326 | 0.209 | 0.107 |
| 33 Holes | | 0.678 | 0.520 | 0.366 | 0.224 | 0.107 |
| 45 Holes | | 0.787 | 0.588 | 0.403 | 0.242 | 0.116 |
| 49 Holes | | 0.855 | 0.636 | 0.436 | 0.264 | 0.128 |

| PATTERN 4 – ANTI-SYMMETRICAL LOAD – R ₁ | | | | | | |
|--|-----|-------|-------|-------|-------|-------|
| η | [-] | 80 | 96 | 120 | 160 | 240 |
| λ / λ_{\max} [-] | | | | | | |
| No Hole | | 0.506 | 0.402 | 0.301 | 0.203 | 0.111 |
| 1 Hole | | 0.521 | 0.414 | 0.310 | 0.207 | 0.113 |
| 5 Holes | | 0.564 | 0.447 | 0.332 | 0.220 | 0.119 |
| 9 Holes | | 0.600 | 0.473 | 0.349 | 0.230 | 0.124 |
| 13 Holes | | 0.570 | 0.447 | 0.326 | 0.209 | 0.107 |
| 17 Holes | | 0.621 | 0.486 | 0.353 | 0.226 | 0.116 |
| 29 Holes | | 0.735 | 0.566 | 0.404 | 0.255 | 0.130 |
| 49 Holes | | 0.855 | 0.636 | 0.436 | 0.264 | 0.128 |

LIVE LOAD RESULTANT: TABLES

| PATTERN 1 – SYMMETRICAL LOAD – R ₁ | | | | | | |
|---|-----|-------|-------|-------|-------|-------|
| η | [-] | 80 | 96 | 120 | 160 | 240 |
| F / F_{\max} [-] | | | | | | |
| No Hole | | 0.910 | 0.581 | 0.340 | 0.172 | 0.068 |
| 1 Hole | | 0.932 | 0.596 | 0.348 | 0.176 | 0.069 |
| 5 Holes | | 0.955 | 0.612 | 0.358 | 0.182 | 0.072 |
| 9 Holes | | 0.989 | 0.637 | 0.376 | 0.193 | 0.078 |
| 13 Holes | | 1.000 | 0.646 | 0.382 | 0.197 | 0.080 |
| 25 Holes | | 0.974 | 0.632 | 0.375 | 0.194 | 0.079 |
| 29 Holes | | 0.970 | 0.627 | 0.369 | 0.188 | 0.075 |
| 49 Holes | | 0.724 | 0.462 | 0.264 | 0.127 | 0.045 |

| PATTERN 2 – SYMMETRICAL LOAD – R ₁ | | | | | | |
|---|-----|-------|-------|-------|-------|-------|
| η | [-] | 80 | 96 | 120 | 160 | 240 |
| F/F _{max} [-] | | | | | | |
| No Hole | | 0.910 | 0.581 | 0.340 | 0.172 | 0.068 |
| 4 Holes | | 0.921 | 0.589 | 0.344 | 0.174 | 0.069 |
| 8 Holes | | 0.924 | 0.590 | 0.344 | 0.174 | 0.068 |
| 12 Holes | | 0.958 | 0.614 | 0.359 | 0.182 | 0.072 |
| 13 Holes | | 0.980 | 0.629 | 0.369 | 0.188 | 0.074 |
| 33 Holes | | 0.801 | 0.510 | 0.293 | 0.143 | 0.051 |
| 45 Holes | | 0.724 | 0.460 | 0.262 | 0.126 | 0.044 |
| 49 Holes | | 0.724 | 0.462 | 0.264 | 0.127 | 0.045 |

| PATTERN 3 – SYMMETRICAL LOAD – R ₁ | | | | | | |
|---|-----|-------|-------|-------|-------|-------|
| η | [-] | 80 | 96 | 120 | 160 | 240 |
| F/F _{max} [-] | | | | | | |
| No Hole | | 0.910 | 0.581 | 0.340 | 0.172 | 0.068 |
| 4 Holes | | 0.848 | 0.532 | 0.303 | 0.148 | 0.055 |
| 8 Holes | | 0.840 | 0.527 | 0.300 | 0.146 | 0.054 |
| 12 Holes | | 0.861 | 0.541 | 0.309 | 0.151 | 0.056 |
| 13 Holes | | 0.879 | 0.554 | 0.317 | 0.155 | 0.058 |
| 33 Holes | | 0.747 | 0.475 | 0.273 | 0.132 | 0.047 |
| 45 Holes | | 0.712 | 0.452 | 0.257 | 0.123 | 0.043 |
| 49 Holes | | 0.724 | 0.462 | 0.264 | 0.127 | 0.045 |

| PATTERN 4 – SYMMETRICAL LOAD – R ₁ | | | | | | |
|---|-----|-------|-------|-------|-------|-------|
| η | [-] | 80 | 96 | 120 | 160 | 240 |
| F/F _{max} [-] | | | | | | |
| No Hole | | 0.910 | 0.581 | 0.340 | 0.172 | 0.068 |
| 4 Holes | | 0.879 | 0.552 | 0.315 | 0.154 | 0.057 |
| 8 Holes | | 0.948 | 0.607 | 0.355 | 0.180 | 0.071 |
| 12 Holes | | 0.933 | 0.599 | 0.351 | 0.179 | 0.071 |
| 13 Holes | | 0.879 | 0.554 | 0.317 | 0.155 | 0.058 |
| 33 Holes | | 0.911 | 0.577 | 0.332 | 0.164 | 0.063 |
| 45 Holes | | 0.919 | 0.585 | 0.337 | 0.167 | 0.064 |
| 49 Holes | | 0.724 | 0.462 | 0.264 | 0.127 | 0.045 |

| PATTERN 1 – ANTI-SYMMETRICAL LOAD – R ₁ | | | | | | |
|--|-----|-------|-------|-------|-------|-------|
| η | [-] | 80 | 96 | 120 | 160 | 240 |
| F/F _{max} [-] | | | | | | |
| No Hole | | 0.673 | 0.463 | 0.292 | 0.159 | 0.065 |
| 1 Hole | | 0.689 | 0.474 | 0.299 | 0.162 | 0.066 |
| 5 Holes | | 0.721 | 0.495 | 0.311 | 0.167 | 0.068 |
| 9 Holes | | 0.754 | 0.518 | 0.325 | 0.176 | 0.073 |
| 13 Holes | | 0.767 | 0.526 | 0.329 | 0.178 | 0.074 |
| 25 Holes | | 0.807 | 0.545 | 0.335 | 0.178 | 0.073 |
| 29 Holes | | 0.801 | 0.537 | 0.326 | 0.171 | 0.070 |
| 49 Holes | | 0.634 | 0.409 | 0.237 | 0.116 | 0.042 |

| PATTERN 2 – ANTI-SYMMETRICAL LOAD – R ₁ | | | | | | |
|--|-----|-------|-------|-------|-------|-------|
| η | [-] | 80 | 96 | 120 | 160 | 240 |
| F/F _{max} [-] | | | | | | |
| No Hole | | 0.673 | 0.463 | 0.292 | 0.159 | 0.065 |
| 4 Holes | | 0.677 | 0.466 | 0.293 | 0.159 | 0.064 |
| 8 Holes | | 0.686 | 0.469 | 0.293 | 0.156 | 0.062 |
| 12 Holes | | 0.719 | 0.491 | 0.306 | 0.163 | 0.066 |
| 13 Holes | | 0.742 | 0.507 | 0.315 | 0.168 | 0.068 |
| 33 Holes | | 0.641 | 0.428 | 0.256 | 0.128 | 0.046 |
| 45 Holes | | 0.622 | 0.403 | 0.234 | 0.114 | 0.040 |
| 49 Holes | | 0.634 | 0.409 | 0.237 | 0.116 | 0.042 |

| PATTERN 3 – ANTI-SYMMETRICAL LOAD – R ₁ | | | | | | |
|--|-----|-------|-------|-------|-------|-------|
| η | [-] | 80 | 96 | 120 | 160 | 240 |
| F/F _{max} [-] | | | | | | |
| No Hole | | 0.673 | 0.463 | 0.292 | 0.159 | 0.065 |
| 4 Holes | | 0.621 | 0.427 | 0.266 | 0.140 | 0.054 |
| 8 Holes | | 0.624 | 0.425 | 0.262 | 0.136 | 0.051 |
| 12 Holes | | 0.642 | 0.436 | 0.267 | 0.138 | 0.052 |
| 13 Holes | | 0.658 | 0.447 | 0.274 | 0.142 | 0.054 |
| 33 Holes | | 0.617 | 0.410 | 0.243 | 0.120 | 0.042 |
| 45 Holes | | 0.613 | 0.397 | 0.229 | 0.111 | 0.040 |
| 49 Holes | | 0.634 | 0.409 | 0.237 | 0.116 | 0.042 |

| PATTERN 4 – ANTI-SYMMETRICAL LOAD – R ₁ | | | | | | |
|--|-----|-------|-------|-------|-------|-------|
| η | [-] | 80 | 96 | 120 | 160 | 240 |
| F/F_{\max} [-] | | | | | | |
| No Hole | | 0.673 | 0.463 | 0.292 | 0.159 | 0.065 |
| 4 Holes | | 0.689 | 0.474 | 0.299 | 0.162 | 0.066 |
| 8 Holes | | 0.714 | 0.490 | 0.307 | 0.165 | 0.067 |
| 12 Holes | | 0.726 | 0.496 | 0.309 | 0.165 | 0.067 |
| 13 Holes | | 0.658 | 0.447 | 0.274 | 0.142 | 0.054 |
| 33 Holes | | 0.688 | 0.466 | 0.286 | 0.148 | 0.057 |
| 45 Holes | | 0.706 | 0.472 | 0.284 | 0.146 | 0.056 |
| 49 Holes | | 0.634 | 0.409 | 0.237 | 0.116 | 0.042 |

UNIFORMLY DISTRIBUTED LIVE LOAD: TABLES

| PATTERN 1 – SYMMETRICAL LOAD – R ₁ | | | | | | |
|---|-----|-------|-------|-------|-------|-------|
| η | [-] | 80 | 96 | 120 | 160 | 240 |
| q/q_{\max} [-] | | | | | | |
| No Hole | | 0.665 | 0.425 | 0.248 | 0.126 | 0.050 |
| 1 Hole | | 0.687 | 0.439 | 0.256 | 0.130 | 0.051 |
| 5 Holes | | 0.738 | 0.473 | 0.277 | 0.140 | 0.056 |
| 9 Holes | | 0.797 | 0.514 | 0.303 | 0.156 | 0.063 |
| 13 Holes | | 0.845 | 0.546 | 0.323 | 0.166 | 0.068 |
| 25 Holes | | 0.954 | 0.619 | 0.368 | 0.190 | 0.077 |
| 29 Holes | | 1.000 | 0.646 | 0.381 | 0.194 | 0.078 |
| 49 Holes | | 0.971 | 0.619 | 0.354 | 0.171 | 0.061 |

| PATTERN 2 – SYMMETRICAL LOAD – R ₁ | | | | | | |
|---|-----|-------|-------|-------|-------|-------|
| η | [-] | 80 | 96 | 120 | 160 | 240 |
| q/q_{\max} [-] | | | | | | |
| No Hole | | 0.665 | 0.425 | 0.248 | 0.126 | 0.050 |
| 4 Holes | | 0.704 | 0.450 | 0.263 | 0.133 | 0.053 |
| 8 Holes | | 0.743 | 0.474 | 0.277 | 0.140 | 0.054 |
| 12 Holes | | 0.806 | 0.516 | 0.302 | 0.153 | 0.061 |
| 13 Holes | | 0.833 | 0.535 | 0.314 | 0.160 | 0.063 |
| 33 Holes | | 0.868 | 0.552 | 0.317 | 0.155 | 0.056 |
| 45 Holes | | 0.920 | 0.585 | 0.333 | 0.160 | 0.056 |
| 49 Holes | | 0.971 | 0.619 | 0.354 | 0.171 | 0.061 |

| PATTERN 3 – SYMMETRICAL LOAD – R ₁ | | | | | | |
|---|-----|-------|-------|-------|-------|-------|
| η | [-] | 80 | 96 | 120 | 160 | 240 |
| q/q _{max} [-] | | | | | | |
| No Hole | | 0.665 | 0.425 | 0.248 | 0.126 | 0.050 |
| 4 Holes | | 0.648 | 0.407 | 0.232 | 0.113 | 0.042 |
| 8 Holes | | 0.673 | 0.423 | 0.240 | 0.117 | 0.043 |
| 12 Holes | | 0.724 | 0.455 | 0.260 | 0.127 | 0.047 |
| 13 Holes | | 0.745 | 0.470 | 0.269 | 0.132 | 0.049 |
| 33 Holes | | 0.810 | 0.515 | 0.296 | 0.143 | 0.051 |
| 45 Holes | | 0.907 | 0.575 | 0.327 | 0.157 | 0.055 |
| 49 Holes | | 0.971 | 0.619 | 0.354 | 0.171 | 0.061 |

| PATTERN 4 – SYMMETRICAL LOAD – R ₁ | | | | | | |
|---|-----|-------|-------|-------|-------|-------|
| η | [-] | 80 | 96 | 120 | 160 | 240 |
| q/q _{max} [-] | | | | | | |
| No Hole | | 0.665 | 0.425 | 0.248 | 0.126 | 0.050 |
| 4 Holes | | 0.648 | 0.407 | 0.232 | 0.113 | 0.042 |
| 8 Holes | | 0.733 | 0.469 | 0.274 | 0.139 | 0.055 |
| 12 Holes | | 0.756 | 0.485 | 0.285 | 0.145 | 0.058 |
| 13 Holes | | 0.745 | 0.470 | 0.269 | 0.132 | 0.049 |
| 33 Holes | | 0.808 | 0.512 | 0.294 | 0.146 | 0.056 |
| 45 Holes | | 0.947 | 0.603 | 0.348 | 0.172 | 0.066 |
| 49 Holes | | 0.971 | 0.619 | 0.354 | 0.171 | 0.061 |

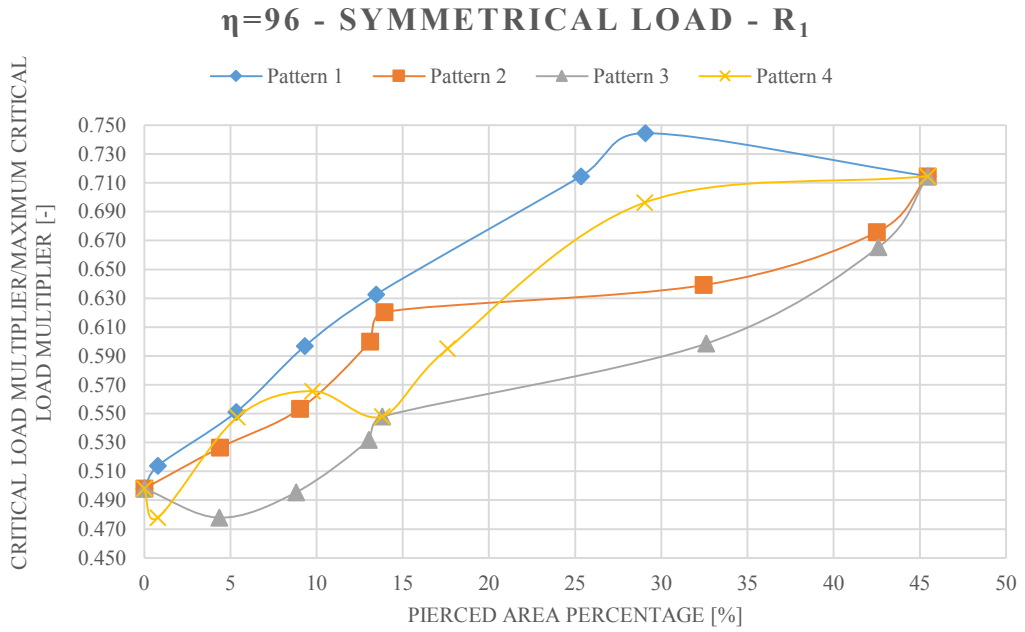
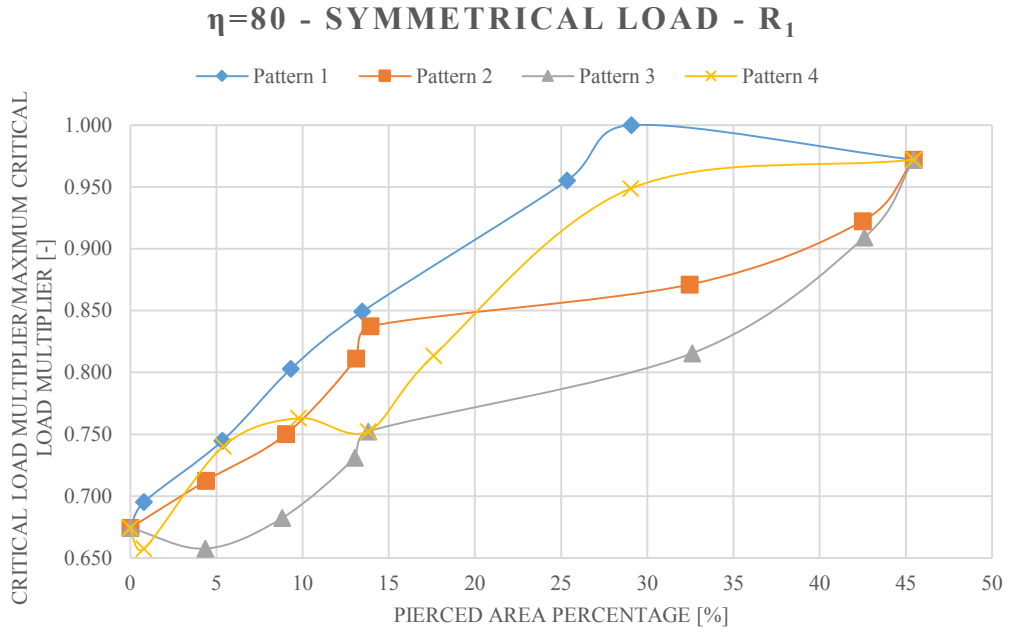
| PATTERN 1 – ANTI-SYMMETRICAL LOAD – R ₁ | | | | | | |
|--|-----|-------|-------|-------|-------|-------|
| η | [-] | 80 | 96 | 120 | 160 | 240 |
| q/q _{max} [-] | | | | | | |
| No Hole | | 0.492 | 0.339 | 0.213 | 0.116 | 0.048 |
| 1 Hole | | 0.508 | 0.350 | 0.220 | 0.119 | 0.049 |
| 5 Holes | | 0.557 | 0.382 | 0.240 | 0.129 | 0.053 |
| 9 Holes | | 0.608 | 0.418 | 0.262 | 0.142 | 0.059 |
| 13 Holes | | 0.648 | 0.444 | 0.278 | 0.150 | 0.063 |
| 25 Holes | | 0.790 | 0.534 | 0.328 | 0.174 | 0.071 |
| 29 Holes | | 0.826 | 0.554 | 0.337 | 0.176 | 0.072 |
| 49 Holes | | 0.851 | 0.549 | 0.318 | 0.155 | 0.056 |

| PATTERN 2 – ANTI-SYMMETRICAL LOAD – R ₁ | | | | | | |
|--|-----|-------|-------|-------|-------|-------|
| η | [-] | 80 | 96 | 120 | 160 | 240 |
| q/q _{max} [-] | | | | | | |
| No Hole | | 0.492 | 0.339 | 0.213 | 0.116 | 0.048 |
| 4 Holes | | 0.518 | 0.356 | 0.224 | 0.121 | 0.049 |
| 8 Holes | | 0.552 | 0.377 | 0.235 | 0.125 | 0.050 |
| 12 Holes | | 0.605 | 0.413 | 0.257 | 0.137 | 0.055 |
| 13 Holes | | 0.630 | 0.431 | 0.268 | 0.143 | 0.058 |
| 33 Holes | | 0.694 | 0.464 | 0.277 | 0.139 | 0.049 |
| 45 Holes | | 0.791 | 0.513 | 0.297 | 0.144 | 0.051 |
| 49 Holes | | 0.851 | 0.549 | 0.318 | 0.155 | 0.056 |

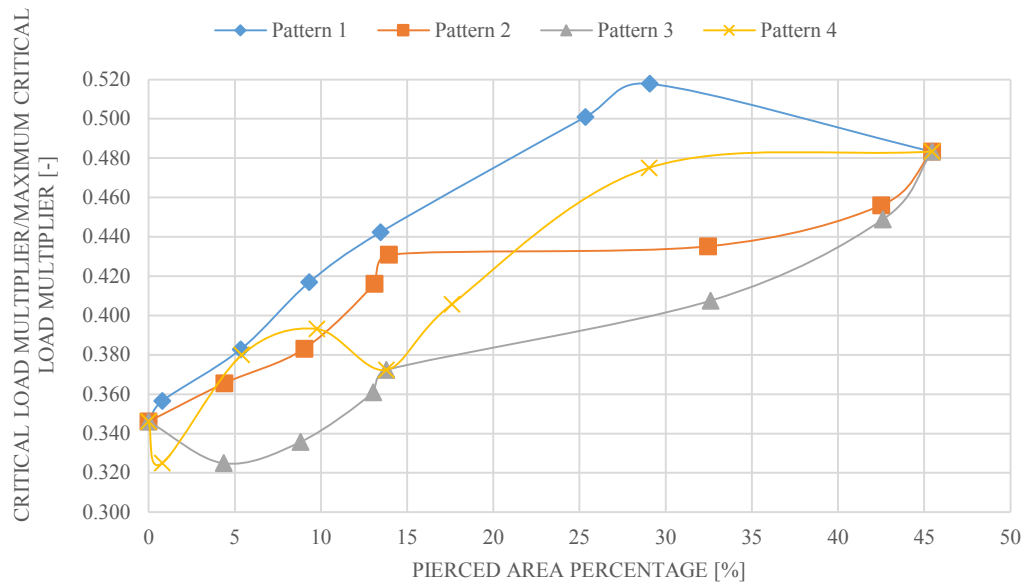
| PATTERN 3 – ANTI-SYMMETRICAL LOAD – R ₁ | | | | | | |
|--|-----|-------|-------|-------|-------|-------|
| η | [-] | 80 | 96 | 120 | 160 | 240 |
| q/q _{max} [-] | | | | | | |
| No Hole | | 0.492 | 0.339 | 0.213 | 0.116 | 0.048 |
| 4 Holes | | 0.475 | 0.326 | 0.203 | 0.107 | 0.041 |
| 8 Holes | | 0.500 | 0.341 | 0.210 | 0.109 | 0.041 |
| 12 Holes | | 0.539 | 0.366 | 0.225 | 0.116 | 0.044 |
| 13 Holes | | 0.558 | 0.379 | 0.233 | 0.120 | 0.046 |
| 33 Holes | | 0.669 | 0.444 | 0.264 | 0.130 | 0.046 |
| 45 Holes | | 0.781 | 0.505 | 0.292 | 0.142 | 0.050 |
| 49 Holes | | 0.851 | 0.549 | 0.318 | 0.155 | 0.056 |

| PATTERN 4 – ANTI-SYMMETRICAL LOAD – R ₁ | | | | | | |
|--|-----|-------|-------|-------|-------|-------|
| η | [-] | 80 | 96 | 120 | 160 | 240 |
| q/q _{max} [-] | | | | | | |
| No Hole | | 0.492 | 0.339 | 0.213 | 0.116 | 0.048 |
| 4 Holes | | 0.508 | 0.350 | 0.220 | 0.119 | 0.049 |
| 8 Holes | | 0.552 | 0.379 | 0.238 | 0.128 | 0.052 |
| 12 Holes | | 0.589 | 0.402 | 0.250 | 0.134 | 0.054 |
| 13 Holes | | 0.558 | 0.379 | 0.233 | 0.120 | 0.046 |
| 33 Holes | | 0.610 | 0.414 | 0.254 | 0.131 | 0.050 |
| 45 Holes | | 0.727 | 0.486 | 0.293 | 0.150 | 0.058 |
| 49 Holes | | 0.851 | 0.549 | 0.318 | 0.155 | 0.056 |

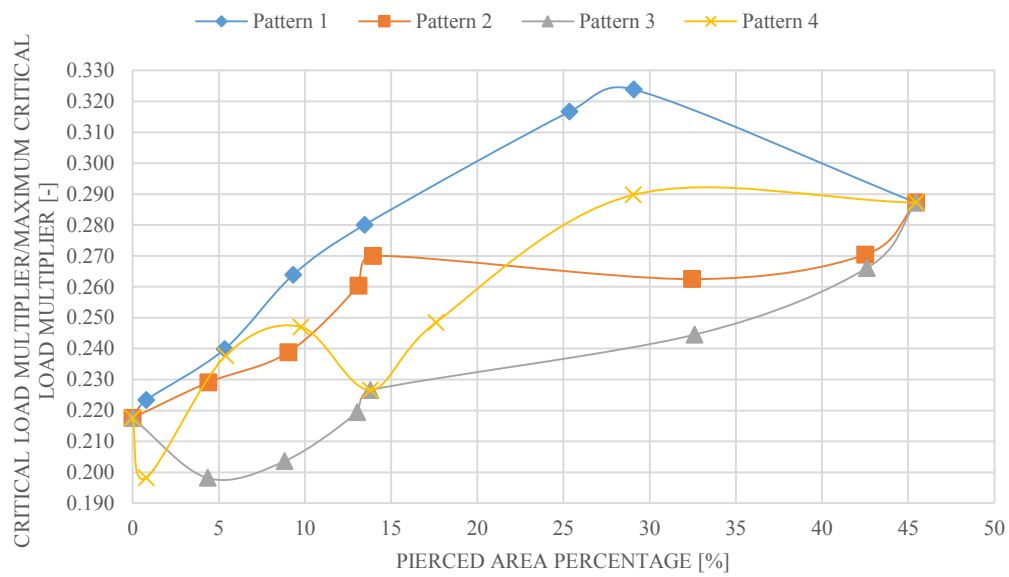
LOAD MULTIPLIER: GRAPHICS



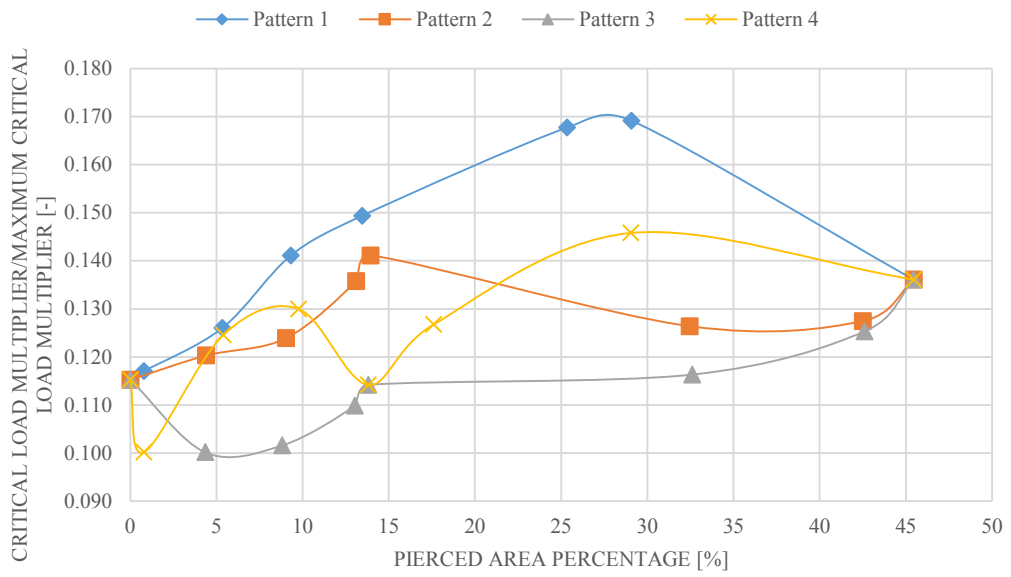
$\eta=120$ - SYMMETRICAL LOAD - R_1



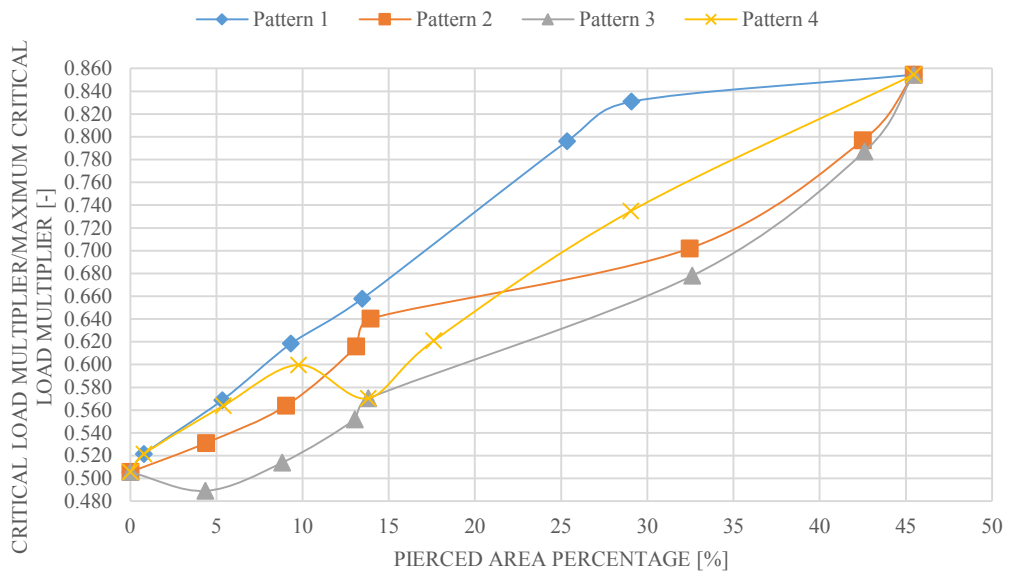
$\eta=160$ - SYMMETRICAL LOAD - R_1



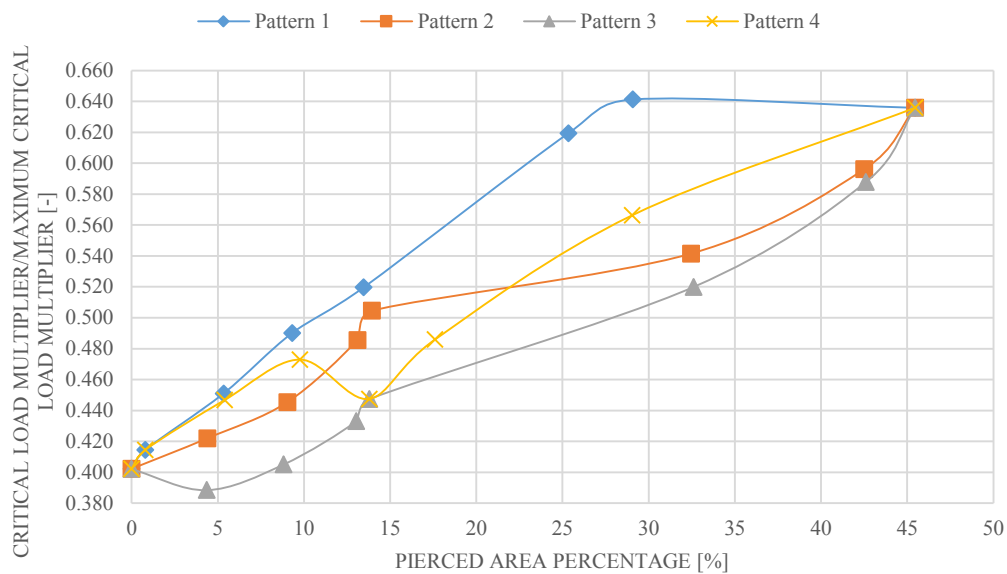
$\eta=240$ - SYMMETRICAL LOAD - R_1



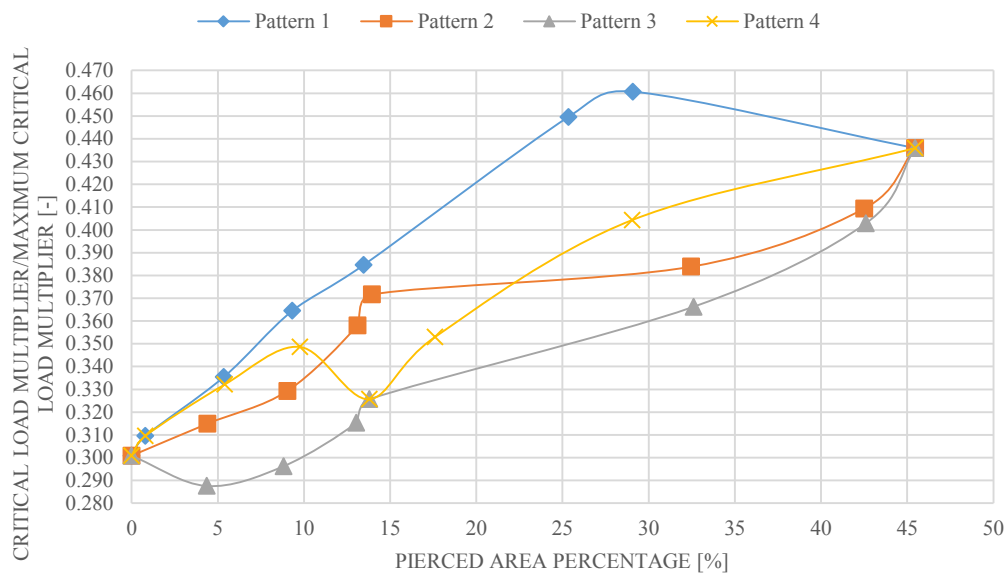
$\eta=80$ - ANTI-SYMMETRICAL LOAD- R_1



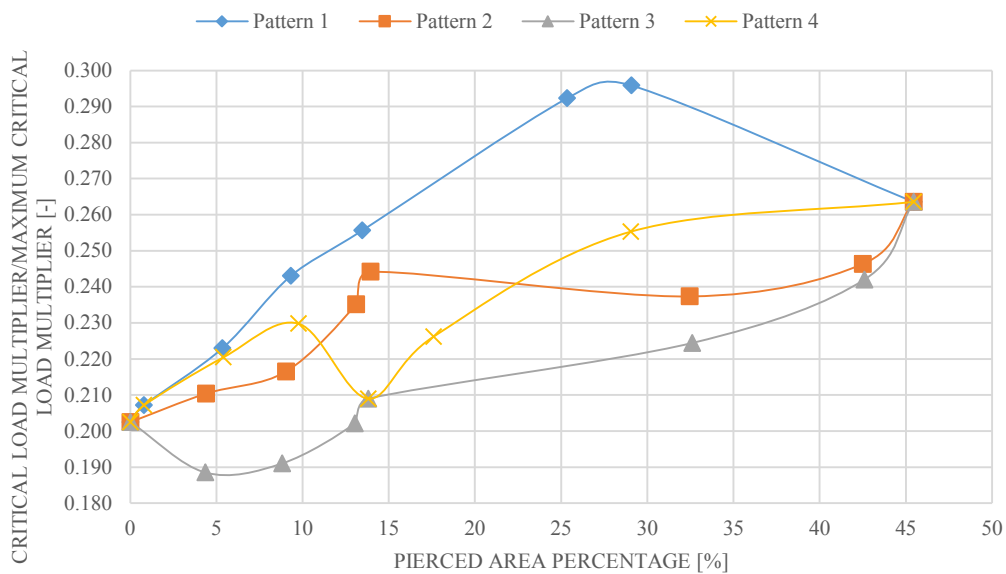
$\eta=96$ - ANTI-SYMMETRICAL LOAD- R_1



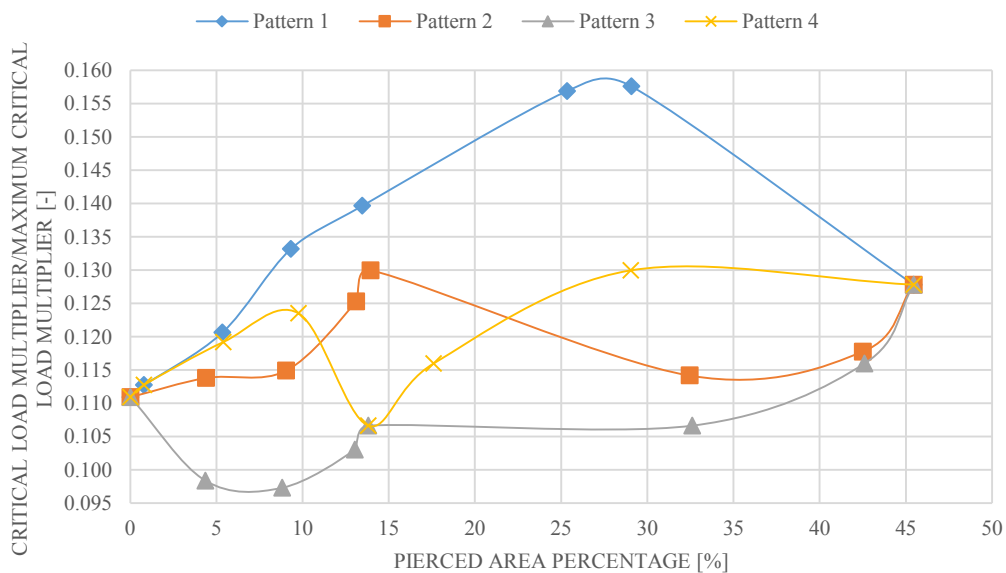
$\eta=120$ - ANTI-SYMMETRICAL LOAD - R_1



$\eta=160$ - ANTI-SYMMETRICAL LOAD- R_1

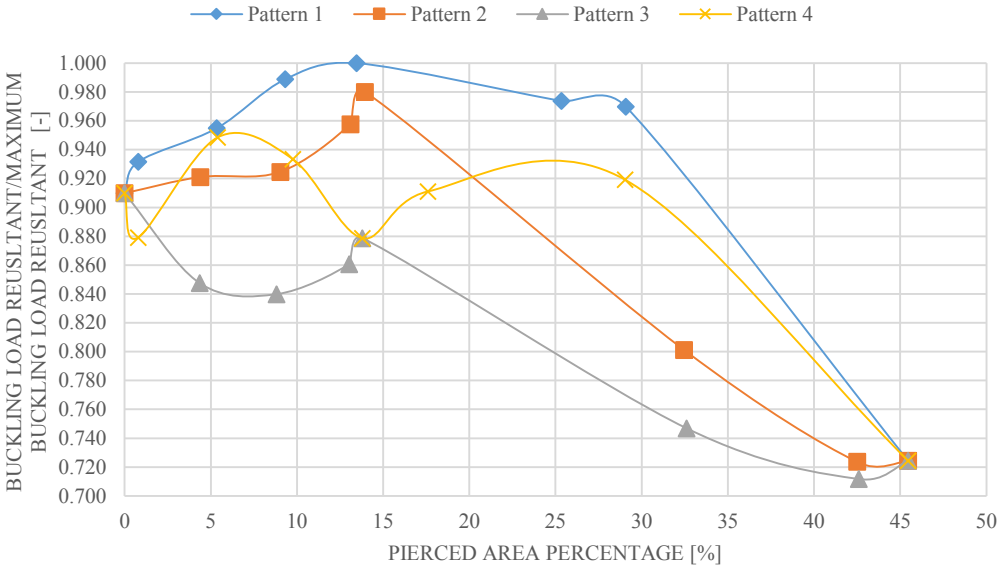


$\eta=240$ - ANTI-SYMMETRICAL LOAD- R_1

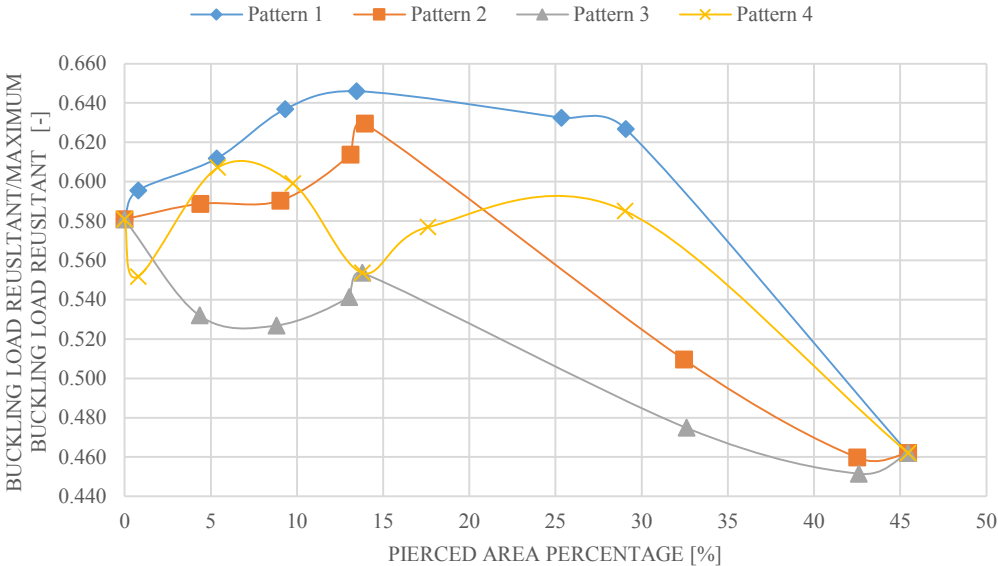


LIVE LOAD RESULTANT: GRAPHICS

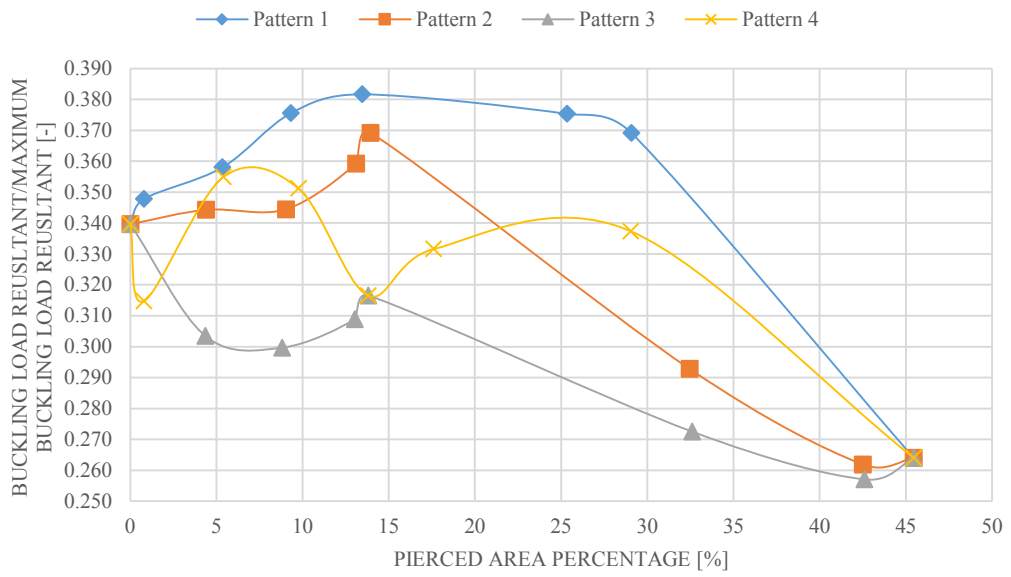
$\eta=80$ - SYMMETRICAL LOAD- R_1



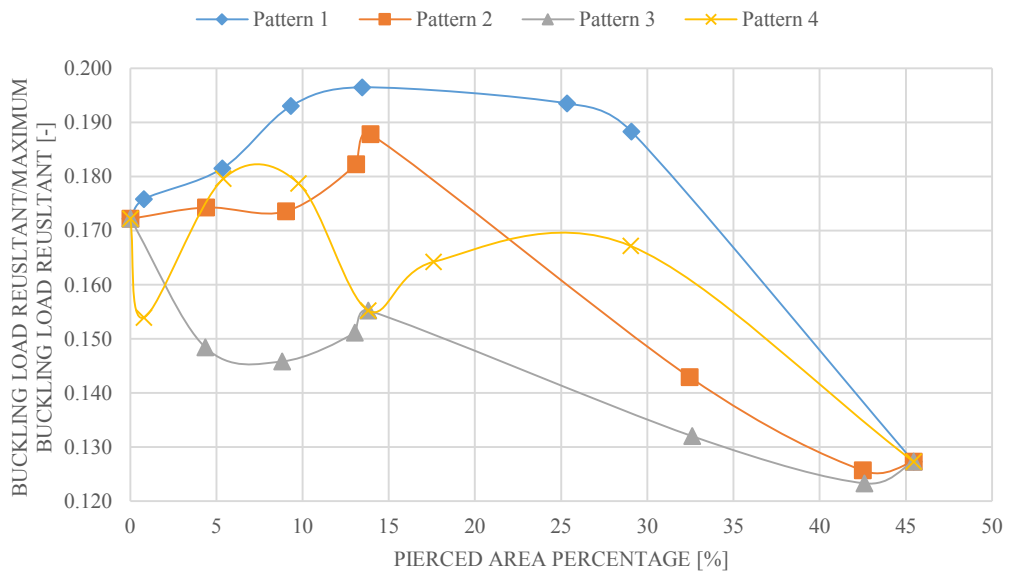
$\eta=96$ - SYMMETRICAL LOAD- R_1



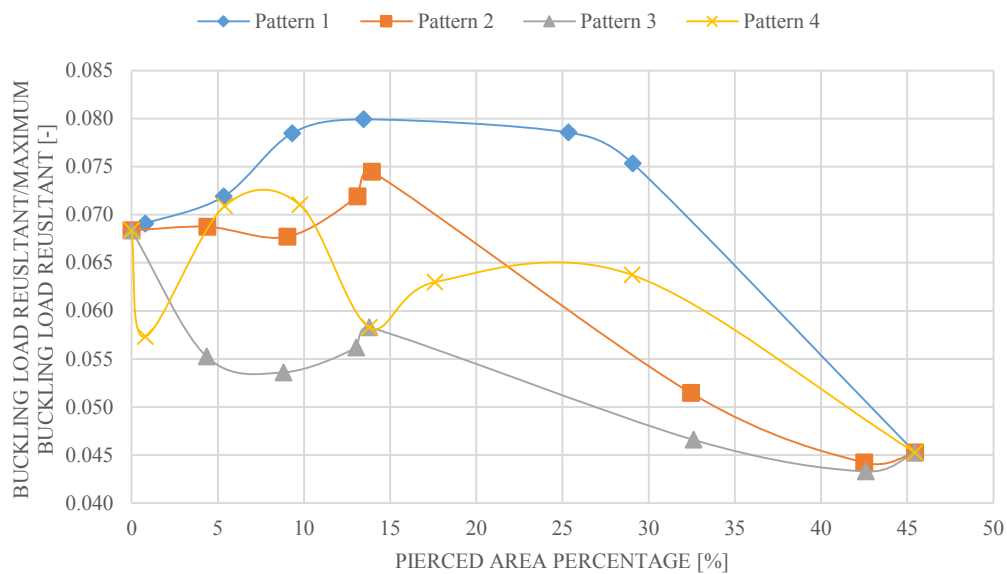
$\eta=120$ - SYMMETRICAL LOAD- R_1



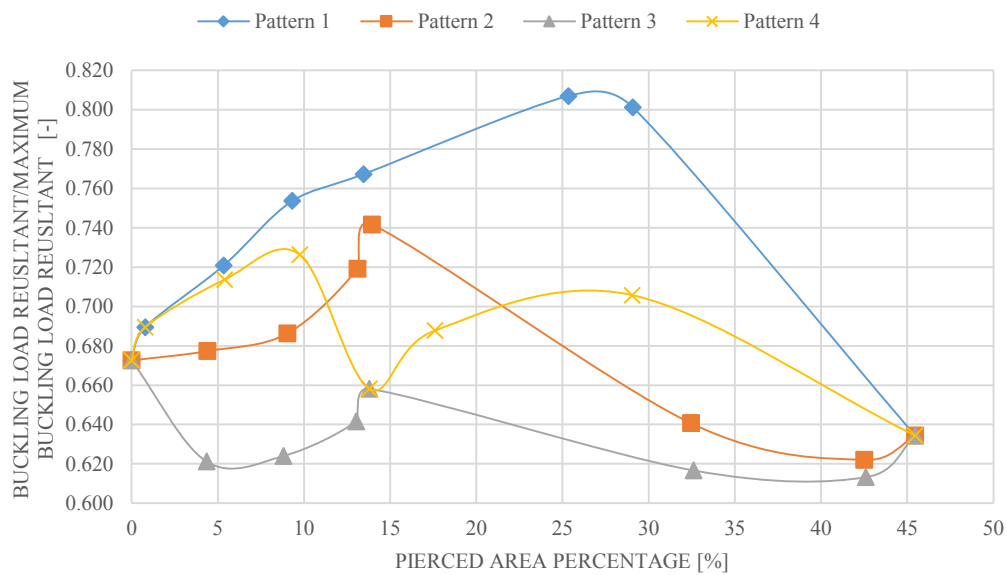
$\eta=160$ - SYMMETRICAL LOAD- R_1



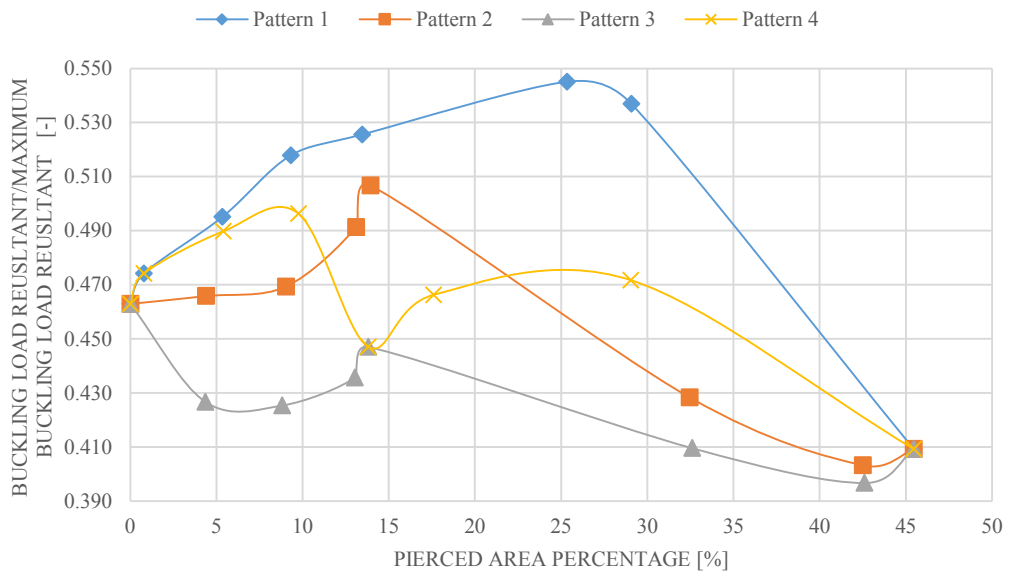
$\eta=240$ - SYMMETRICAL LOAD- R_1



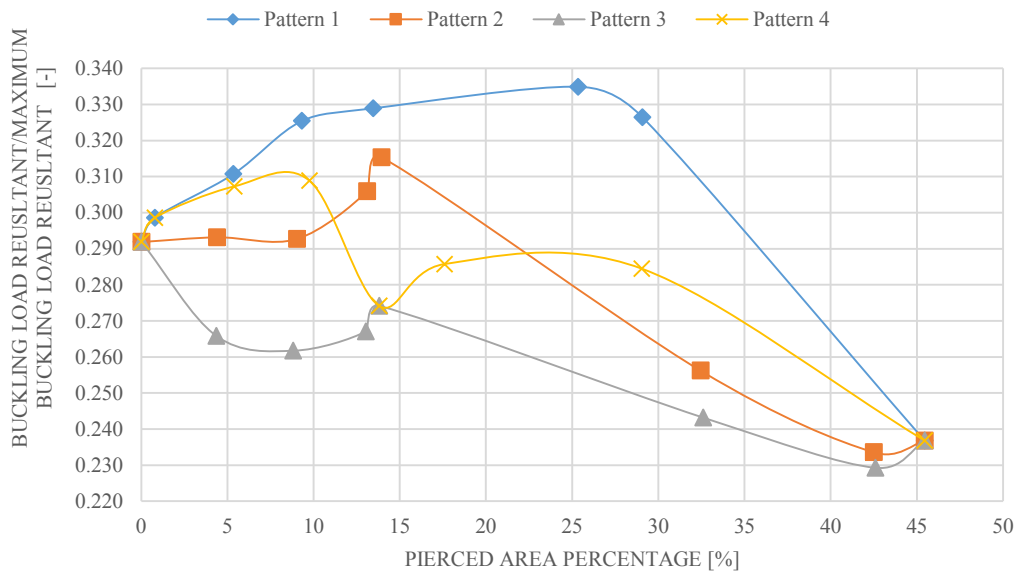
$\eta=80$ - ANTI-SYMMETRICAL LOAD- R_1



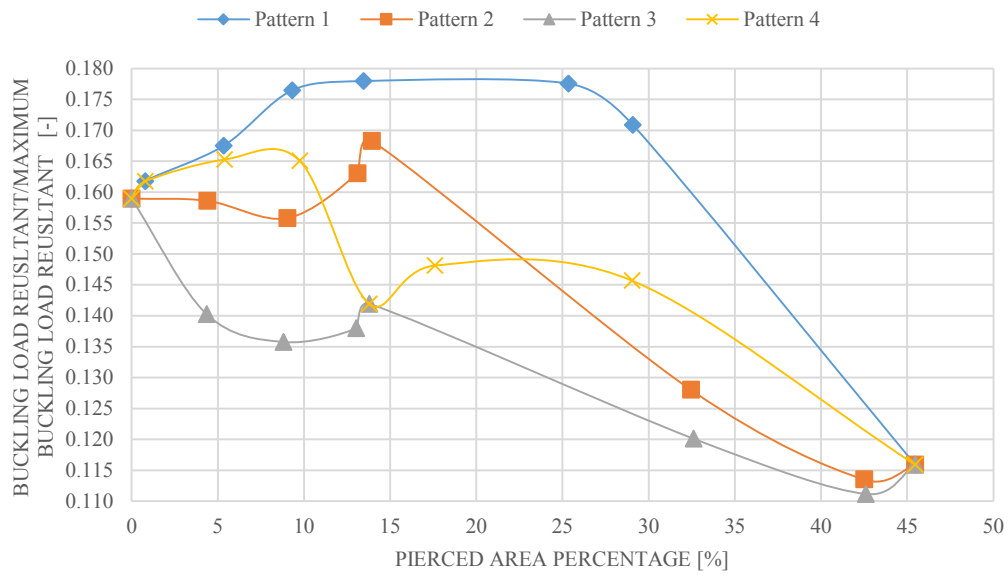
$\eta=96$ - ANTI-SYMMETRICAL LOAD- R_1



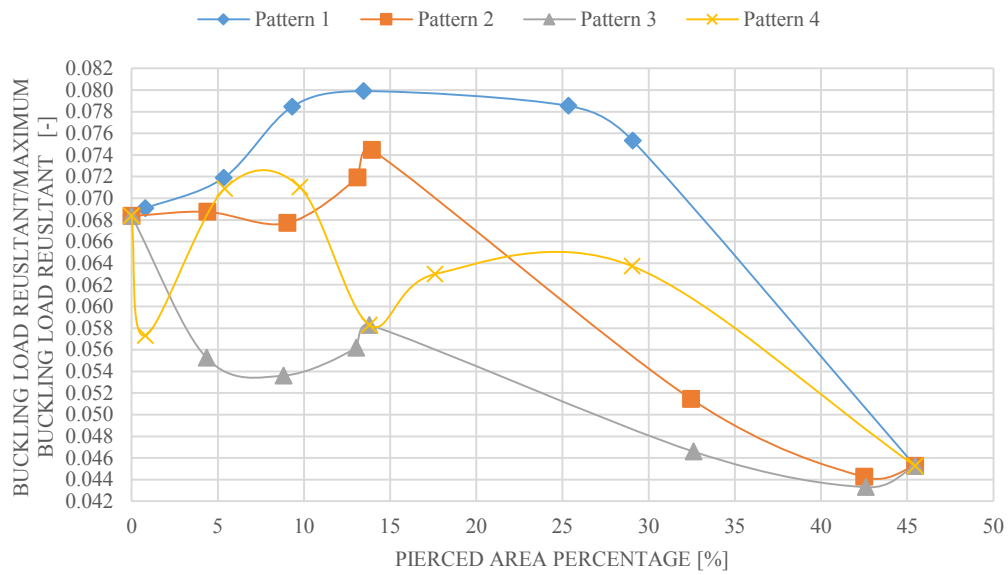
$\eta=120$ - ANTI-SYMMETRICAL LOAD- R_1



$\eta=160$ - ANTI-SYMMETRICAL LOAD - R_1

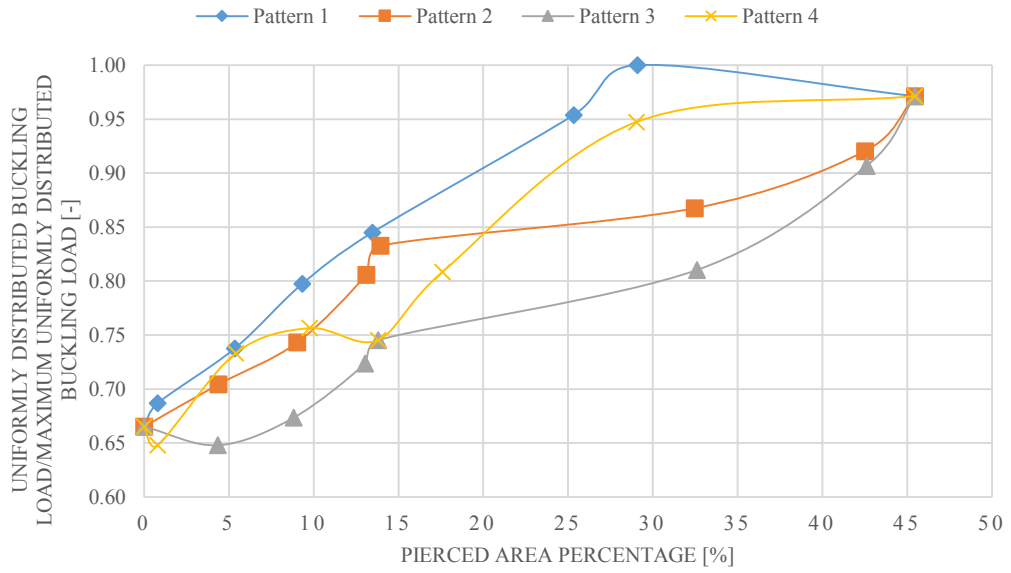


$\eta=240$ - ANTI-SYMMETRICAL LOAD - R_1

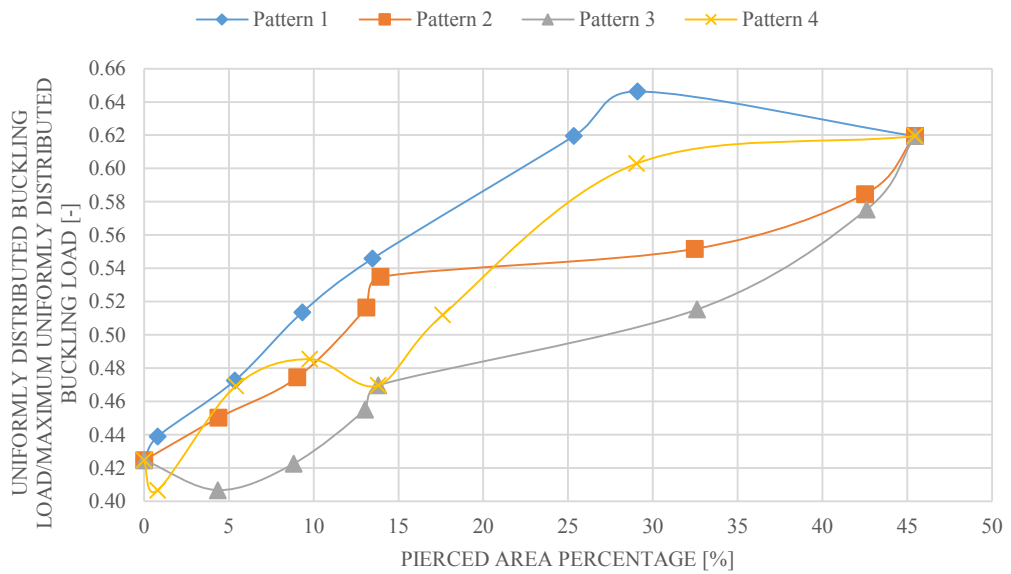


UNIFORMLY DISTRIBUTED LIVE LOAD: GRAPHICS

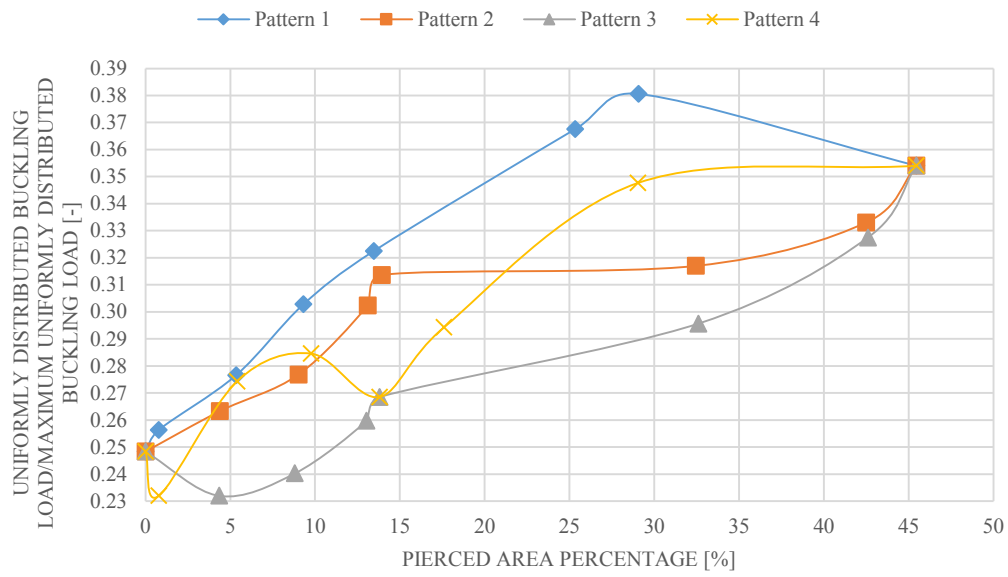
$\eta=80$ - SYMMETRICAL LOAD - R_1



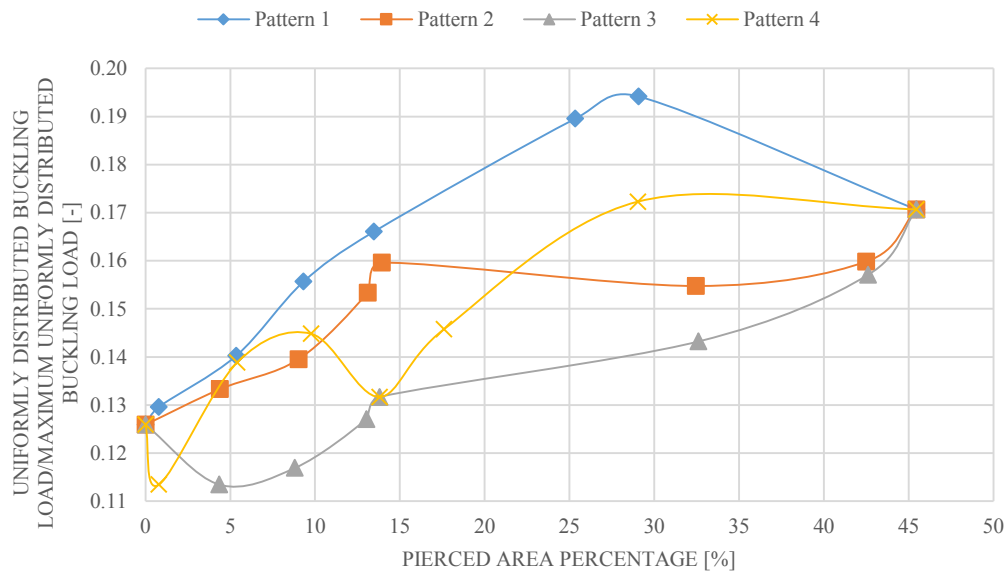
$\eta=96$ - SYMMETRICAL LOAD - R_1



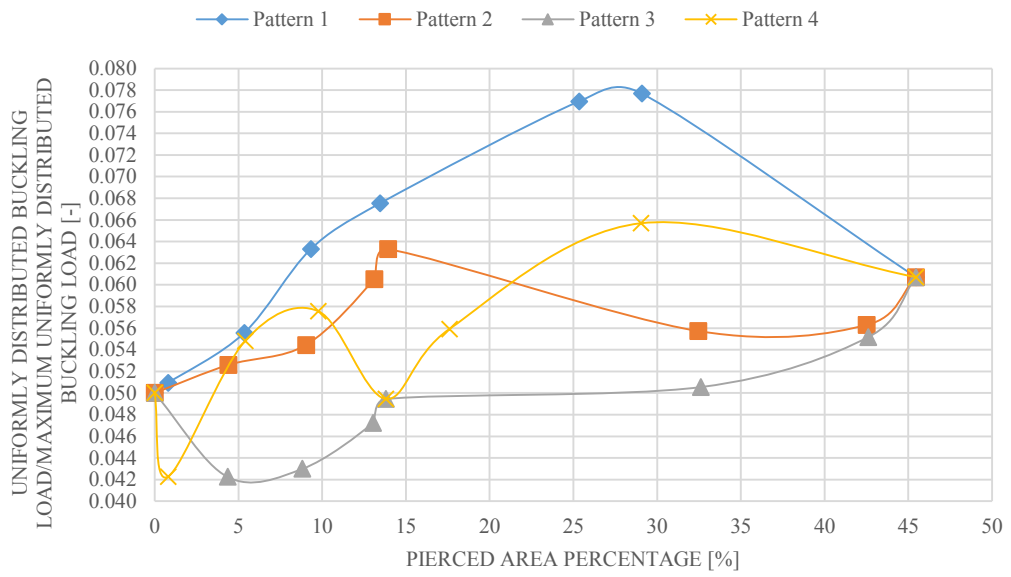
$\eta=120$ - SYMMETRICAL LOAD - R_1



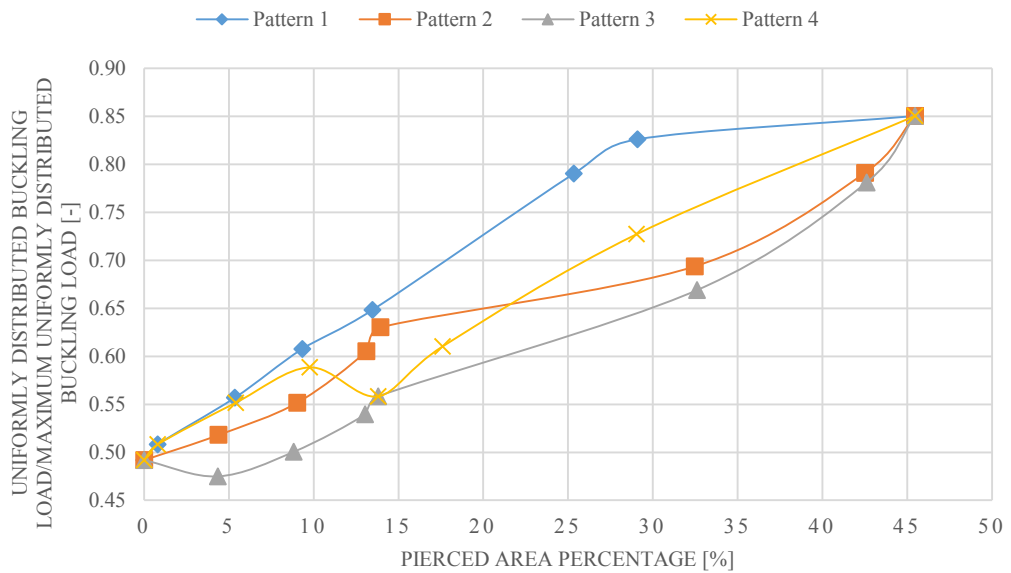
$\eta=160$ - SYMMETRICAL LOAD - R_1



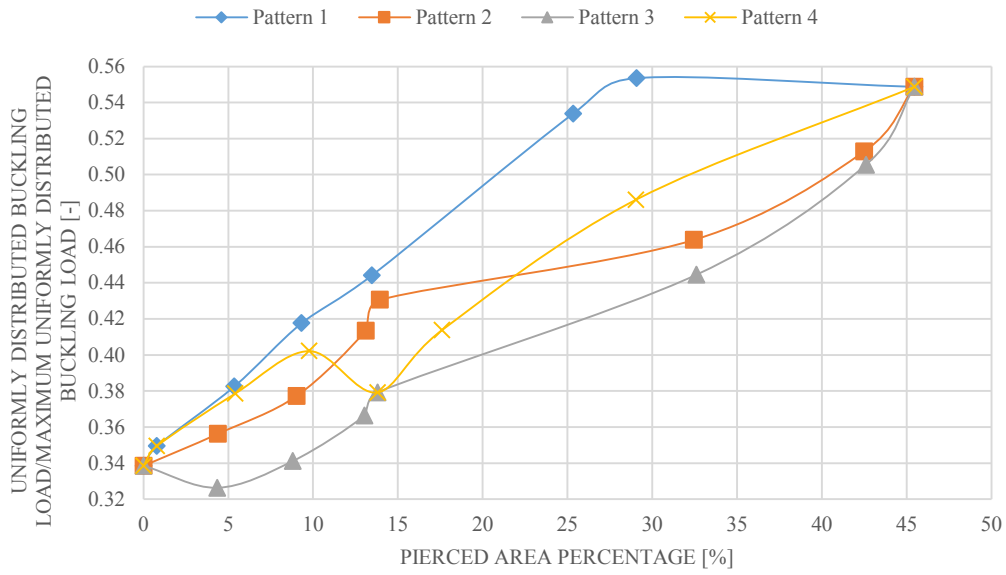
$\eta=240$ - SYMMETRICAL LOAD - R_1



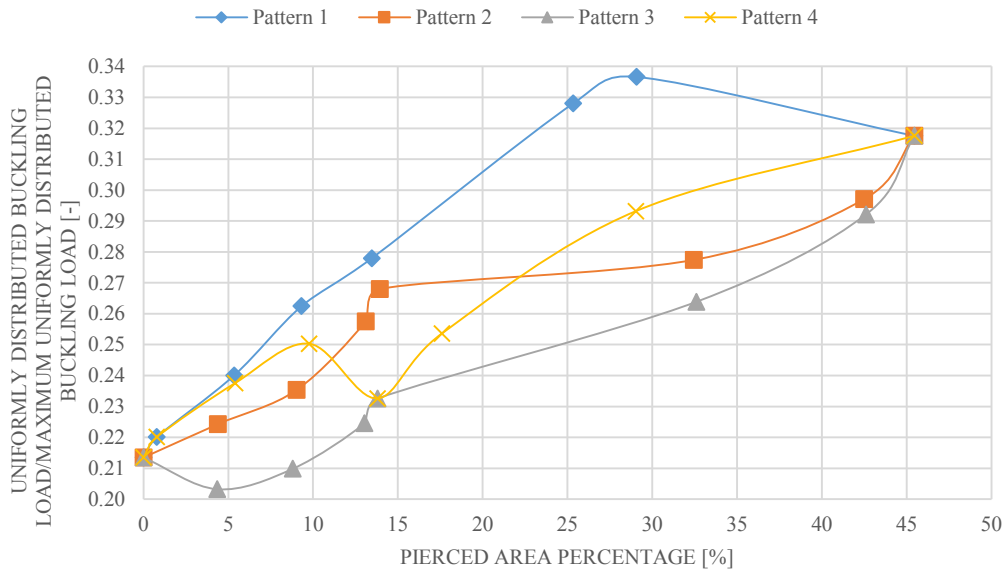
$\eta=80$ - ANTI-SYMMETRICAL LOAD - R_1



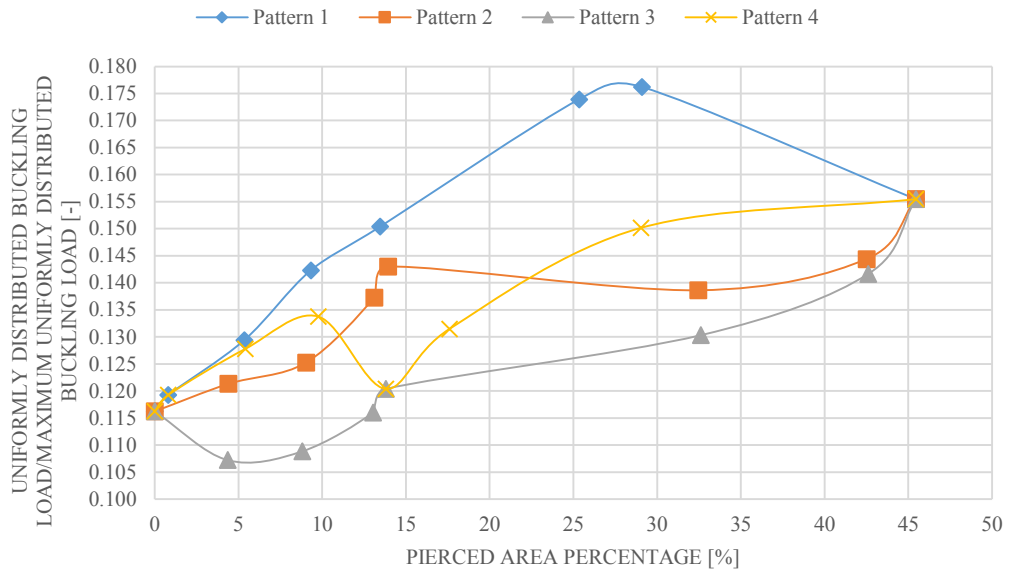
$\eta=96$ - ANTI-SYMMETRICAL LOAD - R_1



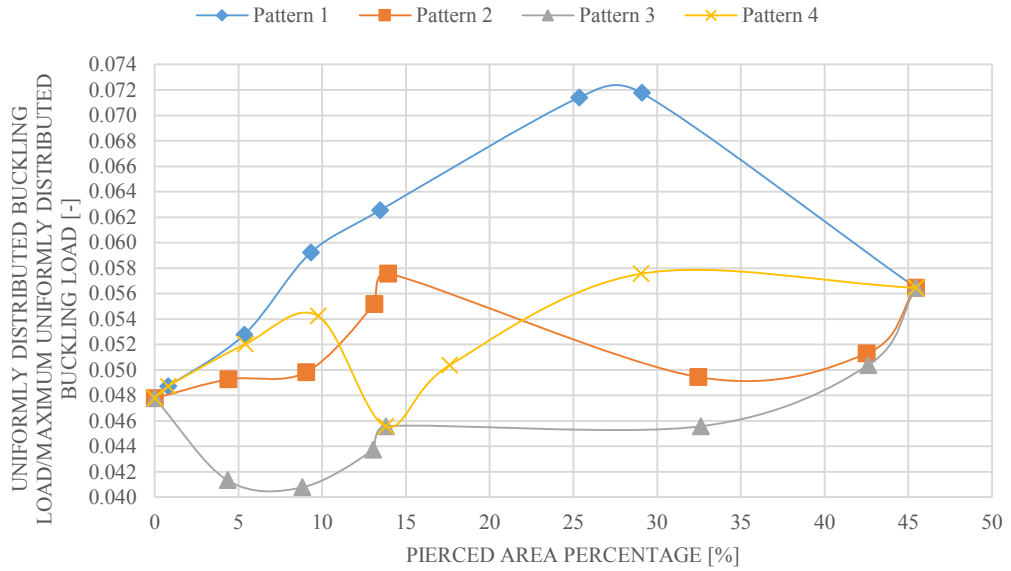
$\eta=120$ - ANTI-SYMMETRICAL LOAD - R_1



$\eta=160$ - ANTI-SYMMETRICAL LOAD - R_1



$\eta=240$ - ANTI-SYMMETRICAL LOAD - R_1



LOAD MULTIPLIER: TABLES

| PATTERN 1 – SYMMETRICAL LOAD – R ₂ | | | | | | |
|---|-----|-------|-------|-------|-------|-------|
| η | [-] | 80 | 96 | 120 | 160 | 240 |
| λ/λ_{\max} [-] | | | | | | |
| No Hole | | 0.359 | 0.251 | 0.163 | 0.095 | 0.045 |
| 1 Hole | | 0.361 | 0.254 | 0.166 | 0.097 | 0.046 |
| 5 Holes | | 0.397 | 0.281 | 0.184 | 0.107 | 0.051 |
| 9 Holes | | 0.422 | 0.301 | 0.198 | 0.116 | 0.056 |
| 13 Holes | | 0.374 | 0.315 | 0.209 | 0.124 | 0.060 |
| 25 Holes | | 0.369 | 0.321 | 0.227 | 0.136 | 0.066 |
| 29 Holes | | 0.335 | 0.286 | 0.238 | 0.142 | 0.067 |
| 49 Holes | | 0.312 | 0.266 | 0.214 | 0.129 | 0.060 |

| PATTERN 2 – SYMMETRICAL LOAD – R ₂ | | | | | | |
|---|-----|-------|-------|-------|-------|-------|
| η | [-] | 80 | 96 | 120 | 160 | 240 |
| λ/λ_{\max} [-] | | | | | | |
| No Hole | | 0.359 | 0.251 | 0.163 | 0.095 | 0.045 |
| 4 Holes | | 0.377 | 0.265 | 0.172 | 0.100 | 0.048 |
| 8 Holes | | 0.285 | 0.233 | 0.179 | 0.104 | 0.049 |
| 12 Holes | | 0.245 | 0.201 | 0.163 | 0.115 | 0.055 |
| 13 Holes | | 0.280 | 0.234 | 0.191 | 0.121 | 0.057 |
| 33 Holes | | 0.257 | 0.214 | 0.175 | 0.121 | 0.055 |
| 45 Holes | | 0.274 | 0.230 | 0.189 | 0.123 | 0.056 |
| 49 Holes | | 0.312 | 0.266 | 0.214 | 0.129 | 0.060 |

| PATTERN 3 – SYMMETRICAL LOAD – R ₂ | | | | | | |
|---|-----|-------|-------|-------|-------|-------|
| η | [-] | 80 | 96 | 120 | 160 | 240 |
| λ/λ_{\max} [-] | | | | | | |
| No Hole | | 0.359 | 0.251 | 0.163 | 0.095 | 0.045 |
| 4 Holes | | 0.361 | 0.251 | 0.161 | 0.092 | 0.042 |
| 8 Holes | | 0.367 | 0.256 | 0.165 | 0.094 | 0.043 |
| 12 Holes | | 0.391 | 0.273 | 0.176 | 0.100 | 0.046 |
| 13 Holes | | 0.404 | 0.283 | 0.183 | 0.104 | 0.048 |
| 33 Holes | | 0.318 | 0.268 | 0.193 | 0.113 | 0.052 |
| 45 Holes | | 0.267 | 0.225 | 0.185 | 0.121 | 0.055 |
| 49 Holes | | 0.312 | 0.266 | 0.214 | 0.129 | 0.060 |

| PATTERN 4 – SYMMETRICAL LOAD – R ₂ | | | | | | |
|---|-----|-------|-------|-------|-------|-------|
| η | [-] | 80 | 96 | 120 | 160 | 240 |
| λ / λ_{\max} [-] | | | | | | |
| No Hole | | 0.359 | 0.251 | 0.163 | 0.095 | 0.045 |
| 1 Hole | | 0.361 | 0.254 | 0.166 | 0.097 | 0.046 |
| 5 Holes | | 0.396 | 0.279 | 0.182 | 0.106 | 0.051 |
| 9 Holes | | 0.400 | 0.282 | 0.185 | 0.107 | 0.051 |
| 13 Holes | | 0.404 | 0.283 | 0.183 | 0.104 | 0.048 |
| 17 Holes | | 0.429 | 0.305 | 0.199 | 0.114 | 0.052 |
| 29 Holes | | 0.452 | 0.337 | 0.229 | 0.136 | 0.063 |
| 49 Holes | | 0.312 | 0.266 | 0.214 | 0.129 | 0.060 |

| PATTERN 1 – ANTI-SYMMETRICAL LOAD – R ₂ | | | | | | |
|--|-----|-------|-------|-------|-------|-------|
| η | [-] | 80 | 96 | 120 | 160 | 240 |
| λ / λ_{\max} [-] | | | | | | |
| No Hole | | 0.232 | 0.174 | 0.124 | 0.081 | 0.043 |
| 1 Hole | | 0.233 | 0.176 | 0.127 | 0.084 | 0.045 |
| 5 Holes | | 0.265 | 0.199 | 0.143 | 0.093 | 0.049 |
| 9 Holes | | 0.289 | 0.218 | 0.155 | 0.101 | 0.053 |
| 13 Holes | | 0.315 | 0.237 | 0.169 | 0.109 | 0.057 |
| 25 Holes | | 0.389 | 0.293 | 0.206 | 0.130 | 0.065 |
| 29 Holes | | 0.413 | 0.310 | 0.217 | 0.134 | 0.066 |
| 49 Holes | | 0.418 | 0.311 | 0.211 | 0.125 | 0.058 |

| PATTERN 2 – ANTI-SYMMETRICAL LOAD – R ₂ | | | | | | |
|--|-----|-------|-------|-------|-------|-------|
| η | [-] | 80 | 96 | 120 | 160 | 240 |
| λ / λ_{\max} [-] | | | | | | |
| No Hole | | 0.232 | 0.174 | 0.124 | 0.081 | 0.043 |
| 4 Holes | | 0.245 | 0.183 | 0.131 | 0.085 | 0.045 |
| 8 Holes | | 0.258 | 0.193 | 0.137 | 0.089 | 0.046 |
| 12 Holes | | 0.288 | 0.217 | 0.154 | 0.099 | 0.051 |
| 13 Holes | | 0.303 | 0.229 | 0.163 | 0.104 | 0.054 |
| 33 Holes | | 0.321 | 0.244 | 0.173 | 0.108 | 0.052 |
| 45 Holes | | 0.390 | 0.291 | 0.199 | 0.118 | 0.055 |
| 49 Holes | | 0.418 | 0.311 | 0.211 | 0.125 | 0.058 |

| PATTERN 3 – ANTI-SYMMETRICAL LOAD – R ₂ | | | | | | |
|--|-----|-------|-------|-------|-------|-------|
| η | [-] | 80 | 96 | 120 | 160 | 240 |
| λ/λ_{\max} [-] | | | | | | |
| No Hole | | 0.232 | 0.174 | 0.124 | 0.081 | 0.043 |
| 4 Holes | | 0.213 | 0.162 | 0.117 | 0.076 | 0.040 |
| 8 Holes | | 0.225 | 0.171 | 0.122 | 0.079 | 0.041 |
| 12 Holes | | 0.244 | 0.185 | 0.132 | 0.085 | 0.043 |
| 13 Holes | | 0.255 | 0.193 | 0.138 | 0.089 | 0.045 |
| 33 Holes | | 0.312 | 0.237 | 0.168 | 0.105 | 0.050 |
| 45 Holes | | 0.381 | 0.285 | 0.196 | 0.117 | 0.054 |
| 49 Holes | | 0.418 | 0.311 | 0.211 | 0.125 | 0.058 |

| PATTERN 4 – ANTI-SYMMETRICAL LOAD – R ₂ | | | | | | |
|--|-----|-------|-------|-------|-------|-------|
| η | [-] | 80 | 96 | 120 | 160 | 240 |
| λ/λ_{\max} [-] | | | | | | |
| No Hole | | 0.232 | 0.174 | 0.124 | 0.081 | 0.043 |
| 1 Hole | | 0.233 | 0.176 | 0.127 | 0.084 | 0.045 |
| 5 Holes | | 0.263 | 0.197 | 0.141 | 0.092 | 0.048 |
| 9 Holes | | 0.279 | 0.210 | 0.149 | 0.096 | 0.050 |
| 13 Holes | | 0.255 | 0.193 | 0.138 | 0.089 | 0.045 |
| 17 Holes | | 0.282 | 0.213 | 0.152 | 0.097 | 0.049 |
| 29 Holes | | 0.360 | 0.271 | 0.191 | 0.119 | 0.059 |
| 49 Holes | | 0.418 | 0.311 | 0.211 | 0.125 | 0.058 |

LIVE LOAD RESULTANT: TABLES

| PATTERN 1 – SYMMETRICAL LOAD – R ₂ | | | | | | |
|---|-----|-------|-------|-------|-------|-------|
| η | [-] | 80 | 96 | 120 | 160 | 240 |
| F/F_{\max} [-] | | | | | | |
| No Hole | | 0.427 | 0.254 | 0.134 | 0.059 | 0.018 |
| 1 Hole | | 0.424 | 0.254 | 0.135 | 0.060 | 0.018 |
| 5 Holes | | 0.449 | 0.271 | 0.145 | 0.065 | 0.020 |
| 9 Holes | | 0.457 | 0.278 | 0.151 | 0.068 | 0.022 |
| 13 Holes | | 0.381 | 0.278 | 0.153 | 0.070 | 0.023 |
| 25 Holes | | 0.323 | 0.244 | 0.144 | 0.068 | 0.023 |
| 29 Holes | | 0.277 | 0.204 | 0.144 | 0.067 | 0.022 |
| 49 Holes | | 0.196 | 0.145 | 0.098 | 0.046 | 0.014 |

| PATTERN 2 – SYMMETRICAL LOAD – R ₂ | | | | | | |
|---|-----|-------|-------|-------|-------|-------|
| η | [-] | 80 | 96 | 120 | 160 | 240 |
| F/F _{max} [-] | | | | | | |
| No Hole | | 0.427 | 0.254 | 0.134 | 0.059 | 0.018 |
| 4 Holes | | 0.430 | 0.257 | 0.137 | 0.060 | 0.018 |
| 8 Holes | | 0.302 | 0.212 | 0.136 | 0.060 | 0.018 |
| 12 Holes | | 0.242 | 0.171 | 0.116 | 0.065 | 0.020 |
| 13 Holes | | 0.278 | 0.200 | 0.137 | 0.068 | 0.022 |
| 33 Holes | | 0.198 | 0.142 | 0.097 | 0.053 | 0.016 |
| 45 Holes | | 0.180 | 0.130 | 0.090 | 0.046 | 0.014 |
| 49 Holes | | 0.196 | 0.145 | 0.098 | 0.046 | 0.014 |

| PATTERN 3 – SYMMETRICAL LOAD – R ₂ | | | | | | |
|---|-----|-------|-------|-------|-------|-------|
| η | [-] | 80 | 96 | 120 | 160 | 240 |
| F/F _{max} [-] | | | | | | |
| No Hole | | 0.427 | 0.254 | 0.134 | 0.059 | 0.018 |
| 4 Holes | | 0.410 | 0.242 | 0.126 | 0.054 | 0.015 |
| 8 Holes | | 0.399 | 0.236 | 0.124 | 0.053 | 0.015 |
| 12 Holes | | 0.406 | 0.241 | 0.127 | 0.055 | 0.015 |
| 13 Holes | | 0.416 | 0.248 | 0.132 | 0.057 | 0.016 |
| 33 Holes | | 0.251 | 0.182 | 0.109 | 0.049 | 0.015 |
| 45 Holes | | 0.175 | 0.127 | 0.088 | 0.045 | 0.013 |
| 49 Holes | | 0.196 | 0.145 | 0.098 | 0.046 | 0.014 |

| PATTERN 4 – SYMMETRICAL LOAD – R ₂ | | | | | | |
|---|-----|-------|-------|-------|-------|-------|
| η | [-] | 80 | 96 | 120 | 160 | 240 |
| F/F _{max} [-] | | | | | | |
| No Hole | | 0.427 | 0.254 | 0.134 | 0.059 | 0.018 |
| 1 Hole | | 0.424 | 0.254 | 0.135 | 0.060 | 0.018 |
| 5 Holes | | 0.447 | 0.268 | 0.144 | 0.064 | 0.020 |
| 9 Holes | | 0.431 | 0.259 | 0.139 | 0.062 | 0.019 |
| 13 Holes | | 0.416 | 0.248 | 0.132 | 0.057 | 0.016 |
| 17 Holes | | 0.422 | 0.257 | 0.138 | 0.061 | 0.018 |
| 29 Holes | | 0.382 | 0.245 | 0.138 | 0.064 | 0.020 |
| 49 Holes | | 0.196 | 0.145 | 0.098 | 0.046 | 0.014 |

| PATTERN 1 – ANTI-SYMMETRICAL LOAD – R ₂ | | | | | | |
|--|-----|-------|-------|-------|-------|-------|
| η | [-] | 80 | 96 | 120 | 160 | 240 |
| F/F _{max} [-] | | | | | | |
| No Hole | | 0.264 | 0.167 | 0.097 | 0.048 | 0.016 |
| 1 Hole | | 0.263 | 0.168 | 0.098 | 0.049 | 0.017 |
| 5 Holes | | 0.288 | 0.184 | 0.108 | 0.054 | 0.019 |
| 9 Holes | | 0.303 | 0.194 | 0.114 | 0.057 | 0.020 |
| 13 Holes | | 0.316 | 0.204 | 0.120 | 0.060 | 0.022 |
| 25 Holes | | 0.341 | 0.221 | 0.129 | 0.064 | 0.022 |
| 29 Holes | | 0.346 | 0.223 | 0.130 | 0.063 | 0.022 |
| 49 Holes | | 0.269 | 0.172 | 0.097 | 0.045 | 0.014 |

| PATTERN 2 – ANTI-SYMMETRICAL LOAD – R ₂ | | | | | | |
|--|-----|-------|-------|-------|-------|-------|
| η | [-] | 80 | 96 | 120 | 160 | 240 |
| F/F _{max} [-] | | | | | | |
| No Hole | | 0.264 | 0.167 | 0.097 | 0.048 | 0.016 |
| 4 Holes | | 0.267 | 0.170 | 0.098 | 0.049 | 0.017 |
| 8 Holes | | 0.270 | 0.171 | 0.099 | 0.049 | 0.017 |
| 12 Holes | | 0.290 | 0.186 | 0.108 | 0.054 | 0.018 |
| 13 Holes | | 0.303 | 0.195 | 0.114 | 0.057 | 0.020 |
| 33 Holes | | 0.253 | 0.164 | 0.096 | 0.046 | 0.015 |
| 45 Holes | | 0.264 | 0.169 | 0.096 | 0.044 | 0.013 |
| 49 Holes | | 0.269 | 0.172 | 0.097 | 0.045 | 0.014 |

| PATTERN 3 – ANTI-SYMMETRICAL LOAD – R ₂ | | | | | | |
|--|-----|-------|-------|-------|-------|-------|
| η | [-] | 80 | 96 | 120 | 160 | 240 |
| F/F _{max} [-] | | | | | | |
| No Hole | | 0.264 | 0.167 | 0.097 | 0.048 | 0.016 |
| 4 Holes | | 0.229 | 0.147 | 0.086 | 0.042 | 0.014 |
| 8 Holes | | 0.233 | 0.149 | 0.087 | 0.042 | 0.013 |
| 12 Holes | | 0.242 | 0.155 | 0.090 | 0.044 | 0.014 |
| 13 Holes | | 0.251 | 0.161 | 0.094 | 0.046 | 0.015 |
| 33 Holes | | 0.246 | 0.159 | 0.093 | 0.045 | 0.014 |
| 45 Holes | | 0.258 | 0.166 | 0.094 | 0.043 | 0.013 |
| 49 Holes | | 0.269 | 0.172 | 0.097 | 0.045 | 0.014 |

| PATTERN 4 – ANTI-SYMMETRICAL LOAD – R ₂ | | | | | | |
|--|-----|-------|-------|-------|-------|-------|
| η | [-] | 80 | 96 | 120 | 160 | 240 |
| F/F _{max} [-] | | | | | | |
| No Hole | | 0.264 | 0.167 | 0.097 | 0.048 | 0.016 |
| 1 Hole | | 0.263 | 0.168 | 0.098 | 0.049 | 0.017 |
| 5 Holes | | 0.286 | 0.182 | 0.106 | 0.053 | 0.018 |
| 9 Holes | | 0.290 | 0.186 | 0.108 | 0.054 | 0.018 |
| 13 Holes | | 0.251 | 0.161 | 0.094 | 0.046 | 0.015 |
| 17 Holes | | 0.267 | 0.172 | 0.101 | 0.050 | 0.016 |
| 29 Holes | | 0.299 | 0.193 | 0.113 | 0.055 | 0.018 |
| 49 Holes | | 0.269 | 0.172 | 0.097 | 0.045 | 0.014 |

UNIFORMLY DISTRIBUTED LIVE LOAD: TABLES

| PATTERN 1 – SYMMETRICAL LOAD – R ₂ | | | | | | |
|---|-----|-------|-------|-------|-------|-------|
| η | [-] | 80 | 96 | 120 | 160 | 240 |
| q/q _{max} [-] | | | | | | |
| No Hole | | 0.341 | 0.203 | 0.107 | 0.047 | 0.014 |
| 1 Hole | | 0.343 | 0.205 | 0.109 | 0.048 | 0.015 |
| 5 Holes | | 0.381 | 0.229 | 0.123 | 0.055 | 0.017 |
| 9 Holes | | 0.406 | 0.247 | 0.134 | 0.061 | 0.019 |
| 13 Holes | | 0.356 | 0.260 | 0.143 | 0.066 | 0.021 |
| 25 Holes | | 0.352 | 0.266 | 0.157 | 0.074 | 0.025 |
| 29 Holes | | 0.317 | 0.234 | 0.165 | 0.077 | 0.025 |
| 49 Holes | | 0.293 | 0.216 | 0.147 | 0.069 | 0.021 |

| PATTERN 2 – SYMMETRICAL LOAD – R ₂ | | | | | | |
|---|-----|-------|-------|-------|-------|-------|
| η | [-] | 80 | 96 | 120 | 160 | 240 |
| q/q _{max} [-] | | | | | | |
| No Hole | | 0.341 | 0.203 | 0.107 | 0.047 | 0.014 |
| 4 Holes | | 0.360 | 0.215 | 0.114 | 0.051 | 0.015 |
| 8 Holes | | 0.266 | 0.187 | 0.120 | 0.053 | 0.016 |
| 12 Holes | | 0.224 | 0.158 | 0.107 | 0.060 | 0.019 |
| 13 Holes | | 0.260 | 0.187 | 0.129 | 0.064 | 0.020 |
| 33 Holes | | 0.236 | 0.170 | 0.116 | 0.064 | 0.019 |
| 45 Holes | | 0.254 | 0.184 | 0.127 | 0.065 | 0.020 |
| 49 Holes | | 0.293 | 0.216 | 0.147 | 0.069 | 0.021 |

| PATTERN 3 – SYMMETRICAL LOAD – R ₂ | | | | | | |
|---|-----|-------|-------|-------|-------|-------|
| η | [-] | 80 | 96 | 120 | 160 | 240 |
| q/q _{max} [-] | | | | | | |
| No Hole | | 0.341 | 0.203 | 0.107 | 0.047 | 0.014 |
| 4 Holes | | 0.343 | 0.202 | 0.106 | 0.045 | 0.012 |
| 8 Holes | | 0.350 | 0.207 | 0.109 | 0.046 | 0.013 |
| 12 Holes | | 0.374 | 0.223 | 0.117 | 0.051 | 0.014 |
| 13 Holes | | 0.388 | 0.232 | 0.123 | 0.053 | 0.015 |
| 33 Holes | | 0.299 | 0.217 | 0.130 | 0.059 | 0.018 |
| 45 Holes | | 0.247 | 0.179 | 0.124 | 0.064 | 0.019 |
| 49 Holes | | 0.293 | 0.216 | 0.147 | 0.069 | 0.021 |

| PATTERN 4 – SYMMETRICAL LOAD – R ₂ | | | | | | |
|---|-----|-------|-------|-------|-------|-------|
| η | [-] | 80 | 96 | 120 | 160 | 240 |
| q/q _{max} [-] | | | | | | |
| No Hole | | 0.341 | 0.203 | 0.107 | 0.047 | 0.014 |
| 1 Hole | | 0.343 | 0.205 | 0.109 | 0.048 | 0.015 |
| 5 Holes | | 0.379 | 0.227 | 0.122 | 0.054 | 0.017 |
| 9 Holes | | 0.384 | 0.231 | 0.124 | 0.055 | 0.017 |
| 13 Holes | | 0.388 | 0.232 | 0.123 | 0.053 | 0.015 |
| 17 Holes | | 0.414 | 0.251 | 0.135 | 0.060 | 0.018 |
| 29 Holes | | 0.437 | 0.280 | 0.158 | 0.073 | 0.023 |
| 49 Holes | | 0.293 | 0.216 | 0.147 | 0.069 | 0.021 |

| PATTERN 1 – ANTI-SYMMETRICAL LOAD – R ₂ | | | | | | |
|--|-----|-------|-------|-------|-------|-------|
| η | [-] | 80 | 96 | 120 | 160 | 240 |
| q/q _{max} [-] | | | | | | |
| No Hole | | 0.211 | 0.134 | 0.077 | 0.038 | 0.013 |
| 1 Hole | | 0.212 | 0.135 | 0.080 | 0.040 | 0.014 |
| 5 Holes | | 0.244 | 0.156 | 0.091 | 0.046 | 0.016 |
| 9 Holes | | 0.269 | 0.173 | 0.101 | 0.051 | 0.018 |
| 13 Holes | | 0.296 | 0.190 | 0.112 | 0.056 | 0.020 |
| 25 Holes | | 0.372 | 0.240 | 0.141 | 0.069 | 0.024 |
| 29 Holes | | 0.397 | 0.256 | 0.148 | 0.072 | 0.025 |
| 49 Holes | | 0.402 | 0.256 | 0.144 | 0.067 | 0.021 |

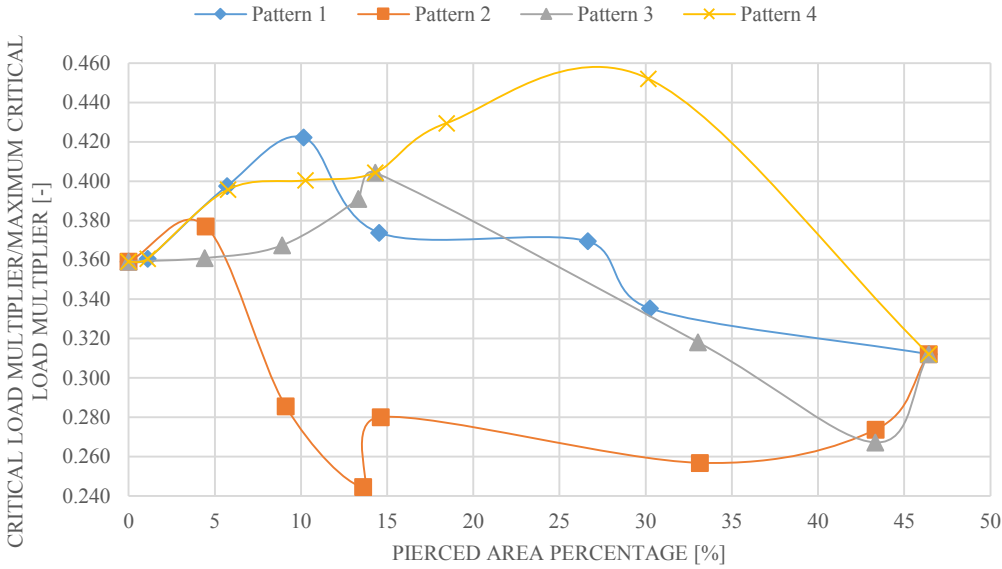
| PATTERN 2 – ANTI-SYMMETRICAL LOAD – R ₂ | | | | | | |
|--|-----|-------|-------|-------|-------|-------|
| η | [-] | 80 | 96 | 120 | 160 | 240 |
| q/q _{max} [-] | | | | | | |
| No Hole | | 0.211 | 0.134 | 0.077 | 0.038 | 0.013 |
| 4 Holes | | 0.224 | 0.142 | 0.082 | 0.041 | 0.014 |
| 8 Holes | | 0.237 | 0.150 | 0.087 | 0.043 | 0.015 |
| 12 Holes | | 0.269 | 0.172 | 0.100 | 0.050 | 0.017 |
| 13 Holes | | 0.284 | 0.183 | 0.107 | 0.053 | 0.019 |
| 33 Holes | | 0.303 | 0.196 | 0.115 | 0.056 | 0.018 |
| 45 Holes | | 0.373 | 0.239 | 0.135 | 0.062 | 0.019 |
| 49 Holes | | 0.402 | 0.256 | 0.144 | 0.067 | 0.021 |

| PATTERN 3 – ANTI-SYMMETRICAL LOAD – R ₂ | | | | | | |
|--|-----|-------|-------|-------|-------|-------|
| η | [-] | 80 | 96 | 120 | 160 | 240 |
| q/q _{max} [-] | | | | | | |
| No Hole | | 0.211 | 0.134 | 0.077 | 0.038 | 0.013 |
| 4 Holes | | 0.192 | 0.123 | 0.071 | 0.035 | 0.011 |
| 8 Holes | | 0.204 | 0.130 | 0.076 | 0.037 | 0.012 |
| 12 Holes | | 0.223 | 0.143 | 0.083 | 0.041 | 0.013 |
| 13 Holes | | 0.234 | 0.150 | 0.088 | 0.043 | 0.014 |
| 33 Holes | | 0.293 | 0.190 | 0.111 | 0.054 | 0.017 |
| 45 Holes | | 0.364 | 0.234 | 0.133 | 0.061 | 0.018 |
| 49 Holes | | 0.402 | 0.256 | 0.144 | 0.067 | 0.021 |

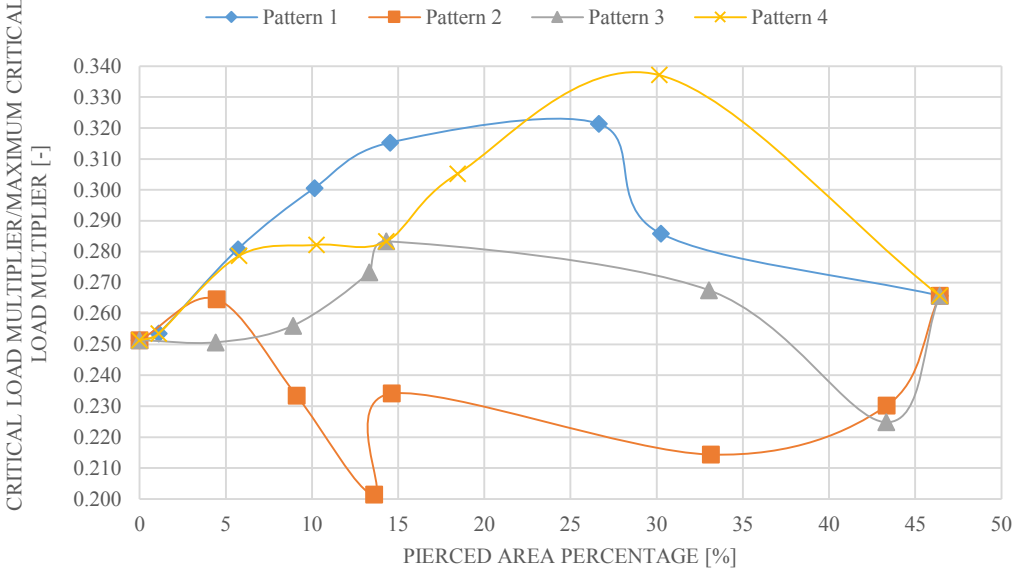
| PATTERN 4 – ANTI-SYMMETRICAL LOAD – R ₂ | | | | | | |
|--|-----|-------|-------|-------|-------|-------|
| η | [-] | 80 | 96 | 120 | 160 | 240 |
| q/q _{max} [-] | | | | | | |
| No Hole | | 0.211 | 0.134 | 0.077 | 0.038 | 0.013 |
| 1 Hole | | 0.212 | 0.135 | 0.080 | 0.040 | 0.014 |
| 5 Holes | | 0.242 | 0.155 | 0.090 | 0.045 | 0.016 |
| 9 Holes | | 0.259 | 0.165 | 0.096 | 0.048 | 0.016 |
| 13 Holes | | 0.234 | 0.150 | 0.088 | 0.043 | 0.014 |
| 17 Holes | | 0.262 | 0.169 | 0.099 | 0.049 | 0.016 |
| 29 Holes | | 0.342 | 0.221 | 0.129 | 0.063 | 0.021 |
| 49 Holes | | 0.402 | 0.256 | 0.144 | 0.067 | 0.021 |

LOAD MULTIPLIER: TABLES

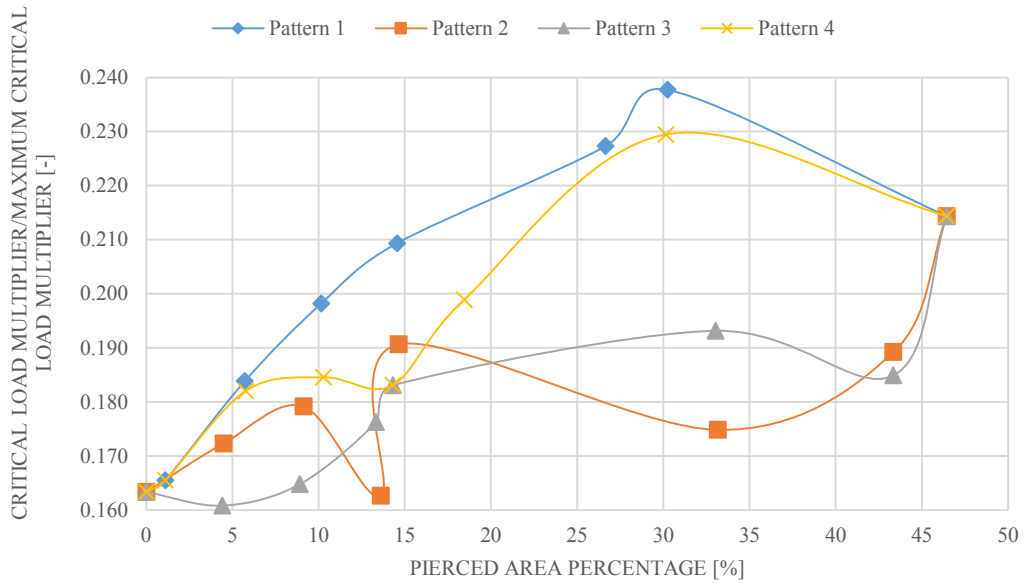
$\eta=80$ - SYMMETRICAL LOAD - R_2



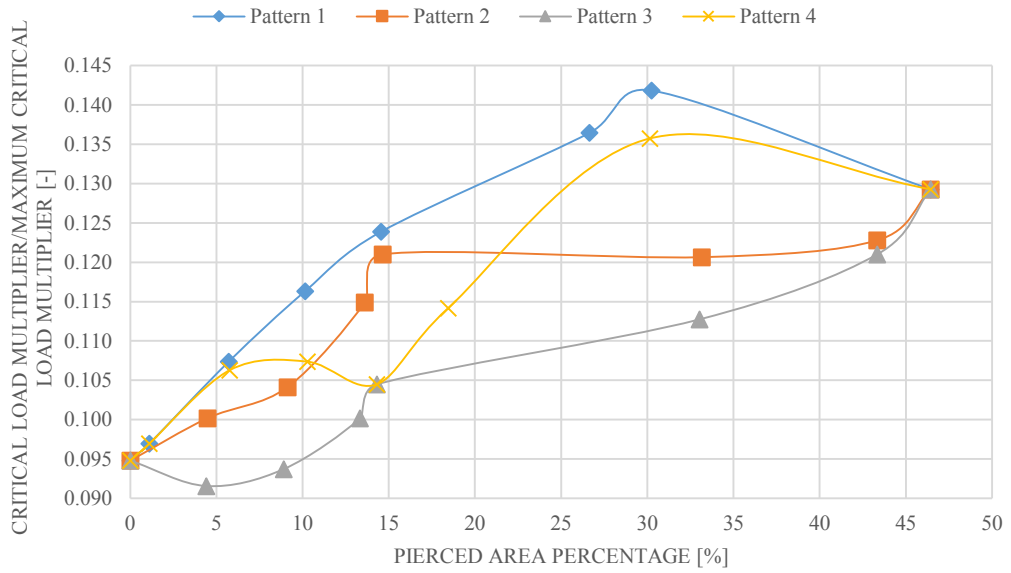
$\eta=96$ - SYMMETRICAL LOAD - R_2



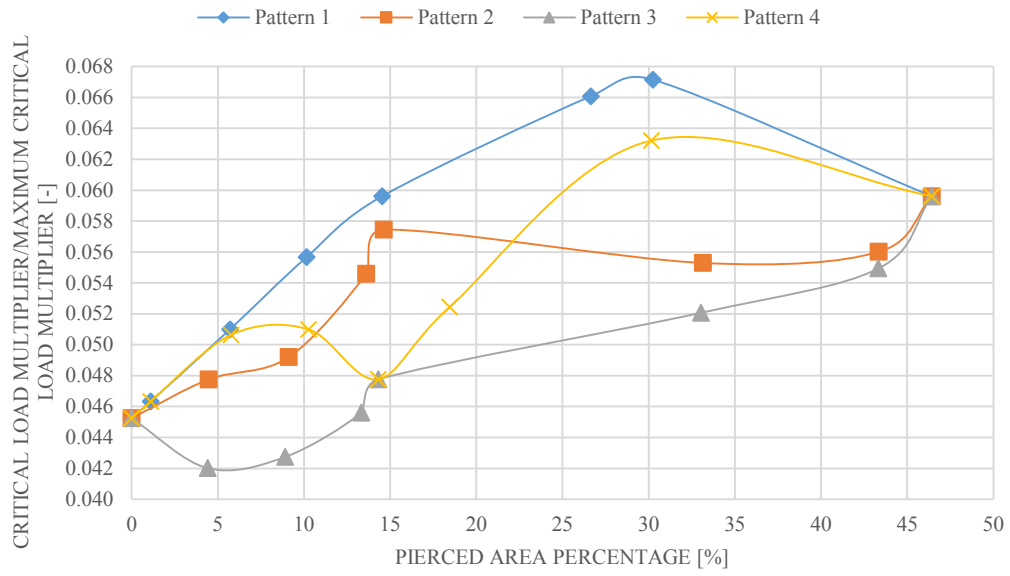
$\eta=120$ - SYMMETRICAL LOAD - R_2



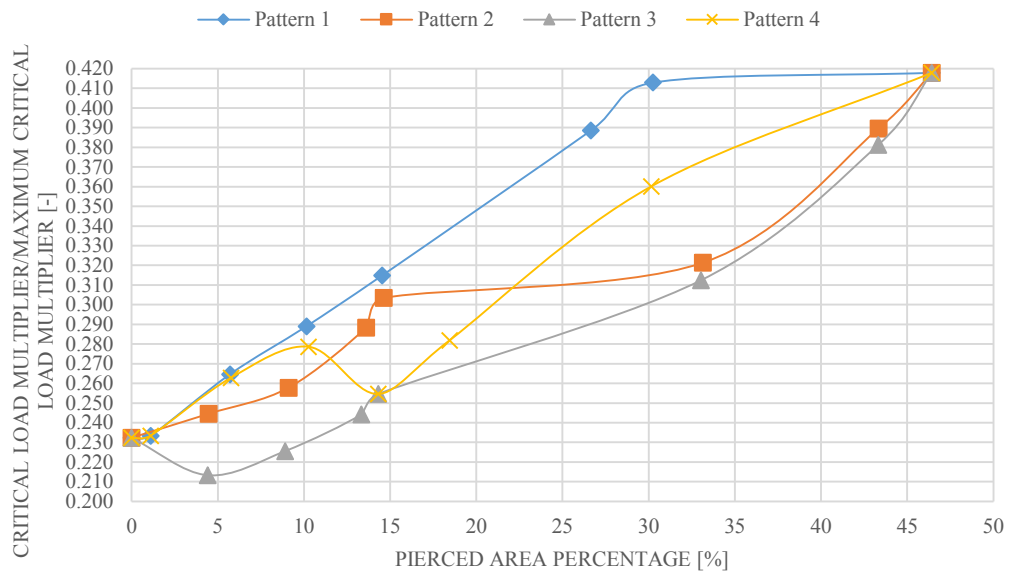
$\eta=160$ SYMMETRICAL LOAD - R_2



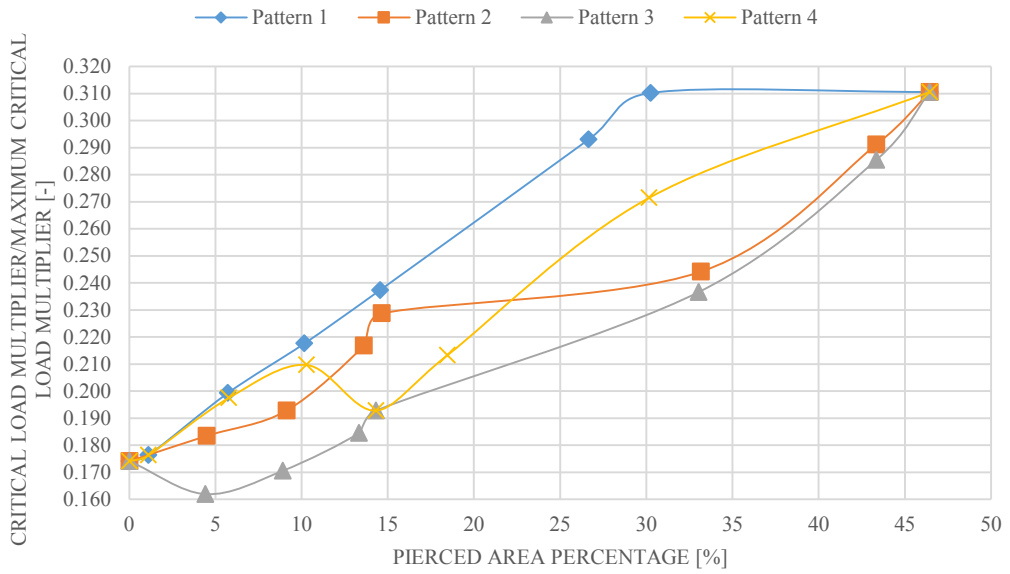
$\eta=240$ - SYMMETRICAL LOAD - R_2



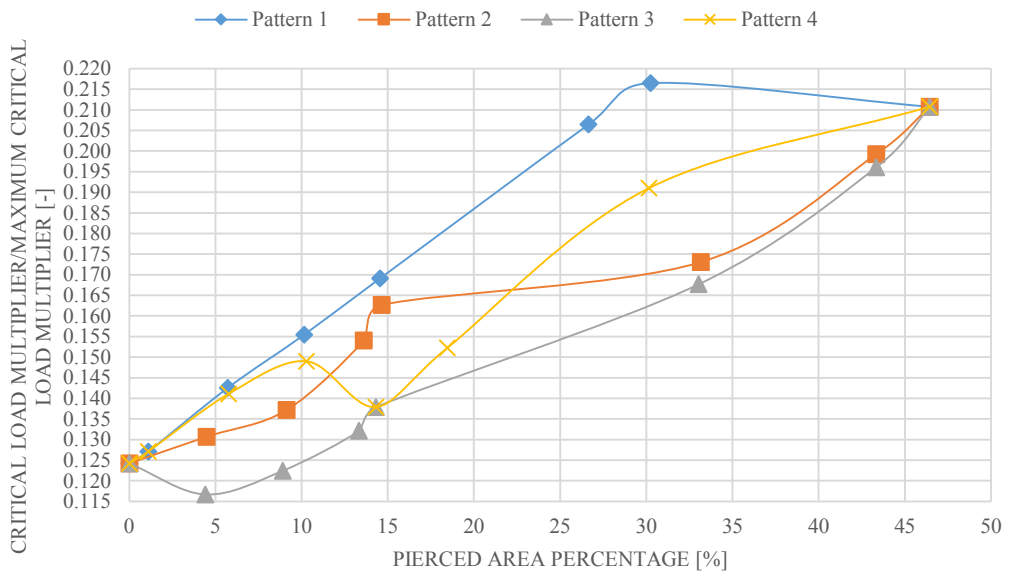
$\eta=80$ - ANTI-SYMMETRICAL LOAD - R_2



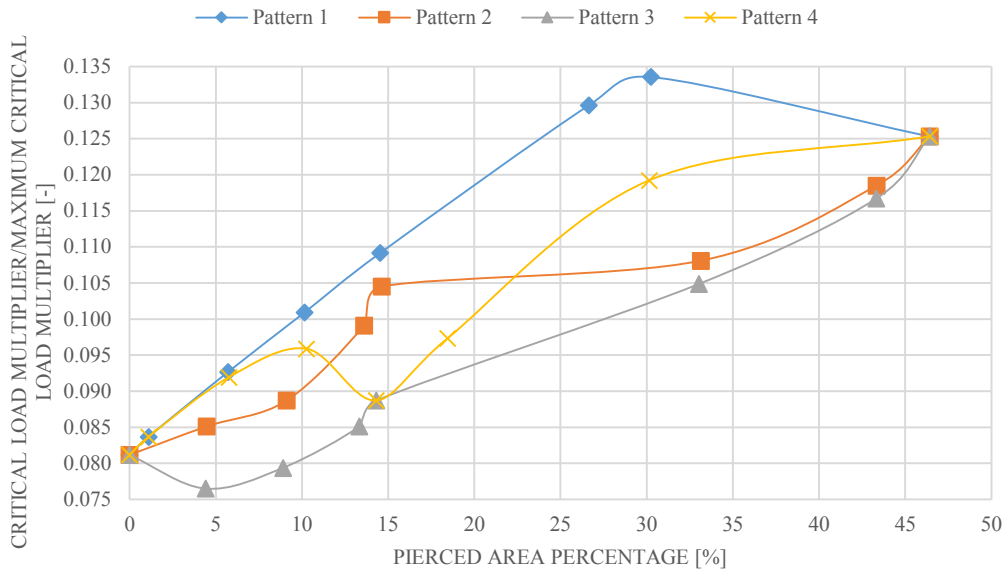
$\eta=96$ - ANTI-SYMMETRICAL LOAD - R_2



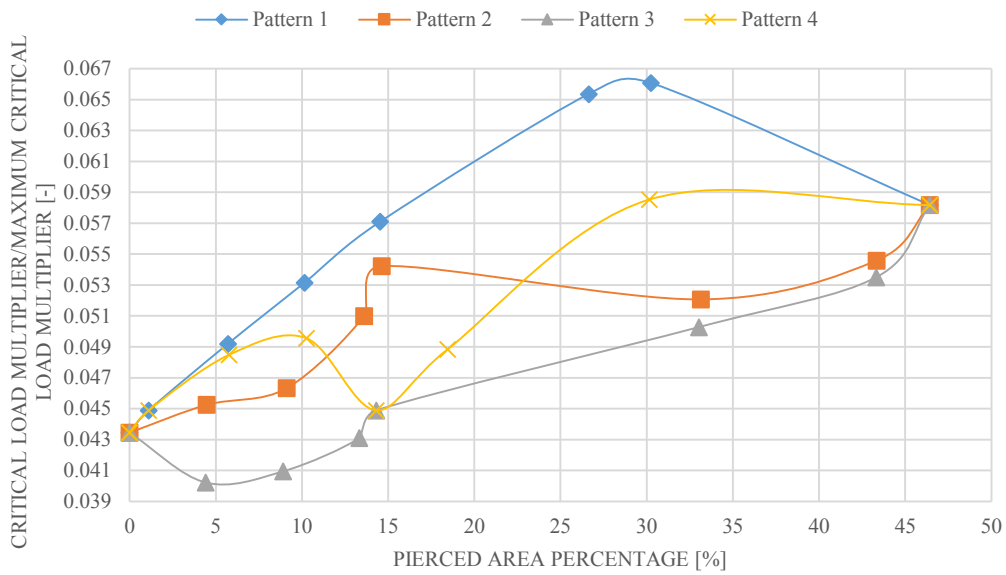
$\eta=120$ - ANTI-SYMMETRICAL LOAD - R_2



$\eta=160$ - ANTI-SYMMETRICAL LOAD - R_2

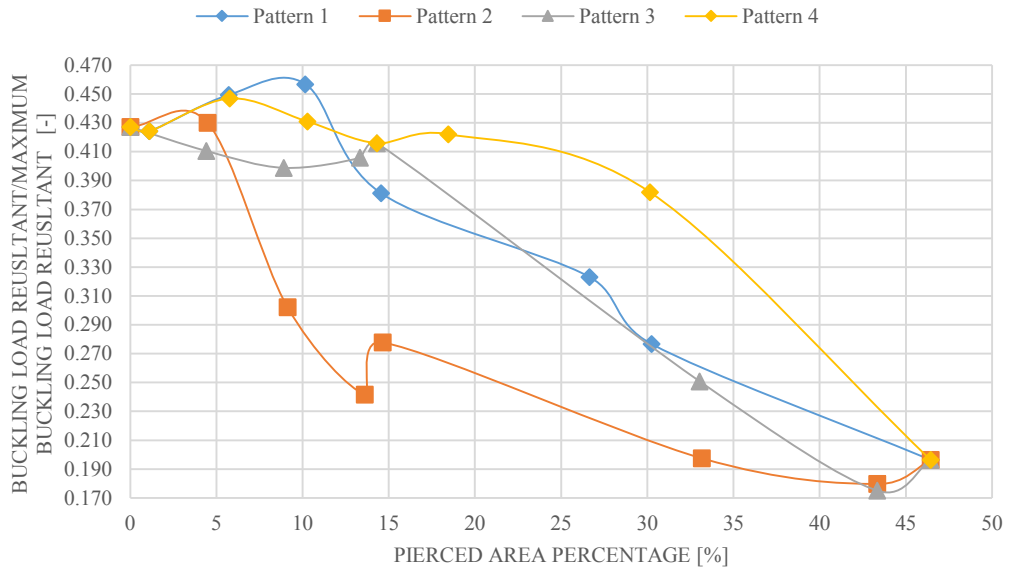


$\eta=240$ - ANTI-SYMMETRICAL LOAD - R_2

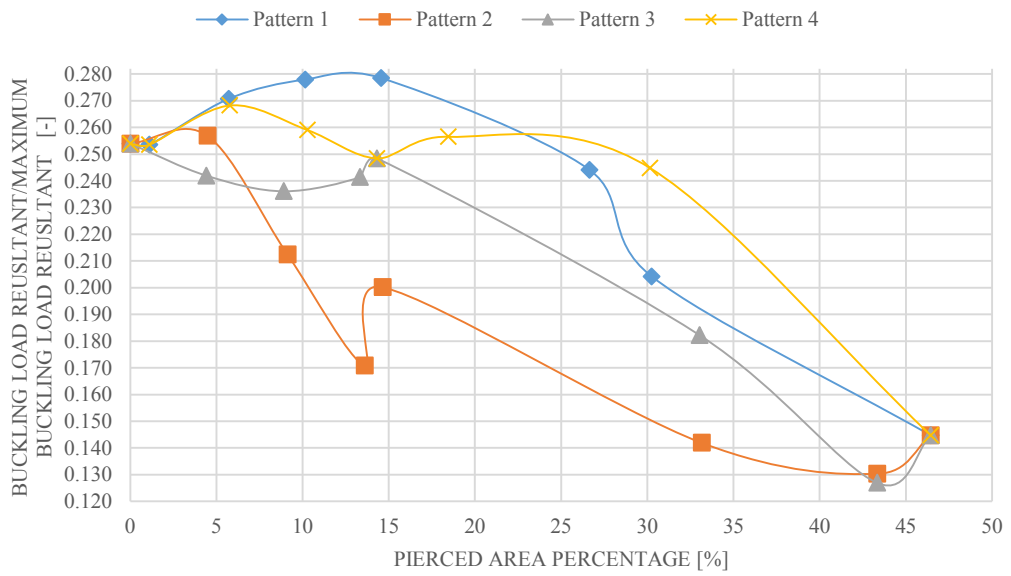


LIVE LOAD RESULTANT: GRAPHICS

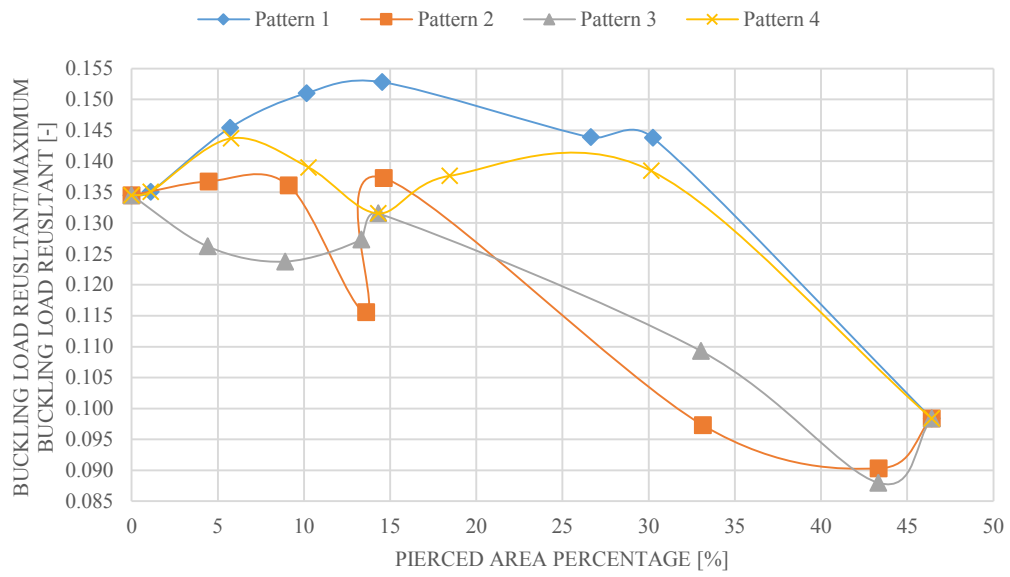
$\eta=80$ - SYMMETRICAL LOAD - R_2



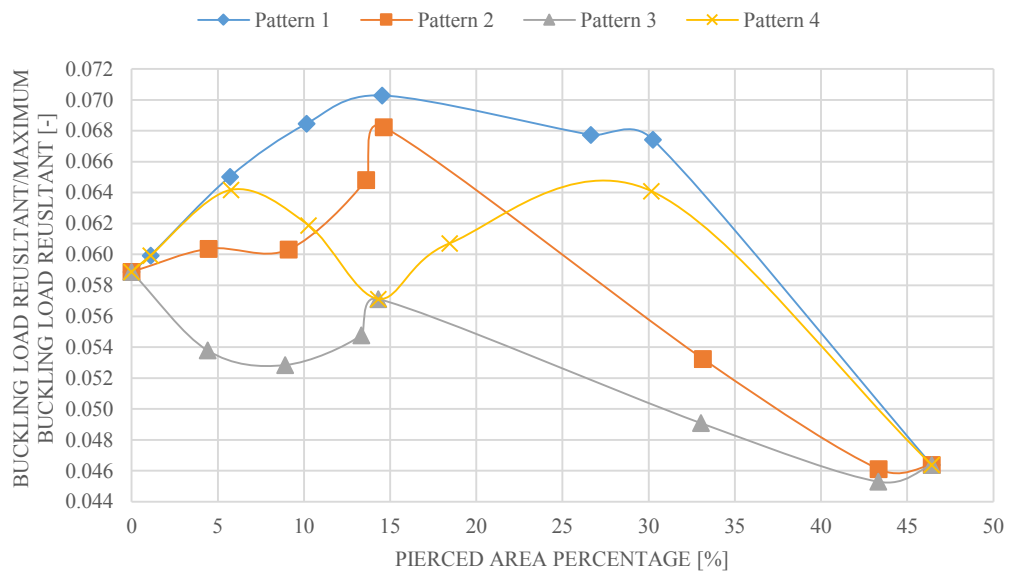
$\eta=96$ - SYMMETRICAL LOAD - R_2



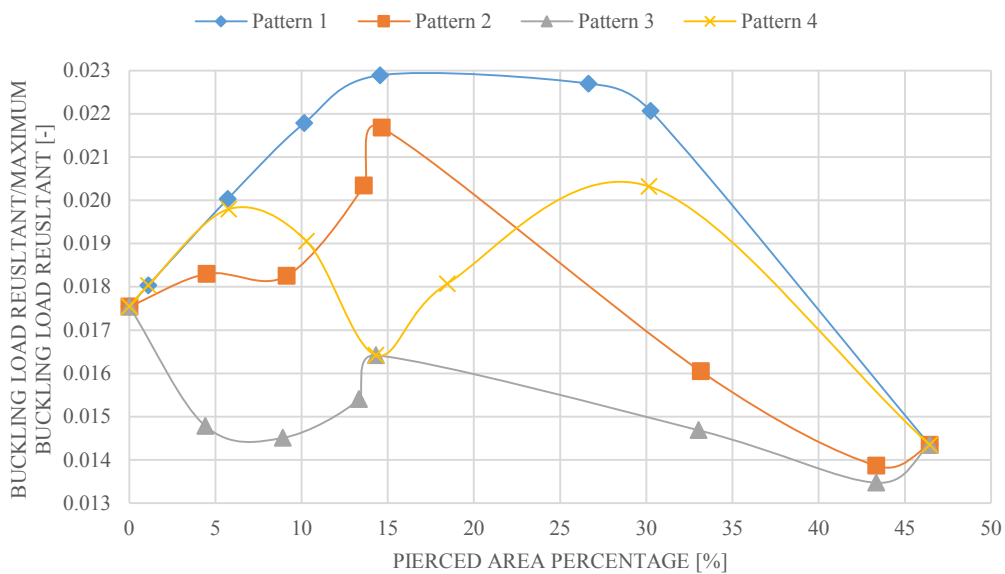
$\eta=120$ - SYMMETRICAL LOAD - R_2



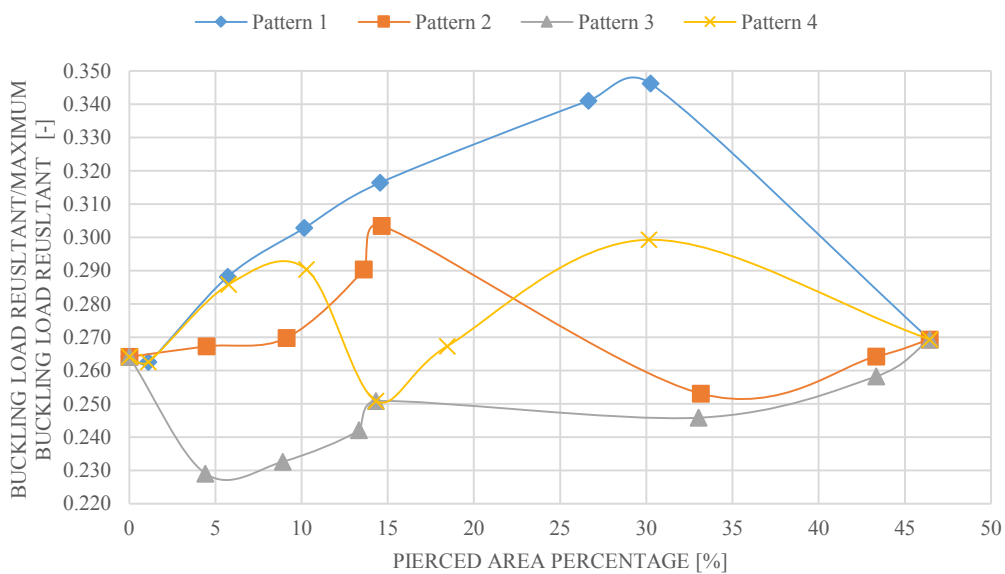
$\eta=160$ - SYMMETRICAL LOAD - R_2



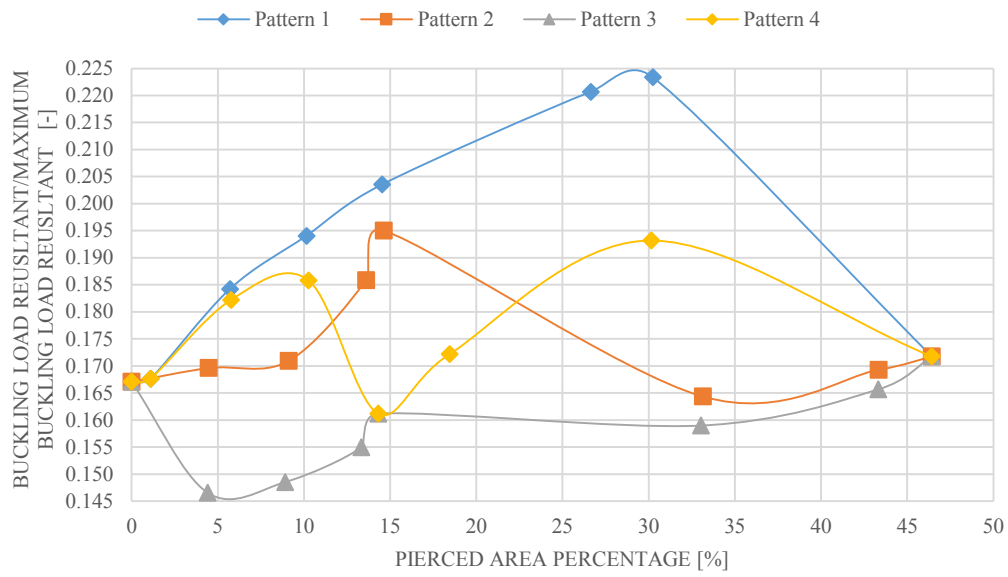
$\eta=240$ - SYMMETRICAL LOAD - R_2



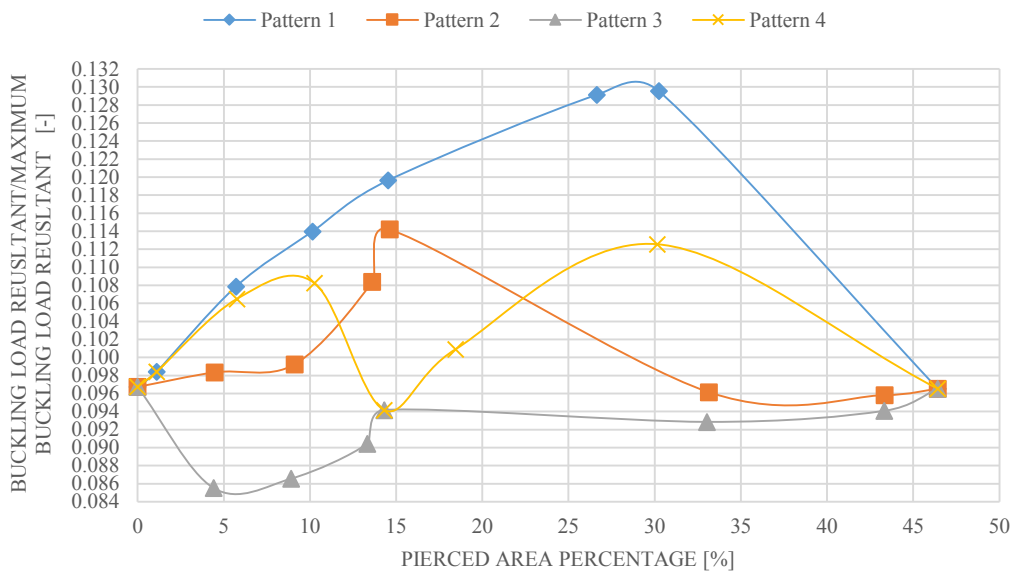
$\eta=80$ - ANTI-SYMMETRICAL LOAD - R_2



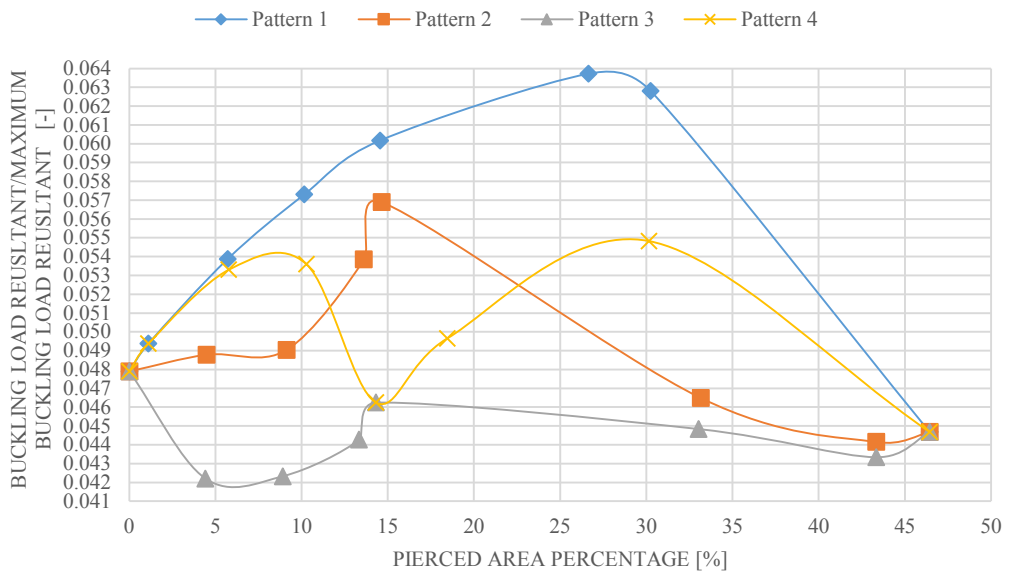
$\eta=96$ - ANTI-SYMMETRICAL LOAD - R_2



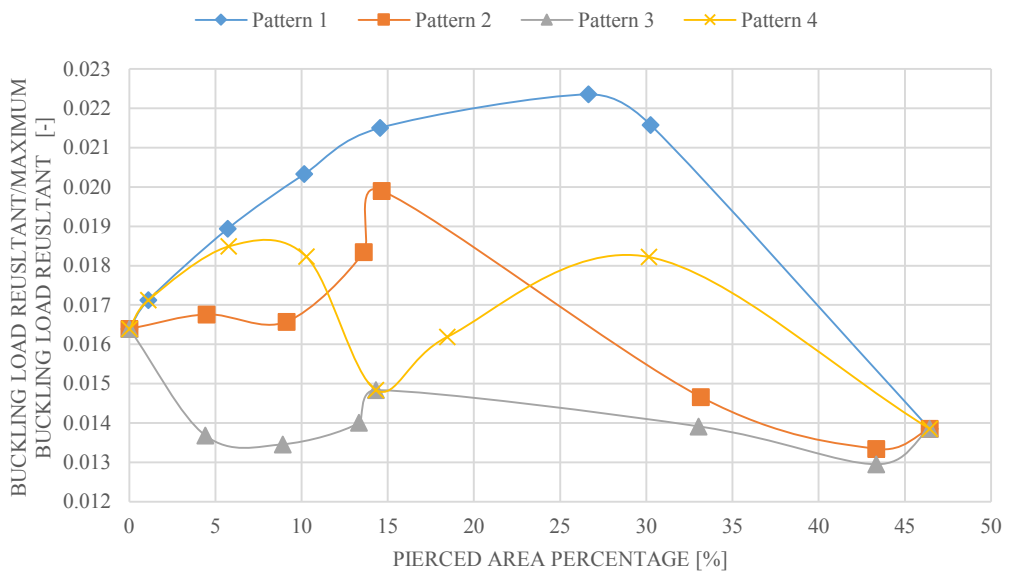
$\eta=120$ - ANTI-SYMMETRICAL LOAD - R_2



$\eta=160$ - ANTI-SYMMETRICAL LOAD - R_2

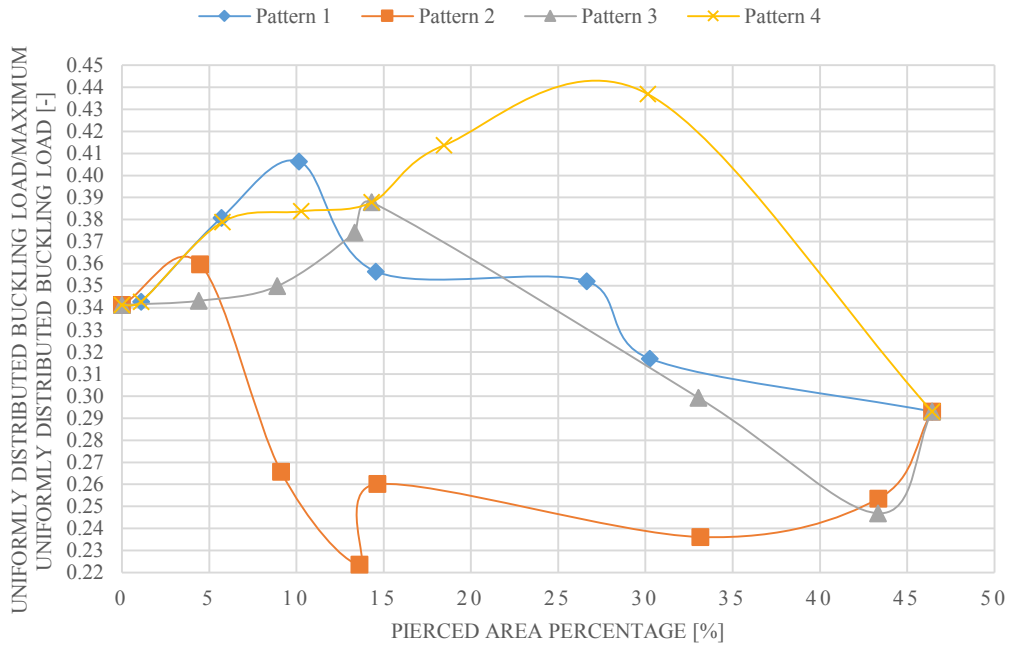


$\eta=240$ - ANTI-SYMMETRICAL LOAD - R_2

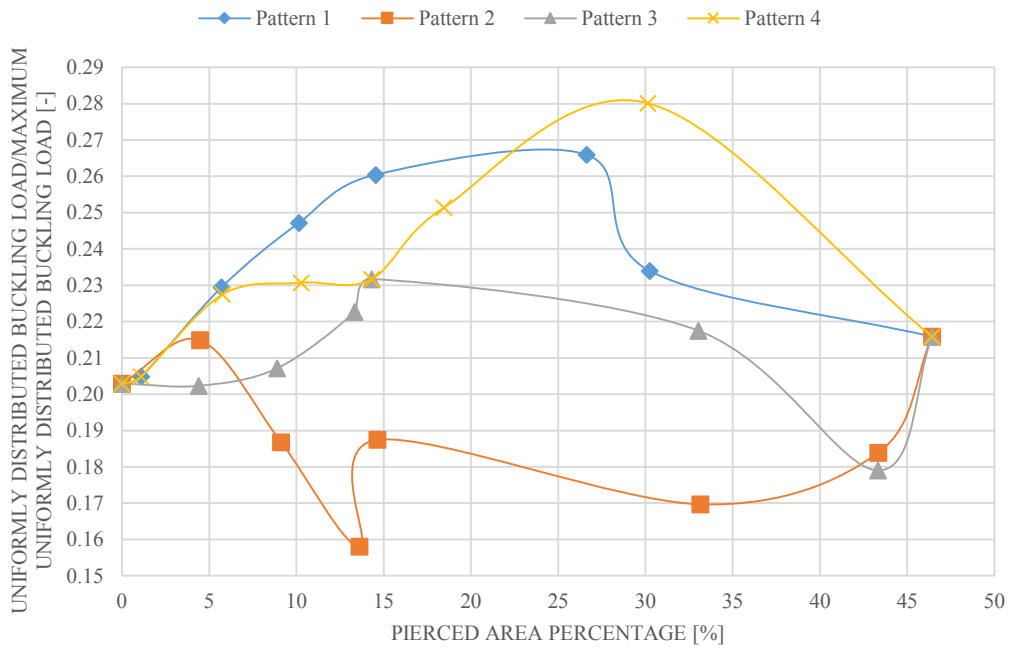


UNIFORMLY DISTRIBUTED LIVE LOAD: GRAPHICS

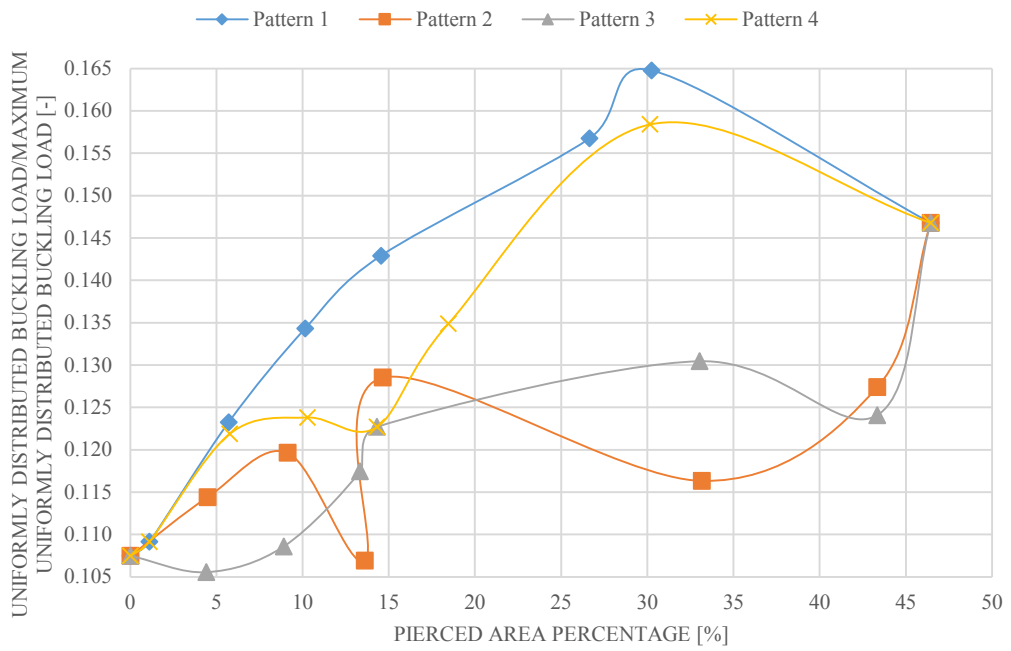
$\eta=80$ - SYMMETRICAL LOAD - R_2



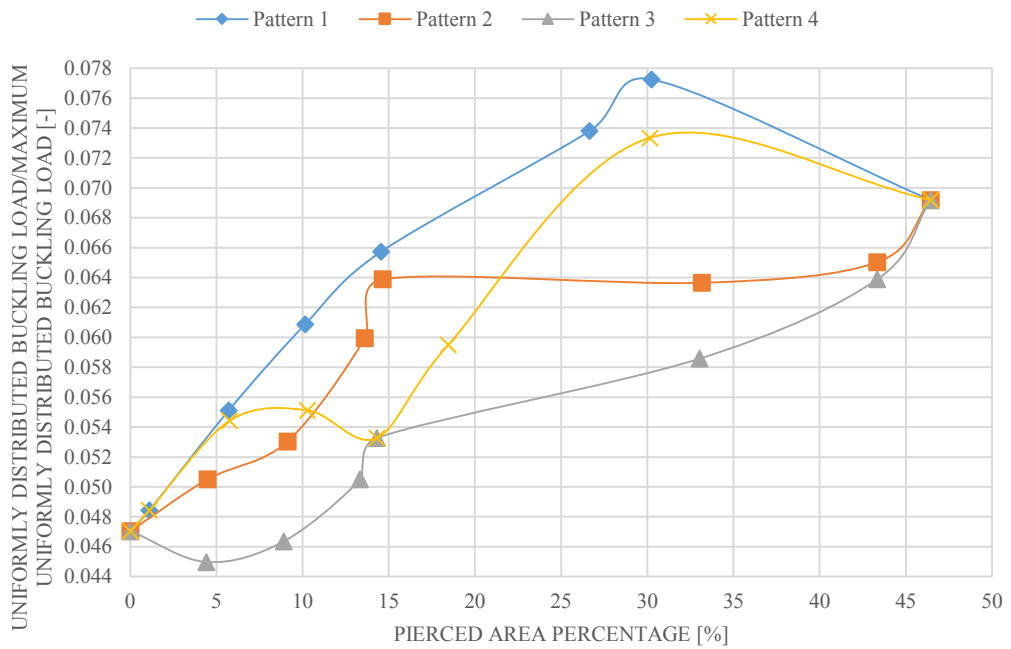
$\eta=96$ - SYMMETRICAL LOAD - R_2



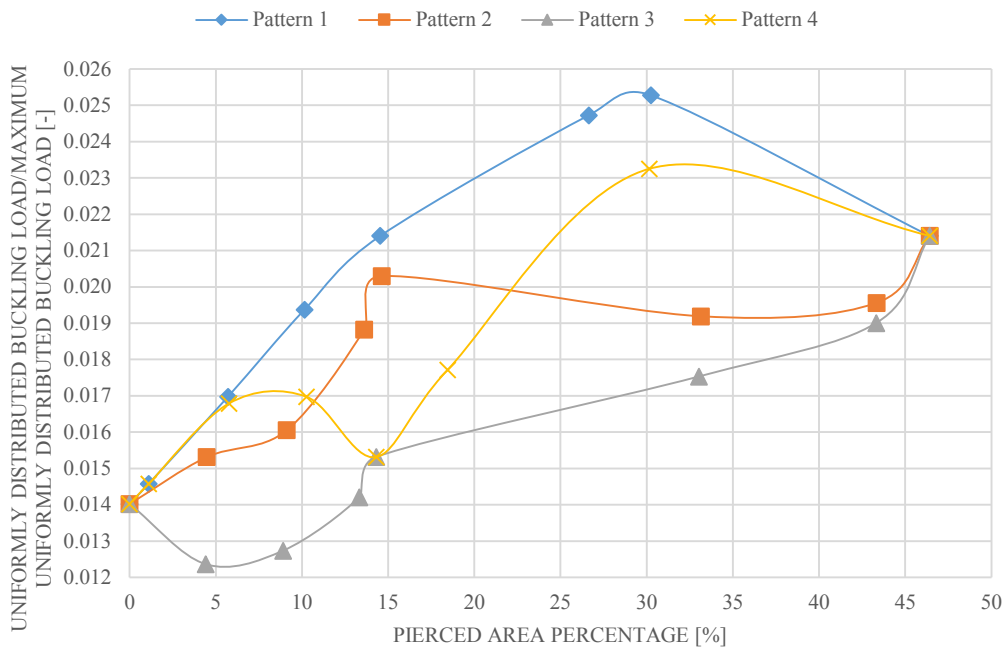
$\eta=120$ - SYMMETRICAL LOAD - R_2



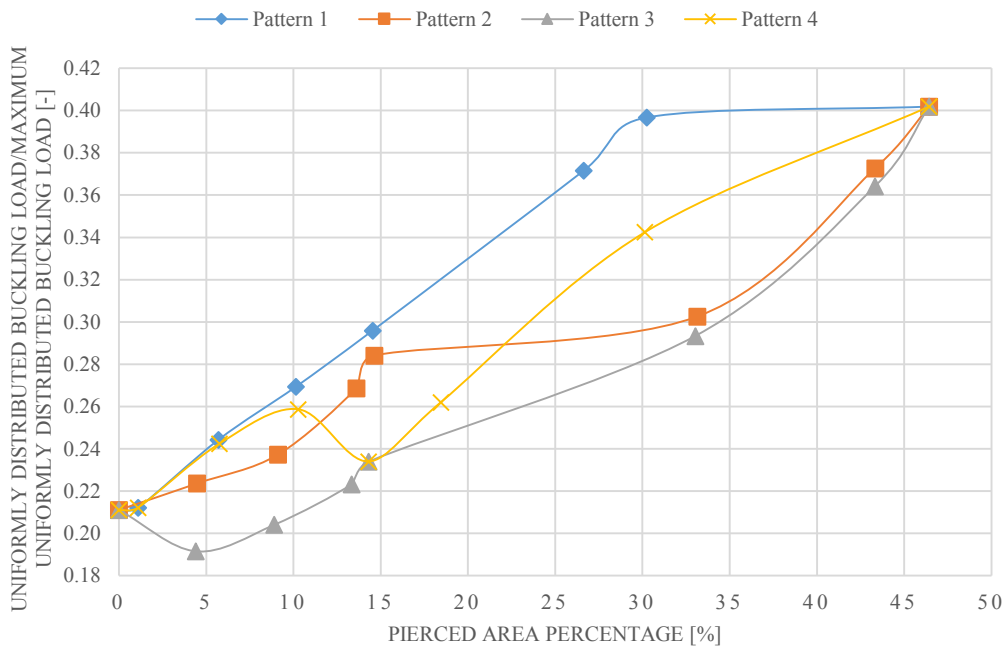
$\eta=160$ - SYMMETRICAL LOAD - R_2



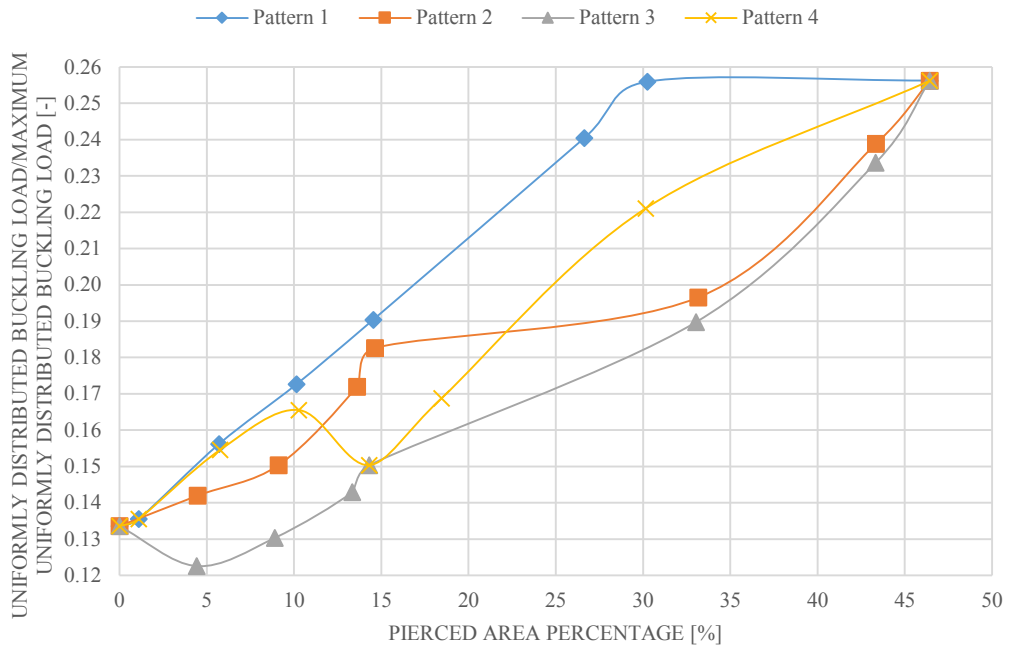
$\eta=240$ - SYMMETRICAL LOAD - R_2



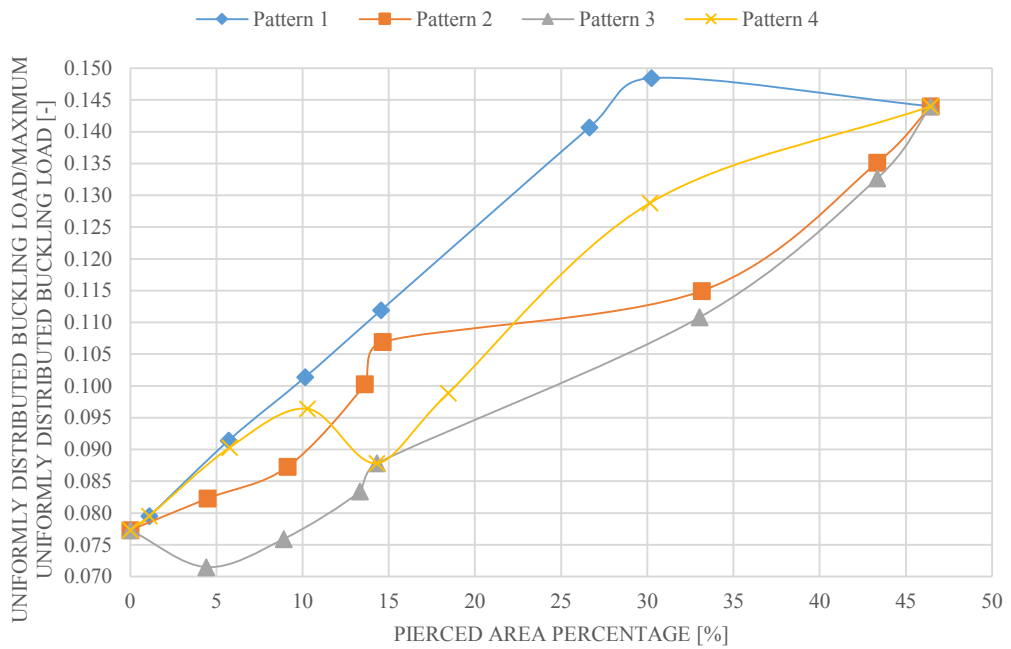
$\eta=80$ - ANTI-SYMMETRICAL LOAD - R_2



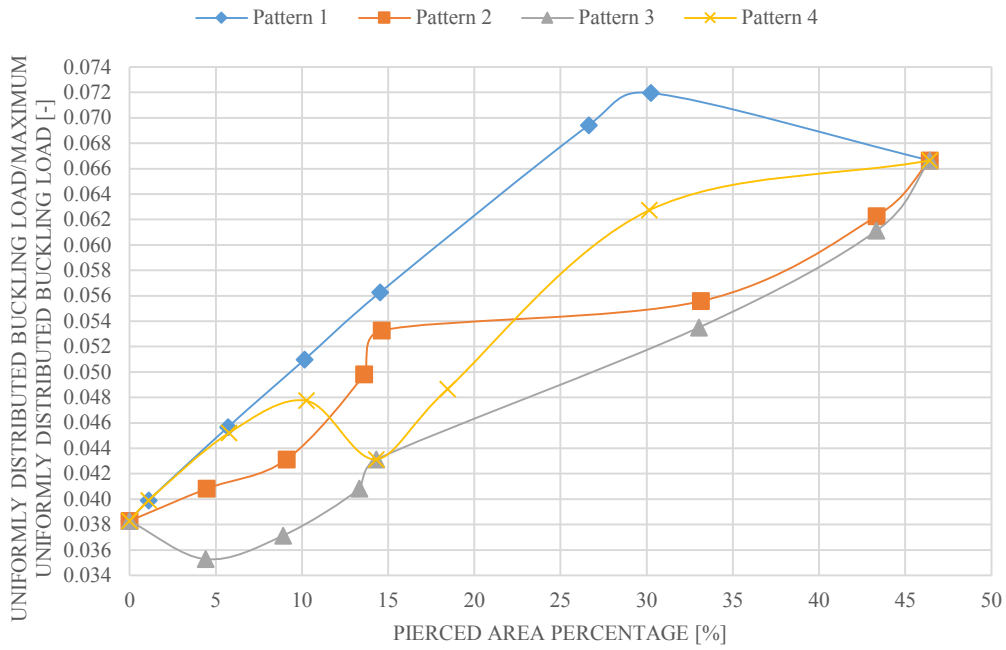
$\eta=96$ - ANTI-SYMMETRICAL LOAD - R_2



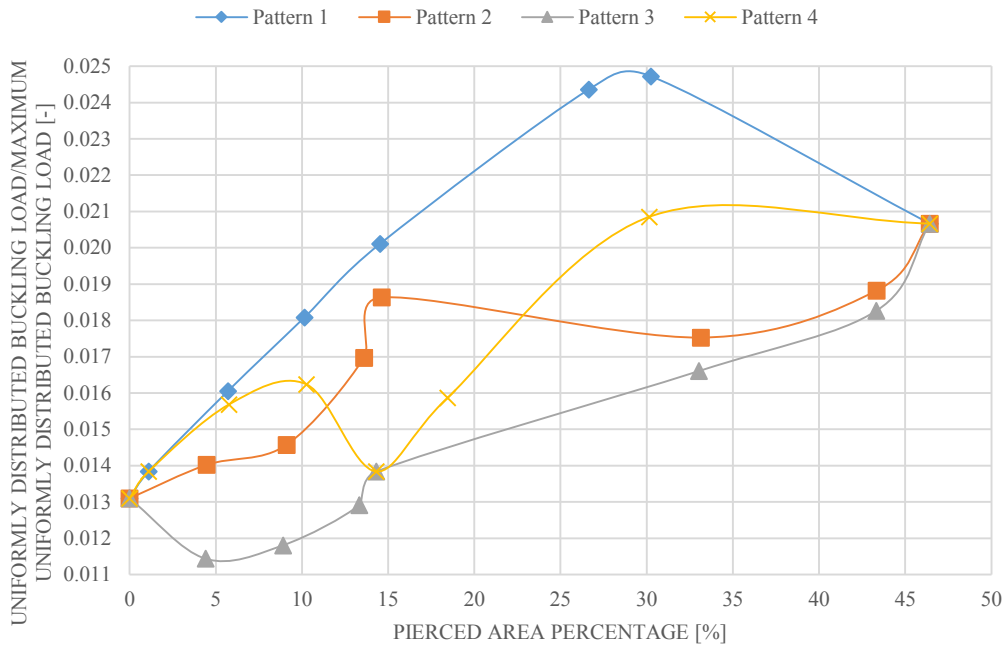
$\eta=120$ - ANTI-SYMMETRICAL LOAD - R_2



$\eta=160$ - ANTI-SYMMETRICAL LOAD - R_2



$\eta=240$ - ANTI-SYMMETRICAL LOAD - R_2



LOAD MULTIPLIER: TABLES

| PATTERN 1 – SYMMETRICAL LOAD – R ₃ | | | | | | |
|---|-----|-------|-------|-------|-------|-------|
| η | [-] | 80 | 96 | 120 | 160 | 240 |
| λ/λ_{\max} [-] | | | | | | |
| No Hole | | 0.664 | 0.504 | 0.361 | 0.237 | 0.136 |
| 1 Hole | | 0.662 | 0.501 | 0.357 | 0.233 | 0.132 |
| 5 Holes | | 0.717 | 0.545 | 0.391 | 0.258 | 0.149 |
| 9 Holes | | 0.761 | 0.581 | 0.419 | 0.278 | 0.162 |
| 13 Holes | | 0.804 | 0.615 | 0.445 | 0.297 | 0.173 |
| 25 Holes | | 0.911 | 0.695 | 0.500 | 0.328 | 0.184 |
| 29 Holes | | 0.957 | 0.728 | 0.521 | 0.339 | 0.186 |
| 49 Holes | | 1.000 | 0.740 | 0.506 | 0.309 | 0.154 |

| PATTERN 2 – SYMMETRICAL LOAD – R ₃ | | | | | | |
|---|-----|-------|-------|-------|-------|-------|
| η | [-] | 80 | 96 | 120 | 160 | 240 |
| λ/λ_{\max} [-] | | | | | | |
| No Hole | | 0.664 | 0.504 | 0.361 | 0.237 | 0.136 |
| 4 Holes | | 0.706 | 0.537 | 0.384 | 0.252 | 0.145 |
| 8 Holes | | 0.748 | 0.569 | 0.409 | 0.270 | 0.156 |
| 12 Holes | | 0.790 | 0.602 | 0.434 | 0.287 | 0.165 |
| 13 Holes | | 0.806 | 0.615 | 0.444 | 0.295 | 0.171 |
| 33 Holes | | 0.862 | 0.644 | 0.448 | 0.277 | 0.138 |
| 45 Holes | | 0.952 | 0.704 | 0.483 | 0.296 | 0.148 |
| 49 Holes | | 1.000 | 0.740 | 0.506 | 0.309 | 0.154 |

| PATTERN 3 – SYMMETRICAL LOAD – R ₃ | | | | | | |
|---|-----|-------|-------|-------|-------|-------|
| η | [-] | 80 | 96 | 120 | 160 | 240 |
| λ/λ_{\max} [-] | | | | | | |
| No Hole | | 0.664 | 0.504 | 0.361 | 0.237 | 0.136 |
| 4 Holes | | 0.627 | 0.467 | 0.326 | 0.207 | 0.112 |
| 8 Holes | | 0.654 | 0.486 | 0.338 | 0.213 | 0.114 |
| 12 Holes | | 0.694 | 0.515 | 0.357 | 0.225 | 0.120 |
| 13 Holes | | 0.706 | 0.524 | 0.364 | 0.229 | 0.122 |
| 33 Holes | | 0.824 | 0.614 | 0.424 | 0.261 | 0.130 |
| 45 Holes | | 0.933 | 0.689 | 0.471 | 0.286 | 0.142 |
| 49 Holes | | 1.000 | 0.740 | 0.506 | 0.309 | 0.154 |

| PATTERN 4 – SYMMETRICAL LOAD – R ₃ | | | | | | |
|---|-----|-------|-------|-------|-------|-------|
| η | [-] | 80 | 96 | 120 | 160 | 240 |
| λ/λ_{\max} [-] | | | | | | |
| No Hole | | 0.664 | 0.504 | 0.361 | 0.237 | 0.136 |
| 1 Hole | | 0.662 | 0.501 | 0.357 | 0.233 | 0.132 |
| 5 Holes | | 0.717 | 0.545 | 0.391 | 0.257 | 0.148 |
| 9 Holes | | 0.741 | 0.563 | 0.403 | 0.264 | 0.150 |
| 13 Holes | | 0.706 | 0.524 | 0.364 | 0.229 | 0.122 |
| 17 Holes | | 0.753 | 0.561 | 0.392 | 0.249 | 0.135 |
| 29 Holes | | 0.894 | 0.668 | 0.467 | 0.295 | 0.158 |
| 49 Holes | | 1.000 | 0.740 | 0.506 | 0.309 | 0.154 |

| PATTERN 1 – ANTI-SYMMETRICAL LOAD – R ₃ | | | | | | |
|--|-----|-------|-------|-------|-------|-------|
| η | [-] | 80 | 96 | 120 | 160 | 240 |
| λ/λ_{\max} [-] | | | | | | |
| No Hole | | 0.519 | 0.421 | 0.322 | 0.223 | 0.129 |
| 1 Hole | | 0.527 | 0.425 | 0.323 | 0.221 | 0.126 |
| 5 Holes | | 0.563 | 0.456 | 0.349 | 0.242 | 0.140 |
| 9 Holes | | 0.601 | 0.487 | 0.371 | 0.257 | 0.149 |
| 13 Holes | | 0.638 | 0.515 | 0.392 | 0.270 | 0.156 |
| 25 Holes | | 0.756 | 0.597 | 0.442 | 0.295 | 0.165 |
| 29 Holes | | 0.792 | 0.622 | 0.455 | 0.301 | 0.166 |
| 49 Holes | | 0.852 | 0.641 | 0.447 | 0.278 | 0.142 |

| PATTERN 2 – ANTI-SYMMETRICAL LOAD – R ₃ | | | | | | |
|--|-----|-------|-------|-------|-------|-------|
| η | [-] | 80 | 96 | 120 | 160 | 240 |
| λ/λ_{\max} [-] | | | | | | |
| No Hole | | 0.519 | 0.421 | 0.322 | 0.223 | 0.129 |
| 4 Holes | | 0.546 | 0.443 | 0.338 | 0.233 | 0.134 |
| 8 Holes | | 0.581 | 0.469 | 0.357 | 0.246 | 0.141 |
| 12 Holes | | 0.620 | 0.499 | 0.378 | 0.258 | 0.147 |
| 13 Holes | | 0.632 | 0.510 | 0.387 | 0.265 | 0.151 |
| 33 Holes | | 0.715 | 0.553 | 0.394 | 0.246 | 0.123 |
| 45 Holes | | 0.808 | 0.610 | 0.425 | 0.263 | 0.134 |
| 49 Holes | | 0.852 | 0.641 | 0.447 | 0.278 | 0.142 |

| PATTERN 3 – ANTI-SYMMETRICAL LOAD – R ₃ | | | | | | |
|--|-----|-------|-------|-------|-------|-------|
| η | [-] | 80 | 96 | 120 | 160 | 240 |
| λ/λ_{\max} [-] | | | | | | |
| No Hole | | 0.519 | 0.421 | 0.322 | 0.223 | 0.129 |
| 4 Holes | | 0.512 | 0.411 | 0.307 | 0.205 | 0.111 |
| 8 Holes | | 0.536 | 0.426 | 0.314 | 0.205 | 0.109 |
| 12 Holes | | 0.567 | 0.449 | 0.329 | 0.214 | 0.113 |
| 13 Holes | | 0.578 | 0.457 | 0.335 | 0.218 | 0.115 |
| 33 Holes | | 0.697 | 0.537 | 0.380 | 0.236 | 0.117 |
| 45 Holes | | 0.798 | 0.600 | 0.416 | 0.257 | 0.131 |
| 49 Holes | | 0.852 | 0.641 | 0.447 | 0.278 | 0.142 |

| PATTERN 4 – ANTI-SYMMETRICAL LOAD – R ₃ | | | | | | |
|--|-----|-------|-------|-------|-------|-------|
| η | [-] | 80 | 96 | 120 | 160 | 240 |
| λ/λ_{\max} [-] | | | | | | |
| No Hole | | 0.519 | 0.421 | 0.322 | 0.223 | 0.129 |
| 1 Hole | | 0.527 | 0.425 | 0.323 | 0.221 | 0.126 |
| 5 Holes | | 0.563 | 0.455 | 0.347 | 0.240 | 0.139 |
| 9 Holes | | 0.595 | 0.477 | 0.359 | 0.244 | 0.138 |
| 13 Holes | | 0.578 | 0.457 | 0.335 | 0.218 | 0.115 |
| 17 Holes | | 0.619 | 0.489 | 0.358 | 0.234 | 0.124 |
| 29 Holes | | 0.720 | 0.560 | 0.405 | 0.260 | 0.137 |
| 49 Holes | | 0.852 | 0.641 | 0.447 | 0.278 | 0.142 |

LIVE LOAD RESULTANT: TABLES

| PATTERN 1 – SYMMETRICAL LOAD – R ₃ | | | | | | |
|---|-----|-------|-------|-------|-------|-------|
| η | [-] | 80 | 96 | 120 | 160 | 240 |
| F/F_{\max} [-] | | | | | | |
| No Hole | | 0.943 | 0.621 | 0.376 | 0.202 | 0.089 |
| 1 Hole | | 0.929 | 0.609 | 0.367 | 0.195 | 0.085 |
| 5 Holes | | 0.976 | 0.645 | 0.392 | 0.211 | 0.095 |
| 9 Holes | | 0.993 | 0.658 | 0.402 | 0.219 | 0.099 |
| 13 Holes | | 1.000 | 0.664 | 0.408 | 0.223 | 0.101 |
| 25 Holes | | 0.977 | 0.648 | 0.396 | 0.213 | 0.093 |
| 29 Holes | | 0.977 | 0.647 | 0.393 | 0.210 | 0.089 |
| 49 Holes | | 0.789 | 0.507 | 0.294 | 0.147 | 0.056 |

| PATTERN 2 – SYMMETRICAL LOAD – R ₃ | | | | | | |
|---|-----|-------|-------|-------|-------|-------|
| η | [-] | 80 | 96 | 120 | 160 | 240 |
| F/F _{max} [-] | | | | | | |
| No Hole | | 0.943 | 0.621 | 0.376 | 0.202 | 0.089 |
| 4 Holes | | 0.960 | 0.633 | 0.384 | 0.206 | 0.091 |
| 8 Holes | | 0.970 | 0.641 | 0.390 | 0.211 | 0.094 |
| 12 Holes | | 0.981 | 0.650 | 0.397 | 0.215 | 0.096 |
| 13 Holes | | 0.997 | 0.662 | 0.405 | 0.221 | 0.099 |
| 33 Holes | | 0.836 | 0.543 | 0.319 | 0.161 | 0.061 |
| 45 Holes | | 0.790 | 0.508 | 0.296 | 0.148 | 0.057 |
| 49 Holes | | 0.789 | 0.507 | 0.294 | 0.147 | 0.056 |

| PATTERN 3 – SYMMETRICAL LOAD – R ₃ | | | | | | |
|---|-----|-------|-------|-------|-------|-------|
| η | [-] | 80 | 96 | 120 | 160 | 240 |
| F/F _{max} [-] | | | | | | |
| No Hole | | 0.943 | 0.621 | 0.376 | 0.202 | 0.089 |
| 4 Holes | | 0.847 | 0.547 | 0.322 | 0.166 | 0.068 |
| 8 Holes | | 0.843 | 0.542 | 0.318 | 0.162 | 0.066 |
| 12 Holes | | 0.856 | 0.550 | 0.323 | 0.165 | 0.067 |
| 13 Holes | | 0.866 | 0.558 | 0.327 | 0.167 | 0.068 |
| 33 Holes | | 0.796 | 0.515 | 0.301 | 0.151 | 0.057 |
| 45 Holes | | 0.769 | 0.493 | 0.286 | 0.141 | 0.054 |
| 49 Holes | | 0.789 | 0.507 | 0.294 | 0.147 | 0.056 |

| PATTERN 4 – SYMMETRICAL LOAD – R ₃ | | | | | | |
|---|-----|-------|-------|-------|-------|-------|
| η | [-] | 80 | 96 | 120 | 160 | 240 |
| F/F _{max} [-] | | | | | | |
| No Hole | | 0.943 | 0.621 | 0.376 | 0.202 | 0.089 |
| 1 Hole | | 0.929 | 0.609 | 0.367 | 0.195 | 0.085 |
| 5 Holes | | 0.971 | 0.641 | 0.389 | 0.210 | 0.093 |
| 9 Holes | | 0.957 | 0.631 | 0.382 | 0.205 | 0.090 |
| 13 Holes | | 0.866 | 0.558 | 0.327 | 0.167 | 0.068 |
| 17 Holes | | 0.886 | 0.573 | 0.338 | 0.175 | 0.073 |
| 29 Holes | | 0.911 | 0.591 | 0.350 | 0.181 | 0.075 |
| 49 Holes | | 0.789 | 0.507 | 0.294 | 0.147 | 0.056 |

| PATTERN 1 – ANTI-SYMMETRICAL LOAD – R ₃ | | | | | | |
|--|-----|-------|-------|-------|-------|-------|
| η | [-] | 80 | 96 | 120 | 160 | 240 |
| F/F _{max} [-] | | | | | | |
| No Hole | | 0.730 | 0.514 | 0.333 | 0.188 | 0.084 |
| 1 Hole | | 0.732 | 0.513 | 0.330 | 0.184 | 0.080 |
| 5 Holes | | 0.759 | 0.535 | 0.347 | 0.197 | 0.088 |
| 9 Holes | | 0.778 | 0.548 | 0.354 | 0.201 | 0.090 |
| 13 Holes | | 0.788 | 0.553 | 0.357 | 0.202 | 0.090 |
| 25 Holes | | 0.807 | 0.554 | 0.348 | 0.191 | 0.082 |
| 29 Holes | | 0.805 | 0.549 | 0.341 | 0.185 | 0.079 |
| 49 Holes | | 0.670 | 0.438 | 0.259 | 0.131 | 0.052 |

| PATTERN 2 – ANTI-SYMMETRICAL LOAD – R ₃ | | | | | | |
|--|-----|-------|-------|-------|-------|-------|
| η | [-] | 80 | 96 | 120 | 160 | 240 |
| F/F _{max} [-] | | | | | | |
| No Hole | | 0.730 | 0.514 | 0.333 | 0.188 | 0.084 |
| 4 Holes | | 0.735 | 0.518 | 0.335 | 0.189 | 0.084 |
| 8 Holes | | 0.746 | 0.524 | 0.338 | 0.190 | 0.085 |
| 12 Holes | | 0.764 | 0.535 | 0.343 | 0.192 | 0.084 |
| 13 Holes | | 0.776 | 0.544 | 0.350 | 0.197 | 0.087 |
| 33 Holes | | 0.689 | 0.463 | 0.279 | 0.142 | 0.054 |
| 45 Holes | | 0.668 | 0.438 | 0.258 | 0.130 | 0.051 |
| 49 Holes | | 0.670 | 0.438 | 0.259 | 0.131 | 0.052 |

| PATTERN 3 – ANTI-SYMMETRICAL LOAD – R ₃ | | | | | | |
|--|-----|-------|-------|-------|-------|-------|
| η | [-] | 80 | 96 | 120 | 160 | 240 |
| F/F _{max} [-] | | | | | | |
| No Hole | | 0.730 | 0.514 | 0.333 | 0.188 | 0.084 |
| 4 Holes | | 0.686 | 0.478 | 0.302 | 0.164 | 0.067 |
| 8 Holes | | 0.685 | 0.472 | 0.294 | 0.156 | 0.063 |
| 12 Holes | | 0.694 | 0.477 | 0.295 | 0.156 | 0.062 |
| 13 Holes | | 0.704 | 0.483 | 0.300 | 0.159 | 0.064 |
| 33 Holes | | 0.670 | 0.448 | 0.268 | 0.135 | 0.051 |
| 45 Holes | | 0.655 | 0.428 | 0.251 | 0.126 | 0.049 |
| 49 Holes | | 0.670 | 0.438 | 0.259 | 0.131 | 0.052 |

| PATTERN 4 – ANTI-SYMMETRICAL LOAD – R ₃ | | | | | | |
|--|-----|-------|-------|-------|-------|-------|
| η | [-] | 80 | 96 | 120 | 160 | 240 |
| F/F _{max} [-] | | | | | | |
| No Hole | | 0.730 | 0.514 | 0.333 | 0.188 | 0.084 |
| 1 Hole | | 0.732 | 0.513 | 0.330 | 0.184 | 0.080 |
| 5 Holes | | 0.756 | 0.531 | 0.343 | 0.194 | 0.087 |
| 9 Holes | | 0.763 | 0.531 | 0.339 | 0.188 | 0.082 |
| 13 Holes | | 0.704 | 0.483 | 0.300 | 0.159 | 0.064 |
| 17 Holes | | 0.724 | 0.496 | 0.308 | 0.164 | 0.066 |
| 29 Holes | | 0.730 | 0.493 | 0.302 | 0.159 | 0.064 |
| 49 Holes | | 0.670 | 0.438 | 0.259 | 0.131 | 0.052 |

UNIFORMLY DISTRIBUTED LIVE LOAD: TABLES

| PATTERN 1 – SYMMETRICAL LOAD – R ₃ | | | | | | |
|---|-----|-------|-------|-------|-------|-------|
| η | [-] | 80 | 96 | 120 | 160 | 240 |
| q/q _{max} [-] | | | | | | |
| No Hole | | 0.656 | 0.432 | 0.262 | 0.140 | 0.062 |
| 1 Hole | | 0.655 | 0.429 | 0.259 | 0.138 | 0.060 |
| 5 Holes | | 0.710 | 0.469 | 0.285 | 0.154 | 0.069 |
| 9 Holes | | 0.756 | 0.501 | 0.306 | 0.167 | 0.075 |
| 13 Holes | | 0.800 | 0.531 | 0.326 | 0.178 | 0.081 |
| 25 Holes | | 0.909 | 0.603 | 0.368 | 0.199 | 0.087 |
| 29 Holes | | 0.956 | 0.632 | 0.384 | 0.205 | 0.088 |
| 49 Holes | | 1.000 | 0.643 | 0.373 | 0.186 | 0.071 |

| PATTERN 2 – SYMMETRICAL LOAD – R ₃ | | | | | | |
|---|-----|-------|-------|-------|-------|-------|
| η | [-] | 80 | 96 | 120 | 160 | 240 |
| q/q _{max} [-] | | | | | | |
| No Hole | | 0.656 | 0.432 | 0.262 | 0.140 | 0.062 |
| 4 Holes | | 0.700 | 0.461 | 0.280 | 0.150 | 0.066 |
| 8 Holes | | 0.742 | 0.491 | 0.299 | 0.161 | 0.072 |
| 12 Holes | | 0.785 | 0.520 | 0.317 | 0.172 | 0.077 |
| 13 Holes | | 0.801 | 0.532 | 0.326 | 0.177 | 0.080 |
| 33 Holes | | 0.859 | 0.558 | 0.328 | 0.166 | 0.063 |
| 45 Holes | | 0.950 | 0.611 | 0.356 | 0.178 | 0.068 |
| 49 Holes | | 1.000 | 0.643 | 0.373 | 0.186 | 0.071 |

| PATTERN 3 – SYMMETRICAL LOAD – R ₃ | | | | | | |
|---|-----|-------|-------|-------|-------|-------|
| η | [-] | 80 | 96 | 120 | 160 | 240 |
| q/q _{max} [-] | | | | | | |
| No Hole | | 0.656 | 0.432 | 0.262 | 0.140 | 0.062 |
| 4 Holes | | 0.619 | 0.399 | 0.235 | 0.121 | 0.050 |
| 8 Holes | | 0.647 | 0.416 | 0.244 | 0.125 | 0.051 |
| 12 Holes | | 0.687 | 0.442 | 0.259 | 0.132 | 0.054 |
| 13 Holes | | 0.699 | 0.450 | 0.264 | 0.135 | 0.055 |
| 33 Holes | | 0.820 | 0.530 | 0.310 | 0.156 | 0.059 |
| 45 Holes | | 0.932 | 0.598 | 0.346 | 0.171 | 0.065 |
| 49 Holes | | 1.000 | 0.643 | 0.373 | 0.186 | 0.071 |

| PATTERN 4 – SYMMETRICAL LOAD – R ₃ | | | | | | |
|---|-----|-------|-------|-------|-------|-------|
| η | [-] | 80 | 96 | 120 | 160 | 240 |
| q/q _{max} [-] | | | | | | |
| No Hole | | 0.656 | 0.432 | 0.262 | 0.140 | 0.062 |
| 1 Hole | | 0.655 | 0.429 | 0.259 | 0.138 | 0.060 |
| 5 Holes | | 0.710 | 0.469 | 0.285 | 0.153 | 0.068 |
| 9 Holes | | 0.735 | 0.484 | 0.294 | 0.157 | 0.069 |
| 13 Holes | | 0.699 | 0.450 | 0.264 | 0.135 | 0.055 |
| 17 Holes | | 0.747 | 0.483 | 0.285 | 0.148 | 0.061 |
| 29 Holes | | 0.892 | 0.579 | 0.343 | 0.177 | 0.073 |
| 49 Holes | | 1.000 | 0.643 | 0.373 | 0.186 | 0.071 |

| PATTERN 1 – ANTI-SYMMETRICAL LOAD – R ₃ | | | | | | |
|--|-----|-------|-------|-------|-------|-------|
| η | [-] | 80 | 96 | 120 | 160 | 240 |
| q/q _{max} [-] | | | | | | |
| No Hole | | 0.508 | 0.358 | 0.232 | 0.131 | 0.058 |
| 1 Hole | | 0.516 | 0.362 | 0.232 | 0.130 | 0.057 |
| 5 Holes | | 0.553 | 0.389 | 0.252 | 0.143 | 0.064 |
| 9 Holes | | 0.592 | 0.417 | 0.270 | 0.153 | 0.069 |
| 13 Holes | | 0.630 | 0.442 | 0.285 | 0.161 | 0.072 |
| 25 Holes | | 0.750 | 0.516 | 0.324 | 0.177 | 0.077 |
| 29 Holes | | 0.788 | 0.537 | 0.334 | 0.181 | 0.077 |
| 49 Holes | | 0.849 | 0.555 | 0.328 | 0.166 | 0.065 |

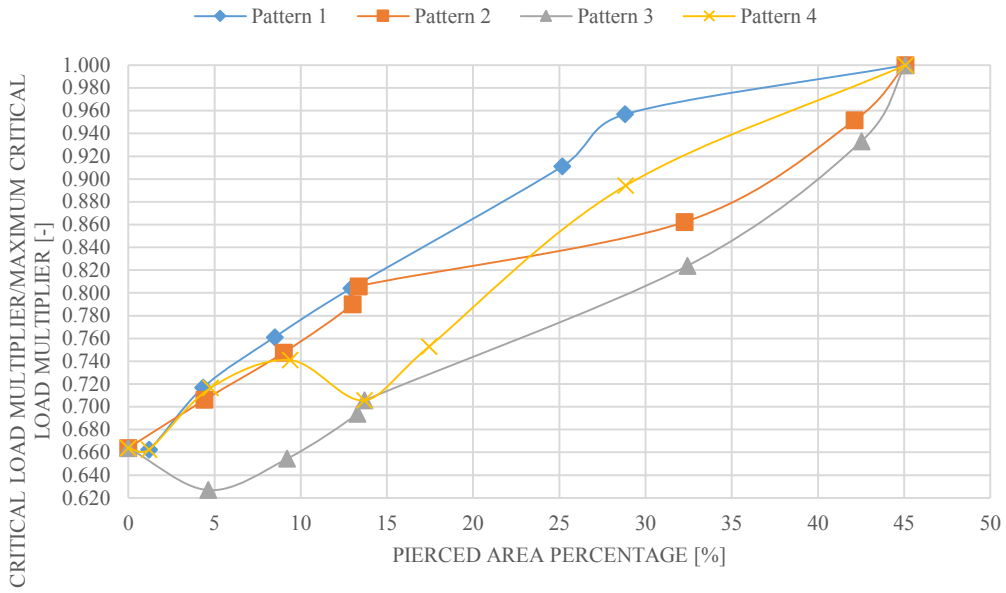
| PATTERN 2 – ANTI-SYMMETRICAL LOAD – R ₃ | | | | | | |
|--|-----|-------|-------|-------|-------|-------|
| η | [-] | 80 | 96 | 120 | 160 | 240 |
| q/q _{max} [-] | | | | | | |
| No Hole | | 0.508 | 0.358 | 0.232 | 0.131 | 0.058 |
| 4 Holes | | 0.535 | 0.377 | 0.244 | 0.138 | 0.061 |
| 8 Holes | | 0.571 | 0.401 | 0.259 | 0.146 | 0.065 |
| 12 Holes | | 0.611 | 0.428 | 0.275 | 0.154 | 0.068 |
| 13 Holes | | 0.624 | 0.437 | 0.281 | 0.158 | 0.070 |
| 33 Holes | | 0.708 | 0.476 | 0.287 | 0.146 | 0.055 |
| 45 Holes | | 0.804 | 0.527 | 0.311 | 0.157 | 0.061 |
| 49 Holes | | 0.849 | 0.555 | 0.328 | 0.166 | 0.065 |

| PATTERN 3 – ANTI-SYMMETRICAL LOAD – R ₃ | | | | | | |
|--|-----|-------|-------|-------|-------|-------|
| η | [-] | 80 | 96 | 120 | 160 | 240 |
| q/q _{max} [-] | | | | | | |
| No Hole | | 0.508 | 0.358 | 0.232 | 0.131 | 0.058 |
| 4 Holes | | 0.501 | 0.349 | 0.221 | 0.119 | 0.049 |
| 8 Holes | | 0.525 | 0.362 | 0.225 | 0.120 | 0.048 |
| 12 Holes | | 0.557 | 0.383 | 0.237 | 0.125 | 0.050 |
| 13 Holes | | 0.568 | 0.390 | 0.242 | 0.128 | 0.051 |
| 33 Holes | | 0.690 | 0.461 | 0.276 | 0.139 | 0.052 |
| 45 Holes | | 0.793 | 0.518 | 0.304 | 0.153 | 0.059 |
| 49 Holes | | 0.849 | 0.555 | 0.328 | 0.166 | 0.065 |

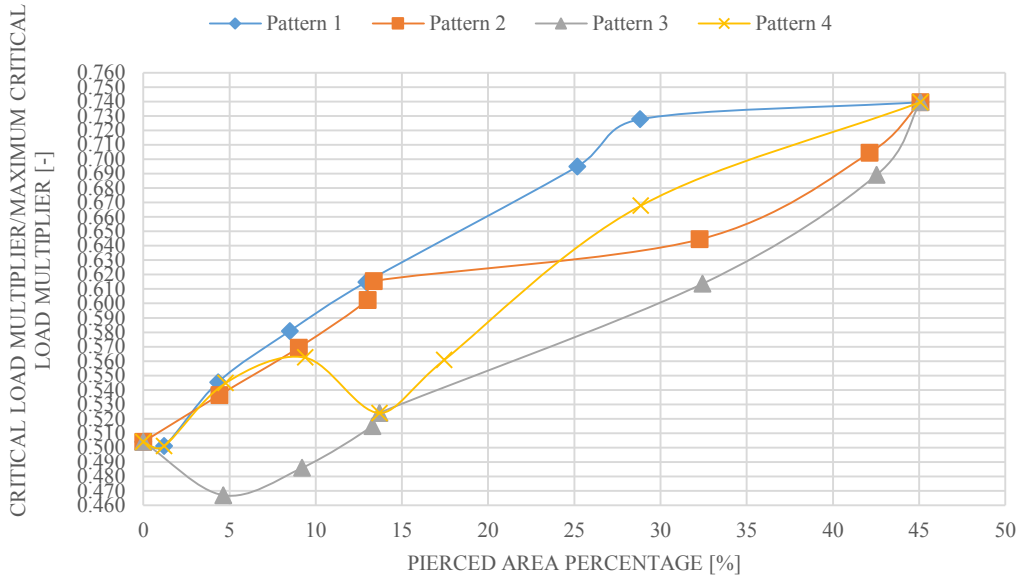
| PATTERN 4 – ANTI-SYMMETRICAL LOAD – R ₃ | | | | | | |
|--|-----|-------|-------|-------|-------|-------|
| η | [-] | 80 | 96 | 120 | 160 | 240 |
| q/q _{max} [-] | | | | | | |
| No Hole | | 0.508 | 0.358 | 0.232 | 0.131 | 0.058 |
| 1 Hole | | 0.516 | 0.362 | 0.232 | 0.130 | 0.057 |
| 5 Holes | | 0.553 | 0.388 | 0.251 | 0.142 | 0.063 |
| 9 Holes | | 0.586 | 0.408 | 0.260 | 0.145 | 0.063 |
| 13 Holes | | 0.568 | 0.390 | 0.242 | 0.128 | 0.051 |
| 17 Holes | | 0.611 | 0.418 | 0.259 | 0.138 | 0.056 |
| 29 Holes | | 0.714 | 0.483 | 0.295 | 0.155 | 0.063 |
| 49 Holes | | 0.849 | 0.555 | 0.328 | 0.166 | 0.065 |

LOAD MULTIPLIER: GRAPHICS

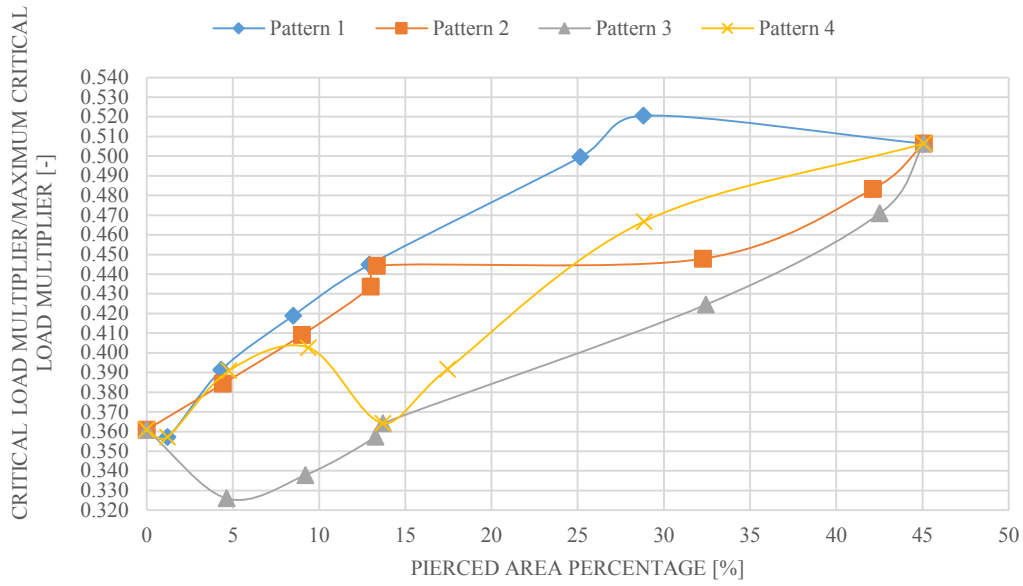
$\eta=80$ - SYMMETRICAL LOAD - R_3



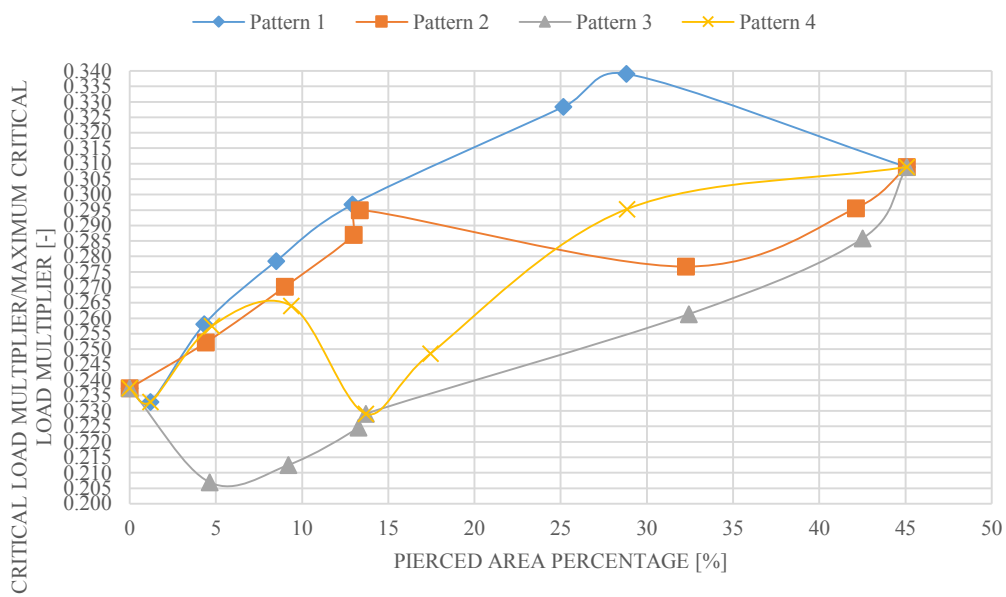
$\eta=96$ - SYMMETRICAL LOAD - R_3



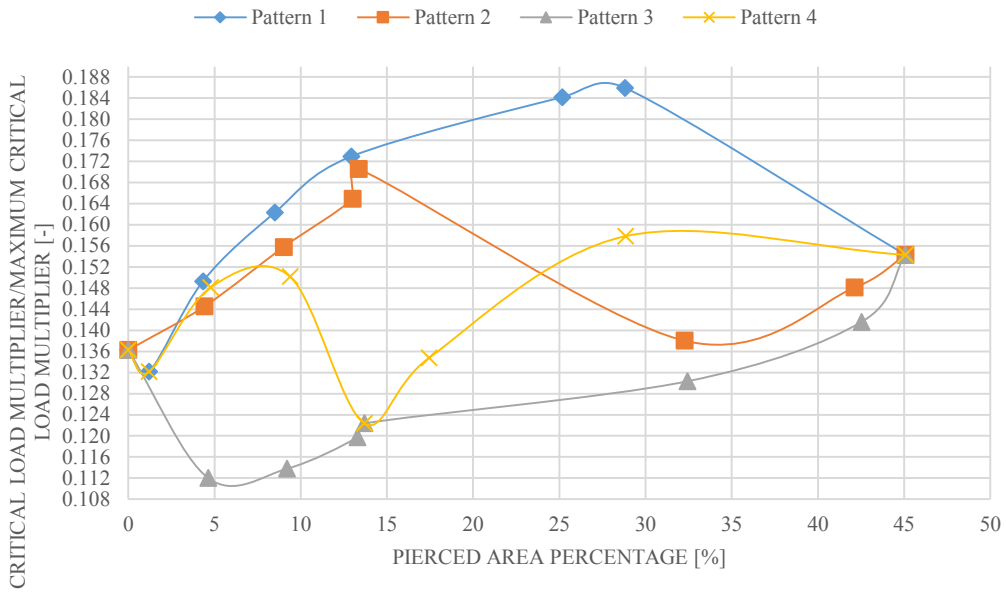
$\eta=120$ - SYMMETRICAL LOAD - R_3



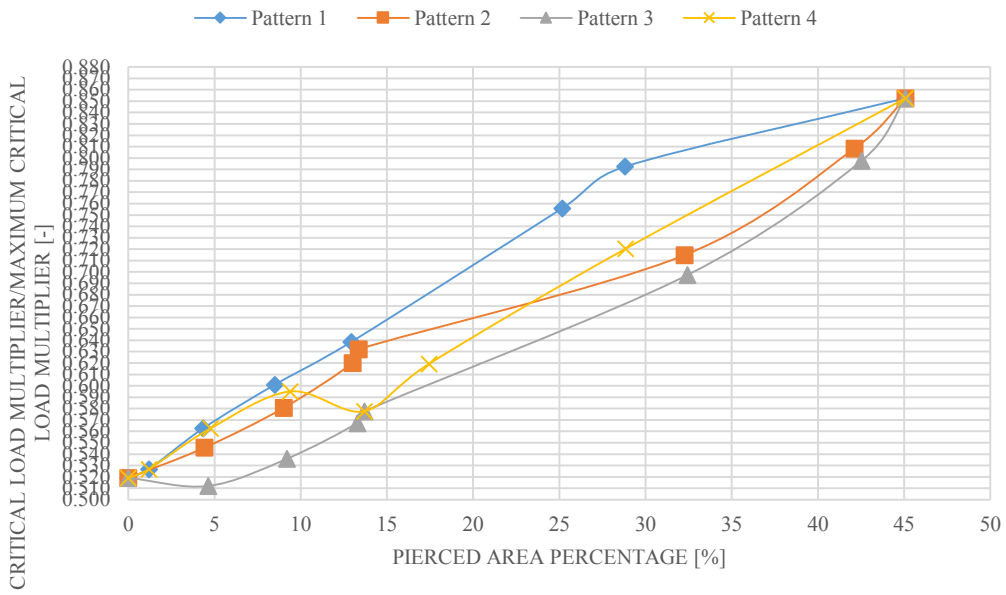
$\eta=160$ - SYMMETRICAL LOAD - R_3



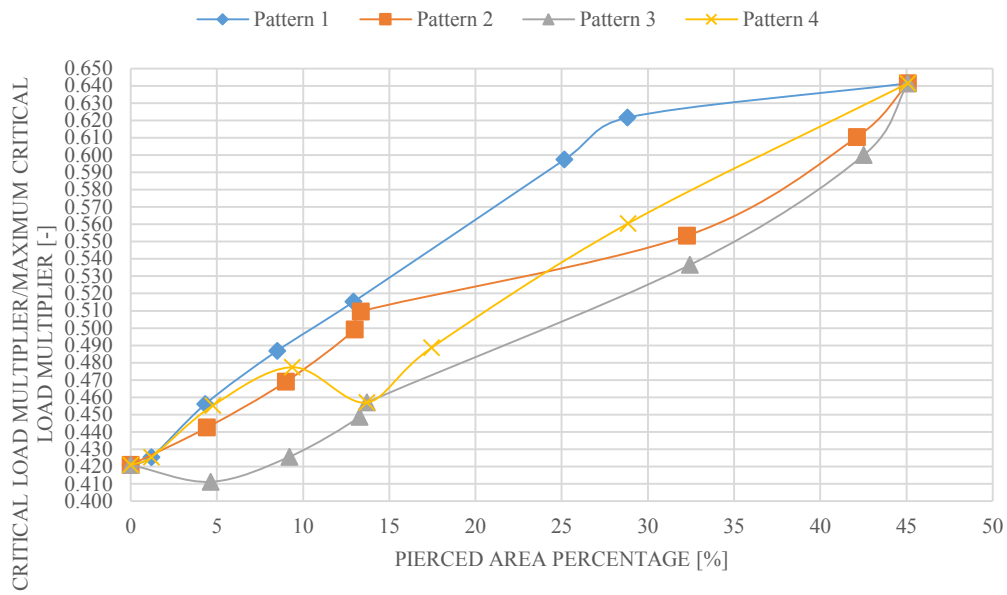
$\eta=240$ - SYMMETRICAL LOAD - R_3



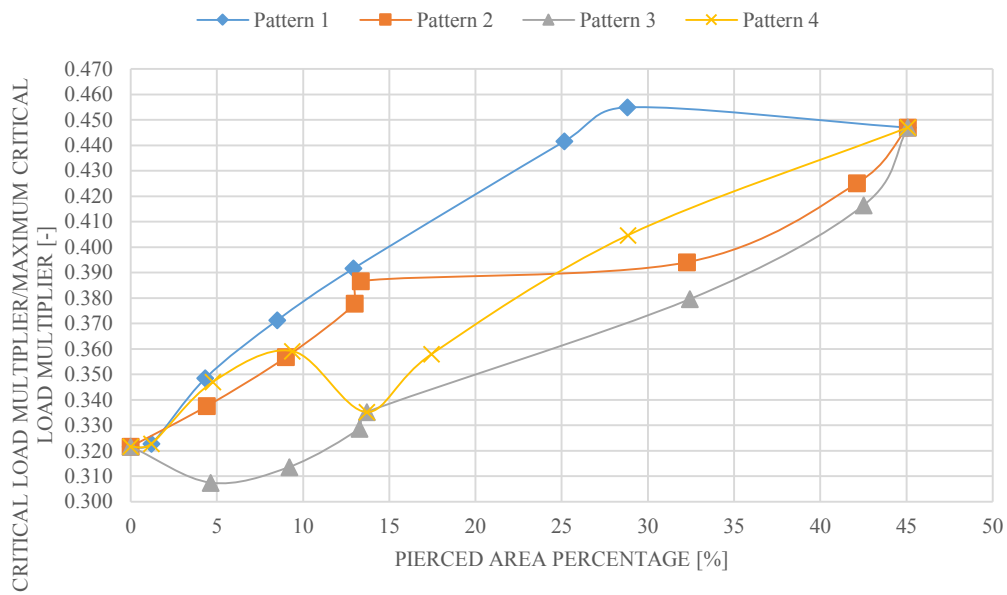
$\eta=80$ - ANTI-SYMMETRICAL LOAD - R_3



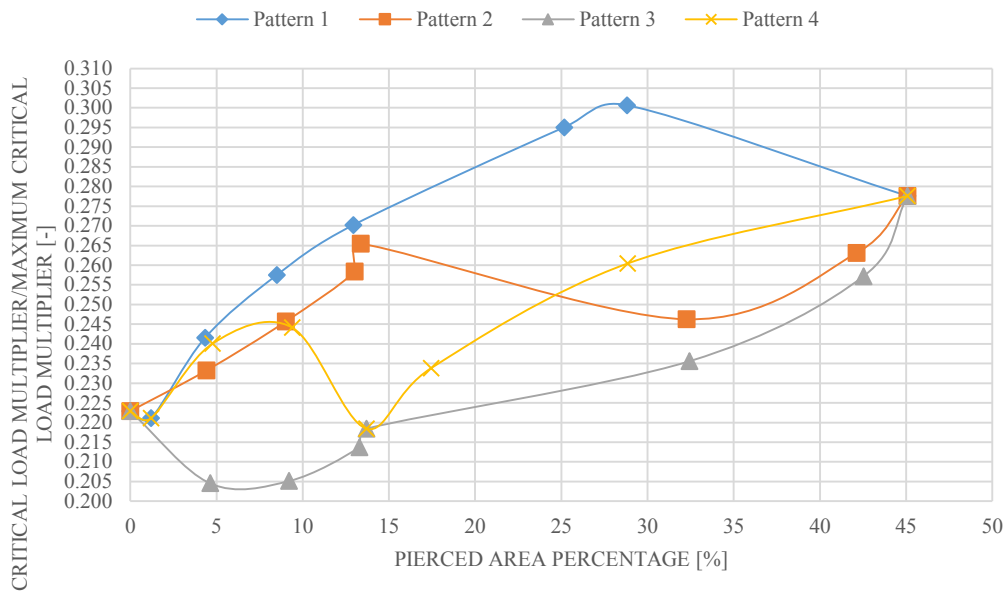
$\eta=96$ - ANTI-SYMMETRICAL LOAD - R_3



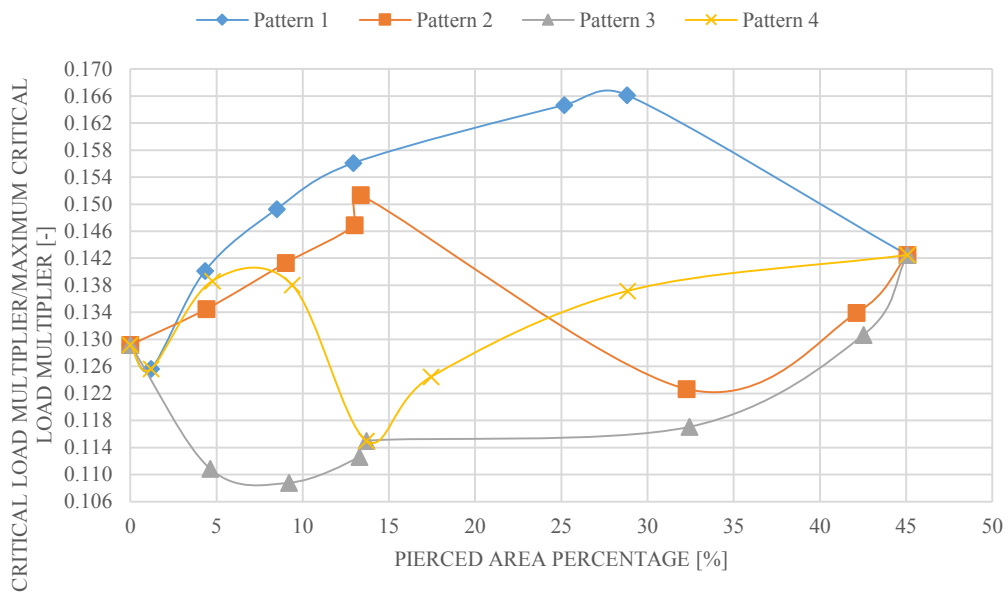
$\eta=120$ - ANTI-SYMMETRICAL LOAD - R_3



$\eta=160$ - ANTI-SYMMETRICAL LOAD - R_3

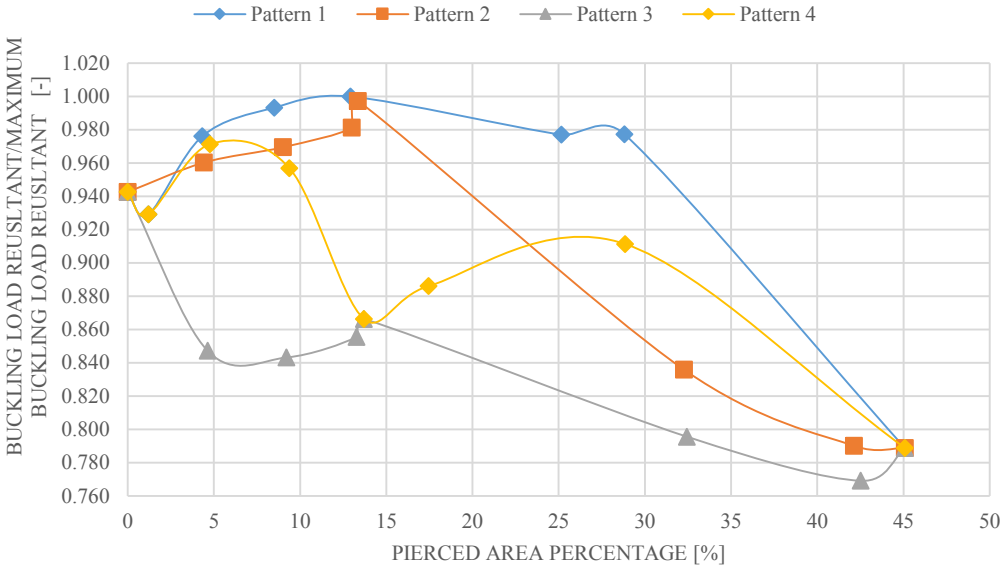


$\eta=240$ - ANTI-SYMMETRICAL LOAD - R_3

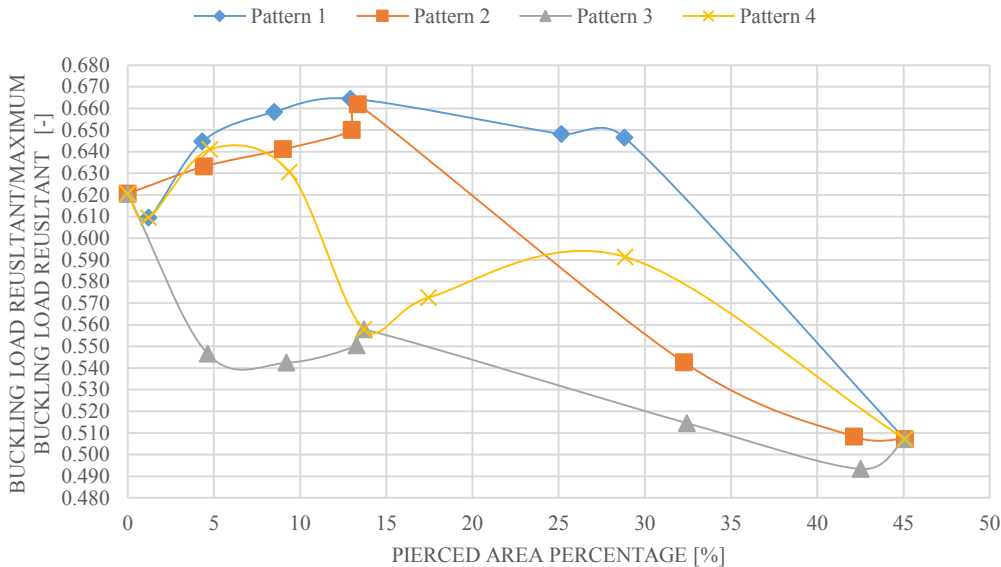


LIVE LOAD RESULTANT: GRAPHICS

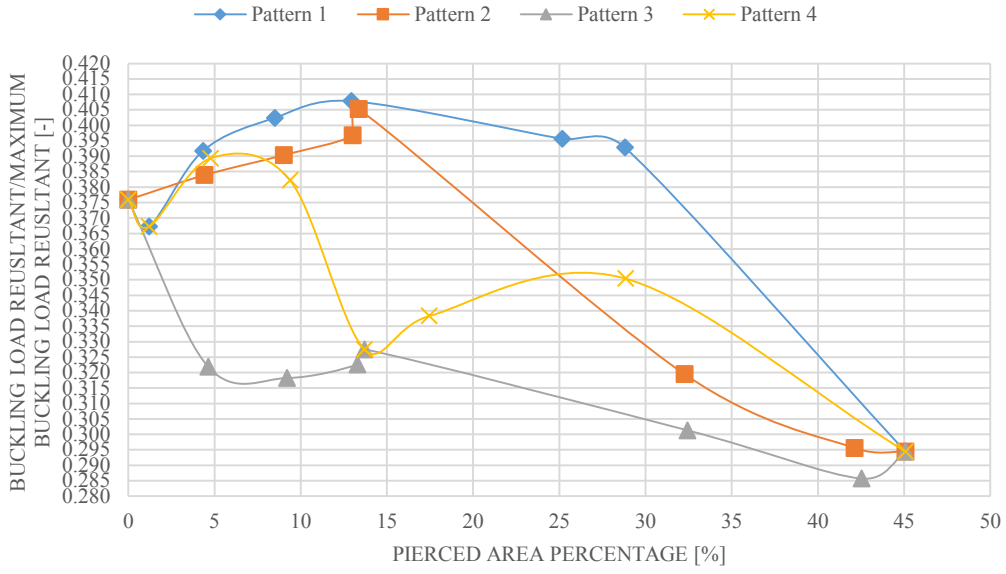
$\eta=80$ - SYMMETRICAL LOAD - R_3



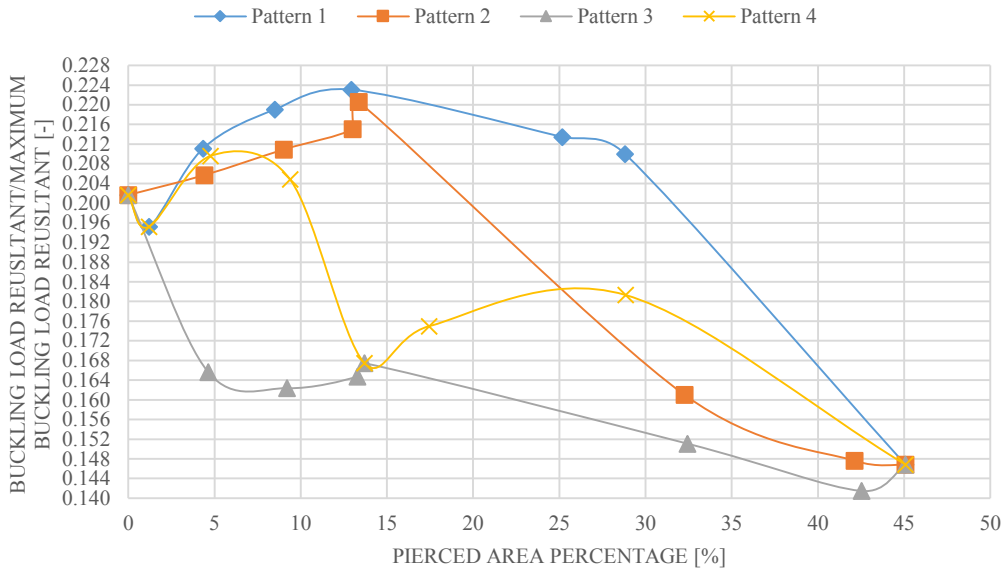
$\eta=96$ - SYMMETRICAL LOAD - R_3



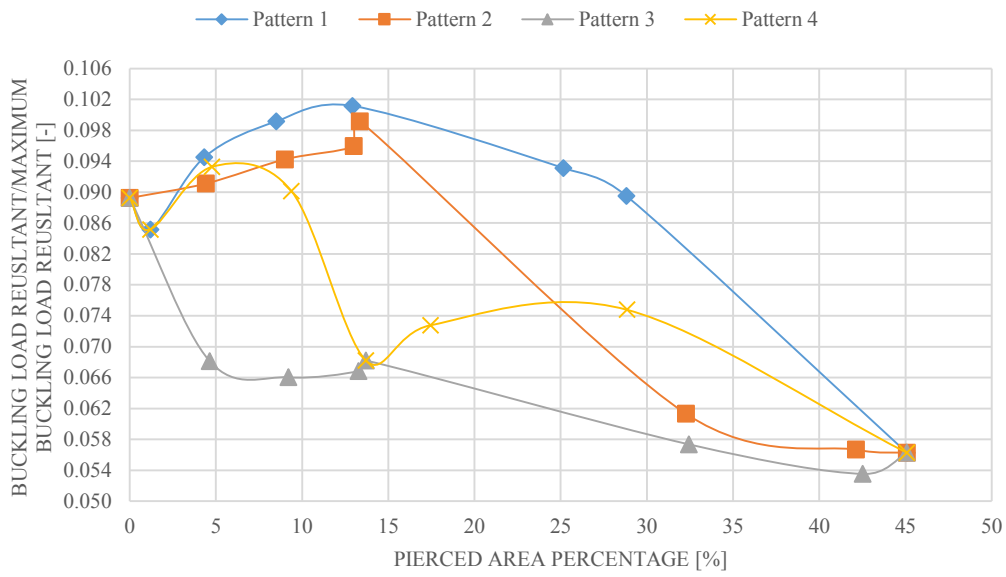
$\eta=120$ - SYMMETRICAL LOAD - R_3



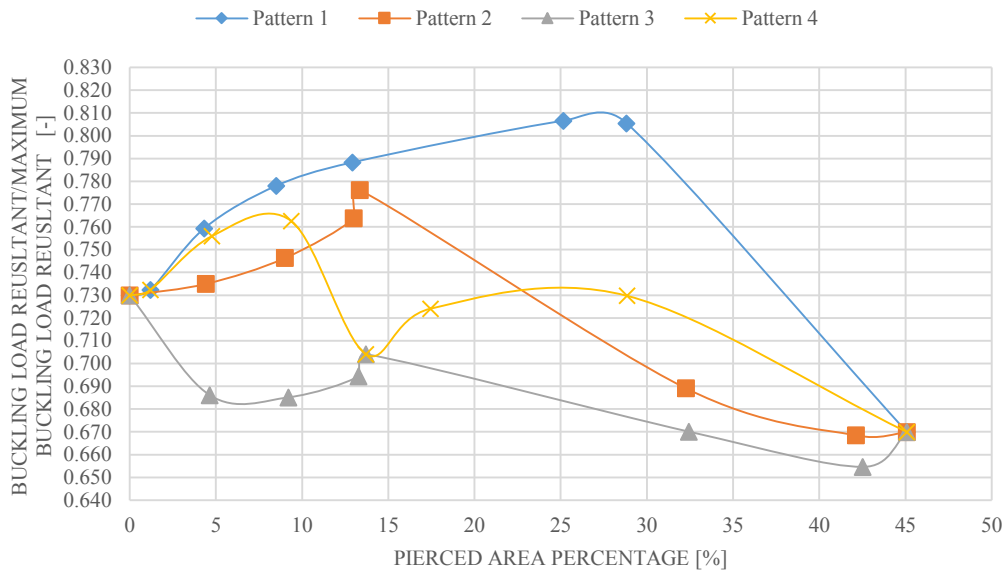
$\eta=160$ - SYMMETRICAL LOAD - R_3



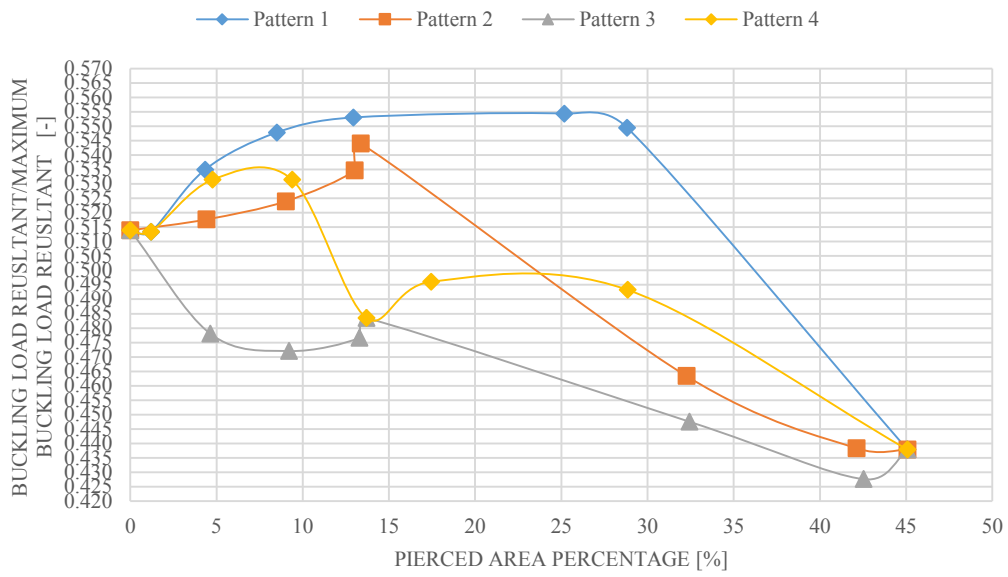
$\eta=240$ - SYMMETRICAL LOAD - R_3



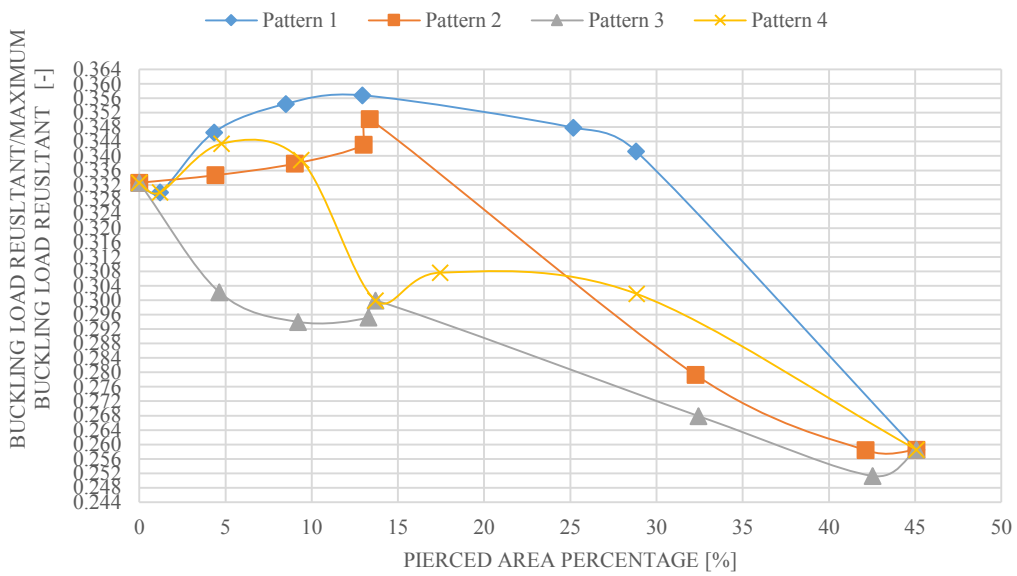
$\eta=80$ - ANTI-SYMMETRICAL LOAD - R_3



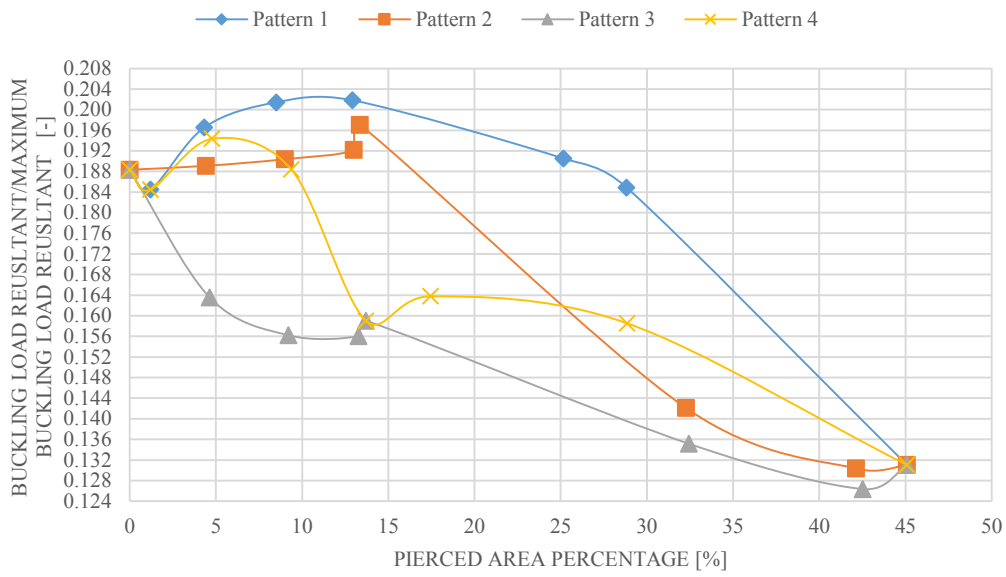
$\eta=96$ - ANTI-SYMMETRICAL LOAD - R_3



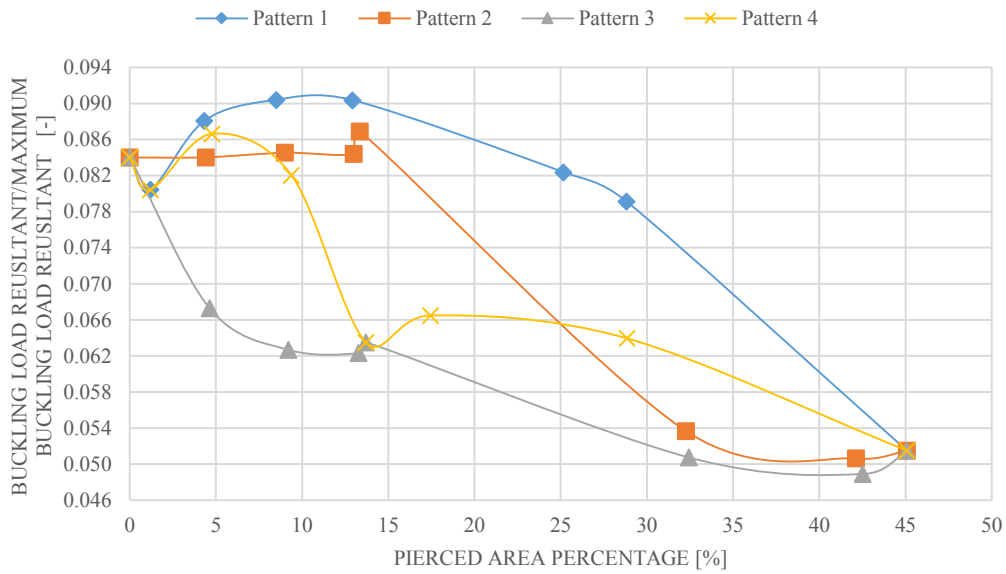
$\eta=120$ - ANTI-SYMMETRICAL LOAD - R_3



$\eta=160$ - ANTI-SYMMETRICAL LOAD - R_3

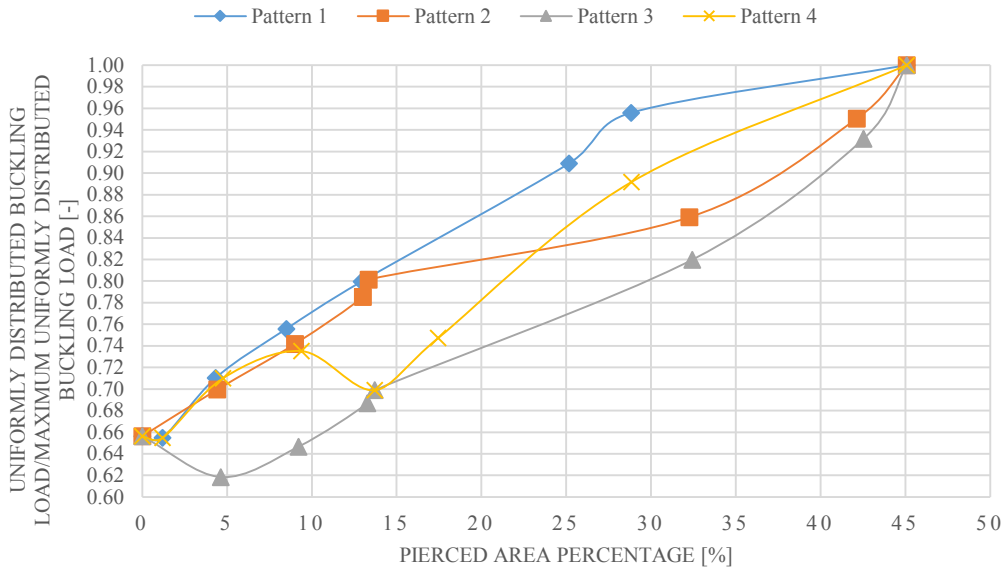


$\eta=240$ - ANTI-SYMMETRICAL LOAD - R_3

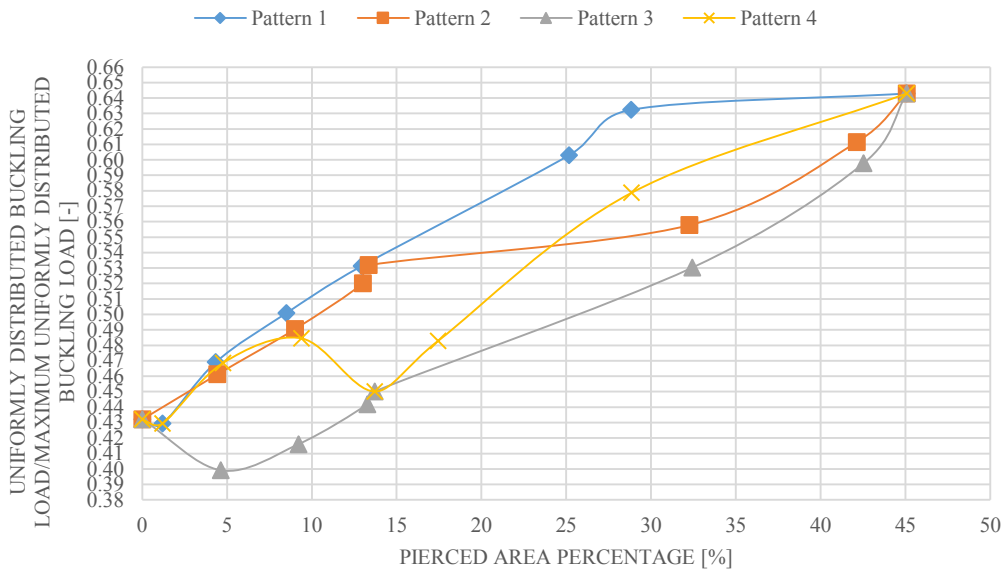


UNIFORMLY DISTRIBUTED LIVE LOAD: GRAPHICS

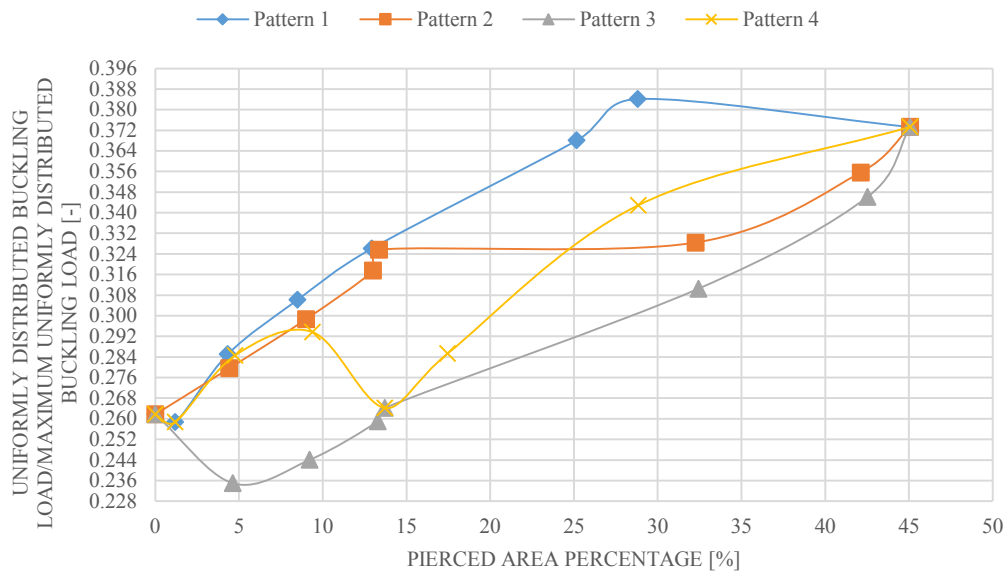
$\eta=80$ - SYMMETRICAL LOAD - R_3



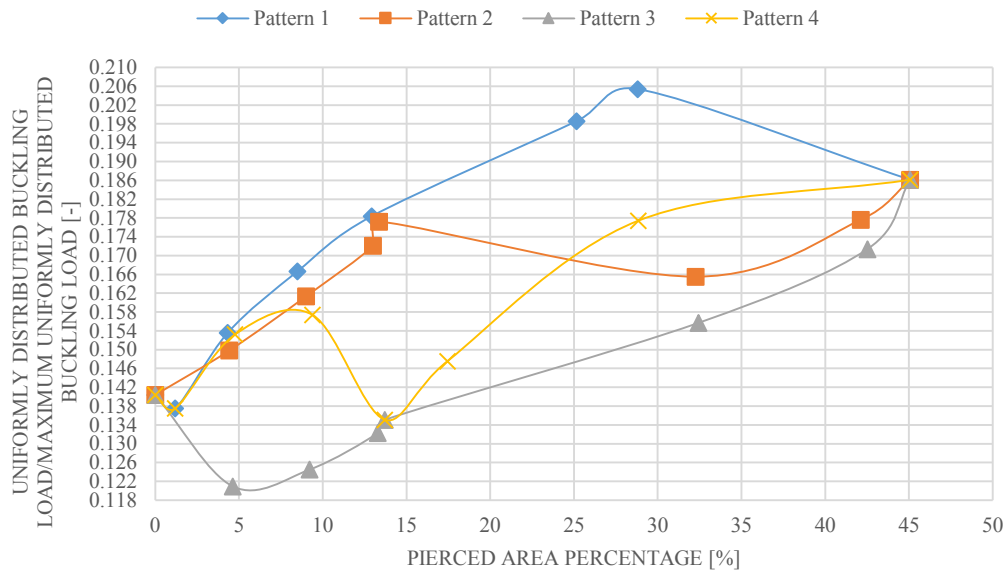
$\eta=96$ - SYMMETRICAL LOAD - R_3



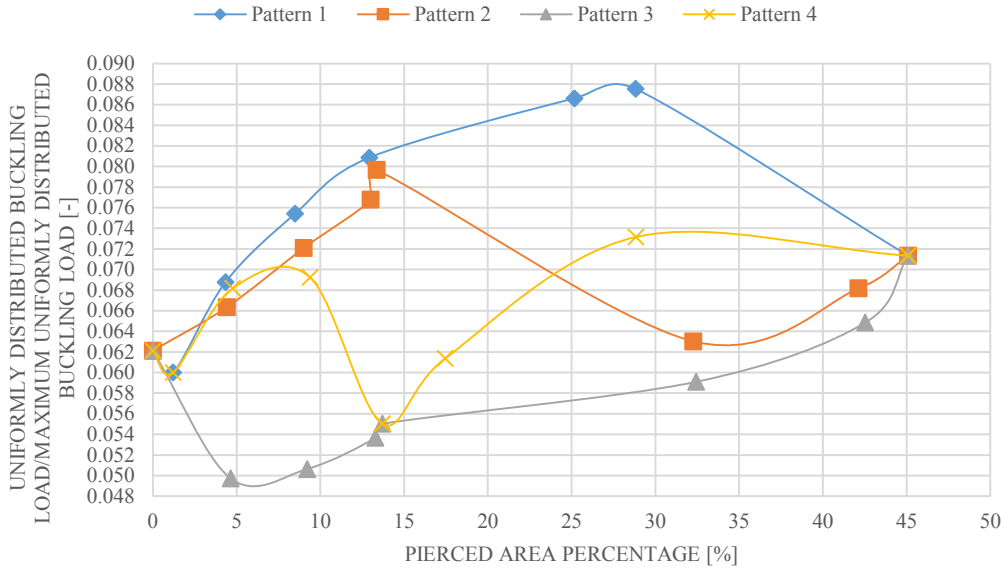
$\eta=120$ - SYMMETRICAL LOAD - R_3



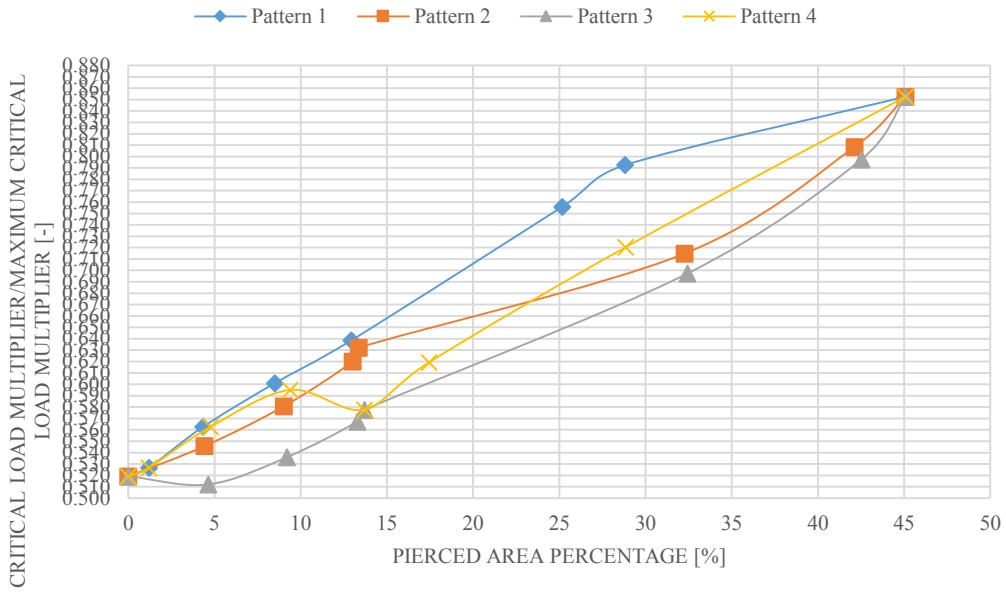
$\eta=160$ - SYMMETRICAL LOAD - R_3



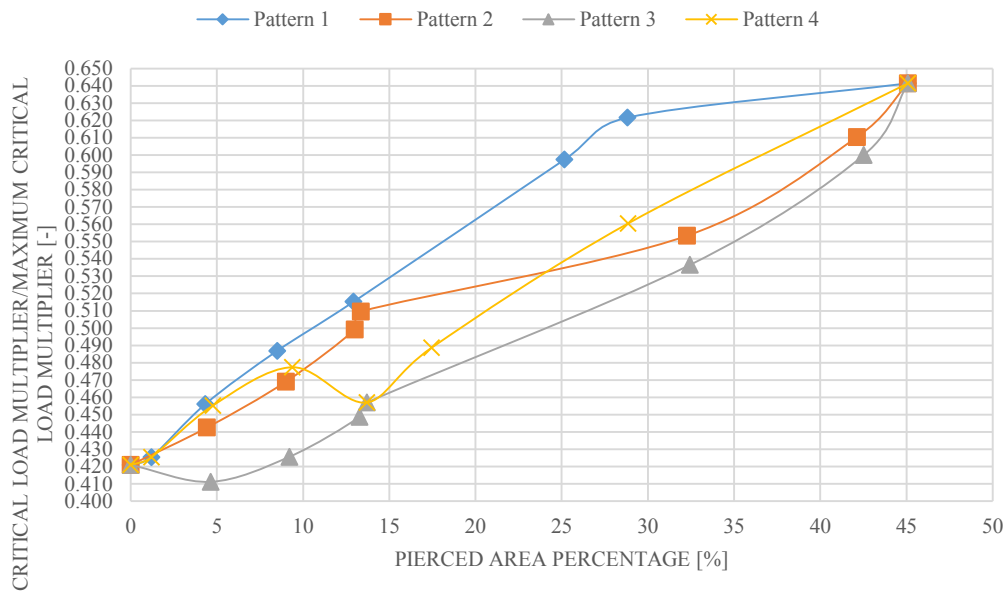
$\eta=240$ - SYMMETRICAL LOAD - R_3



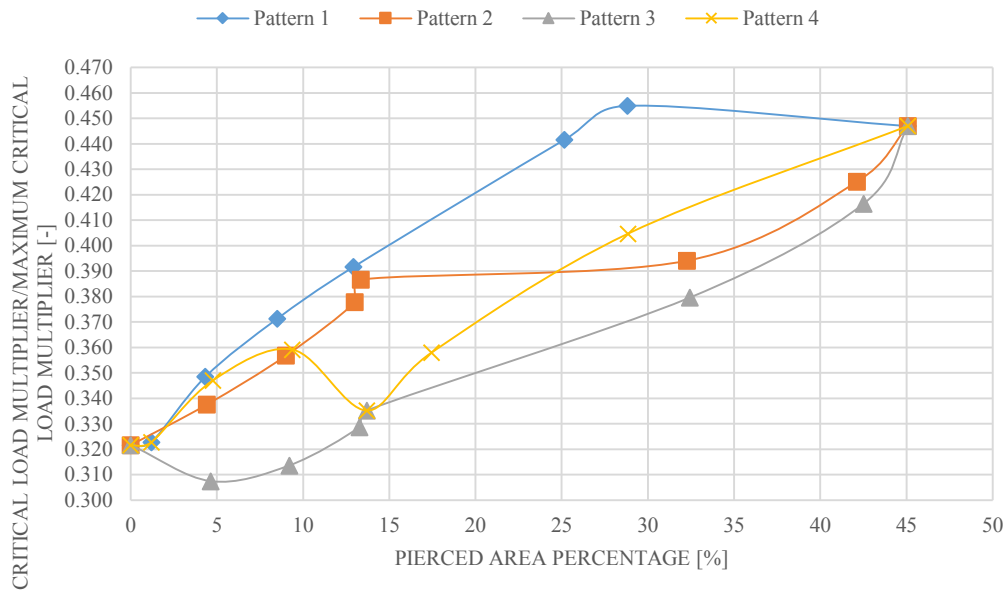
$\eta=80$ - ANTI-SYMMETRICAL LOAD - R_3



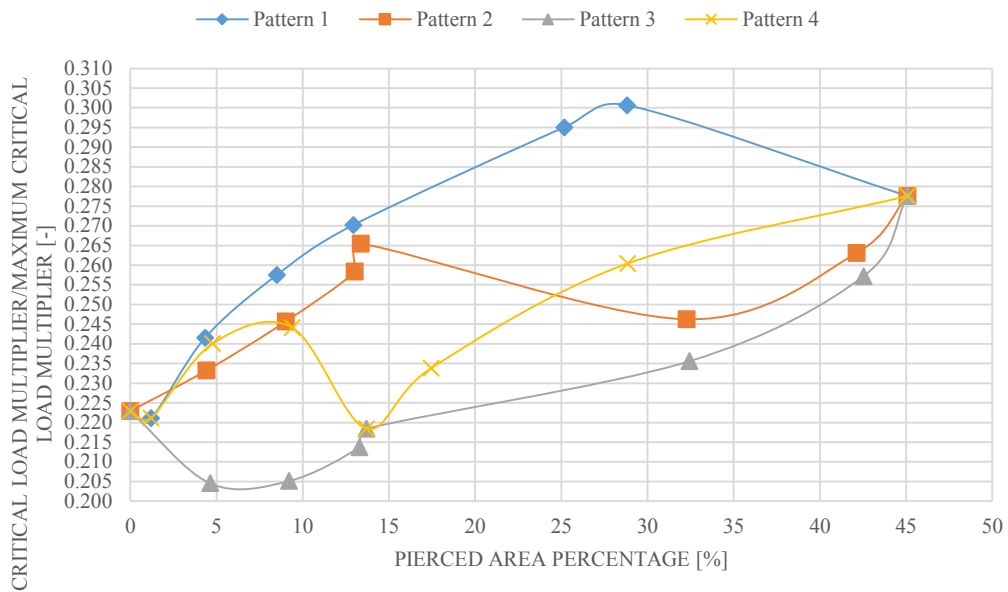
$\eta=96$ - ANTI-SYMMETRICAL LOAD - R_3



$\eta=120$ - ANTI-SYMMETRICAL LOAD - R_3



$\eta=160$ - ANTI-SYMMETRICAL LOAD - R_3



$\eta=240$ - ANTI-SYMMETRICAL LOAD - R_3

